Femtosecond Reaction Dynamics

Royal Netherlands Academy of Arts and Sciences
P.O. Box 19121, 1000 GC Amsterdam, the Netherlands

Proceedings of the colloquium 'Femtosecond Reaction Dynamics',
Amsterdam, 17–19 May 1993

ISBN 0-444-85776-1

Koninklijke Nederlandse Akademie van Wetenschappen
Verhandelingen, Afd. Natuurkunde, Eerste Reeks, deel 42

Femtosecond Reaction Dynamics

Edited by Douwe A. Wiersma

North-Holland, Amsterdam/Oxford/New York/Tokyo, 1994

Preface

The idea for a Colloquium on *Femtosecond Reaction Dynamics* was inspired by the fast advancements that have been made in the field of 'femtosecond spectroscopy.' The recent discovery that an argon ion pumped Ti: sapphire laser can produce pulses of 10 fs or less and that such pulses can be amplified to terrawatt pulses of less than 50 fs, at kHz repitition rates, has made it clear that a new era in physics and spectroscopy has begun. For laser physicists this situation may present a problem as vividly expressed by Wayne Knox,[1] who concluded his paper on *The revolution in femtosecond near-infrared pulse generation* with: 'Ultimately, we suppose that femtosecond lasers will be as ubiquitous as 9 V batteries. Then what shall we do?' For physical chemists, on the contrary, this new situation presents a challenge to find novel use of femtosecond pulses in experiments that probe deeper into the question of molecular reactivity. In fact many people in our community have taken up this challenge already and this work is finding recognition by a broad audience in chemistry, as demonstrated by the fact that professor Zewail was awarded the Wolf Prize in Chemistry for 1993.

It is very satisfying that all speakers at the Colloquium have contributed a paper to the Proceedings of the Meeting. Because of the great diversity of topics addressed, these Proceedings of the Royal Netherlands Academy Colloquium on *Femtosecond Reaction Dynamics* contain a good overview of the state-of-the-art in the field of 'Femtoscience.'

The organization of the Royal Netherlands Academy Colloquium on Femtosecond Reaction Dynamics was only possible through the efforts of several people and financial support by many organizations. We gratefully acknowledge the indispensable help and advice of Ms. M. Kooy from the Royal Netherlands Academy of Arts and Sciences and Mrs. G. Lap-Koekkoek from the University of Groningen. For financial support we are foremeost indebted to the Royal Netherlands Academy of Arts and Sciences. Without its generous financial support this meeting would never have been possible. Support from the other sponsors has also been vital to financing of the meeting and of the social activities.

[1] W.H. Knox, Optics and Photonics News *3*, 10 (1992).

In particular we wish to thank Spectra Physics The Netherlands for generous financial support of the Colloquium and of the dinner in the Frans Hals museum in Haarlem, and Coherent Benelux for sponsorship of a dinner in restaurant De Doelen in Muiden. We are also grateful to Optopia for providing a free (boat) ride to Muiden. Finally, thanks are also due to the John van Geuns Fund, the Materials Science Centre and the Faculty of Sciences of the University of Groningen for financial support.

The Organizing Committee

Chairman: Prof. dr. D.A. Wiersma (University of Groningen)

Prof. dr. M. Glasbeek	(University of Amsterdam)
Prof. dr. A. Lagendijk	(AMOLF and University of Amsterdam)
Prof. dr. T.J. Schaafsma	(University of Wageningen)
Prof. dr. S. Stolte	(Free University, Amsterdam)
Prof. dr. J.W. Verhoeven	(University of Amsterdam)
Prof. dr. H. Woerdman	(University of Leiden)

Opening address Royal Netherlands Academy Colloquium on Femtosecond Reaction Dynamics

On behalf of the organizing committee of the Royal Netherlands Academy Colloquium on *Femtosecond Reaction Dynamics* I would like to welcome you to The Trippenhuis here in Amsterdam and to this Meeting. Both the timing of this Meeting and its location seem just right. With respect to the timing: yesterday prof. Zewail was awarded the Wolf Prize in Chemistry for his outstanding work in the field of 'Femtochemistry.' Regarding the place: Amsterdam in many ways is a magical town; many were and are drawn to it because of its tolerance; others come here to admire the paintings of van Gogh, Rembrandt or enjoy listening to the world-famous Royal 'Concertgebouw' orchestra. Amsterdam has also a rich history in science; it was the home town of Johannes Diderik van der Waals who was the first physics professor at the University of Amsterdam. His forces hold many of the systems we study together. His successor was Pieter Zeeman. Who in this audience has not at one time or another used the Zeeman effect in her or his work? Jacobus van 't Hoff, the founding father of stereo chemistry has also been a professor at the University of Amsterdam. All these scientists received the Noble prize for their seminal contributions to science. This Conference site: the headquarters of the Royal Netherlands Academy of Arts and Sciences keeps their memories and those of other prominent Dutch scientists in many ways very much alive.

This Meeting is not an ordinary meeting: the fact that so many distinguished scientists are gathered here makes it very special; the small number of scientists (about 50) participating in this Colloquium sollicits for strong interactions among the participants and the Meeting's subject is at the front of research in the field of Optical Sciences. We therefore expect the Proceedings of this Colloquium to become an important milestone in the field of *Femtosecond Reaction Dynamics.*

This field is moving very fast indeed, not only by the increasing pace of technological innovations, but also by the fact that short optical pulses are finding constantly new applications in chemistry, physics, biology and even medicine. So one of the points to be addressed at this Symposium is: what is the future of femtoseconds pulses in our field and what are the challenges in this next decade?

Before calling on the first speaker I would like to announce a few changes in the Programme: the first is connected with the fact that professor Zewail could not make it on time because of the Wolf prize ceremony yesterday. Professor Shank has been so kind to agree to change places with professor Zewail. Professor Shank will therefore also be the Chairman of tomorrow mornings session. Professor Castner will present his lecture on Wednesday instead of Tuesday. This gives the speakers in the after-coffee session on Wednesday a little more time.

Then now the time has come to call on the first speaker of this morning: professor Shank, professor at the University of California at Berkeley and Director of Lawrence Berkely Laboratory. Despite his youthful appearance professor Shank is, to many of us, the founding father of femtoseconds. His work together with Ippen and the other members of the Shank group at Bell Laboratories have made a lasting contribution to the field of ultrafast lasers and ultrafast phenomena. I wish you a very good and pleasant Meeting.

Amsterdam, May 17, 1993

Douwe A. Wiersma
(Chairman of the Academy Colloquium)

Contents

Ahmed H. Zewail

Femtosecond Reaction Dynamics

Elementary Processes, from Isolated to Solvated Reactions

Abstract

The field of femtochemistry is reviewed with particular focus on femtosecond reaction dynamics, from isolated to solvated reactions. As an example, the nuclear motion of a two-atom system is examined in the gas phase/molecular beam, in the presence of one (or few) solvent atoms, and in solvent cages of clusters and at high-pressure phases. We conclude by discussing future directions relating to molecular control and to the development of ultrafast diffraction.

I. Introduction

This article is the outcome of an overview lecture presented at the Royal Netherlands Academy of Arts and Sciences as part of a conference organized by Professor Dr. Douwe A. Wiersma (May 17-19, 1993). The meeting, which was superbly organized, was crafted to focus on femtosecond reaction dynamics, covering studies from the isolated-system limit to the condensed phase. The following is the contribution of research from the California Institute of Technology. Personally, I am grateful for the warm and sincere reception by colleagues at the Conference on the occasion of the awarding of the 1993 Wolf Prize in Chemistry (for this field). I wish to thank Professor Wiersma for his generous and kind efforts, and Professor John van der Waals for his thoughtful introduction and presentation of the Royal Academy Medal.

The field of 'molecular reaction dynamics' (Levine, 1987) is concerned with the understanding of chemical reactivity of *isolated* (single, full- or half-collision) systems at the molecular level. In such systems, the motion of atoms during the breaking and making of bonds involves several dynamical phenomena. Fundamentally, there are three types of ultrafast dynamics common to all chemical reactions: (1) the process of intramolecular vibrational (and rotational) energy redistribution (IVR); (2) the reactants-to-products microcanonical reaction rates, state-resolved; and (3) the dynamics of the transition states and their structures. Over the past 15 years, much progress has been made in observing and studying these processes in real-time. For a recent review, the reader is referred to Khundkar, 1990 and Zewail (1993 & 1994).

Since atoms and molecules have typical velocities on the order of 1 km/s, the elementary dynamics of transition-state structures at a resolution of angstroms are on the femtosecond (fs) time scale. This classical estimate of the femtosecond time scale for nuclear motion is also evident from transition-state theory of reaction rates:

$$k_{reaction} = (kT/h)(Q^{\ddagger}/Q_r)\, e^{-E_a/kT}$$
$$\equiv (kT/h)\, K^{\ddagger}. \tag{1}$$

In the above expression, Q_r is the product of partition functions for the reactants, and $Q^{\ddagger}$ is that of the activated complex (less the one of the reaction coordinate). $K^{\ddagger}$ is the equilibrium constant between the reactants and the activated complexes. The upper limit of kT/h is about 10^{13} sec^{-1}; this is the 'rate' at which the nuclei are expected to change their position. Thus, with sufficient time resolution, the transition-state structures can be 'frozen out.' Quantum mechanically, this picture of localization is also valid, as with fs pulses the de Broglie wavelength of a chemical system is sub-angstrom, a key feature in the studies of the

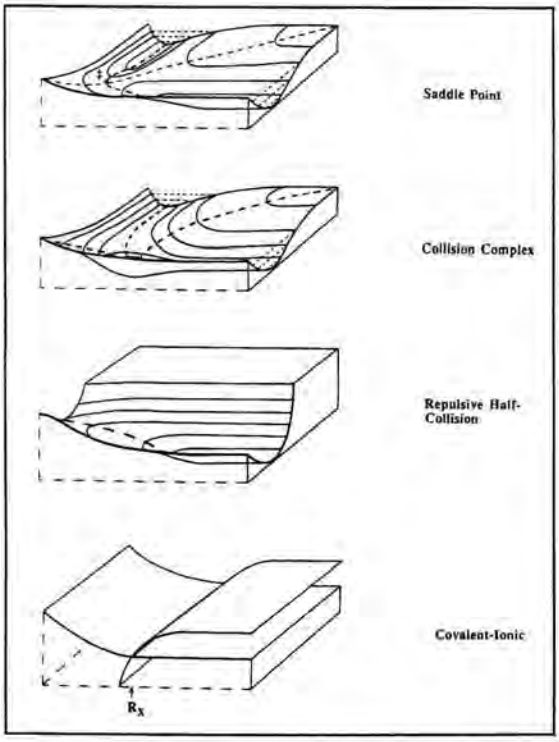

Fig. 1. Some generic potentials describing nuclear motions for different types of reactions. Drawn by Dr. M. Gruebele.

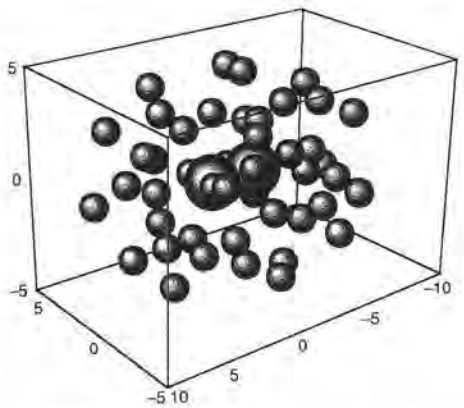

Fig. 2. Molecular dynamics simulations of the solvation structure in clusters; in this case, for iodine in argon. The atomic size is not to scale exactly (changed for better visualization).

evolution of chemical reactions in real-time. Femtochemistry (for reviews, see Zewail, 1988; 1991; 1993; 1994) is concerned with the very act of chemical transformation: the process of breaking one chemical bond and making another.

The scope of this research has spanned applications in the gas phase/ molecular beams, in clusters, on surfaces, and at the interface to the condensed

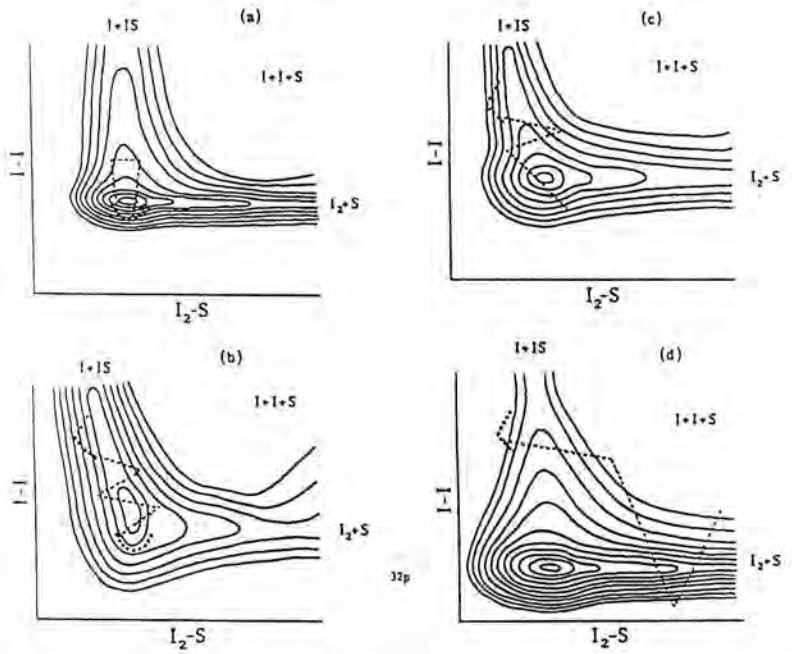

Fig. 3. Some global potentials describing the solvent-solute coordinate and the chemical I-I coordinate. [P.S. Dardi and J.S. Dahler, *J. Chem. Phys.* **98**, 363, (1993)].

phase. These applications were exemplified in the recent conference on femtochemistry in Berlin (Appendix I). The range of reactions studied includes two classes: (1) unimolecular (half-collision); and (2) bimolecular (full-collision) reactions. Fig. 1 gives some generic potentials describing the motions in these classes of reactions studied by Femtosecond Transition-state Spectroscopy (FTS). Specifically, they include: dissociation, isomerization, barrier crossing (saddle-point), intermediates of collision-complexes (potential well), electron

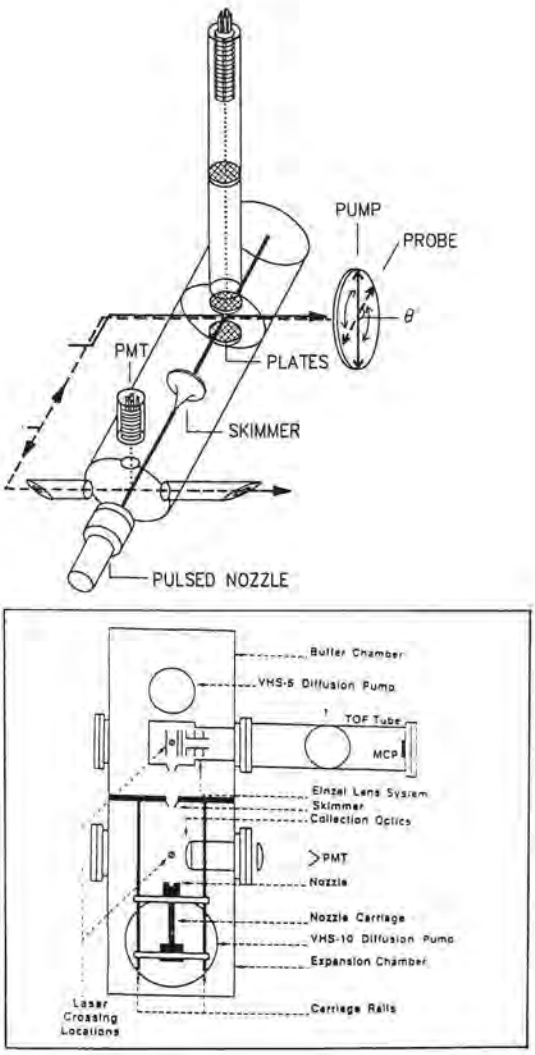

Fig. 4. (Top) Molecular beam apparatus with time-of-flight mass-spectrometer and with a laser-induced fluorescence arrangement. (Bottom) A schematic with details of another similar, but larger, beam apparatus.

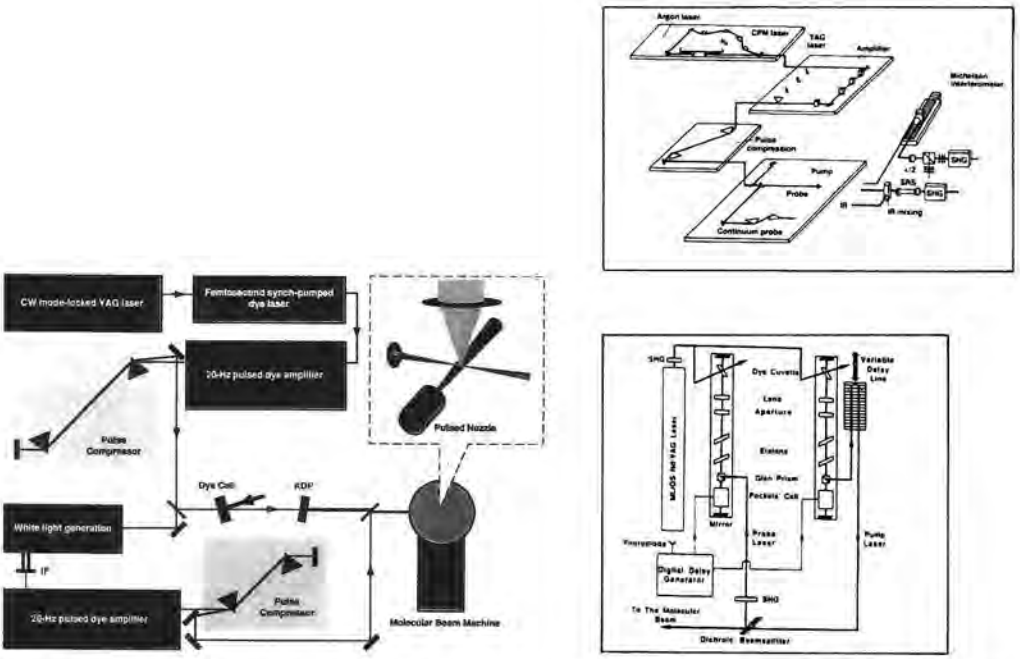

Fig. 5. Three laser systems used in these studies. (Top right) the CPM laser/amplifier system; (Bottom right) a mode-locked Q-switched Nd : YAG system with two dye lasers pumped in synchrony; (Left) A CW mode-locked YAG system with a synch-pumped dye laser, together with two amplifiers and pulse continuum generation and compression arrangements.

and proton transfers, etc. Elsewhere, these studies have been reviewed by Khundkar (1990), Porter (1992), Beddard (1993), Dantus (1991), and Zewail (1988, 1989, 1991, 1992, 1993, 1994).

Here, we wish to examine the simplest elementary reaction of two atoms in isolation and in a controlled solvent environment, developing both the concepts and the methodology. The system is that of molecular iodine and iodine with *one*, *few*, or *shells* of solvent (He, Ne, Ar, Xe) cages (Fig. 2). This systematic study allows us to examine the dynamics of elementary reactions on ultrashort time scales, 'before' and 'during' the solvent motion. Accordingly, in analogy with the description given in Fig. 1, we can now examine the trajectory of the motion, including the solvent-solute coordinate as part of the global potential (Fig. 3). The experimental approach utilizes the FTS methodology with molecular beams (or high pressure cells) (Fig. 4), along with the now standard methods of detection: laser-induced fluorescence (LIF) and mass-spectrometry. The three laser systems used are shown in Fig. 5.

II. The Potential of Free-Solute Motion

When iodine is excited with a femtosecond pulse, a wave packet is formed with the nuclei, at a given internuclear distance, localized to $\sim$0.1-0.2 Å. Fig. 6 shows

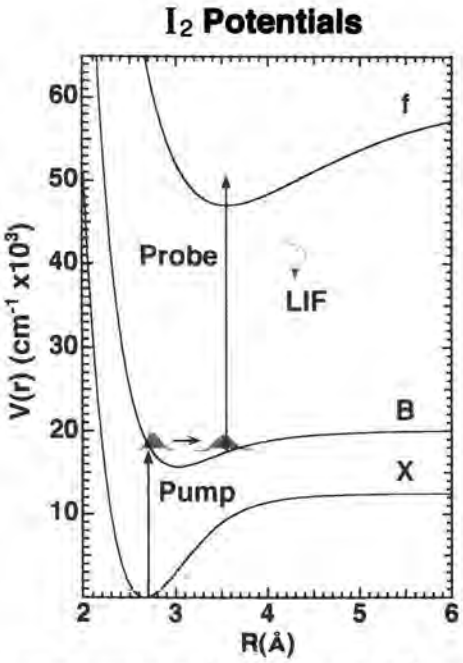

Fig. 6. The potentials for iodine, together with a typical scheme for wave packet preparation and probing [from Yan, 1992].

the wave packet preparation on the bound B-state and the probing by laser-induced fluorescence. We can also prepare wave packets above dissociation (to I + I* atoms) on the B-state potential, as well as on the A-state (not shown) to yield I + I ground-state atoms. Before considering the solvation of iodine, it is useful to show how we can deduce the potential from the femtosecond experiments (Gruebele, 1993).

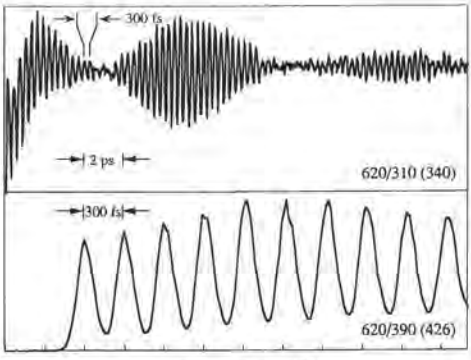

Fig. 7. The wave packet motion in iodine excited to the B-state at 620 nm, observed by LIF [R.M. Bowman, M. Dantus, and A.H. Zewail, *Chem. Phys. Lett.* **161**, 297 (1989); see also Gruebele, 1993].

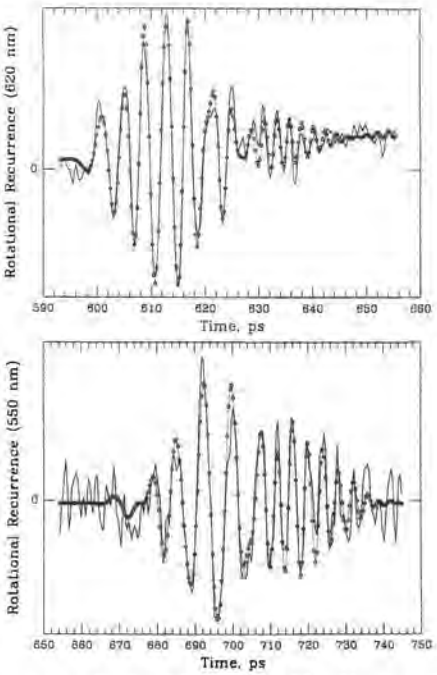

Fig. 8. The rotational recurrences observed for iodine [M. Dantus, R.M. Bowman, and A.H. Zewail, *Nature* **343**, 737 (1990); see also Gruebele, 1993].

The wave packet dynamics of *vibrational* and *rotational* motions show separate time scales corresponding to *scalar* and *vector* dependencies in the time evolution. In Figs. 7 and 8, the vibrational (femtosecond) and rotational (subnanosecond) transients are shown, and in Fig. 9 the influence of the initial temperature (beam versus cell) is displayed. From these results, one can invert the data, using, e.g., the RKR method, and obtain the potential. Experimentally, the initial position of the wave packet and the translation energy are varied by changing the total energy. In Fig. 10, three examples of wave packets, bound, dissociative, or quasi-bound, are shown and will be part of the studies of solvation discussed below. This coherent motion of a wave packet in reactive and nonreactive systems (Zewail, 1993) has become general to many systems. In solutions and clusters, such transients provide the nature of the dynamics, particularly at the early times, significant to the elementary processes.[1,2]

[1] In solutions, see the work of S. Ruhman (I_3^-), G. Fleming and N. Scherer (I_2), R. Hochstrasser (HgI_2), P. Barbara (I_2^-) in this proceeding.
[2] In clusters, see the work of C. Lineberger [$I_2^-/(CO_2)_n$], A.W. Castleman, Jr. $(NH_3)_n$, L. Wöste (Na_3), and our group (I_2/Ar_n): Papanikolas, 1992; Wei, 1992; Schreiber, 1992; and Potter, 1992; Liu, 1993. For the work of G. Gerber (Na_2, Na_3), see this proceeding and Baumert, 1992.

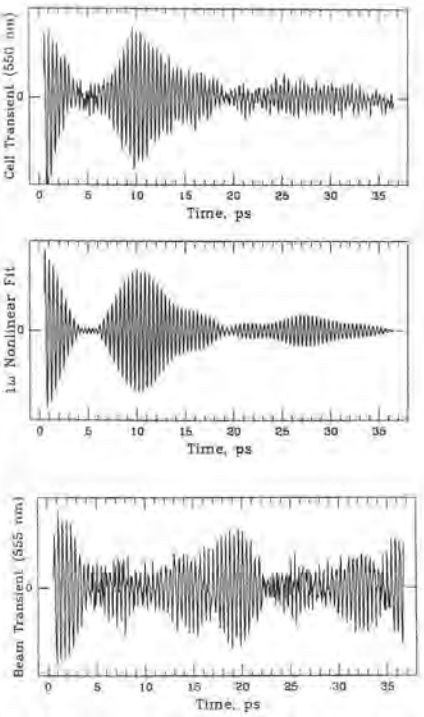

Fig. 9. Wave packet dynamics of iodine observed in a molecular beam and in a cell. The middle transient is a theoretical simulation of the top transient [Gruebele, 1993].

III. The One (and Few) Solvent-Atom Case

The simplest case for solvation is that of a one-rare gas atom attached to iodine by van der Waals forces. This complex can be made in a molecular beam and its identification and structure can be obtained from the spectroscopy. The structure of, e.g., the iodine/neon system is sketched in Fig. 11. Here, we employ an ultrafast pulse to excite the I_2 vibration (quantum number v_i') in the $I_2 \cdot Ne_n$ complex and subsequently detect the nascent I_2 in $v_{f'}$ (Fig. 12). The state-to-state dynamics can then be probed directly (Fig. 13), and the v_i' dependence of the microcanonical rates can be determined (Fig. 14). These rates allow us to describe the dynamics along the second potential coordinate, namely the intermolecular solute-solvent motion.

Designating the iodine nuclear motion by the coordinate r and the iodine-rare gas by R (Fig. 12), then the Hamiltonian can be written as follows:

$$U(r, R) = U(r_0, R) + V(r, R), \tag{2}$$

where r_0 designates the equilibrium value. The rate for the rare gas atom

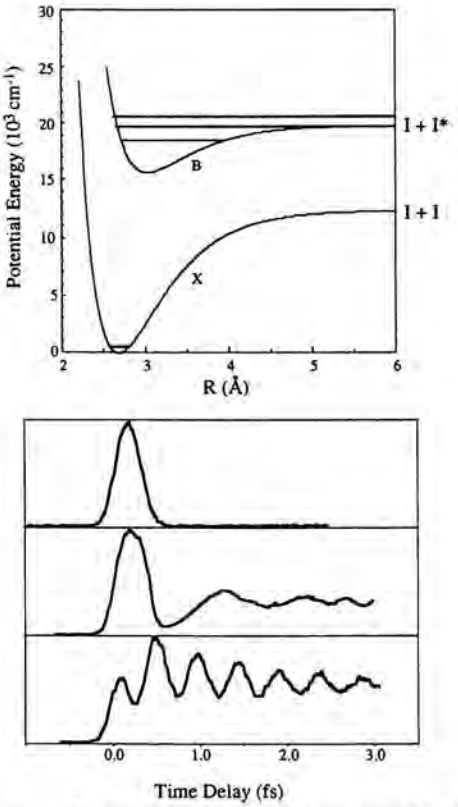

Fig. 10. Wave packet dynamics (bottom) of iodine at three energies (top); below, at, and above dissociation to I + I*.

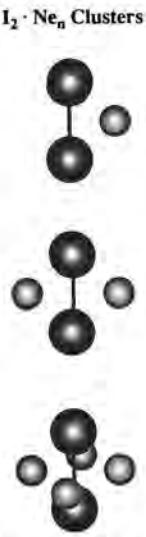

Fig. 11. View of the structures of $I_2 \cdot Ne_n$ with $n = 1, 2, 4$.

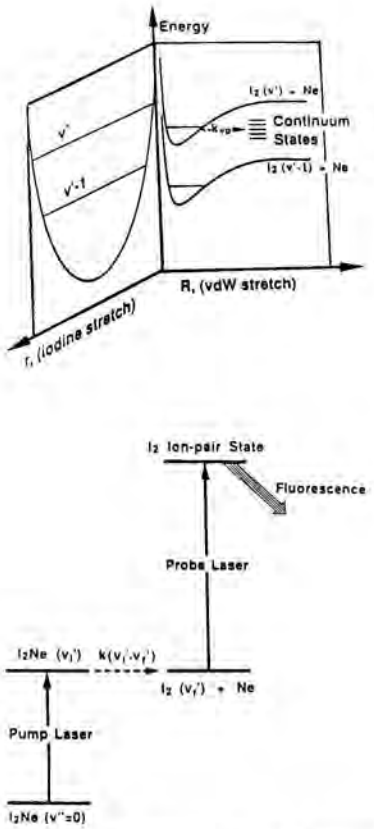

Fig. 12. (Top) The potential of I_2Ne along the intra- and intermolecular coordinates. (Bottom) The pump (reactant)-probe (product) scheme used for probing the state-to-state rates [Gutmann, 1992; Gutmann, 1992].

'evaporation' (predissociation) can be written in a simple form using a Fermi-Golden rule expression:

$$\tau^{-1} \equiv k(v_i', v_f') = \pi |\langle v_i' l' | V | v_f' \varepsilon' \rangle|^2$$
$$\equiv \pi |\langle v_i' | (r - r_0) | v_f' \rangle|^2 \, |\langle l' | (\partial U / \partial Q)_0 | \varepsilon' \rangle|^2. \quad (3)$$

Beswick and Jortner (Beswick, 1981) have shown that the first matrix element describes the v_i' dependence of the intramolecular part, and the second matrix element describes the intermolecular effect (l' is the quantum number of the vdW coordinate and ε' describes the translational continuum). A model potential and geometry can now be invoked to obtain the rates. Instead, we shall use a recent simplified model which makes it straightforward to deduce characteristic of the intermolecular potential at short distances. In this Landau-Teller-Nikitin theory, the half-collision predissociation problem is transferred to the reverse rare gas atom plus iodine full collision (Willberg, 1993). Accordingly, the rates are given

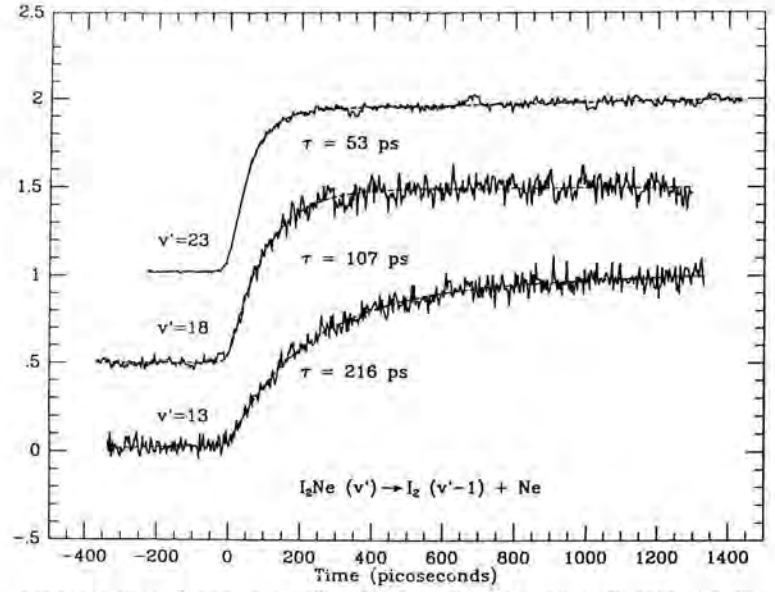

Fig. 13. Typical transients for $I_2 \cdot Ne$, following the scheme outlined in Fig. (12) [Gutmann, 1992; Gutmann, 1992].

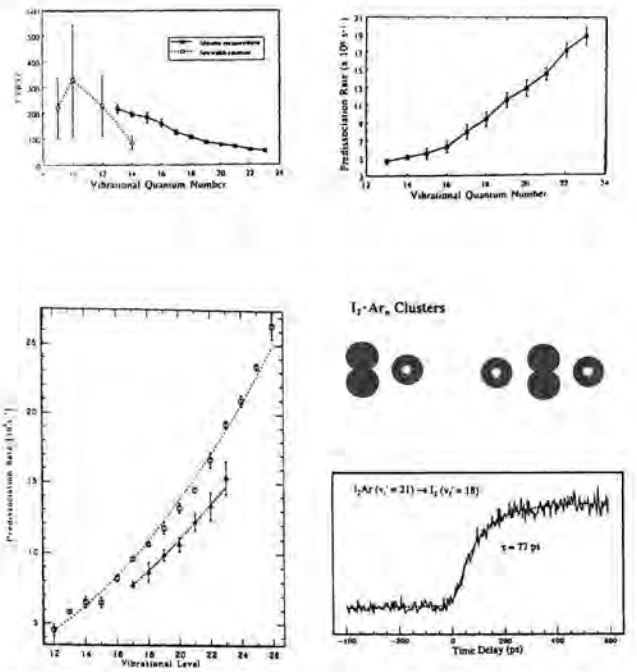

Fig. 14. The dependence of the resonance lifetime and state-to-state rates on the initial vibrational quantum number v_i'. (Top) for I_2Ne; (Bottom) left is for I_2He (Solid curve; real-time data and dashed curve is linewith data), and (Bottom) right is for $I_2 \cdot Ar$ [Gutmann, 1992; Gutmann, 1992].

by the dependence of the translational (inter) to vibrational (intra) coupling on (i) the amplitude of the vibrational motion of the iodine and (ii) the Franck-Condon factor between translational functions of a free-free transition. It is straightforward to show that (Willberg, 1993):

$$k = cv_i' e^{\gamma v_i'}, \tag{4}$$

with a highly nonlinear v_i' dependence (Fig. 14). Now γ defines the nature of the repulsive potential (exponential) and is directly related to α, the length parameter of the potential. Such treatment for iodine solvated with He, Ne, or Ar, together with real-time studies of the rates, can be found in Gutmann, 1992. The potential parameter α is typically 1.2 $Å^{-1}$ indicating a length approach of ~ 0.8 Å.

For larger number of rare gas atoms, the rates change dramatically as shown

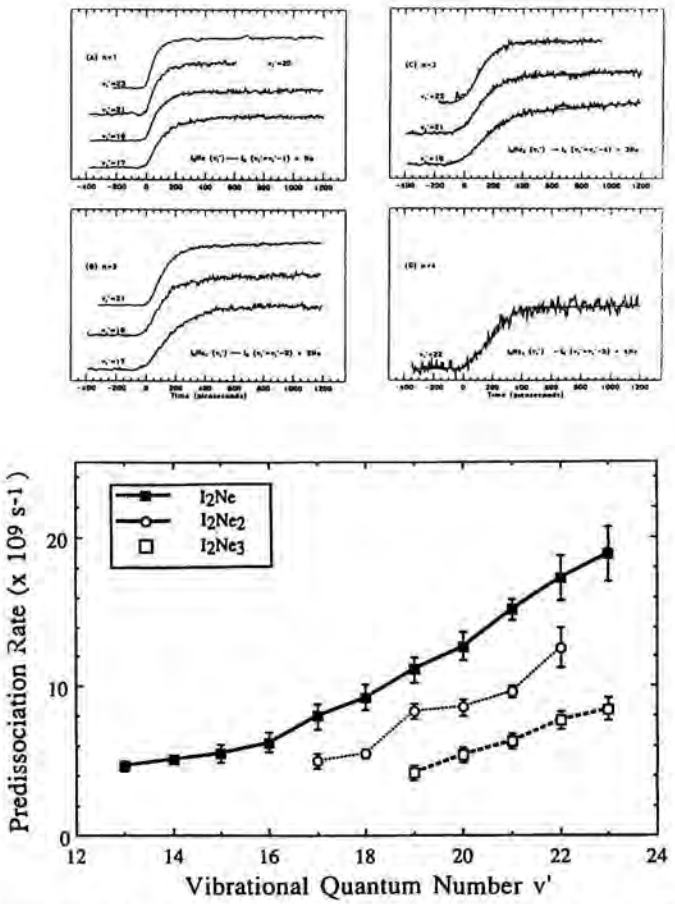

Fig. 15. The dependence of the rates on the cluster size (Ne; $n = 1, 2, 3, 4$), and on the initial vibrational quantum number [Gutmann, 1992; Gutmann, 1992].

in Fig. 15. It is useful to note that as the number of solvent atoms increases, the rates decrease. Furthermore, the 'onset' for vibrational relaxation (i.e., condensed phase effect) begins with two solvent atoms on this *picosecond* time scale (Gutmann, 1992).

Changing the rare gas atom to argon results in a new channel. In addition to evaporation, the argon causes the breakage of the chemical I-I bond. The solvent, in this case, mixes the bound state with a repulsive potential ('electronic predissociation'), producing $I + I + Ar$, in addition to the $I_2 + Ar$. We shall return to these two processes of evaporation and bond breakage when we consider the solvation effects in larger I_2/Ar_n clusters.

IV. Solvation in Large Cluster Cages

Solvation dynamics of chemical reactions in cluster cages offer a unique opportunity to examine the effect of a solvent on the elementary processes of bond breaking or bond making. The solvent may, for example, facilitate the remaking of a bond, in what has been termed the 'cage effect' (Frank, 1934), or it may behave as a 'chaperone' (Porter, 1992) with new reaction intermediates formed. With the ability to resolve the elementary femtosecond (fs) nuclear motions of reactions, it is of great interest to probe such motions in the presence of solvent shells that reach a unique quasi-condensed phase (Saenger, 1981; Jortner, 1990; Berry, 1990).

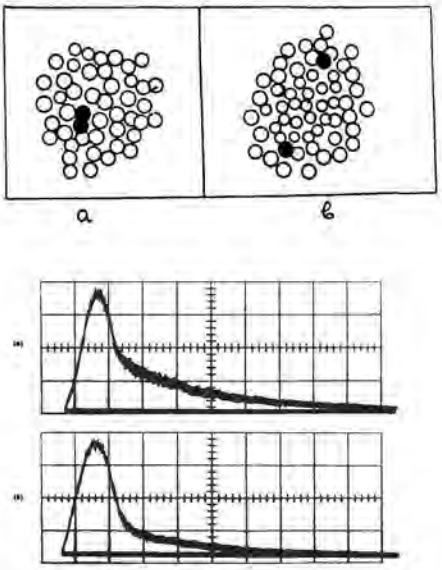

Fig. 16. Two historical figures related to iodine dissociation studies over the past 60 years. (Top) The caging idea in liquids [Frank, 1934], and (bottom) the oscilloscope traces of light output from flash lamps used in the initial flash photolysis of iodine [Porter, 1992].

In this section, we discuss studies of the real-time fs dynamics of neutral iodine dissociation and caging in clusters of argon atoms (typically 40 to 150). On this time scale, we observe the 'solvent-frozen' coherent motion of the iodine nuclei at times less that 1 ps, and the subsequent caging after the two iodine atoms are chaperoned by the argon atoms for less than 300 fs. The fs experiments give a unified picture of the mechanism which crucially depends on (i) the time scale for bond breakage and (ii) the effective temperature of the solvent. Molecular dynamics simulations are also discussed to help visualize details of the motion of the iodine solute in the argon solvent.

Direct real-time studies of clusters on the picosecond (Papanikolas, 1991; Felker, 1983; Breen, 1990; Syage, 1991; Gutmann, 1992) and femtosecond (Baumert, 1992; Potter, 1992; Papanikolas, 1992; Wei, 1992; Schreiber, 1992) timescales and molecular dynamics simulations (Amar, 1984; Alimi, 1992; Stace, 1981) have revealed the dependence of the dynamics on the solvent and on the number of solvent atoms or molecules. From the large solvent complexes to the one-atom cages formed in molecular beams, these iodine systems provide a new way for examining solvation, and help the understanding of the asymptotic bulk properties in liquids, solids, or in compressed gases/liquids. On the ps-fs time

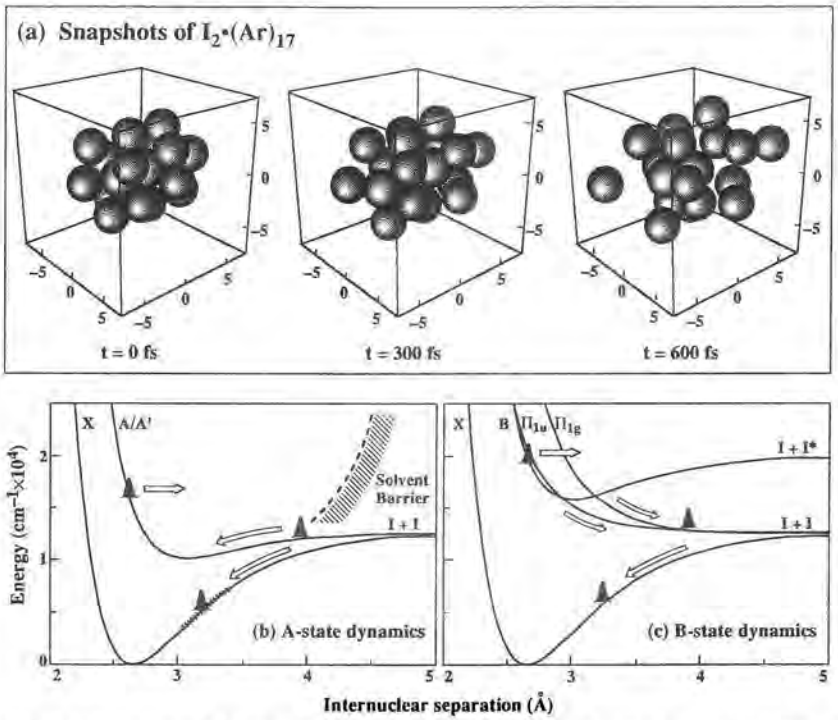

Fig. 17. (Top) Snapshots of the dynamics of iodine dissociation in argon at three times. (Bottom) The potentials describing the wave packet motion in the gas phase and in the solvent cage (schematic barrier); see Liu, 1993.

scale, the recent work in solutions (Harris, 1988; Scherer, 1992) is of great interest for comparison. Fig. 16 shows, in two cases, the earlier historical role of iodine reactions over the past 60 years.

In our experiments, the clusters of neutral iodine molecules in argon were made in a molecular beam and the femtosecond dynamics were probed following the methodology developed earlier (Khundkar, 1990; Zewail, 1988, 1993) (see Figs. 4, 5). The dissociation reaction was initiated by a femtosecond laser pulse which prepares a wave packet either on the A state above its dissociation limit (to I + I), or on the B state at different energies below or above dissociation (to I + I*). The snapshots in Fig. 17 show the deduced structures in the cluster (see below), and the relevant ground and excited state potentials (X, A/A′, B, and Π) governing the nuclear motions. A second fs pulse is used to probe (Gruebele,

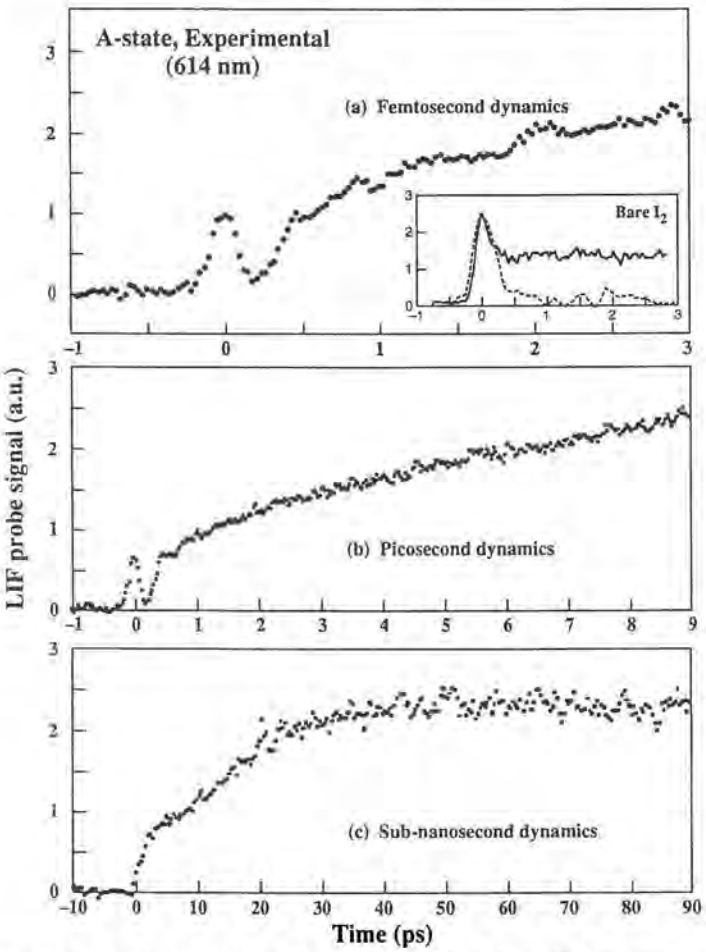

Fig. 18. Femtosecond to sub-nanosecond dynamics of iodine dissociation in argon solvent cages. The excitation is at 614 nm, and the probing is by LIF [Liu, 1993]; see text.

1993) the motion of the wave packet by detecting (Potter, 1992) the laser-induced fluorescence of I_2 in the Ar clusters at its characteristic emission (Fei, 1992). From electron diffraction, the average size of the clusters formed is estimated to range from 40 to 150 argon atoms, with an average temperature of 30 K or less. To compare the dynamics in the clusters to those of bare iodine (Gruebele, 1993), argon gas was replaced by helium which is known to form no such clusters under these expansion conditions.

Fig. 18 shows typical experimental transients obtained when iodine molecules were initially excited at 614 nm. In Fig. 18a, the first peak rise characterizes the preparation of the wave packet. The following decay reflects the fact that the wave packet is moving into a region where iodine can no longer absorb the probe pulse. In about 200 fs, the signal drops to almost zero. A fast and prompt recovery was then observed in another ~ 300 fs, which indicates that the wave packet coherently moves back to optical regions of the probe. At longer times, the signal starts to increase almost 'linearly' and much more slowly, as shown in Fig. 18b. A steady-state value is reached about 30 ps later. For the pump wavelengths ranging from 590 to 700 nm, the transients exhibit similar behaviors. The inset in Fig. 18a shows the corresponding transients obtained for the iodine-helium expansion ($\lambda_{pump} = 614$ and 640 nm), and should be compared with the behavior shown in Figs. 7 and 10.

When the pump wavelength was shorter than 590 nm (below the dissociation to $I + I^*$), the initial fs dynamics discussed above are replaced by a picosecond decay (~ 15 ps). The signal also rises again in ~ 30 ps, as shown in Fig. 19 for $\lambda_{pump} = 510$ nm. In the inset of Fig. 19 (top), a transient obtained by the same pump and probe (310 nm) is shown for the helium expansion. This transient shows the ~ 600 fs modulation which reflects the vibrational period of bare iodine molecules on the B state at this energy (Gruebele, 1993); see Figs. 7, 10. Above the B-state dissociation into $I + I^*$, we also observe the caging [Fig. 19 (bottom)], but the dynamics, as discussed below, are different.

The above results demonstrate that bare iodine (in helium expansions) behaves as expected when free of the solvent influence (Gruebele, 1993), as discussed above. In argon clusters, the motion of the wave packet is dramatically different and clearly reflects the initial coherence and the caging dynamics. To help understand details of the motion in the solvent cages, we have performed molecular-dynamics (MD) simulations. The clusters were assumed to have 17 or 44 argon atoms which form one or two argon shells about the iodine molecule (Potter, 1992). Iodine with one argon atom was also considered. A simulated transient was obtained by accumulating the time when the trajectories of the iodine molecules were within the probe windows. Fig. 20 shows the MD transients of the A-state dynamics, and those of the B-state, together with the intrinsic change in the I-I distance with time. The MD simulations reproduce essentially all major features of the experimental fs and ps transients. They also show how the bond energy, distance, and cluster temperature change with time.

The microscopic picture of the motion in the solvent cage now develops. Fundamentally, we observe the different types of motion which lead to what we

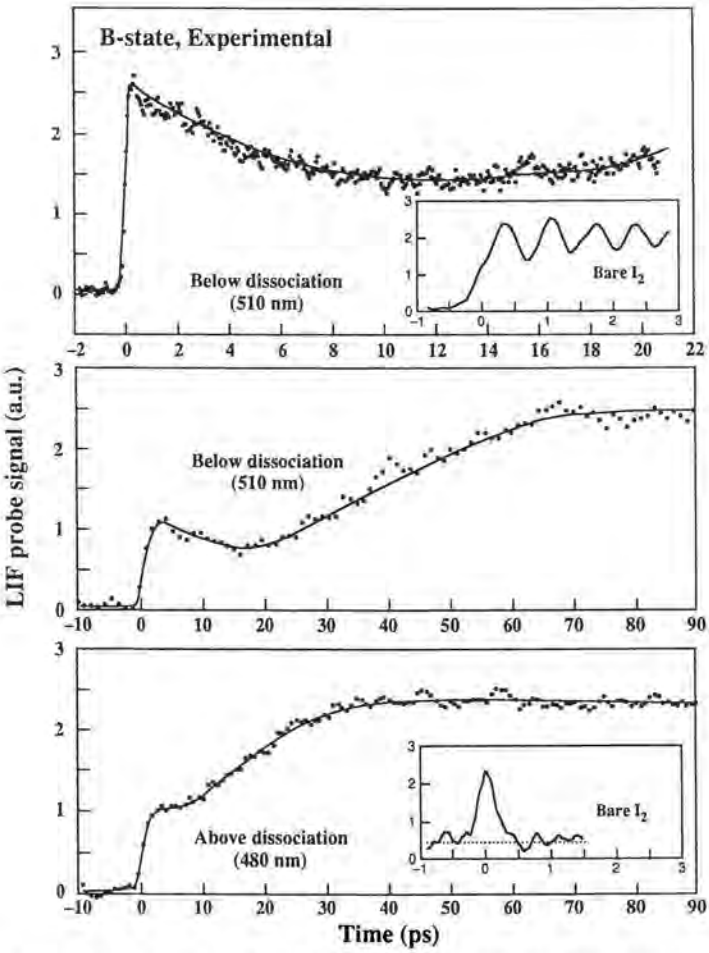

Fig. 19. The same condition as in Fig. (18), but with the initial excitation either at 510 nm (below dissociation) or at 480 nm (above dissociation). Note the contrast with the results in Fig. (18); see text.

term '*coherent*' and '*diffusive*' caging. When iodine is excited above dissociation into I + I (A-state), the wave packet moves to the region of the solvent barrier made of the repulsion with argon atoms. It then bounces back and reaches the probe window coherently and the first prompt recovery of the signal is observed (Fig. 18). On this ~ 500 fs time scale, the solvent is still 'frozen' and from the observed time delay, we estimate a solvent barrier at ~ 4.4 Å. Transferring energy to argon through periodic collisions, the iodine recombines and relaxes on the X and/or A/A′ states. If this energy release is 'non-statistical,' one expects a step-wise build-up of the signal because of the step-wise motion into more favorable regions of the probe as the I-I distance decreases towards the equi-

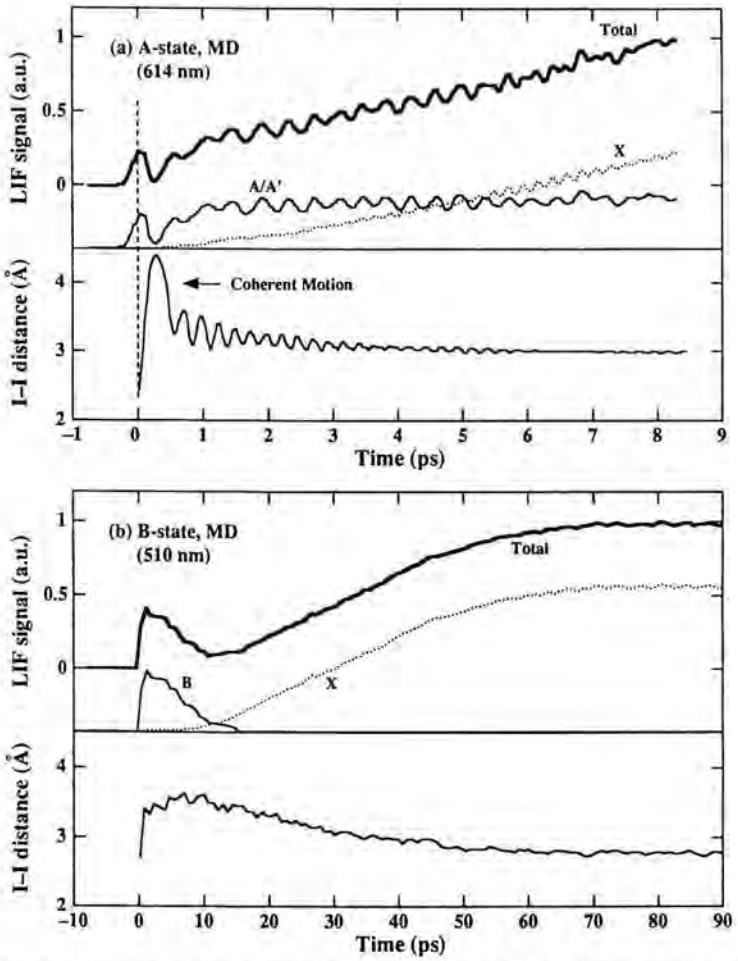

Fig. 20. Molecular dynamics (MD) simulations of A-state and the B-state type behavior. Both the LIF signal and the change in the I-I distance are displayed. (Not shown are the changes in energy, temperature and cluster size with time [Potter, 1992, and work to be published]; Liu, 1993, see text.

librium value. The slope of this linear rise depends on the cluster size, but the shape is indicative of caging.

The time scale of bond breakage is fundamental to the subsequent caging dynamics. For the A-state type dissociation (or for the repulsive states), it is typically 200-400 fs, consistent with the time scale for coherent caging. It also indicates that argon chaperone of iodine is no longer than 300 fs. Bond breakage on the quasi-bound B-state takes a much longer time. Iodine with one argon predissociates in about 70 ps (depending on the energy, see Section III) (Gutmann, 1992); and in our clusters, we observe an initial decay of ~ 15 ps instead of the coherent decay of ~ 200 fs on the A-state. The long ps B-state dynamics

allow for efficient energy transfer and for the cluster to soften its structure and the solvent barrier to decrease in energy. As supported by MD simulations, once dissociated, the two iodine atoms can be found at long internuclear distances, allowing solvent atoms to intervene between them.

The consequence of this 'diffusive' solvent motion is a longer caging time and equilibration (exponential rise; see Figs. 19, 20) in the recombination. The caging time in this case ranges from 5-10 ps (delay time for the rise); this too is evident in the theoretical simulations and in the experimental transients here and also in (Potter, 1992). The phenomenon of diffusive caging brings an analogy to liquids, where the motion of the solvent and the finite temperature could mask the coherent caging observed here. In a matrix at low-temperatures, the rigidity should allow for the observation of the direct motion (Alimi, 1992), provided the matrix phonons are not a problem for energy relaxation and dephasing of the initial packet. Work on caging of I_2 in argon matrices would be of interest, and this system is currently under study in the groups of A. Apkarian and D. Imre.

Above the B-state dissociation limit, we observe the A-state type caging, in addition to quasi-bound B-state contribution. On the B-state, above its dissociation, caging is achieved by energy transfer to argon and trapping in the bound potential, with the packet oscillation back and forth.

Future extension of this work (Liu) in this laboratory will be aimed at experimental and theoretical studies of the dynamics in the cluster phase (different compositions), as shown here, or at high pressures as reported before[3] and discussed below. Since our focus is on neutral systems, we will not be able to reach the mass-resolution of the original studies of $I_2^-(CO_2)_n$ (Papanikolas, 1992). However, our interest is in large solvation shells and the scaling laws of cluster size are quite adequate. With the help of MD in clusters and at high pressures, these studies promise a new direction for fs dynamics of solvation.

V. At the Interface to Liquids

The same systems have been studied at high pressures in order to change the 'degree of order' of the solvent around the solute. Unlike cluster cages, at high pressures there is no stacking geometry. Instead, the radial distribution function reflects the structure of the solvent shells. For iodine in argon, say at 100 atmospheres, the density of argon is about 3 atoms per nm^3, and the radial distribution function is typically that shown in Fig. 21.

The solvation effect is manifested in a number of ways depending on the total energy below dissociation in the B state, and above dissociation to $I + I^*$. In Fig. 21, the influence of this density change on the dephasing and rephasing of the isolated wave packet [Fig. 7] is shown. At three energies (see Fig. 10), the

[3] See Zewail, 1992 for work up to 100 atmospheres. For studies at higher pressures, up to 2000 atmospheres, see Lienau (1993).

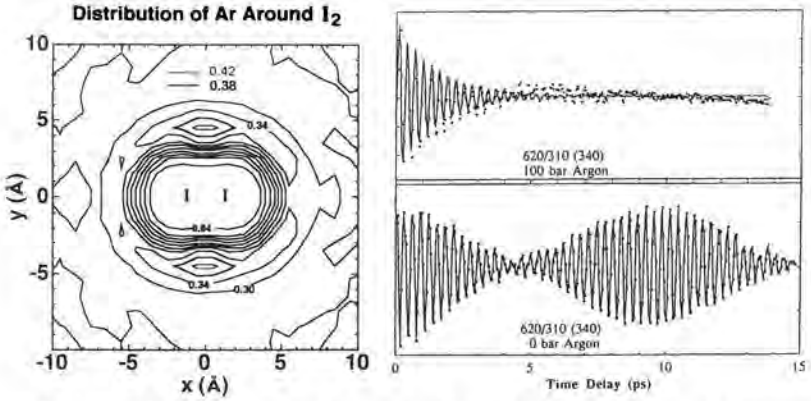

Fig. 21. (Left) The distribution of argon around iodine at 100 atmospheres of pressure. (Right) The effect of the pressure on the wave packet motion [Zewail, 1992; Yan, 1992].

behavior at 100 atmospheres is contrasted with that of 'zero pressure' (Fig. 22). Significant changes are observed. For bare iodine, we observe energy-dependent dynamics. Above dissociation, the wave packet of iodine freely moves to longer internuclear separations without return. Near dissociation, the packet returns with almost 50% probability, displaying a 'chirped-packet' behavior. Below dissociation, the wave packet returns back and oscillates between the turning points, just as described before in Fig. 10.

At high pressures, the changes are significant in showing the effect of the solu-

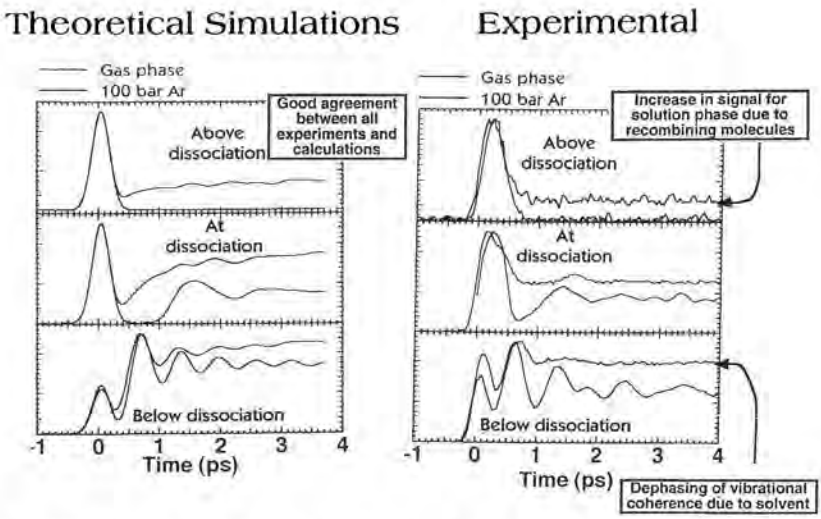

Fig. 22. Experimental and molecular dynamics studies of the wave packet motion in the gas phase and at 100 atmospheres of pressure for three energies; above, at, and below dissociation. The gas phase data are 'below' those of the high-pressure data [Zewail, 1992; Yan, 1992].

tion phase on the caging and relaxation. Unlike the cluster case, the caging observed when the I-I bond is broken above the dissociation limit shows no clear evidence of the coherent motion discussed above. This indicates the phase averaging imposed by the dynamic solvent effect at high pressures. At dissociation, there is change in the asymptotic level and one also observes changes in the nature of the oscillating motion at $t = 0$ and longer times. Below dissociation, we observe the dephasing of vibrational coherence due to the solvent (see Fig. 22).

The Wilson's group (Yan, 1992) has shown (Fig. 22) that the dynamics at high pressures can be simulated from 'ab initio' dynamical calculations. (See also Section IV.) At the three energies studied, the simulations reproduce the major features of the experiments and quantify the contributions of caging, vibrational relaxation, and dephasing on the time scale of their occurrence.

Much more work will be forthcoming in this area as we hope to examine the role of solvation at more than 100 atmospheres of pressure to compare and contrast with the cluster cage work, described above, and also with the liquid and matrix work. The apparatus for these very high pressures is now completed at Caltech and data for I_2 in argon at $\sim 2{,}000$ atmospheres have already been obtained (Lienau, 1993).

VI. Reactions and Their Control

This section describes the extension of the above studies to the xenon system, and, additionally, the use of this system to demonstrate the control of chemical reaction yield on the femtosecond time scale.

Before discussing this reaction yield control, it is useful to show the control of wave packet population with femtosecond pulses. Stimulated by earlier work on multiple and phase-coherent (ns) pulse techniques (Warren, 1983; Orlowski, 1978), we have used two fs pump pulses (instead of one) to prepare two wave packets either fully *in-phase* or *out-of-phase*. A third pulse is used to probe the motions of the two packets. This pulse sequence defines a phase angle (between the first two pulses) for a 2-D wave packet transients with $\theta = \omega_1 \tau_1$, where ω_1 is a frequency that can be made to match any of the packet frequencies (i.e., periods of motions) and τ_1 is the delay time. For a period of say 300 fs, if we use τ_1 of 150 fs, then $\theta = \pi$. Accordingly, the phase should be 180° shifted (see Fig. 23). Prepared in such a way, the two packets will then be out-of-phase and no oscillations should be observed. On the other hand, if $\theta = 4\pi$, then we should be able to double the population *in-phase*. This is reminiscent of the first observation of *in-phase* and *out-of-phase* coherence in studies of IVR by Felker et al. (Felker, 1983; Felker, 1988), but now provides an opportunity for packet population control with the phase of the motion well defined.

The experimental results (Gerdy, 1990) relating to these concepts are shown in Fig. 23, also for iodine. The results indicate that one is able to prepare two wave packets in-phase or out-of-phase with minimum spreading and a high degree of localization. We therefore should be able to use this approach to con-

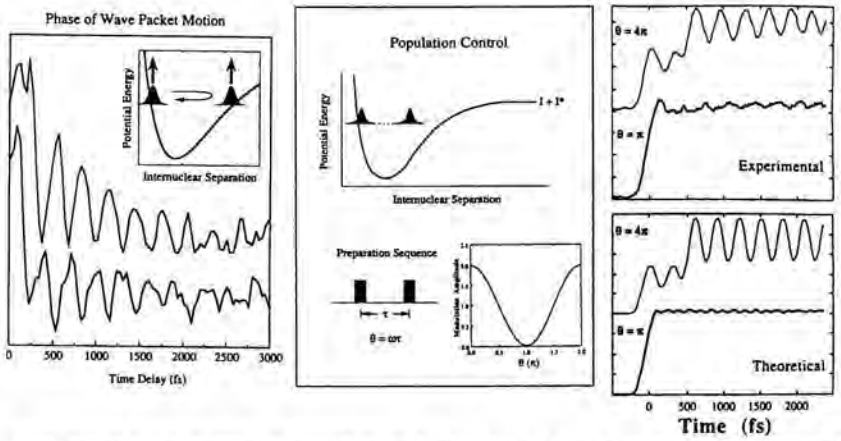

Fig. 23. Control of wave packet population in iodine using a pair of pulses for preparation and a third one for probing. (Left) The in-phase and out-of-phase motions as probed at the two turning points. (Middle) Scheme for packet transfer and phase angle (θ) control. (Right) Experimental and theoretical results [Gerdy, 1990]; see text and also [R.M. Bowman, M. Dantus, and A.H. Zewail, *Chem. Phys. Lett.* **174**, 546 (1990)].

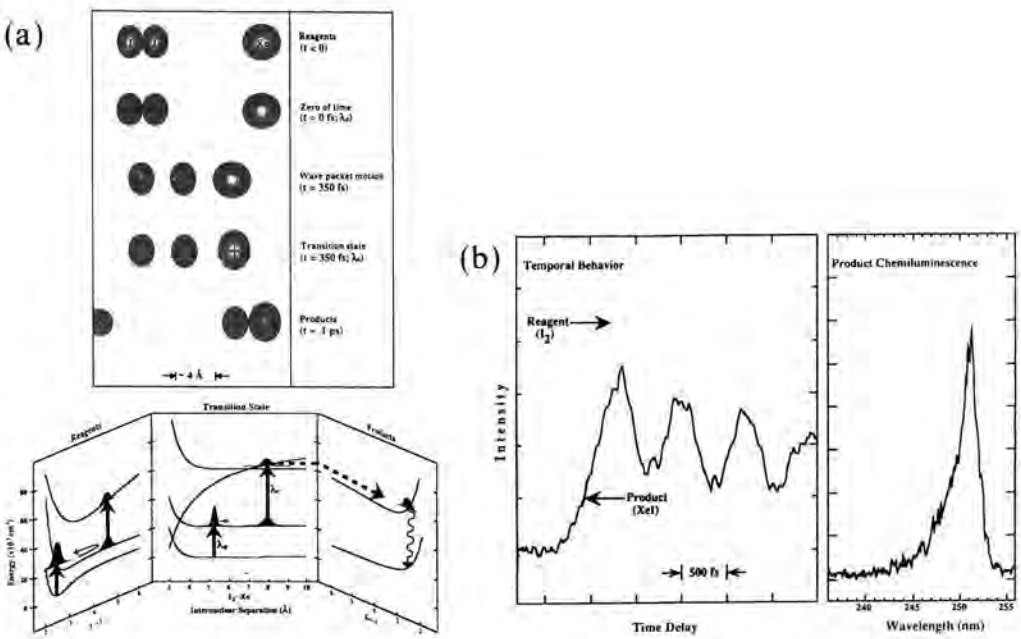

Fig. 24. Control of reaction yield with fs pulses. (a) Schematic of the motion and the potentials involved. (b) Experimental results for $I_2 + Xe$ reaction. The product yield is monitored through its chemiluminescence, which follows the 'harpoon' process. Note that the modulation of the yield of XeI follows that of the nuclear motion (Reference: E.D. Potter, J.L. Herek, S. Pedersen, Q. Liu, and A.H. Zewail, *Nature* **355**, 66 (1992)]; see text.

trol the reactivity of a chemical reaction since both the *timing* and the *phase* of the motion can be established. Recent theoretical studies by Tannor (Somloi, 1993) have explored control pathways in I_2 and further experiments should utilize this experimental approach. We have not specified the phase of the pulses as done in the earlier ns work (Warren, 1983; Orlowski, 1978), also on I_2, but the recent fs work (Scherer and Fleming) has obtained the wave packet dynamics with specified pulse phases, giving an additional feature to the control experiments on the fs time scale.

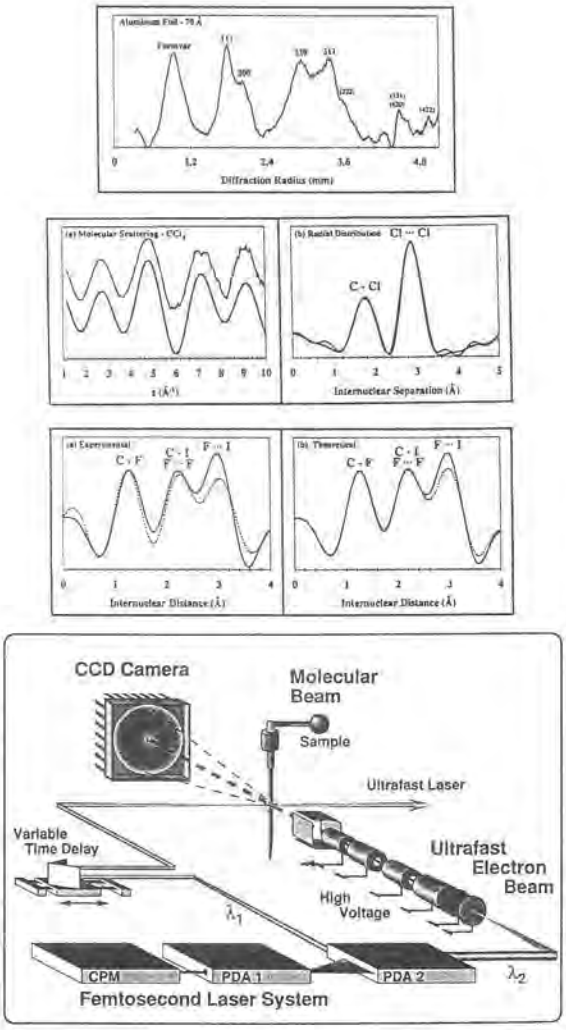

Fig. 25. Ultrafast electron diffraction. (Top) Experimental results taken for different systems (aluminum foil - 70 Å, CCl_4, CF_3I) and (bottom) the apparatus which includes a fs laser system, a CCD camera, electron optics, and the molecular beam [Williamson, 1991; 1992; 1993; 1994].

Iodine reacts with xenon to form xenon iodide with the following elementary steps:

$$Xe + I - I^* \rightarrow [Xe^+ \cdots I^- \cdots I]^{*\ddagger} \rightarrow XeI^* + I. \qquad (5)$$

This reaction is a type of 'harpoon reaction' and proceeds by electron transfer in the transition-state region, Fig. 24. When iodine is excited into the B-state, the wave packet moves toward the outer turning point with the change in phase shown above. If a second (control) pulse is used, this packet can be promoted (at the critical time and with the relevant phase) to the harpoon region of the potential, thus inducing product formation. Conceptually, the idea is to exploit the timing of the motion of the packet by the two pulses and to monitor the yield of the product XeI (through its chemiluminescence). If the packet arrives at 'the right time at the right place' for the controlling pulse to promote, we should then see a yield, but if the packet is not at this particular configuration, then no yield will be observed.

Fig. 24 shows this control of the yield for the $Xe + I_2$ system with the 'period of yield modulation' following the period of the nuclear motion in the reactant I_2. (The modulation depth is $\sim 100\%$, here limited by the width of our uv pulses). It is remarkable that this effect, which we termed the 'switch effect,' clocks the bimolecular encounter and controls the outcome of the product. Naturally, we are extending these first studies to a number of systems. Studies are also planned in large and small solvent clusters in the beam to explore their relevance to the solvation of iodine (in the series He, Ne, Ar, Kr, and Xe) and for the precursor-geometry effect on bimolecular reactions (Scherer, 1990; Ionov, 1992). The mechanism of the control of the wave packet as related to the switch effect in the reactants or in the transition-state is of considerable interest to us. Theoretically, this control of the wave packet on the fs time scale has been advanced for different schemes (Tannor, 1988; Manz, 1992; Wilson, Warren, this proceeding), and more experiments will surely be forthcoming; perhaps the chemists' dream of ultimate control will be fulfilled using ultrashort laser pulses (Zewail, 1980; Bloembergen, 1984).

VII. Concluding Remarks

Studies of molecular reaction dynamics on their fundamental time scale - femtoseconds - have opened up new and exciting opportunities for understanding chemical reactions as they actually happen. Studies in femtochemistry include reactions in the gas phase/molecular beams, in clusters, on surfaces, and at the interface to the condensed phase (see Appendix I). Larger and more complex sytems have also been studied [see Zewail, 1993, 1994, and references therein]. In addition to the FTS methodology, which is the standard technique for such studies, we are also advancing the recently developed ultrafast electron diffrac-

tion method (Williamson, 1991; 1992; 1993; 1994; Dantus, 1994) (see Fig. 25) for studies of complex structures in real-time.

This article focused on the application to one elementary reaction in the isolated (gas phase/molecular beam) phase, in solvent cages, and in solutions. Some recent developments, including extensions to the control of the reaction population and yield, are also discussed.

The important contributions in this volume is a testimony to the versatility and to the diversity in the field. Studies of reactions and molecular dynamics with fs resolution are now finding significant and bread applications in Chemistry and Biology. We have reached the ultimate time scale for the nuclear motions to observe and study the elementary transition states, and to localize the motion (wave packet). The field is continuing to expand with a large community for research in both experiment and theory.

References

Alimi, R., Gerber, R.B., McCaffray, J.G., Hunz, H., Schwentner, N., *Phys. Rev. Lett.* **69**, 856, 1992.

Amar, F.G., Berne, B.J., *J. Phys. Chem.* **88**, 6720, 1984.

Baumert, T., Engle, V., Meier, C., Gerber, G., *Chem. Phys. Lett.* **200**, 488, 1992.

Beddard. G., *Rep. Prog. Phys.* **56**, 63, 1993.

Berry, R.S., *Proceedings of the International School of Physics*, ed., Scoles, G., North-Holland, Amsterdam, p. 3, 1990.

Beswick, J. A., Jortner, J., *Adv. Chem. Phys.* **47**, 363, 1981.

Breen, J.J., Peng, L.W., Willberg, D.M., Heikal, A., Cong, P., Zewail, A.H., *Chem. Phys.* **92**, 805, 1990.

Bloembergen, N., Zewail, A.H., *J. Phys. Chem.* **88**, 5459, 1984.

Dantus, M., Roberts, G., *Comments Atomic & Mol. Phys.* **26**, 131, 1991.

Dantus, M., Kim, S.B., Williamson, J.C., Zewail, A.H., *J. Phys. Chem.* **98**, 2782 (1994).

Fei, S., Zheng, X., Heaven, M., Tellinghuisen, J., *J. Chem. Phys.* **97**, 6057, 1992.

Felker, P.M., Zewail, A.H., *Chem. Phys. Lett.* **94**, 454 (1983).

Felker, P.M., Zewail, A.H., *J. Chem. Phys.* **78**, 5266 (1983).

Felker, P.M., Zewail, A.H., *Chem. Phys. Lett.* **102**, 113, 1983.

Felker, P.M., Zewail, A.H., *Adv. Chem. Phys.* **70**, 265, 1988.

Fleming, G., Scherer, N., Ziegler, L.: in this proceeding.

Frank, J., Rabinovitch, E., *Trans. Faraday Soc.* **30**, 120, 1934.

Gerdy, J., Dantus, M., Bowman, R.M., Zewail, A.H., *Chem. Phys. Lett.* **171**, 1, 1990.

Gruebele, M., Zewail, A.H., *J. Chem. Phys.* **98**, 883; and references therein, 1993.

Gutmann, M., Willberg, D.M., Zewail, A.H., *J. Chem. Phys.* **97**, 8037, 1992.

Gutmann, M., Willberg, D.M., Zewail, A.H., *J. Chem. Phys.* **97**, 8048, 1992.

Harris, A.L., Brown, J.K., Harris, C.B., *Ann. Rev. Phys. Chem.* **39**, 341, 1988.
Ionov, S.I., Brucker, G.A., Jaques, C., Valachovic, L., Wittig, C., *J. Chem. Phys.* **97**, 9486, 1992.
Jortner, J., Scharf, D., Ben-Horin, N., Even, U., Landman, U., *Proceedings of the International School of Physics*, ed., Scoles, G., North-Holland, Amsterdam, p. 43, 1990.
Khundkar, L.R., Zewail, A.H., *Ann. Rev. Phys. Chem.* **41**, 15; and references therein, 1990.
Levine, R.D., Bernstein, R.B., 'Molecular Reaction Dynamics and Chemical Reactivity,' Oxford University Press, Oxford, 1987.
Lienau, C., Williamson, J.C., Zewail, A.H., *Chem. Phys. Lett.* **213**, 289 (1993).
Liu, Q., Wang, J.-K., Zewail, A.H.: *Nature* - **364**, 427 (1993).
Manz, J., *Faraday Discuss. Chem. Soc.* **91**, 358, 1991.
Manz, J., *Chem. Phys. Lett.* **198**, 483, 1992.
Orlowski, T.E., Jones, K.E., Zewail, A.H., *J. Chem. Phys.* **54**, 197, 1978.
Papanikolas, J.M., Gord, J.R., Levinger, N.E., Ray, D., Vorsa, V., Lineberger, W.C., *J. Phys. Chem.* **95**, 8028, 1991.
Papanikolas, J.M., Vorsa, V., Nadal, M.E., Campagnola, P.J., Gord, J.R., Lineberger, W.C., *J. Chem. Phys.* **97**, 7002, 1992.
Porter, G., 'The Chemical Bond: Structure and Dynamics', ed., Zewail, A.H., Academic Press, Boston, p. 113, and references therein, 1992.
Potter, E.D., Liu, Q., Zewail, A.H., *Chem. Phys. Lett.* **200**, 605, 1992.
Saenger, K.L., McClelland, G.M., Herschbach, D.R., *J. Chem. Phys.* **85**, 333, 1981.
Scherer, N.F., Ziegler, L.D., Fleming, G.R., *J. Chem. Phys.* **96**, 5544, 1992.
Scherer, N.F., Sipes, C., Bernstein, R.B., Zewail, A.H., *J. Chem. Phys.* **92**, 5239, 1990.
Schreiber, E., Kühling, H., Kobs, K., Rutz, S., Wöste, L., ber. Bunsenges, *Phys. Chem.* **96**, 1301, 1992.
Somloi, J., Kazakov, V., Tannor, D.J., *Chem. Phys.* **172**, 85, 1993.
Stace, A.J., *J. Chem. Soc. Faraday Trans II* **77**, 2105, 1981.
Syage, J., Steadman, J., *J. Chem. Phys.* **95**, 2497, 1991.
Tannor, D.J., Rice, S.A., *Adv. Chem. Phys.* **70**, 441, 1988.
Warren, W.S., Zewail, A.H., *J. Chem. Phys.* **78**, 2298, 1983.
Wei, S., Purnell, J., Buzza, S.A., Stanley, R.J., Castleman, Jr., A.W., *J. Chem. Phys.* **97**, 9480, 1992.
Willberg, D.M., Gutmann, M., Nikitin, E.E., Zewail, A.H., *Chem. Phys. Lett.* **201**, 506, 1993.
Williamson, J.C., Zewail, A.H., *Proc. Natl. Acad. Sci.* **88**, 5021, 1991.
Williamson, J.C., Dantus, M., Kim, S.B., Zewail, A.H., *Chem. Phys. Lett.* **196**, 529, 1992.
Williamson, J.C., Zewail, A.H., *Chem. Phys. Lett.* **208**, 10, 1993.
Williamson, J.C., Zewail, A.H., *J. Phys. Chem.* **98**, 2766 (1994).
Yan, Y., Whitnell, R.M., Wilson, K.R., Zewail, A.H., *Chem. Phys. Lett.* **193**, 402, 1992.

Zewail, A.H., *Science* **242**, 1645, 1988.
Zewail, A.H., Bernstein, R.B., *Chemical & Engineering News*, p. 24–43, November 7, 1988.
Zewail, A.H., *Faraday Discuss. Chem. Soc.* **91**, 207; and references therein, 1991.
Zewail, A.H., J. Chem. Soc., *Faraday Trans.* 2 **85**, 1221, 1989.
Zewail, A.H., Dantus, M., Bowman, R.M., Mokhtari, A., *J. Photochem. Photobiol. A: Chem.* **62/3**, 301, 1992.
Zewail, A.H., *Phys. Today* **33**, 27, 1980.
Zewail, A.H., *J. Phys. Chem.* **97**, 12427 (1993).
Zewail, A.H., in Femtosecond Chemistry, J. Manz and L. Wöste (eds.) VCH Verlagsgesellschaft, Weinheim (1994).

Appendix I

Some Femtochemistry Research Groups

(Source: Invited Speakers Program of the Berlin Conferences)*

Femtochemistry in Gases I
A. H. Zewail, S. Y. Lee, M. Shapiro, Y. Chen, R. Schinke, J. H. Glownia, G. Stock

Femtochemistry in Gases II
J. L. Knee, H. D. Meyer, R. M. Bowman, H. Köppel, C. Daniel, A. A. Stuchebrukhov

Femtochemistry in Clusters I
L. Wöste, C. Wittig, P. M. Felker, G. Gerber, J. P. Visticot, M. Gruebele, V. Engel, B. Soep

Femtochemistry in Clusters II
F. G. Amar, A. W. Castleman, R. B. Gerber, J. L. Bowman, J. A. Syage, W. C. Lineberger

Femtochemistry at Surfaces
T. F. Heinz, S. Holloway, E. Mazur, T. Uzer, J. W. Gadzuk

J. Manz

Femtochemistry from Spectroscopy
J. C. Polanyi, E. J. Heller, R. D. Levine, J. L. Kinsey, D. M. Neumark, P. R. Brooks, J. P. Simons, W. H. Miller

From Femtochemistry into New Domains
G. Porter, S. H. Lin, M. Quack

Femtochemistry from Gases to Solutions
N. P. Ernsting, N. F. Scherer, D. Imre, J. Troe, S. Ruhman, T. Elsaesser, I. H. Gersonde

Femtochemistry and Laser Control
K. R. Wilson, W. Jakubetz, P. B. Corkum, R. Kosloff, A. D. Bandrauk, D. J. Tannor, G. K. Paramonov

J. L. Kinsey

* Not including other works in the condensed phases and in biology. Other groups working in the gas phase (and not present) include those at Illinois (EE & Chemistry), Colorado, Michigan State, Free University of Amsterdam, Köln University, and Université Paul Sabatier.

Author's Address

Arthur Amos Noyes Laboratory of Chemical Physics
California Institute of Technology
Pasadena, California 91125

Contribution Number 8810 from the California Institute of Technology. This research was supported by the National Science Foundation and by the Air Force Office of Scientific Research.

T. Baumert, R. Thalweiser, V. Weiss, E. Wiedenmann and G. Gerber

Femtosecond Dynamics of Molecules and Clusters

Abstract

The real-time dynamics of multiphoton ionization and fragmentation of molecules — Na_2, Na_3 — and clusters — Na_n, Hg_n — has been studied in molecular beam experiments employing ion and electron spectroscopy together with femtosecond pump-probe techniques. Experiments with Na_2 and Na_3 reveal unexpected features of the dynamics of the absorption of several photons as seen in the one- and three dimensional vibrational wave packet motion in different potential surfaces and in high laser fields. Cluster size dependent studies of physical properties such as absorption resonances, lifetimes and decay channels have been performed using tunable femtosecond light pulses in resonance enhanced multiphoton ionization (REMPI) of the cluster size under investigation. This method failed in ns-laser experiments due to the ultrafast decay of the studied cluster. For Na_n cluster we find that for cluster sizes $n \leqslant 21$ molecular excitations and properties prevail over collective excitations of plasmon-like resonances. In the case of Hg_n cluster prompt formation of singly and doubly charged cluster are observed up to $n \approx 60$. The transient multiphoton ionization spectra show a 'short' time wave packet dynamics, which is identical for singly and doubly charged mercury clusters while the 'long' time fragmentation dynamics is different.

Introduction

Multiphoton ionization of small molecules has been studied in recent years by a variety of techniques and is generally well understood. The ionization is predominantly due to resonance-enhanced multi-photon (REMPI) processes, whereas nonresonant multiphoton processes only play a minor role. Dynamical aspects of the interaction of laser radiation with molecules and details of the excitation processes and the different decay channels of highly excited states, embedded in the ionization and in the fragmentation continuum, are rarely studied up to now. Recently we reported on the interaction of a bound doubly excited molecular state with different continua and the competition between the various decay channels (1). In that study we used femtosecond laser pulses as an

experimental tool to distinguish between the dissociative ionization of the molecule and the neutral fragmentation with subsequent excited-fragment photoionization. Both processes are difficult to distinguish when using nanosecond or even picosecond laser pulses. This distinction is of particular importance in multiphoton ionization studies of metal cluster systems. The multiphoton ionization and fragmentation of alkalimetal molecules and, in particular, of Na_2 and Na_3 has attracted considerable current interest. In many experiments with Na_2 it has been found that, in conjunction with the formation of Na_2^+ ions, ionic fragments Na^+ are also formed. Resonance-enhanced multiphoton ionization (REMPI) processes via the $A\,^1\Sigma_u^+$ or the $B\,^1\Pi_u$ states are responsible for this observation (2). The sodium trimer Na_3 is probably the most studied and best known small metal-cluster (3). Its excitation spectrum consists of several bands due to different excited electronic states among which the B-state with an onset at 625 nm is of greatest interest. This is because of the observed pseudorotational features in the spectra. In a series of beautiful experiments Zewail and coworkers (4) have demonstrated the enormous advantage of applying femtosecond lasers to the study of molecular dynamics. Their pioneering work in the field of femtosecond photochemistry and transient molecular fluorescence spectroscopy has initiated other time-resolved ultrafast laser studies (5).

In recent years cluster and in particular metal cluster have been the fascinating subject of many experimental and theoretical studies. Cluster form the link between surface chemistry and molecular physics. Metal cluster exhibit distinct features ranging from molecular properties seen in small particles to solid state-like behaviour of larger aggregates. Studies of cluster properties like geometric structures, the evolution of the electronic states from localized to delocalized in nature and the real-time dynamics of ionization and fragmentation have yet not been studied in detail as a function of cluster size. In this contribution we report the first experiments in cluster physics employing ultrashort laser pulses to time-resolved studies of cluster ionization and fragmentation processes. Alkali cluster, which are easily formed in supersonic expansions, are attractive species to be studied experimentally and theoretically, because there is only one valence electron per atom.

Time-resolved measurements often open up new directions and provide a more comprehensive view of the physical and chemical processes. Due to recent developments in the generation and amplification of ultra-short light pulses, direct measurements of transient ionization and fragmentation spectra with femtosecond time resolution are now possible. This allows a closer look at the dynamical aspects of multiphoton ionization and fragmentation of molecules and clusters.

In this paper we discuss experimental results of time-resolved studies of multiphoton ionization and fragmentation processes of sodium and mercury molecules and cluster in molecular/cluster beam experiments applying femtosecond pump-probe techniques and ion and electron spectroscopy.

Experiment

In our femtosecond laser-molecular/cluster beam studies of time-resolved multiphoton ionization and fragmentation processes, we employed a combination of different experimental techniques. Femtosecond pump-probe techniques are used to induce and to probe cluster transitions, to resolve the interactions and to display the evolution of coherences and populations in real-time. A seeded supersonic beam provides the molecules and cluster in a collision-free environment and restricts the initial states to the very lowest vibrational and rotational states. Time-of-Flight (TOF) spectroscopy is used to measure the final continuum states, the cluster-size distributions and to determine the released kinetic energy of the ionic fragments and the energy distribution of the ejected electrons. Fig. 1 shows the schematic experimental arrangement of the cluster beam, the femtosecond laser pulses and the ion and electron TOF-spectrometers. The sodium cluster Na_n are produced by coexpansion of sodium vapor (50-100 mbar) with the inert carrier gas argon (1-8 bar) through a small cylindrical nozzle of about 100 μm diameter. This technique provides efficiently cooled sodium cluster with about 30-50 K vibrational temperatures. For mercury cluster Hg_n, the necessary oven temperatures are much lower. Femtosecond light pulses are generated in

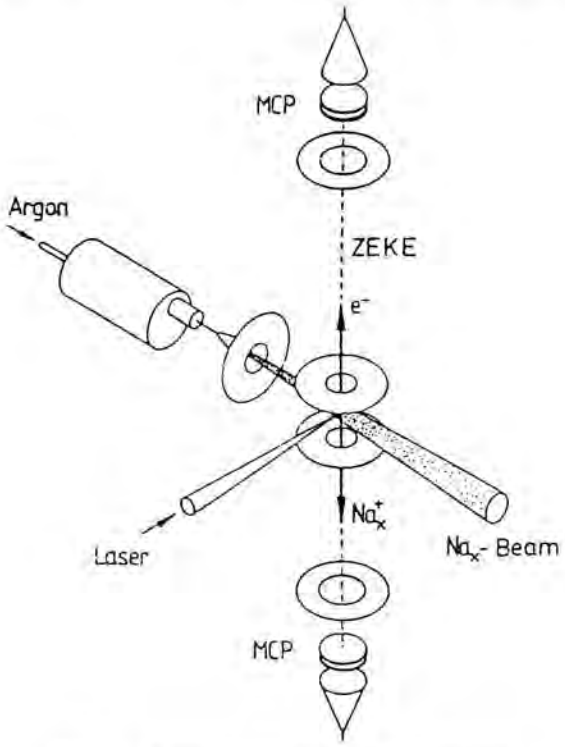

Fig. 1. Schematic experimental arrangement.

two different home-built laser systems. Tunable femtosecond pulses of 50 fs-100 fs time duration and of 0.1 μJ-50 μJ energy in the wavelength range 420 nm to 750 nm are generated in the laser system shown in Fig. 2. The output pulses of a colliding-pulse mode-locked ring dye laser (CPM) are amplified in a bow-tie amplifier, which is pumped by an excimer laser at 308 nm, pulse compressed and focussed into a cell containing methanol to generate a white light continuum. Light pulses at specific wavelengths selected from the white light con-

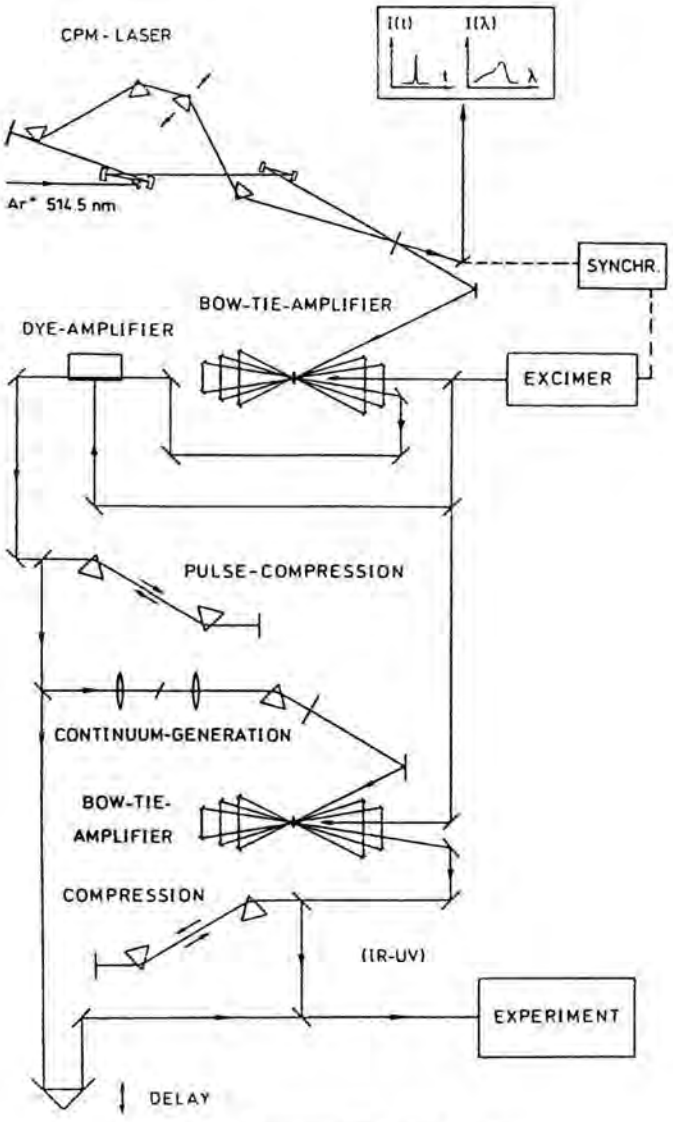

Fig. 2. Femtosecond laser system.

tinuum are amplified again in another bow-tie and compressed before entering the interaction region. A Michelson arrangement was used to delay the probe laser relative to the pump laser.

The second femtosecond laser system makes use of a home-built Ti : Sapphire laser oscillator. This Ti : Sapphire laser produces light pulses of 20 fs-70 fs time duration in the wavelength range 700 nm to 850 nm. Using again a bow-tie amplifier, pulse energies sufficient for multiphoton ionization of metal clusters are obtained.

Results and Discussion

Na_2-*Dimer*

We have recently reported femtosecond time-resolved multiphoton ionization and fragmentation dynamics of the Na_2 molecule. From the real-time observation of vibrational wave packet motions it was concluded, that two different physical processes determine the time evolution of multiphoton ionization (6). The observed femtosecond pump-probe delay spectrum of the molecular ion (Na_2^+) signal is shown in Fig. 3. Evident from the beat structure seen in Fig. 3, there are two frequencies involved and therefore there are two contributions to the transient ionization spectrum, and the envelope intensity variation reveals them to be 180° out of phase. A Fourier analysis of this spectrum yields two groups of frequencies, one centered at 108.7 cm^{-1} and a second one centered at 92.0 cm^{-1}. From the observed two oscillation periods, the 180° phase shift and the additionally measured time-resolved Na^+ photofragmentation spectrum (7),

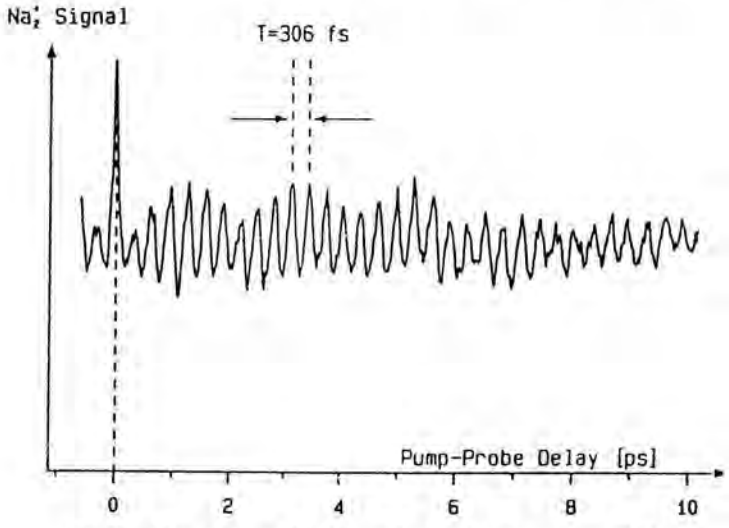

Fig. 3. Transient multiphoton-ionization spectrum of Na_2.

we concluded that for Na_2 two different multiphoton ionization processes exist, to require incoherent addition of the intensities to account for the observations. The direct photoionization of an excited electron, where one pump photon creates a vibrational wave packet in the $A\ ^1\Sigma_u^+$ state and two probe photons transfer that motion via the $2\ ^1\Pi_g$ state into the ionization continuum, is one (REMPI) process. The second involves excitation of two electrons and subsequent electronic autoionization. Here two pump photons create a wave packet at the inner turning point, in the $2\ ^1\Pi_g$ Rydberg state, which then propagates to the outer turning point, where the probe laser transfers the motion into the continuum by exciting a second electron, forming a doubly excited neutral $Na_2^{**}(nl, n'l')$ molecule. This happens only at the outer turning point of the $2\ ^1\Pi_g$ state periodically after each round trip. In this case the probe photon is absorbed at the earliest about 180 fs after the pump photons were absorbed. In the one electron direct photoionization process all three photons are absorbed at the inner turning point at once or at least within the time duration of the light

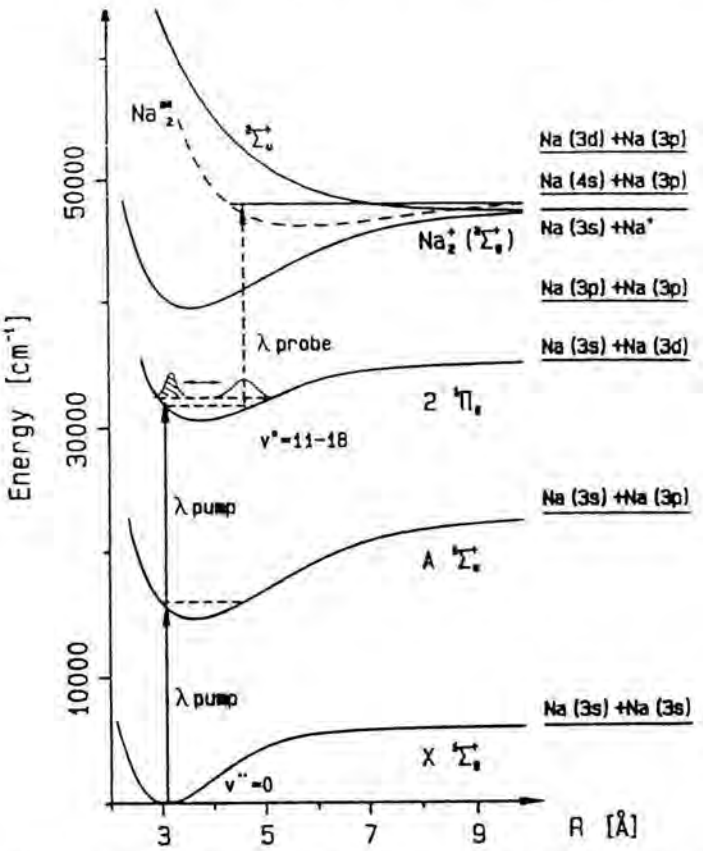

Fig. 4. Potential curve diagramm illustrating the preparation of the wave packet in the $2\ ^1\Pi_g$ state.

pulses. Figure 4 illustrates the two-photon-pump and one-photon-probe ionization process which involves excitation and decay of doubly excited states.

The Na_2 case is the first example of a femtosecond molecular multiphoton ionization study. It was only through time domain measurements that the existence of a second major ionization process was established. A comprehensive discussion including a comparison between experiment and quantum mechanical calculations can be found in a recent publication (8). In a further study the dependence of the total Na_2^+ ion signal on the intensity of the femtosecond pulses was investigated in detail (9). For higher laser intensities the relative contribution from the $A\ ^1\Sigma_u^+$ and the $2\ ^1\Pi_g$ states change dramatically, indicating the increasing importance of the two-electron versus the one-electron process. For even stronger fields (10^{12} W/cm^2) a vibrational wave packet in the electronic ground state $X\ ^1\Sigma_g^+$ is formed through stimulated emission during the time the ultrashort pump pulse interacts with the molecule, and its dynamics is also seen in the transient Na_2^+ signal. The spreading and recurrence of the vibrational wave packet in the bound $A\ ^1\Sigma_u^+$ electronic state has been studied in pump-probe experiments and compared with time-dependent quantum calculations (10).

Na_3-*Trimer*

The same experimental set up and techniques have now been employed to study the ionization and fragmentation dynamics of the cluster Na_3(11). In all the pump-probe experiments discussed here the same color has been used for the pump and the probe laser. This has the experimental advantage of a precise zero delay time determination and it facilitates the interpretation of weak structures superimposed on some decay curves. In the case of the B-state an ultrashort 60 fs pump pulse with photons of 623 nm excites a coherent superposition of the lowest vibrational and pseudorotational levels due to its bandwidth of about 300 cm^{-1}. The generated vibrational and pseudorotational wave packets propagate in the excited state potential surfaces. A time delayed probe photon of the same wavelength and the same 60 fs time duration probes the motion of the wave packet and the decay of the excited state population. This is done by time delayed probe photon ionization. The transient ionization spectrum of Na_3 obtained for a central wavelength of 623 nm is shown in Fig. 5. This time domain spectrum is more complex than that observed for the dimer Na_2. But still there are distinct recognizable time patterns, like the 320 fs separation of the major peaks, which corresponds to an energy of 105 cm^{-1}, and the dip around zero time delay caused by fragmentation of the formed Na_3^+ by the intense laser fields at $\Delta t = 0$. It is in agreement with earlier high resolution two photon ionization (via B-state) spectra (12) that we do not observe a decay of the B-state for delay times up to 10 ps. As the Fast Fourier Transformation (FFT) spectrum, displayed in Fig. 6, shows, the dynamics of the two photon ionization process is determined by three dimensional wave packet motions in the Na_3 B-state and in the X-state as well. At the applied laser intensity both states are involved. The

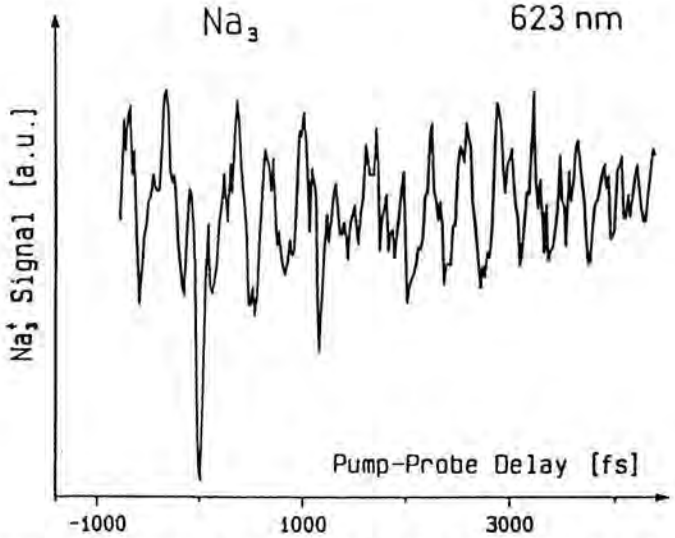

Fig. 5. Pump-probe ionization spectrum of Na_3 (B) using 60 fs light pulses at 623 nm.

pump laser generates a wave packet in the intermediate B-state and simultaneously a wave packet in the X electronic ground state through stimulated emission pumping during the pump pulse. The contributions in the FFT spectrum (Fig. 6) near 140 cm^{-1}, 90 cm^{-1} and 50 cm^{-1} are attributed to the symmetric stretch, to the asymmetric stretch and to the bending mode in the Na_3 electronic ground state. This assignment is based upon the analysis of Broyer et al. (13). The wave packet dynamics in the excited B-state seems to be dominated by the symmetric stretch mode with frequencies close to 105 cm^{-1}. According to calculations of Meyer et al. (14) and Cocchini et al. (15), the Eigenfrequencies

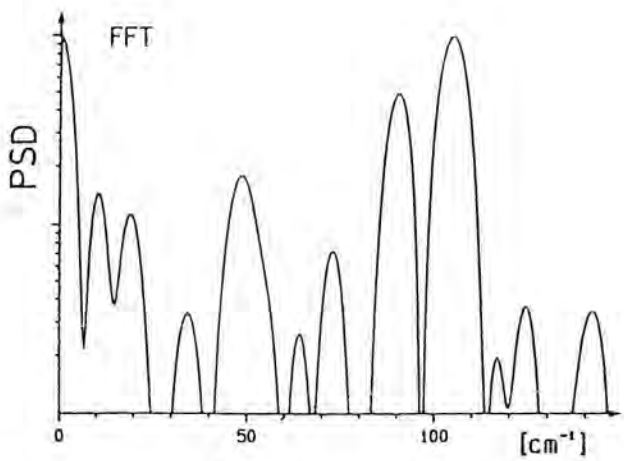

Fig. 6. Fourier (FFT) spectrum of Na_3 (B) transient ionization spectrum shown in Fig. 5.

of the symmetric stretch modes of the 4 $^2A_1$ and the 3 $^2B_2$-states are in the range of 94 cm^{-1} to 111 cm^{-1}. The contribution around 72 cm^{-1} is tentatively assigned to the bending and asymmetric stretch mode of the 3 $^2B_2$ state.

The other observed frequencies 8.5-12 cm^{-1}, 17.5-20 cm^{-1} and 30.5-35 cm^{-1} are assigned to a free pseudorotational wave packet motion in the potential surface of the B-state. The energy differences of successive pseudorotational j-states are experimentally determined as assigned by Delacretaz et al. (12) on the basis of a pure Jahn-Teller distortion of the B-state to half-integer j-values. For $v = 0$, ($v = 1$), these values are Δ_j: 1/2, $-3/2 = 2.5$; (5) cm^{-1}, Δ_j: $-3/2$, $3/2 = 12$; (13.5) cm^{-1}, Δ_j: 3/2, $5/2 = 18$; (20) cm^{-1}, Δ_j: 7/2, $9/2 = 34$; (30) cm^{-1}, respectively. It is however very interesting to note, that in our experiment the corresponding radial component (128 cm^{-1}) of the pseudorotational motion plays only a minor role, if at all. In contrast to this, high resolution spectroscopy of the B-X system exhibits a strong contribution of the radial pseudo-rotational component (12). Theoretical studies of Meiswinkel and Köppel (16) showed, that the observed high resolution spectra can also be explained taking into account a Pseudo-Jahn-Teller (PJT) model with integer pseudorotational j-values. In that model the vibronic coupling of the accidentally degenerate (D_{3h})-states 3 $^2E'$ (B) and 2 $^2A_1'$ is responsible for the observed vibronic structure. So far, it is not yet clear, which of the two models is more appropriate to explain the observed pseudorotational wave packet motion, since the ultrashort dynamics depend on the pseudorotational energy *differences*.

Na_n-*Cluster*

Recently we reported the first femtosecond time-resolved experiments in cluster physics (17), where the photofragmentation dynamics of small sodium cluster ions Na_n^+ have been studied with pump-probe techniques. Ultrashort laser pulses of 60 fs duration are employed to photoionize the sodium cluster and to probe the neutral photofragments. We find that the ejection of dimer Na_2 and trimer Na_3 photofragments occur on ultrashort time scales of 2.5 ps and 0.4 ps, respectively. This and the absence of cluster heating reveals that direct photo-induced fragmentation processes are important at short times rather than the statistical unimolecular decay.

Femtosecond laser pulses have been applied by our group to study cluster size-dependent properties like energy, bandwidth and lifetime(s) of intermediate resonances (Na_n^*) in beam experiments (18). Since the complexity of the spectroscopy and dynamics of metal cluster strongly increases with the number of atoms we have restricted our studies in the case of sodium cluster to sizes $n \leqslant 21$, whereas for mercury cluster we followed the size dependent properties up to $n \approx 45$.

The photoabsorption spectra of neutral metal cluster are of particular interest in view of the size-dependent transition from molecule-like absorption to collective excitation of the valence electrons. For larger cluster Na_n with $n \geqslant 4$, these

resonances are yet not observed in two photon ionization spectroscopy employing nanosecond or picosecond laser pulses because of the anticipated fast decay of the intermediate Na_n^* states. However, using nanosecond laser depletion spectroscopy, Knight (19) and Kappes (20) measured these spectra for selected cluster sizes. We have measured the energy and the bandwidth of Na_n^* ($n = 4$-21) metal cluster absorption resonances by femtosecond two-photon ionization spectroscopy in the range 1.5 eV-3.0 eV with tunable laser pulses. The most striking results, which are discussed in this contribution, are obtained for the cluster Na_8 and Na_{20}. Within the shell model (21) for the electronic structure of metal cluster, these cluster-sizes have a closed electronic shell and are therefore spherically symmetric. On the basis of the Jellium model, the Mie-Drude theory predicts for this spherically symmetric metallic cluster a single intense band corresponding to a classical surface-plasma oscillation. In more elaborate calculations based on (RPA) random-phase-approximations (22) or (TDLDA) time-dependent local-density-approximations (23) the photoabsorption strength, of for instance Na_{20}, splits into two strong and several weaker peaks. However, the fs-two photon ionization spectra of Na_8 - displayed in Fig. 7 - and Na_{20} - displayed in Fig. 8 show several strong resonances, in better agreement with ab initio molecular type calculations (24), with different bandwidths and as discussed later different lifetimes (25). This indicates that the simple physical picture based on the Jellium model has to be modified in order to explain these data.

No measurements of the intermediate resonance lifetime(s) have been reported so far. In our first experiments we have employed femtosecond pump-probe spectroscopy with tunable fs-laser pulses to measure the decay time(s) of the different absorption resonances of all Na_n cluster-sizes up to $n \leqslant 21$. In particular, the results obtained for Na_8 and Na_{20} are discussed in the following. Three transient ionization spectra of Na_8, each obtained with the fs-laser tuned to the

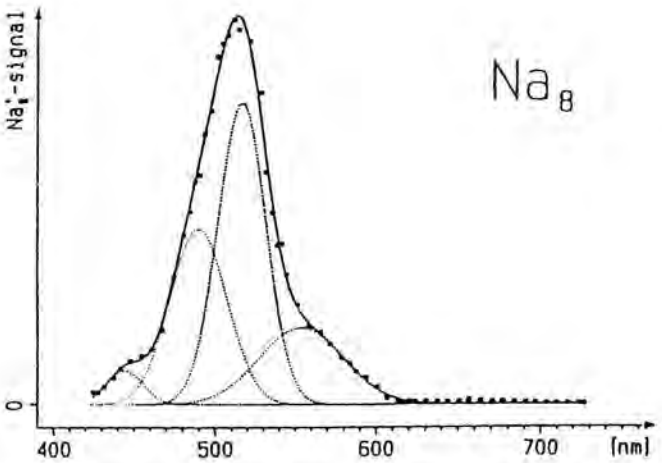

Fig. 7. Femtosecond two-photon ionization spectrum of Na_8.

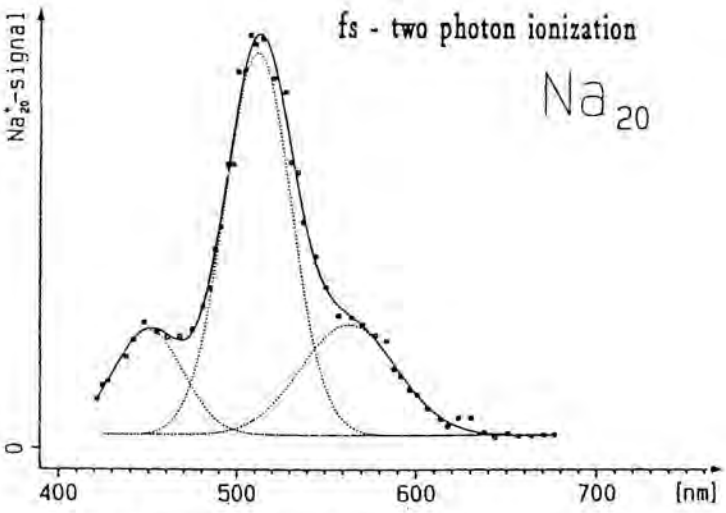

Fig. 8. Femtosecond two-photon ionization spectrum of Na_{20}.

center wavelength of the individual resonance, are displayed in Fig. 9. A pump pulse of about 80 fs time duration excites the Na_8 cluster while a time delayed identical probe pulse probes the residual population by photoionizing Na_8^*, the intermediate excited electronic states. As already discussed we have applied this technique to Na_2, Na_3 and Na_n^+ to investigate wavepacket motion and fragmentation dynamics of these systems. Figure 9 shows the transient Na_8^+ spectra at 493 nm, 518 nm and 540 nm, where the Na_8^+ signal is plotted versus the pump-probe delay time. These spectra are symmetric with respect to zero delay time, because pump and probe pulses have the same time duration and intensity. In order to get the decay time constants we have fitted the transient spectra with a sum of exponential decay functions. At 518 nm the best fit is achieved by taking into account two functions with time constants of 0.5 ps and of about 4 ps. The transient spectrum at 493 nm shows only a single exponential decay with a time constant of 0.45 ps. What is however clearly demonstrated by the spectra in Fig. 9 is that each resonance has its own decay dynamics. Besides the decay there is also for each resonance an additional superimposed oscillatory structure. For the 518 nm resonance we find a regular oscillation with a time interval of about 160 fs, while at 493 nm there are at least two different series with time intervals of 360 fs and 270 fs. The transient spectrum of the 540 nm resonance is quite different from the others. Here we observe a much slower dynamics with time constants of 0.8 ps and of 2.8 ps. A Fast Fourier Transformation (FFT) of each of the time domain spectra clearly shows the corresponding frequencies and some additional frequencies in the range 30 cm^{-1} to 150 cm^{-1}. All these frequencies are in the range of the known vibrational Eigenfrequencies of Na_3 and Na_4 as determined by ZEKE-photo-electron spectroscopy (26). Thus, we believe the observed superimposed fast oscillations are due to wave packet motions in the potential surfaces of these metal-cluster. With the fs-laser tuned to 511 nm,

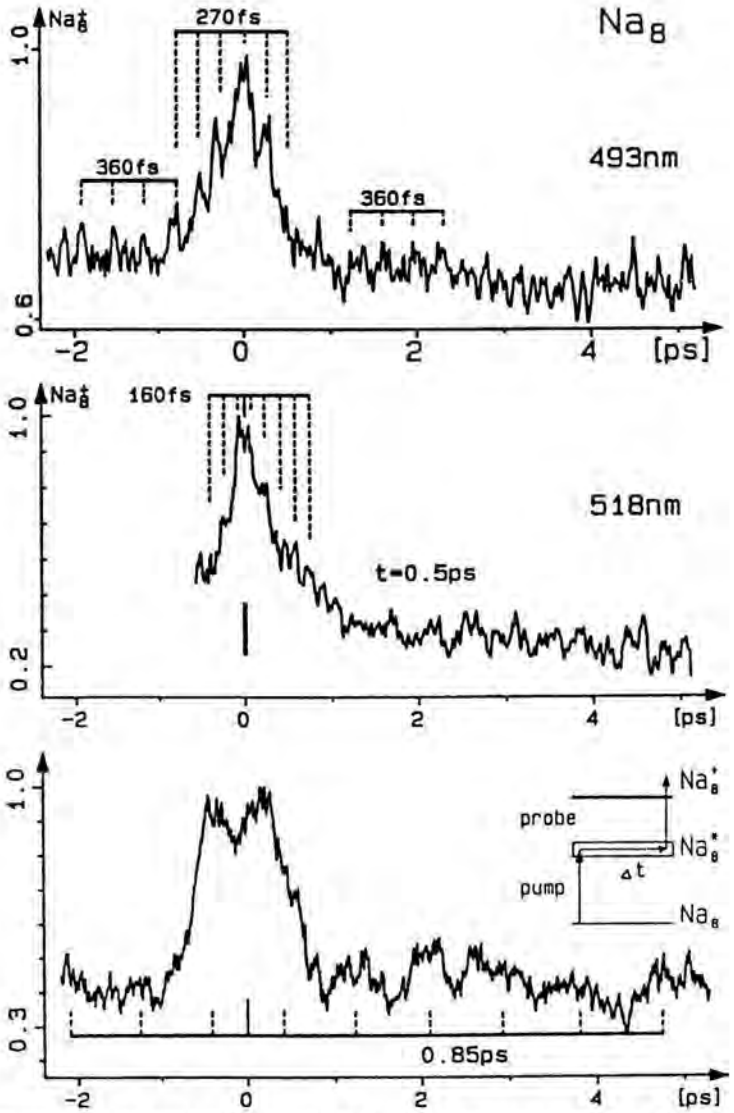

Fig. 9. Femtosecond time-resolved decay of the Na_8^* resonance at 493 nm, 518 nm and 540 nm measured with 80 fs pump and probe pulses.

the wavelength of the strongest resonance measured for Na_{20}, we observed a pump-probe spectrum which can be fitted by a single exponential decay with a time constant of 0.9 ps. Again there is an oscillatory structure superimposed with a time period of 360 fs. Note that also for Na_{20}, the decay time constant as well as the superimposed faster dynamics depend on the particular resonance. From these measurements with ultrafast laser pulses it is evident that the simple picture of a homogeneously broadened surface plasmon resonance is clearly not

appropriate to describe the optical excitations of small ($n \leqslant 21$) sodium metal-cluster. Furthermore the wavelength dependence of the decay time constants and the superimposed fast dynamics is in much better agreement with the measured structure of the cluster absorption resonances. As for the cluster resonances, the pump-probe measurements are much better understood taking into account molecular structures and excitations rather than considering the small Na_n cluster to be a metal with excitations of delocalized electrons. On the basis of the observed cluster absorption resonances, their ultrashort lifetimes and different decay patterns, we conclude that at least for cluster sizes Na_n with $n \leqslant 21$, molecular excitations and properties prevail over collective excitations and surface-plasmon like properties.

Hg_n-*Cluster*

Cluster form a new class of materials, which often exhibit unexpected properties. A very interesting situation arises with mercury cluster. The mercury atom has a $5d^{10}\,6s^2\,np^0$ closed shell electronic configuration with an ionization potential of 10.4 eV. Diatomic Hg_2 and other small mercury cluster are predominantly van der Waals bound systems. However, the electronic structure changes strongly with increasing cluster size and finally converges towards the bulk, where the 6s- and 6p bands overlap, giving mercury its metallic properties. This means that for the divalent Hg_n-cluster a size dependent transition from van der Waals to covalent to metallic binding exists. Therefore mercury provides the

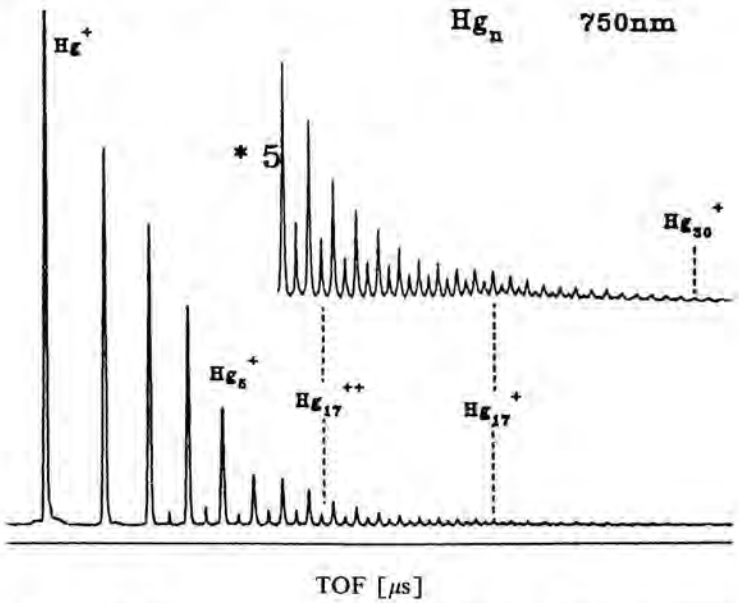

Fig. 10. Time-of-Flight mass spectrum of singly and doubly charged mercury cluster.

ideal system to study the size-dependent nonmetal-metal transition. For neutral mercury cluster the ionization potentials are reasonably well known (27), but other optical properties are practically unknown. The situation is much better for singly and doubly ionized Hg_n cluster with the recently reported ionization potentials and optical absorption spectra (28).

Here we report studies of multiphoton ionization and fragmentation of mercury cluster in the femtosecond time domain. We observe the prompt formation of singly and doubly charged cluster ions, and measure directly the decay of parent ions due to photofragmentation, together with the subsequent growth of daughter species. Furthermore we observe size-selected ion intensity oscillations in pump-probe measurements indicating wave packet dynamics in both singly and doubly charged cluster. For these experiments we have used a Ti:Sapphire laser generating a train of light pulses of 20 fs-70 fs time duration. The pulses are amplified, compressed and delayed to form a sequence of pump-probe pairs. Time-of-Flight (TOF) spectroscopy determines the mass of the cluster ion and the initial kinetic energy of the ionic fragments.

Figure 10 shows a TOF mass spectrum of singly and doubly charged Hg_n cluster ions produced by 30 fs pulses at 750 nm. The most striking features of the spectrum are first, that a multiphoton (6/12 photons) absorption forms singly and doubly ionized cluster and second, that the intensity ratio between singly and doubly charged cluster of the same mass is in most cases favour of the doubly charged species. Furthermore this ratio does not change for up to ten times lower laser intensity, but the ratio does change strongly with wavelength. For Hg_{17} clusters the ratio $Hg_{17}^{+\,+}$ to Hg_{17}^{+} varies from 5:1 for 750 nm to 1:2 for 620 nm laser radiation. The lower part of Fig. 11 shows the transient ionization signal for the mercury dimer for short delay times while the upper part shows the evolution of the transient signal up to 160 ps delay. The oscillating signal at short delay times is due to a very strongly damped vibrational wave packet motion in an unknown excited electronic state of the mercury dimer. A Fourier analysis yields about 30 cm^{-1}, which is close to vibrational Eigenfrequencies of the van der Waals bound Hg_2 molecule. At longer delay times the figure shows first a 6 ps recovery and than a 20 ps decay of the total Hg_2^+ signal. It is inferred from the fragmentation kinetics of larger cluster, that Hg_{15}^+ fragments with a decay constant of 6 ps. Although nothing definitive can be stated without thorough analysis of all possible decay channels, the data suggest that at least one of the Hg_{15}^+ fragments is the dimer Hg_2.

A very surprising result of our time-resolved studies of size-selected neutral mercury cluster is shown in Fig. 12. The figures detail the first five picoseconds of the pump-probe measurement in singly and doubly charged Hg_{17}. Even more surprising is our finding that cluster masses from the monomer up to at least $n = 43$ exhibit quite similar, if not identical, Fourier spectra in both singly and doubly charged species. We interpret the regular modulation of the ion intensity as demonstrating wave packet motion in a neutral cluster excited-state manifold. Fourier analysis reveals a very simple frequency spectrum of a group of low-frequency peaks around 26 cm^{-1}.

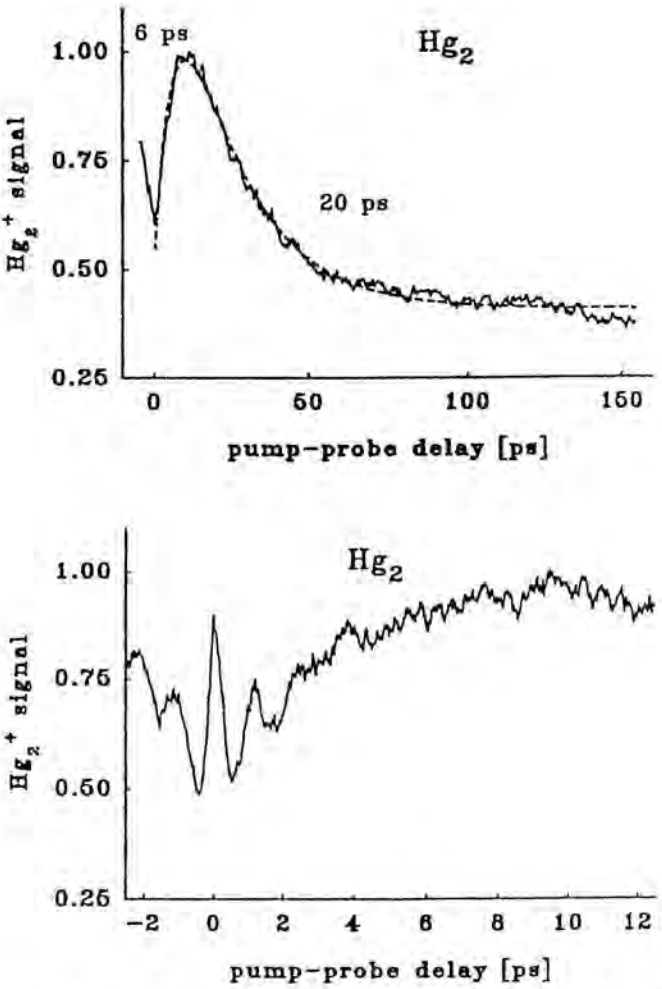

Fig. 11. Transient multiphoton ionization spectra of the mercury dimer obtained with 60 fs laser pulses at 620 nm.

The simplicity and similarity of the wave packet Fourier spectrum over a broad range of cluster masses lead us to propose multiphoton absorption to a core Hg_2^* 'chromophore' imbedded within and common to all the Hg_n neutral cluster examined in these experiments. The fact that blocking the probe pulse effectively quenches all ion signals and that the pump-probe spectrum with a weaker pump (or probe) is still symmetric with respect to $t = 0$ means that the pump pulse must excite a manifold of high-lying Rydberg states near but below the individual cluster ionization limit. Wave packets associated with the Hg_2^*-core form and evolve within this manifold, and the variable-delay probe pulse

detects them by transfering the wave packet motion into both singly and doubly charged cluster ion channels. In addition to the simplicity and universality of the wave packet spectra, previous measurements of one-photon Hg_n-cluster absorption spectry by Brechignac et al. (29) support the idea of a common Hg_2^* chromophore. Their results show the persistence of autoionization features in the ionization spectra of mercury clusters up to $n \approx 35$.

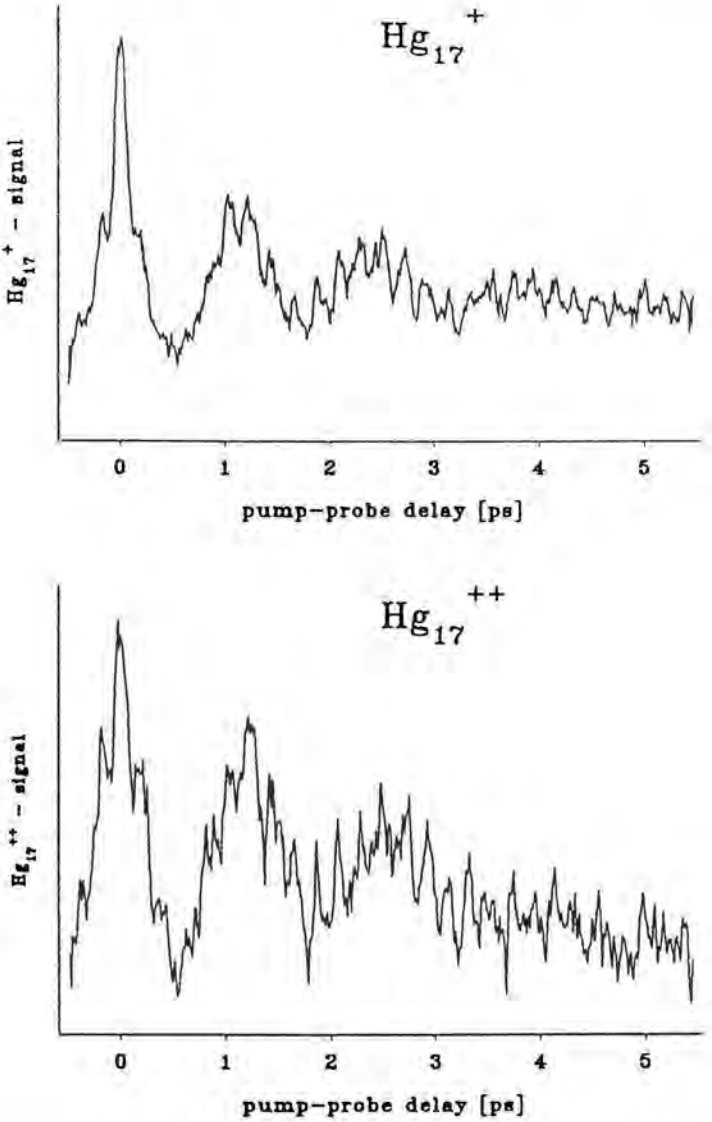

Fig. 12. Transient multiphoton ionization spectra of singly (upper part) and doubly (lower part) charged Hg_{17} cluster.

From the transient ionization spectra of singly and doubly charged Hg_{17}, shown in Fig. 12, it is clear that a maximum ion signal is observed for both species at precisely zero delay time. Note, this suggests that double ionization occurs directly through a transition from the neutral to the doubly charged manifold and not via the singly ionized continuum as it is observed in many high laser field experiments with atoms and molecules.

Summary

The real-time dynamics of multiphoton ionization and fragmentation of sodium and mercury molecules and cluster have been studied in beam experiments employing femtosecond pump-probe techniques and ion- and electron spectroscopy. Sodium with one valence electron per atom is an experimentally and theoretically very attractive system and metal prototype, whereas the divalent mercury offers the unique possibility to study the size dependent nonmetal-metal transition. Femtosecond time-resolved multi-photon ionization of sodium and mercury reveals unexpected features in the dynamics of the absorption of several photons like the observation of a second major REMPI process in Na_2 involving two electrons. Vibrational wave packet motions in dimers, trimers and even much larger systems like Na_8 and Na_{20} have been studied. The spreading and recurrence of a vibrational wave packet as well as its behaviour in strong laser fields have been studied in detail.

Cluster physics bridge the gap between molecular and solid state physics. Cluster size-dependent studies of physical properties such as absorption resonances, lifetimes and decay channels have been performed with tunable, ultrashort light pulses. A major result of our femtosecond experiments is that the conventional view of the optical response of metal-cluster, e.g. the absorption, ionization and decay processes as well as the corresponding time scales, had to be changed. Our results clearly show that for cluster sizes Na_n with $n \leqslant 21$, the molecular structure, excitations and properties prevail over collective excitations and surface-plasmon like properties. It is however obvious that for even larger cluster the optical response must finally be dominated by collective interactions. The preliminary analysis of the time-resolved mercury experiments gives astonishing results. First, the observation of singly and doubly ionized cluster in direct multiphoton ionization transitions and second, an almost identical vibrational wave packet motion in both singly and doubly charged cluster up to $n = 43$ is very surprising. Probably a Hg_2^*-chromophore imbedded within and common to all Hg_n neutral cluster carries the oscillator strength and determines the 'short' time wave packet dynamics.

These real-time studies of the dynamics of ionization and fragmentation with femtosecond time resolution open up new and very exciting fields in molecular and cluster physics and yield results which in many cases are not accessible in nanosecond or picosecond laser experiments.

We gratefully acknowledge the discussions with V. Engel and J. Weiner and the contributions of A. Assion, V. Gerstner, B. Lang, F. Sattler, V. Seyfried, C. Rothenfußer, C. Röttgermann and S. Vogler to various experiments.
This work has been supported by the Deutsche Forschungsgemeinschaft through the Sonderforschungsbereich 276 in Freiburg.

References

1. Baumert, T, Bühler, B., Thalweiser, R., and Gerber, G., *Phys. Rev. Lett.* **64**, 733, 1990.
2. Keller, J., and Weiner, J., *Phys. Rev.* **A30**, 213, 1984; Burkhardt, C.E., Garver, W.P., and Leventhal, J.J., *Phys. Rev.* **A31**, 505, 1985.
3. Broyer, M., Delacretaz, G., Labastie, P., Whetten, R.L., Wolf, J.P., and Wöste, L., *Z. Phys.* **D 3**, 131, 1986.
4. Khundkar, L., and Zewail, A.H., *Annu. Rev. Phys. Chem.* **41**, 15,1990, and references therein.
5. Ultrafast Phenomena VIII, eds. J.L. Martin, A. Migus, G.A. Mourou, and A.H. Zewail, Springer Series in Chemical Physics Vol. **55**, Springer Verlag, 1993.
6. Baumert, T., Grosser, M., Thalweiser, R., and Gerber, G., *Phys. Rev. Lett.* **67**, 3753, 1991.
7. Baumert, T., Bühler, B., Grosser, M., Thalweiser, R., Weiss, V., Wiedenmann, E., and Gerber, G., *J. Phys. Chem.* **95**, 8103, 1991.
8. Engel, V., Baumert, T., Meier, Ch., and Gerber, G., *Z. Phys.* **D 28**, 37, 1993.
9. Baumert, T., Engel, V., Meier, C., and Gerber, G., *Chem. Phys. Lett.* **200**, 488, 1992.
10. Baumert, T., Engel, V., Röttgermann, C., Strunz, W.T., and Gerber, G., *Chem. Phys. Lett.* **191**, 639, 1992.
11. Baumert, T., Thalweiser, R., and Gerber, G., *Chem. Phys. Lett.* **209**, 29, 1993.
12. Delacretaz, G., Grant, E.R., Whetten, R.L., Wöste, L., and Zwanziger, J.F., *Phys. Rev. Lett.* **56**, 2598, 1986.
    Rakowsky, S., Herrmann, F.W., and Ernst, W.E., *Z. Phys.* **D26**, 1993.
13. Broyer, M., Delacretaz, G., Ni, G.Q., Wetten, R.L., Wolf, J.P., and Wöste, L., *Phys. Rev. Lett.* **62**, 2100, 1989.
14. Meyer, W., priv. communication.
15. Cocchini, F., Upton, T.H., and Andreoni, W., *J. Chem. Phys.* **88**, 6068, 1988.
16. Meiswinkel, R., and Köppel, H., *Chem. Phys. Lett.***144**, 177, 1990.
17. Baumert, T., Röttgermann, C., Rothenfußer, C., Thalweiser, R., Weiss, V., and Gerber, G., *Phys. Rev. Lett.* **69**, 1512, 1992.
18. Baumert, T., Thalweiser, R., Weiss, V., and Gerber, G., *Z. Phys.* **D 26**, 131 (1993).
19. Selby, K., Vollmer, M., Masui, J., Kresin, V., de Heer, W.A., and Knight, W.D., *Phys. Rev.* **B40**, 5417 (1989).

20. Wang, C.R., Pollak, S., Cameron, D., and Kappes, M.M., *J. Chem. Phys.* **93**, 3, 1990.
21. Kresin, V., Physics Reports **220**, 1 (1992)
22. Yannouleas, C., and Broglia, R.A., *Phys. Rev.* **A44**, 5793, 1991.
23. Ekardt, W., *Phys. Rev.* **B31**, 6360, 1985; Ekardt, W., Penzar, Z., ibid. **B43**, 1322, 1991.
24. Bonacic-Koutecky, V., Fantucci, P., and Koutecky, J., *Chem. Rev.* **91**, 1035, 1991 and *J. Chem. Phys.* **93**, 3802, 1990.
25. Rothenfußer, C., Thalweiser, R., Weiss, V., and Gerber, G., *Phys. Rev. Lett.* - submitted.
26. Thalweiser, R., Vogler, S., and Gerber, G., SPIE Proceedings Vol. **1858**, 196, 1993.
27. Rademann, K., Kaiser, B., Even, U., and Hensel, F., *Phys. Rev. Lett.* **59**, 2319, 1987.
28. Haberland, H., v. Issendorf, B., Yufeng, J., Kolar, T., and Thanner, G., *Z. Phys.* **D 26**, 8, 1993.
29. Brechignac, C., Broyer, M., Cahuzac, Ph., Delacretaz, G., Labastie, P., Wolf, J.P., and Wöste, L., *Phys. Rev. Lett.* **60**, 275, 1988.

Authors' Address:

Fakultät für Physik
Universität Freiburg
Herrmann-Herder-Str. 3
D-79104 Freiburg
Germany

S. Ruhman, U. Banin, A. Waldman, R. Kosloff and I. Benjamin

Coherent Effects in Solution Photochemistry

Abstract

In this contribution we report time domain studies of photochemistry in liquids. The impulsive nature of photoexcitation using femtosecond pulses results in induction of vibrational coherence in excited, ground, and reaction product electronic states. Theoretical modeling is used in order to interpret the observed time and solvent dependencies of these motions. Coherent vibrations induced are demonstrated to be vital dynamic observables, providing profound insight into the details of solution chemical reactivity. Transient resonance impulsive stimulated scattering is introduced for the first time in order to probe reaction fragments undergoing rapid vibrational relaxation.

Introduction

The introduction of new theoretical and experimental tools[1,2], capable of addressing chemical reaction dynamics in the liquid phase, has generated an explosive growth of interest in this field over the last few years. The ultimate aim of this endeavor is to appreciate how, for a wide array of chemical reactions, solvation influences reactivity in the liquid phase. How a solvent arranges itself around the reactants, and how this alters the intramolecular forces[3]. What degree of inhomogeneity exists in the arrangement of the solvent, and what the timescale is for the structural variations of the solvent shell[4]. Which modes of motion in the solvent couple to the reaction coordinate, and how efficiently energy is dissipated from the reactants into the liquid surroundings, or the other way around[5]. To understand and be able to quantitatively reproduce the series of events which lead from the activated reactant, to thermalized products, or in the case of solvent caging, back to the relaxed reactants. In such a case we wish to quantitatively rationalize the microscopic mechanisms which determine the degree of such caging.

While these objectives are similar in nature to those of chemical dynamics in isolated molecules, methodology in the liquid phase differs markedly in one major respect. Due to the irreversible nature of the solvent induced relaxation processes which very rapidly dissipate the chemistry related motions of the reactants and products, one cannot infer the course of a chemical reaction by prob-

ing the products after the fact. Sorting out the chronology of liquid phase photoinduced reactions, and deciphering the mechanisms of solvation in each stage of molecular evolution, requires following the reacting system as chemical change is under way. In principle, this is a daunting proposition, since in many cases photoinduced chemical rearrangement may be nearly complete in no more than 50-100 fsec[6].

In practice, the application of femtosecond laser spectroscopy, enables us to come close to realizing this. The wide spectrum and short duration of femtosecond pulses ensures simultaneous coherent population of numerous excited state vibronic levels. Disregarding broadening effects due to finite pulse durations, such 'Impulsive' photoexcitation can initiate phase coherent photochemistry in molecular ensembles, starting with uniform initial conditions defined by the equilibrium ground state configuration of the reactant, and evolving concertedly in time under the hamiltonian of the upper state. Finally, by spectroscopically probing this ensemble with a delayed ultrashort laser pulse (Pump-Probe), the evolution of induced chemical change is recorded[7]. This evolution can in certain cases give rise to nonstationary coherent superpositions of vibrations in photochemical products. If the excitation pulse is also impulsive with respect to ground state vibrations, through stimulated Raman interaction coherence can even be instilled in the ground vibronic manifold.

In the following we present a summary of recent femtosecond photochemical work on two molecular systems. Most of the following deals with photolysis of the triiodide ion in polar solvents. In a recently published paper a comprehensive study of this system was reported in which virtually all of the envisioned coherences were recorded[8]. Through a comparative solvent dependence study, and computer simulations, along with a report of preliminary results concerning a new solvated species, $(Cr(C_6H_6)(CO)_3)$ we will demonstrate the vitality of these newly available dynamic variables in providing unprecedented insight into the dynamics of liquid phase chemical change.

Experimental

The laser system has been described in detail elsewhere[8]. Briefly, an anti-resonant ring synch-pumped dye laser constructed in lab is pumped by a mode locked Nd;YLF laser. The output is further amplified at a repetition rate of 1 kHz, using the frequency doubled output of a Nd;YLF regenerative cavity to pump a dye amplifier. The ultimate output consists of 55-65 fsec pulses, centered at 616 nm, containing 20-30 mJ of energy. One portion of this output is frequency doubled to produce an excitation pulse in the UV, and initiates the photolysis of triiodide ions in the solution. Probing pulses are either derived again by doubling the fundamental in order to produce a UV probe, or by generating a white continuum from which a single frequency band probe is isolated by interference filtering. This portion is continuously delayed to produce the experimental scans. A reference and probe are derived by beam splitting, and

the latter is focused onto the sample together with the excite and push pulses. The transmitted probe is spectrally filtered and detected by photodiode. Data collection was carried out by introducing a chopper wheel into the excitation beams, and differentially detecting the signal using a lock-in amplifier (SR 530). All experiments were conducted in a 200 micron flow cell, equipped with ultra-thin quarz windows, using a sample concentration of a few millimolar. Specific details concerning experimental arrangements will be reported in the relevant part of the text.

Triiodide Photodissociation

Background, and Summary of Previous Results

Triiodide is a linear negative ion, stable in many polar solvents[8]. It absorbs in two intense and broad bands centered at 295 and 350 nm, dissociating with a solvent dependent quantum yield into diiodide ions, and atomic iodine. Anywhere from 1.5, to 2.5 eV of excess photon energy is available to the fragments, depending whether the iodine atom is electronically excited or in its ground state. The diiodide also absorbs with medium intensity in two broad bands centered at 360 and 740 nm at room temperature, depending slightly on the solvent. While the former overlaps with I_3^- absorption, the later is spectrally isolated allowing selective probing of the product population. All transitions in the parent and daughter ions are parallel. Further spectrochemical data are provided in previous publications.

This system was chosen as a model triatomic photolysis reaction, since it is strongly perturbed by the solvent, and the intramolecular vibrations in both reactant and product ions are time resolvable with the described laser system. In order to record the course of this reaction in ethanol solution, two types of transient transmission scans following UV photolysis of I_3^- were undertaken. In the first, probing was conducted in the visible and near IR in order to follow the evolution in the nascent I_2^- fragments. Throuthout this spectral region an instantaneous rise and rapid partial decrease of absorption within ~ 250 fsec was observed. The former was associated with absorption of I_3^- in the reactive excited state, the later with the stage of bond cleavage. Following these features a leveling off of the absorption was discerned, upon which 95 cm^{-1} oscillations decaying with a time constant of ~ 400 fsec were superimposed. Observation of a 1π phase shift in these oscillations upon varying the probe frequency from the 'blue' to the 'red' of the I_2^- band center supported our assignment of these modulations to coherent vibrations of the nascent fragment ions. Finally a subsequent gradual narrowing of the transient spectrum around the band center on a timescale of ~ 4 psec was interpreted to be the signature of vibrational product relaxation. Photoselective probing also provided a timescale of ~ 5 psec for reorientation of the newly formed I_2^-.

Two main findings resulted from transient probing in the UV. The instanta-

neous photoinduced bleach in I_3^- absorption undergoes partial replenishment in two phases. The first very rapid one takes place within 5 picoseconds. It has been assigned tentatively with primary geminate recombination, and the duration of this component is suspected to be determined by vibrational relaxation. The second phase which takes place on a 70 psec timescale is accordingly assigned as secondary geminate recombination. However at very short probe delays the bleach signal is superimposed with 111 cm^{-1} oscillations, precisely the frequency of the symmetric stretch vibration in I_3^-, starting immediately at $t = 0$, and decaying with a time constant of ~ 1.5 psec. These modulations are the spectral signature of vibrational coherence in the ground state of the parent ion, excited through Resonance Impulsive Stimulated Raman Scattering (RISRS)[9].

Results in Various Solvents

In order to appreciate the role played by the solvent in triiodide photochemical dynamics, similar transient transmission experiments were performed using water and a series of alcohols as solvents.

Transient transmission scans at 600 and 860 nm for short probe delays in a water solution of triiodide are depicted in Fig. 1. At first glance they look very similar to the results in ethanol, including the clear antiphased spectral modulations appearing after the initial fall off in absorption. However a comparison of transmission scans at a probing frequency near 600 nm in water, ethanol and

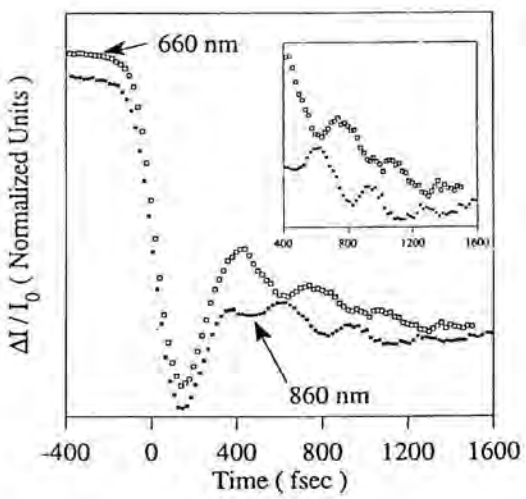

Fig. 1. Transient transmission data at early delay times for water solution at two wavelengths 600 and 880 nm. The inset depicts a portion of the data on an expanded scale.

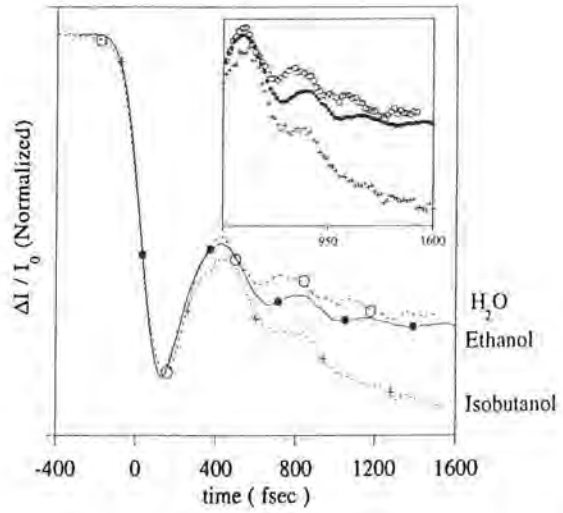

Fig. 2. Transient transmission data at short delays near 600 nm, for triiodide solutions in water, ethanol and isobutanol.

iso-butanol show substantial systematic difference, as shown in Fig. 2. The instantaneous rise and subsequent rapid fall in absorption are remarkably alike in all three solvents. In water the ensuing oscillations appear earlier and are most pronounced, are highest in frequency, and relax most slowly. In the heavier alcohol modulations appear later, and relax so rapidly that they are reduced to a single lobe. In this respect ethanol is intermediate between the two.

Marked solvent dependence is observed in the UV transients as well. In contrast to the observations in the visible, water solvent is almost twice as efficient as ethanol in dephasing RISRS induced coherence in the symmetric stretch of I_3^- as depicted in Fig. 3. Furthermore, the prominence of the primary and secondary phases of recombination are strongly solvent dependent as can be seen in Fig. 4. In solutions of heavier alcohols the rapid phase of bleach recovery is more substantial. In terms of caging, water is pathological, and behaves similarly to the heavy alcohols, exhibiting a prominent rapid phase of absorption recovery, which is extremely short in duration. This finding is in line with recent results of geminate recombination following I_2^- photodissociation[10].

The strong dependence of our observations upon the solvent provides enticing riddles concerning the dynamics of this reaction. Would we not expect a light and strongly interacting solvent such as water to be most efficient in dephasing vibronic coherences, regardless if they are made up of highly excited levels in nascent diiodide ions, or near the bottom of the I_3^- potential well? If so, is it possible that the solvent molecules can interfere so effectively as to mold vastly different vibrational distributions of the emerging I_2^-? It is reasonable that the spectral signature of bond fission is so similar in the studied solvents, and is the

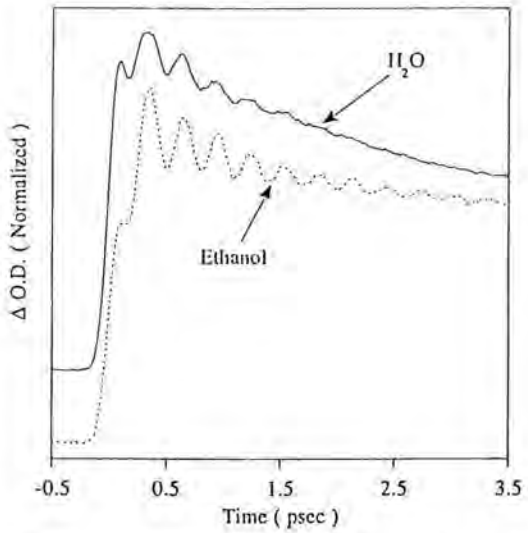

Fig. 3. Short delay transient transmission probing at 308 nm for water and ethanol solutions.

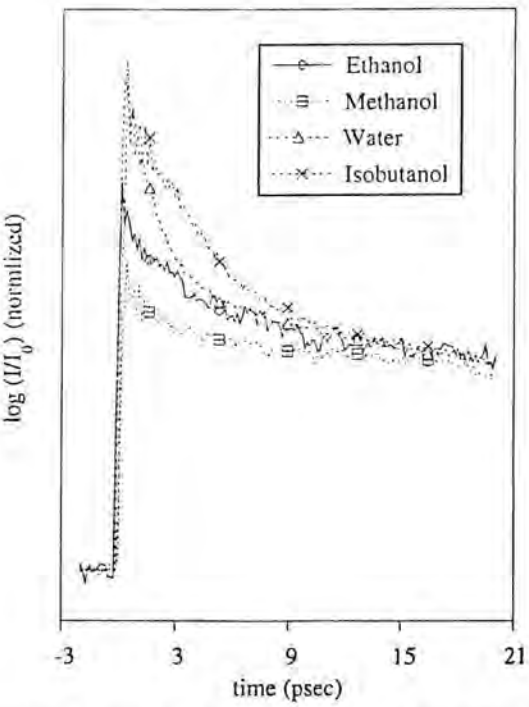

Fig. 4. Transient transmission data in the UV at long delays for triiodide solutions in a series of alcohols and in water.

timescale of ~200-250 fsec for the appearance of separated fragments a realistic time span? In order to begin sorting out these and other fundamental questions concerning the case study at hand, computer simulations were conducted, and are described in the next section.

Computer Simulations

In leu of a reliable model for the excited reactive multidimensional potential surface of I_3^-, a simple LEPS type surface was parametrized to at once fit the basic thermochemistry, and the known absorption spectrum of triiodide[11]. This surface reduces asymptotically to a Morse potential assigned to I_2^-, and is based on the working hypothesis that absorption into the upper band in triiodide leads predominantly to iodine atoms in their spin excited state. The parameters of the reactive surface are given in Table 1. Using this model for the upper state involved in photolysis, two different simulation schemes were run.

The first involved quantum simulations of isolated ion photodissociation performed using fourier wave packet propagation methods in a collinear two dimensional calculation[12]. The calculations are initiated by instantaneous promotion of the zeroth vibrational level of ground state triiodide onto the LEPS surface. The harmonic ground surface potential leads to a gaussian ground state wavefunction. Fig. 5 shows snapshots of the wavefunction at different times after the initial packet was placed on the excited surface. The initial motion is along the symmetric stretch. The striking feature is a large dispersion along the antisymmetric stretch exhibited by the wavefunction which is approximately 2 angstroms after 200 fsec. This dispersion eventually leads the wavefunction into the asymptotic channels with negligible amplitude into the three-body dissociation channel, although this channel is energetically allowed. Even before a detailed evaluation of these results begins, our conclusions concerning the assignment of the first ~300 fsec to the initial act of bond fission gains support. We see that the first 12,000 A.T.U. (300 fsec) go by before substantial 'filling' of the asymptotic exit channels begins.

In order to make sense of this complex wavefunction we have reduced the wavepacket in one dimension, and produced a histogram of $P(R)$, the probabil-

Table 1. Parameters for the I_3^- Potential Surfaces

ground state potential for I_3^-;	
$r_{(I\text{-}I)}^{eq} = 2.97$ Å	$\omega_{sym.} = 110\ cm^{-1}$ $\omega_{asym.} = 149\ cm^{-1}$
excited state potential for I_3^-; (LEPS potential)	
${}^1r^{eq} = 3.23$ Å	${}^3r^{eq} = 2.983$ Å
${}^1\beta = 1.16\ Å^{-1}$	${}^3\beta = 1.00\ Å^{-1}$
${}^1D = 1.1$ eV	${}^3D = 1.009$ eV

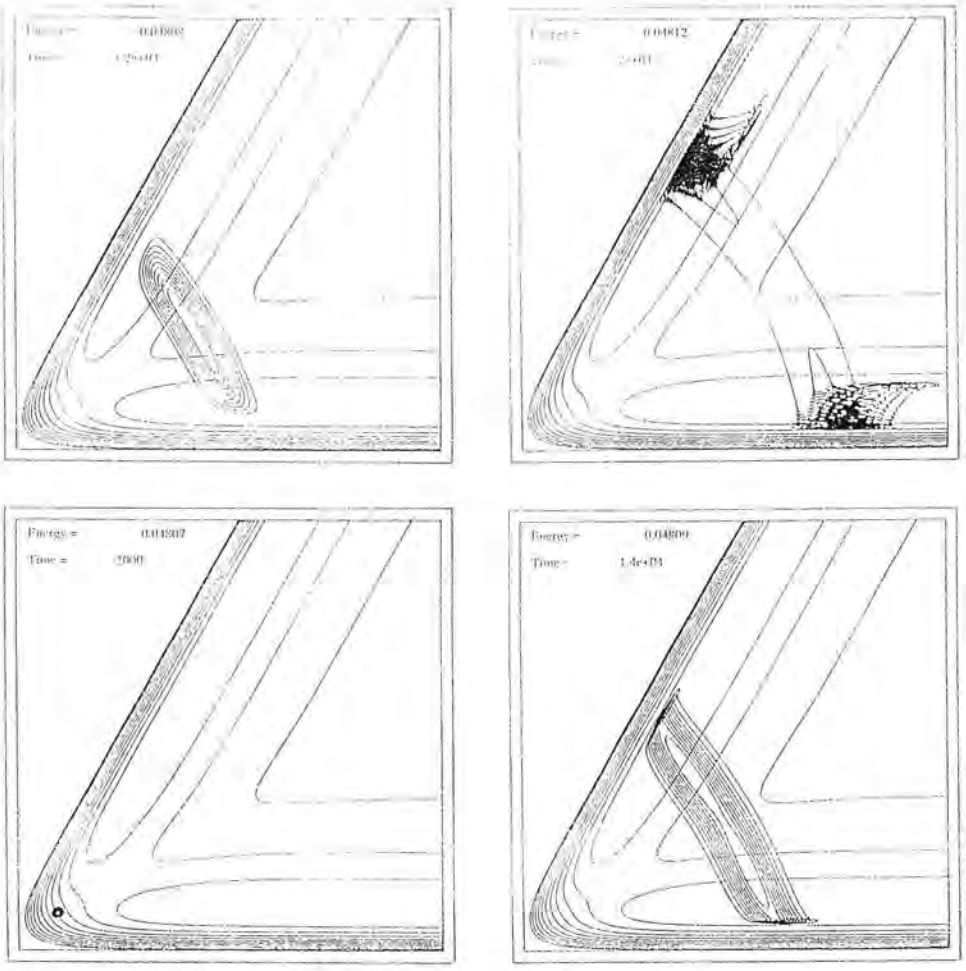

Fig. 5. A series of snapshots of the evolving wavepacket following instantaneous photoexcitation at $t = 0$. The wave function is depicted as contours connecting points where $|\psi^2|$ has equal values. Along with the wavefunction we have also depicted equipotential contours of the reactive LEPS potential.

ity for fragment diiodide ions to be distanced by internuclear radius R, at various delay times. This series of histograms is shown in Fig. 6. We see that in spite of the fact that 'late comers,' or those portions of the wavefunction that enter the dissociation channel after $t = 16{,}000$ are still entering the channel throughout the delays studied, the influx is steadily reduced. The portion of dissociating systems which entered directly at early times has already experienced an intramolecular 'collision,' and re-extended to the large radius turning point of the motion.

In order to evaluate the distribution of vibrational energies in the fragment

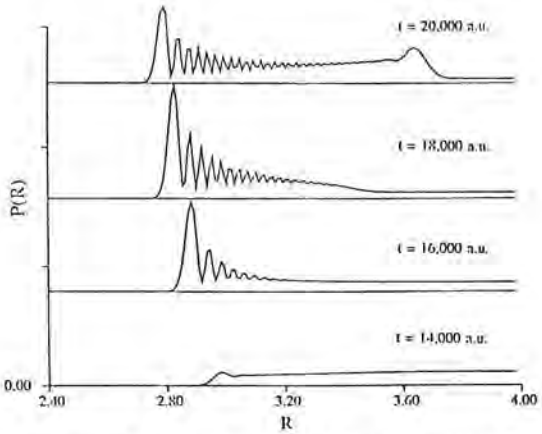

Fig. 6. An overlay of histograms depicting the probability of nascent diiodide fragments to be at a certain internuclear distance.

ions within the exit channel, the portion of the wavepacket described in Fig. 6 was resolved into eigenstates at two delays - at 14,000 and 20,000 A.T.U. These distributions are depicted in Fig. 7. We see that the population of fragment ions produced directly at early times produces a very wide distribution maximized at rather high quanta of $\sim v = 40$. The 'late comers' make a completely different contribution to the distribution which is very localized in vibronic eigenspace, with an acute maximum above $v = 42$. In either case the average portion of excess energy directed into vibration agrees very well with the prediction of 25% derived from kinematic considerations alone.

As stated above, the quantum simulations chart the course of dissociation for an isolated parent ion. While the results serve as an important reference, in order to deepen our understanding of the effects of solvation, a realistic solvent must be included in the simulation. For this purpose classical MD simulations

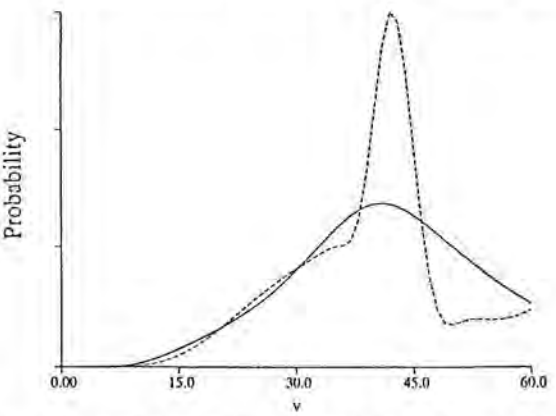

Fig. 7. A resolution into eigenstates of the portion of the wavefunction which has reached the exit channel at two delay times, 14,000 (solid line) and 20,000 (dashed line) A.T.U.

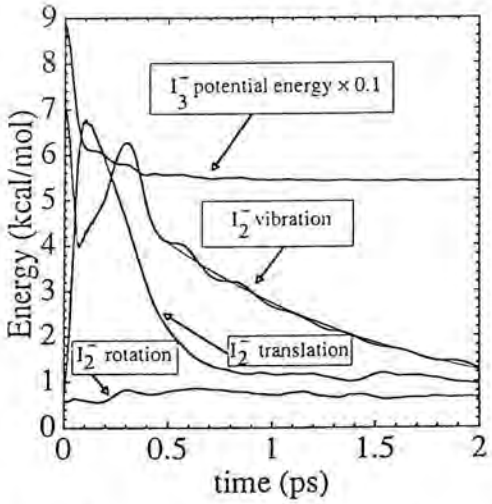

Fig. 8. The average time dependent energies of I_2^- products following photodissociation of triiodide in ethanol.

were conducted using the identical potential immersed in a model ethanol consisting of 216 solvent molecules[13]. Methyl and methylene groups were modeled as a united atom, and further details of the interparticular interactions are provided in our full report. Following instantaneous switching to the excited potential, trajectories were simulated for multiple initial configurations. The charges on the reacting ion are distributed according to a continuous charge switching function, which determines by the degree of asymmetry, which terminal iodine

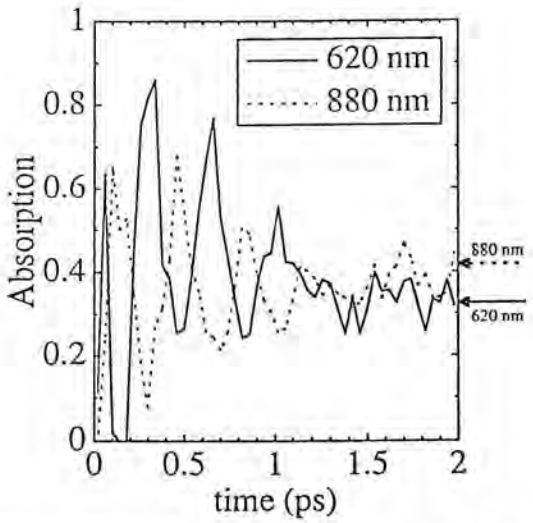

Fig. 9. MD simulated spectral intensities of I_2^- at 620 and 880 nm as a function of time.

atom is on its way to participating in an I_2^- bond. No curve crossing to the ground state, and therefore no caging effects are included at this stage.

The results of the MD calculations are depicted in Fig. 8. Very rapid solvent induced quenching of the translational and vibrational degrees of freedom in the daughter ions is manifest, the former within 250 fsec, the later on a picosecond timescale. At its peak, the distribution over the vibrational manifold reaches an average excess energy which is barely half that obtained in the isolated molecule quantum calculations. It is noteworthy that at this excess energy the vibrational frequency calculated from published vibronic constants for diiodide would be precisely that observed in the coherent oscillations following ethanol dissociation. Using a Franck Condon reflection procedure, the absorption intensity for transient probe pulses at 620 and 880 nm were calculated as a function of the delay time, and are presented in Fig. 9. The agreement with experiment is remarkable. Clear oscillations of opposed phase are observed, dephasing almost precisely on the same timescale as the experimental observable.

'TRISRS' Experiments

Before attempting integration of the above into a unified picture, we wish to relate one more experimental effort, in which impulsive Raman is for the first time employed as a transient vibrational spectroscopy in order to characterize the vibrational relaxation of nascent diiodide fragments in ethanol. Theoretical simulations of the RISRS process using wave packet propagation techniques indicate that in most situations, the coherent superposition in the ground state which is, for example, responsible for producing the spectral modulations observed in Fig. 3, involves coherent transfer of population to a limited number of levels surrounding those initially populated before the impulsive interaction with the laser pulse[9a, 14]. In view of this, as long as all the initially populated ground state levels can interact with the excitation pulse, the decay of the induced spectral modulations nearly mirrors the initial incoherent distribution of population in the ground state vibronic manifold.

Grossly speaking, through this spectroscopy one approximately records a free Raman induction decay of the vibrational distribution at the instant of the push excitation[15]. The duration of free induction decay defines the minimum time that a dynamic variable must be followed in order to reconstruct its power spectrum. Impulsive Raman spectroscopy is accordingly one of the most rapid methods for obtaining vibrational spectral information.

Above the overall narrowing of the product absorption band which follows the stage of coherence dephasing in the fragments, was assigned as the spectral signature of vibrational relaxation in the product ions. This stage is depicted in Fig. 10 at three probe frequencies. In order to obtain independent corroboration of this assignment, an additional method for directly probing the vibrational dynamics was deemed necessary. We have chosen to implement transient RISRS or TRISRS, with its characteristic high time resolution, in order to extract the

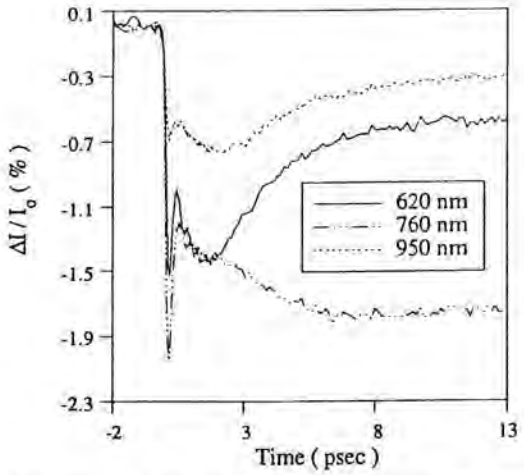

Fig. 10. Transient transmission data for triiodide in ethanol at three probe frequencies.

temporal evolution of the vibrational distribution. This involves a sequence of three ultrashort pulses. A primary photolyzing pulse in the UV initiates the triiodide dissociation. At a certain time after the photolysis which can be varied from one experiment to another, here forth denoted the push delay, a secondary intense 'push' pulse sets in motion ground state coherent vibration (in the nascent fragments!). The decay of the coherence is followed via periodic transmission modulations of a continuously delayed weak probing pulse.

TRISRS data were collected at three push delays, 2, 2.7 and 4 picoseconds after the excitation pulse. In order to clarify sequence of events, Fig. 11 depicts an overlay of two transient transmission scans probed at 840 nm, with and

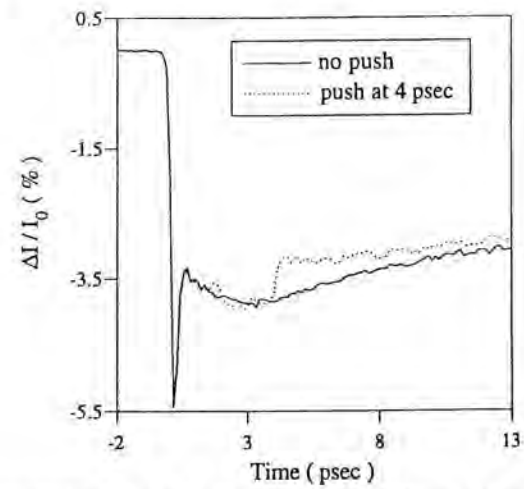

Fig. 11. Transient transmission data at 840 nm with and without the secondary TRISRS push interaction at a delay of 4 psec.

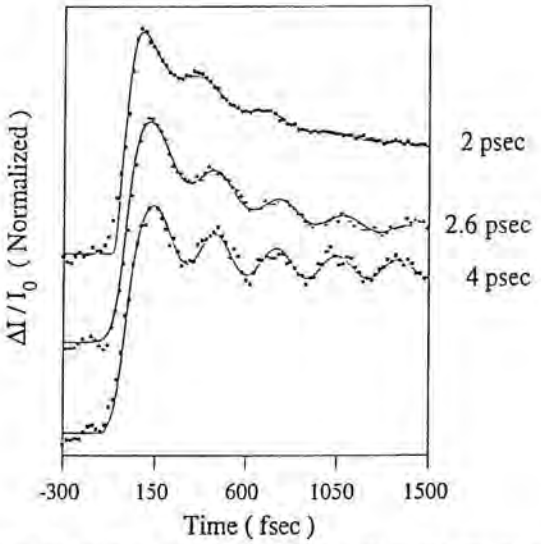

Fig. 12. TRISRS data recorded at three different push delays. Oscillations in transmission are fit to a convolved analytical response.

without the introduction of a push pulse. This second pulse introduces a substantial bleach which recovers to a certain degree but is not completely replenished at 13 picoseconds. The TRISRS bleaches at the three delays are shown in Fig. 12. The data for 2 picoseconds push delay involves probing at 680 nm, while results at later delays were obtained with an 840 nm probe pulse. The zero of time in Fig. 12 relates to the center of the pushing pulse in all three scans. At all these delays periodical oscillations of the transmission are observed. Figs generated by a nonlinear least squares method are depicted, after convolution with our instrument response, along with the data. The oscillatory feature was fit to the functional form $\sin(\omega t + \phi)\exp(e^{-t/\tau})$, and the best fit was afforded by parameters displayed in Table 2.

The first push delay immediately supersedes the decay of spectral oscillations due to bond fission, and the fragment distribution must be broad, involving highly excited vibrational levels. It may however have undergone substantial cooling since its inception about 200 fsec after the UV excitation. The mean vibrational quantum level of the coherent vibrations are experimentally and theoretically determined to be at $n \approx 20$[13,8]. Using the documented vibrational

Table 2

PUSH DELAY (psec)	ω (cm^{-1})	τ (psec)	ϕ (radians)
2.0	102 +/− 4	0.5 +/− 0.2	0.2 +/− 0.4
2.67	105 +/− 3	0.9 +/− 0.2	−1.2 +/− 0.4
4.0	112 +/− 2	1.2 +/− 0.3	−2.0 +/− 0.4

constants of I_2^-[16], the coherence frequency of 102-103 cm^{-1} indicates that the earliest TRISRS induced superposition is made up of levels centered around $n \approx 13$. The ultrafast rate of coherence dephasing (~ 500 fsec) at this push delay cannot be due to anharmonicity alone, and must involve substantial homogeneous contributions such as pure dephasing and population relaxation. Inhomogeneity of the solvent following the violent act of bond fission may also contribute to rapid vibrational dephasing.

As the push delay is increased, the population of fragment ions has relaxed further, leading to a reduction of both the first and second moments of the vibrational distribution. Accordingly, the frequency and the timescale of RISRS coherence dephasing should increase. The frequency will increase due to the larger level spacings closer to the bottom of the potential well. The dephasing is prolonged because of a reduction in the rate of pure dephasing at low v levels[17], and a reduced contribution of anharmonicity which is proportional to $\omega_e\chi_e$ times the second moment of the distribution. These trends are in fact observed. Within 4 psec of push delay, the modulations have already reached the asymptotic vibrational frequency, within our experimental error. The accumulating evidence from this experiment, along with the previous transient transmission data, show clearly that the highly vibrationally excited population of diiodide ions does in fact lose most of its excess vibrational energy within a few picoseconds. This finding agrees with a growing body of work on vibrational relaxation of molecular ions in polar solvents[18, 10].

Discussion

Solvation plays a major role in the reaction studied, as attested to both by simulations and experiments. In the simulation of isolated triiodide dissociation the excess vibrational energy deposited in the diiodide fragment is much higher than is expected by any of the criteria we have previously discussed, such as the frequency of the spontaneous coherence, or the breadth of the absorption spectrum in nascent diiodide. This is not surprising since we have not included the influence of the solvent. It is however tempting to speculate how the seemingly distinct two populations, the 'early and latecomers' should fare upon encounter with the solvation layer. The MD simulations demonstrate that by far the most rapidly dephased and dissipated motion in solution will be fragment translation[19]. The population which decides early on which pair of iodine nuclei will be diiodide, will from that point on vibrationally evolve relatively independently of the solvent. These early-comers will therefore behave similarly if not identically in gas phase and solution with respect to vibrational coherence.

The late comers in contrast continue to evolve along the symmetric stretch coordinate as if all intramolecular motion were translation. This should lead to an all and all crash of the system into the solvent shell, leading to extensive energy transfer and dephasing of this portion of the wavefunction, which in our isolated ion model forays deep into the region of three atom separation, before settling into a two body dissociation. For this reason we believe that upon solva-

tion any coherence in vibration must be due predominantly to the early formed diiodide ions, and the more delayed dissociation should produce relatively cold and dephased fragments.

The MD simulations definitively show that the solvent can absorb large amounts of excess energy from the reaction in very short times, and mold the coherent portion of the vibrational distribution into a sufficiently compact packet in order to reproduce the observed oscillations. A more polar and rapidly responding solvents will at once accept larger amounts of excess vibration during the early stages of bond fission, and stabilize the breaking of symmetry along this initial track, thereby assisting the decision of 'who will become the molecular fragment.' This may well explain why water leads to such high frequency and slowly dephasing fragment coherences, indicating a lower excess energy content and a narrower distribution of vibrational energies in the products. This notion is further supported by the TRISRS results which vividly demonstrate the profound dependence of the dephasing rate on the excess vibrational energy content.

That the very initial stages of photolysis may be relatively insensitive to solvation, and resemble that in the isolated species, is not surprising. The question is when the presence of the solvent will begin to have impact on the spectroscopy, one which will be answerable only when good images of the higher excited states triiodide to which absorption takes place at short delay times are available. Our simulations do, as stated, support our estimates for the appearance of free fragments.

Finally the issue of caging needs further consideration. Our simulations can not guide us on this issue. The importance of mass in the alcohol series in inducing direct recombination portrays a ballistic image of this process. However the case of water demonstrates that this need not always be the case, and that when sufficiently strong interactions between solvent molecules prevail, the strongly knit solvent shell can take a beating even though the individual solvent particles are lightweight. Only further solvent studies will determine if in fact water is singularly unique in this respect.

Preliminary results on $Cr(C_6H_6)(CO)_3$

Up to this point our discussion has involved impulsively induced periodically evolving vibrational coherences in the photo reactant ground state, and in photochemical product states as well.

In the following case we believe that during the first few hundred femtoseconds following photoexcitation of $Cr(C_6H_6)(CO)_3$ in ethylene glycol solution, oscillations due to vibrational coherence in a metastable reactive state are detected.

The primary photochemical event of this complex has been studied, and shown to consist exclusively of carbonyl loss followed mainly by ligand replacement or recombination[20]. The strong band into which we pump at 308 nm, is

assigned as a metal to benzene charge transfer transition. We have conducted a series of transient transmission measurements in analogy with those reported for the triiodide system.

Throughout the visible and near infrared portion of the spectrum an instantaneous rise of absorption is observed, followed by an absorption decay to a nonzero value with a time constant of 1 psec. At very early times a faint oscillatory feature is observed. A representative scan probing at 740 nm is depicted in Fig. 13, along with a best fit. The fitting procedure indicates that the rapidly damped oscillation is best represented as a $160 +/- 15\ cm^{-1}$ vibration, decaying extremely rapidly, with a 120 fsec time constant. In order to test whether we are directly observing a photochemical product or, at least initially, the reactive excited state, simultaneously optical Kerr effect scans where run in a 150 micron thick quartz flat. The rise in absorption is displayed along with the relevant Kerr scan in Fig. 14. To within our experimental error, the zero of time or maximum in pump and probe overlap, is symmetrically situated with respect to the rise. Simulations show that only a dissociation process which induces an exponential rise in the spectrum, with $\tau \sim 10$ fsec, would elude detection in our measurement.

Therefore we tentatively assign the observed absorption and oscillations to the initially excited state, and the 1 psec decay to the act of carbonyl loss. This interpretation is contrary to findings in earlier work on metal hexacarbonyls where the carbonyl ligand was found to dissociate directly[21]. If our assignment is correct, the process of bond fission may require electronic relaxation to low lying ligand field excited states eluded to in the literature[20]. Determining the precise shift in equilibrium structure which gives rise to the observed oscillations will require more work. Bending motions of the benzene-metal-CO system fall

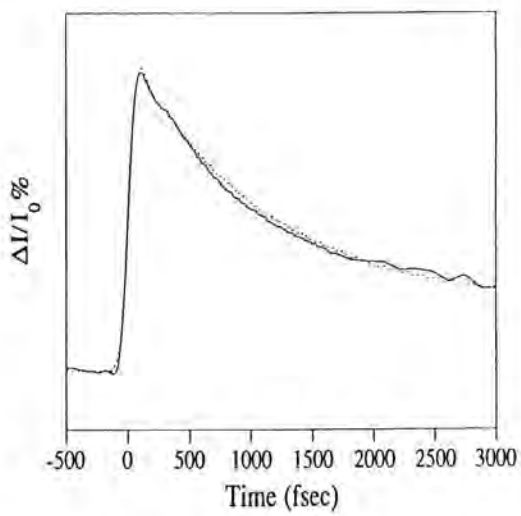

Fig. 13. Transient transmission data of $Cr(C_6H_6)(CO)_3$ at 740 nm, along with best fit.

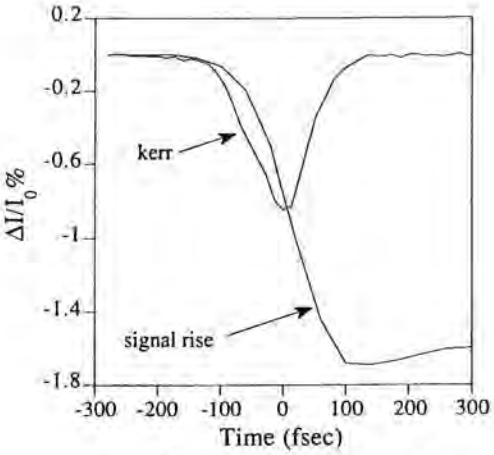

Fig. 14. Rise of the transmission data depicted in the previous figure, along with optical Kerr data.

within this frequency range in the ground state[22]. For this coordinate to be preferentially active would require a Jahn-Teller type symmetry braking in the excited states. Work is ongoing to increase our appreciation of these points.

Conclusion

In this report we have described the application of impulsive photoexcitation on the femtosecond time scale in order to study detailed chemical dynamics of small molecular species in solution. We have demonstrated how monitoring of coherent nuclear motions so induced in ground, excited, and product electronic states, provides new insight into the microscopic mechanisms of solution photochemistry, and allows us to comprehensively characterize the course of photochemical evolution. In particular we have demonstrated the experimental feasibility of the TRISRS scheme, and applied it to measure the vibrational dynamics of rapidly relaxing diiodide ions.

Acknowledgement

We thank Dr. E. Mastov for technical assistance. This work was supported by the Israel Science Foundation of the Israeli Academy of Sciences, by the Israel-US Binational Science Foundation, and by the German Israeli James Frank program for laser matter interactions. The Farkas and F. Haber Centers are supported by the Bundesministerium für die Forschung, and the Minerva Gesellschaft für die Forschung. I.B. thanks the US national science foundation for support.

References

1. Hynes, J.T., in *The Theory of Chemical Reaction Dynamics*, M. Bear Ed., Vol. IV, CRC press, 1988.
2. Martin, J.L., Migus, A., Mourou, G.A., and Zewail, A.H., Ed., *Ultrafast Phenomena VIII*, Springer Verlag, 1992.
3. a) Markovich, G., Giniger, R., Levin, M., and Cheshnovsky, O., *J. Chem. Phys.* **95**, 9416, 1991.
   b) Wei, S., Shi, Z., and Castelman, A.W., *J. Chem. Phys.* **94**, 3268, 1991, Castelman, A.W., and Keese, R.G., *Chem. Rev.* **86**, 589, 1986.
   c) Perera, L., and Berkowitz, M.L., *J. Chem. Phys.* **95**, 5793, 1991.
   d) Myers, A.B., and Markel, F., *Chem. Phys.* **149**, 21, 1990.
   e) Bopp, P., in *The Physics and Chemistry of Aqueous Ionic Solutions*, M.C. Bellissent, and G.W. Neilson, Eds., Reidel 1987.
5. a) Gertner, J., Whitnell, R.M., Wilson, K.R., and Hynes, J.T., *JACS* **113**, 74, 1991.
   b) Ben-nun, M., and Levine, R.D., *J. Phys. Chem.* **96**, 1523, 1992.
   c) Harris, C.B., Smith, D.E., and Russell, D.J., *Chem. Rev.* **90**, 481, 1990.
6. Lenderink, E., Dupen, K., and Wiersma, D.A., *Chem. Phys. Lett.* **194**, 403, 1992.
7. a) Zewail, A.H., *Farad. Discuss. Chem. Soc.* **91**, 207, 1991, references therein.
   b) Scherer, N.F., Ziegler, L.D., and Fleming, G.R., *J. Chem. Phys.* **96**, 5544, 1992.
8. Banin, U., and Ruhman, S., *J. Chem. Phys.* **98**, 4391, 1993; Banin, U., Kosloff, R., and Ruhman, S., *Israel J. Chem.*, in press.
9. a) Hartke, B., Kosloff, R., and Ruhman, S., *Chem. Phys. Lett.* **158**, 238, 1988.
   b) Pollard, W.T., and Mathis, R.A., *Ann. Rev. Phys. Chem.* **43**, 497, 1992.
   c) Yan, Y.-X., Cheng, L.T., and Nelson, K.A., in *Advance in Nonlinear Spectoscopy*, R.G.H. Clarke, R.E. Hester, Wiley, New York, 1987.
   d) Chesnoy, J., and Mokhtari, A., *Phys. Rev. A* **38**, 3566, 1988.
   e) Walmsley, I.A., Wise, F.W., and Tang, C.L., *Chem. Phys. Lett.* **154**, 315, 1989.
   f) Ruhman, S., and Kosloff, R., *J. Opt. Soc. Am. B.* **7**, 1748, 1990.
   g) Baumert, T., Engel, V., Rottgermann, C., Strunz, W.T., and Gerber, G., *Chem. Phys. Lett.* **191**, 639, 1992.
10. a) Kliner, D.A.V., Alfano, J.C., and Barbara, P.F., *J. Chem. Phys.* **98**, 5375, 1993.
    b) Papanikolas, J.M., Vorsa, V., Nadal, M.E., Campagnola, P.J., Gord, J.R., and Lineberger, W.C., *J. Chem. Phys.* **97**, 7002, 1992.
11. Levine, R.D., and Bernstein, R.B., in *Molecular Reaction Dynamics and Chemical Reactivity*, (New York, Oxford Univerity Press, 1987).
12. Kosloff, R., and Tal-Ezer, H., *Chem. Phys. Lett.* **127**, 223, 1986; Kosloff, R., *J. Phys. Chem.* **92**, 2087, 1988.
13. Benjamin, I., Banin, U., and Ruhman, S., *J. Chem. Phys.*, in press.

14. Banin, U., Bartana, A., Kosloff, R., and Ruhman, S., in preparation.
15. Dexheimer, S.L., Wang, Q., Peteanu, L.A., Pollard, W.T., Mathies, R.A., and Shanck, C.V., *Chem. Phys. Lett.* **188**, 61, 1992.
16. Tripathi, G.N.R., Schuler, R.H., and Fessenden, R.W., *Chem. Phys. Lett.* **113**, 563, 1985.
17. Kosloff, R., and Rice, S.A., *J. Chem. Phys.* **72**, 4591, 1980.
18. Li, M., Owrutsky, J., Sarisky, M., Culver, J.P., Yodh, A., and Hochstrasser, R.M., *J. Chem. Phys.* **98**, 5499, 1993.
19. Benjamin, I., and Wilson, K.R., *J. Chem. Phys.* **90**, 4176, 1989.
20. Geoffrey, G.L., and Wrighton, M.S., *Organometalic Photochemistry*, Academic Press, 1979, and references therein.
21. Joly, A.G., and Nelson, K.A., *Chem. Phys* **152**, 69, 1991.
22. Chhor, K., and Lucazeau, G., *J. Raman Spect.* **13**, 235, 1982.

Author's Address

U. Banin, S. Ruhman and A. Waldmann; The Department of Physical Chemistry, and the Farkas center for light-induced processes, the Hebrew University, Givat Ram, Jerusalem, 91904 Israel.
R. Kosloff; The Department of Physical Chemistry, and the Fritz Haber center for Chemical Reaction Dynamics, the Hebrew University, Givat Ram, Jerusalem, 91904 Israel.
I. Benjamin; Department of Chemistry, the University of California, Santa Cruz, CA 95064.

Y. Kimura, Joseph C. Alfano, P.K. Walhout and Paul F. Barbara

Ultrafast Dynamics of the Solvated Electron and I_2^- in Polar Solvents

Abstract

The ultrafast dynamics of the solvated electrons and I_2^- have been investigated in polar solvents. The internal conversion, geminate recombination, and vibrational relaxation down the top 70% of the potential of I_2^- in water are complete within the instrumental time resolution (<0.3 ps). Vibrational relaxation at the bottom of the potential occurs with a time constant of ~ 3 ps. Formation of solvated electrons was observed during these experiments and their dynamics studied. A kinetic model reproduced the observed spectral dynamics, yielding an excited state lifetime of 310 ± 80 fs and a 1.1 ± 0.2 ps timescale for ground state cooling and solvation. The excited *p*-state absorption spectrum was red-shifted from that of the ground state, peaking at wavelengths longer than 1060 nm, in agreement with previous work.

I. Introduction

Reaction dynamics of charged species in polar solvents is a fascinating area of study, owing to the strong electrostatic coupling between the solute and solvent bath. Recent experimental (Banin and Ruhman, 1993; Kliner et al., 1993; Li et al., 1993; Papanikolas et al., 1992) and theoretical (Benjamin and Whitnell, 1993; Whitnell et al., 1992) studies suggest that the efficiency of vibrational relaxation is sensitive to the magnitude of electrostatic interactions between the solute and solvent. The accelerated vibrational relaxation of charged species in polar solvents is believed to result from the long-range coulombic interaction between solute and solvent. This is seen in the vibrational relaxation of I_2^- in ethanol (Kliner et al.,1993) which is much faster than the relaxation time for the corresponding neutral species (Harris et al., 1988).

Solute-solvent electrostatic interactions are also believed to play an important role in the relaxation of excited excess electrons. Excess electrons are a primary photoproduct in aqueous pulse radiolysis experiments, and play an important role in the complicated radiation chemistry of water. Solvated electrons also are important in solution photochemistry and photoelectrochemistry.

Time-resolved dynamical studies of electron localization and solvation follow-

ing electron ejection in bulk water by multiphoton ionization revealed the existence of a presolvated precursor species having a red-shifted IR absorption band which evolved to the equilibrated aqueous electron spectrum on a sub-picosecond timescale (Long et al., 1990; Migus et al., 1987). This IR absorbing precursor was proposed to be the lowest excited state of the aqueous electron, known as the '*p*-state' (Long et al., 1990; Rossky and Schnitker, 1988). The lifetime of the excited *p*-state was reported as 240 fs (Migus et al., 1987) and 540 ± 50 fs (Long et al., 1990). This 'two-state' model was successful in reproducing the experimental data.

The aqueous solvated electron has been subject to a wide range of theoretical investigations. Adiabatic simulations have probed the dynamics of electron solvation following injection of an excess electron into a solvent cavity (Rossky and Schnitker, 1988) or sudden change in electronic state of the electron (Barnett et al., 1989). These studies show electron solvation in water to proceed on two timescales — an 'inertial' component which occurs on a 20-30 fs timescale and accomplishes most of the solvation, and a second, slower component occurring on a 200-500 fs timescale.

Finally, non-adiabatic MD simulations have probed the nature of the excited state relaxation. The non-adiabatic relaxation and solvation of an electron was investigated using both classical rigid SPC water and flexible SPC water, yielding an excited state lifetime of ~ 1 ps and 164 fs respectively (Webster et al., 1991; Murphrey and Rossky, 1993). Ground state solvation was again observed to occur with two timescales - a fast inertial component and a slower 200 fs component. Finally, the non-radiative rate for the equilibrated *p*-state was evaluated using a Golden-Rule expression (Neria et al., 1991), giving an excited state lifetime of ~ 120 fs for water.

In this paper, we report recent experiments examining vibrational relaxation of I_2^- in water. Vibrational relaxation at the top of the vibrational manifold is extraordinarily fast, while relaxation at the bottom of the well occurs with a ~ 3 ps timescale. Additionally, we present results of direct IR pump-probe spectroscopy on the solvated electron, which yields an excited state lifetime of 310 ± 80 fs, a ground state cooling time of 1.1 ± 0.2 ps, and an excited state absorption spectrum characterized by a broad red-shifted absorption band peaking in the infrared region.

II. Experimental

The ultrafast transient absorption spectrometer used in these experiments has been described in detail elsewhere (Kliner et al., 1993). An Ar^+-pumped Ti:sapphire oscillator produced pulses of ~ 90 fs duration, which were amplified using the technique of chirped pulse amplification (Salin et al., 1991). In this technique, the 90 fs oscillator pulses were temporally lengthened to ~ 130 ps in a grating stretcher and amplified in a Nd:YLF-pumped (527 nm, 6 W, 300 ns, 2 KHz) Ti:sapphire regenerative amplifier. After amplification the cavity-dum-

ped pulses were temporally recompressed with a grating pair to yield pulses of 130 fs duration, centered at 780 nm, with an energy of 200 μJ at a repetition rate of 2 kHz.

About 45% of the amplified output pulse was separated and frequency doubled to produce the UV synthesis pulse (390 nm, 30 μJ) which was used to generate solvated electrons via either multiphoton ionization of the neat solvent or electron photodetachment of aqueous iodide anions. After a 4.4 ns delay, a 780 nm pump pulse (25 μJ) was used to excite the excess electrons or I_2^- to the excited state. After a variable time delay (0-100 ps) a probe pulse (540-1060 nm) interrogated the system.

III. Results

Fig. 1a shows a pump-probe absorption transient of I_2^- in water. The transient contains contributions from both I_2^- species as well as spectral contamination from solvated electrons. The UV synthesis pulse generates excess electrons by multiphoton ionization of water (or photodetachment of I^-), and the 780 nm pump pulse promotes the electrons to an excited '*p*'-state whose temporal evolution is shown in Fig. 1d. Acid solutions were used to circumvent this problem. Protons scavenge excess electrons via the process

$$H_3O^+ + e^- \rightarrow H_2O + H$$

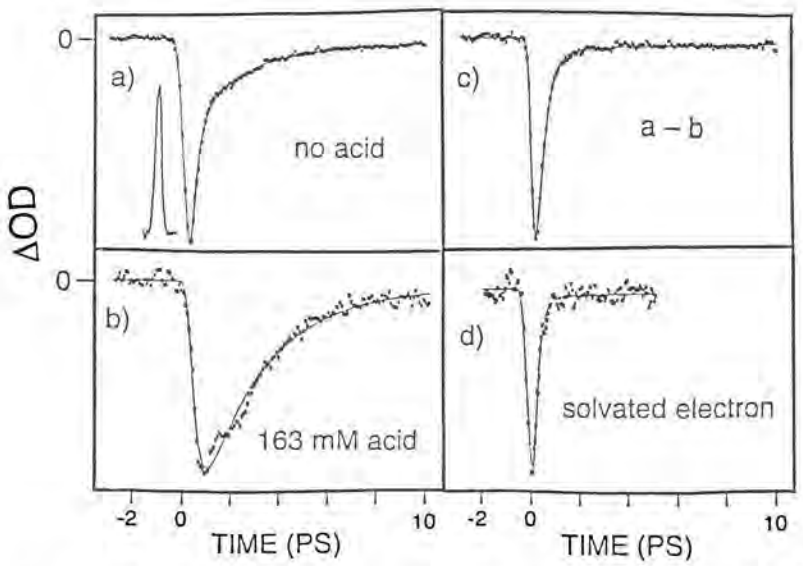

Fig. 1. Pump-probe absorption transients in water at 720 nm. a) I_2^- with no acid. b) I_2^- with 163 mM $HClO_4$. c) Change in transient signals caused by addition of the acid., i.e. transient 1a-transient 1b. d) Neat water. The instrument response function is 0.3 ps FWHM and is shown in Fig. 1a.

A transient obtained with a solution of 3 nm I_2 and 5 mM KI which is 160 mM in $HClO_4$ is seen in Fig. 1b. At this concentration of $HClO_4$, approximately >99.99% of the excess electrons are scavenged in the ~4.4 ns delay between the synthesis and pump pulses. Fig. 1c shows the difference transient obtained by subtracting Fig. 1b from Fig. 1a, which illustrates the change in the absorption transient caused by the acid quencher. The transient in Fig. 1c is identical to that of the aqueous solvated electron (Fig. 1d), confirming that the net effect of the acid is to remove solvated electron contamination from the I_2^- spectrum.

Pump-probe absorption transiens of solvated electrons in 50 mM aqueous solution of KI are shown in Fig. 2. Transients on the blue edge of the ground state absorption band show an instrument-limited reduction in optical density, or bleach, followed by bleach recovery having a fast component with most of the amplitude and a slower picosecond component. The transients on the red edge of the absorption band show an instrument-limited *increase* in optical density, followed by decay on several timescales. Absorption transients probing at the intermediate spectral region show nonmonotonic behavior, having a bleach at early times, followed by bleach recovery which overshoots to yield a transient increased absorption.

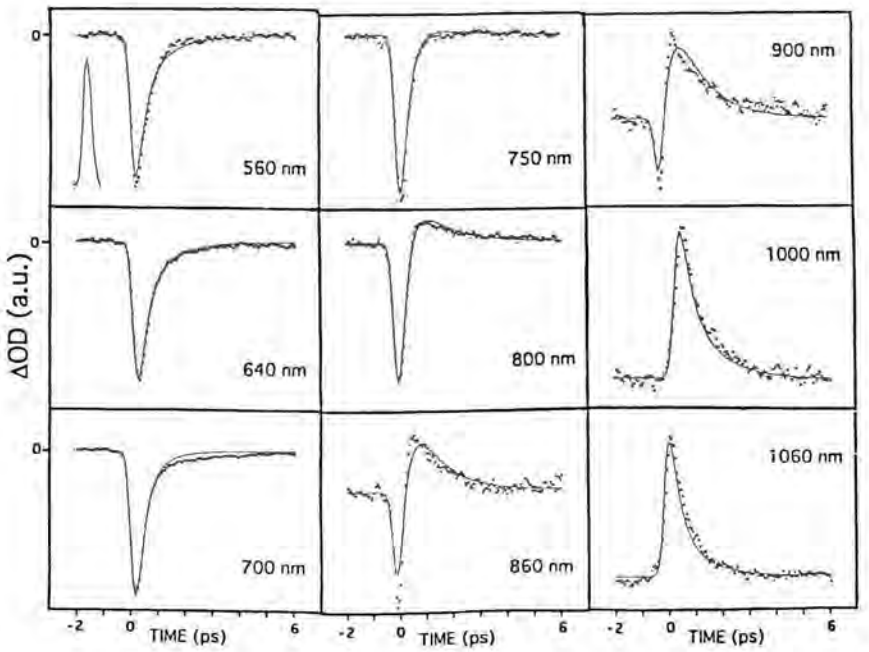

Fig. 2. Transient absorption spectra of the solvated electron in aqueous 50 mM KI solutions. The solid lines show the best fit of the photodynamic model.

IV. Modeling of Dynamics

a. I_2^- Dynamics

Previous modeling of I_2^- has shown that for $t < 1.5$ ps, the change in optical density for wavelengths near the ground state absorption maximum is proportional to the excess average vibrational energy (Kliner et al., 1993). Thus the absorption transient at 720 nm in water (Fig. 1b) can be used to estimate the vibrational relaxation time near the bottom of the well. Such a procedure results in a value of ~ 3 ps for the vibrational relaxation time of I_2^- in water ($v \leqslant 20$). This value of ~ 3 ps is very similar to, but slightly faster than, the value of ~ 4 ps for I_2^- in ethanol.

b. Solvated Electron Dynamics

Previous experiments successfully modeled their data using a strictly two-state model, neglecting the spectral effects of solvation and solvent heating. For our data this model predicts that all transients should show the identical temporal behavior. Thus, the transient bleach recovery obtained probing at all wavelengths on the blue edge of the absorption band should be equal to the timescale of the transient increased absorption decay on the red-edge of the absorption band. The wavelength where the ground and excited state absorption bands cross should act as an isosbestic point, with no dynamical behavior at this probe wavelength. Finally, all observed spectral dynamics should be monotonic.

The predictions of this two-state model are not in accord with our observations. We have thus modified the strictly two-state model to incorporate transient solvation and local heating following the electronic relaxation. The kinetic model is

$$e^-_{s\text{-state}} \xrightarrow{h\nu} e^-_{p\text{-state}} \xrightarrow{k_1} e^{-*}_{s\text{-state}} \xrightarrow[\text{continuous shift}]{k_2} e^-_{s\text{-state}}$$

where $e^{-*}_{s\text{-state}}$ represents a ground state electron which is not fully solvated and/or has a sudden increase in the local temperature of the surrounding solvent environment. This model assumes that solvation in the excited state plays no role in the spectral dynamics. While this is not strictly true, MD simulations show the excited state to be much less sensitive to transient solvation effects than the ground state (Barnett et al., 1989). Additionally this model assumes only a single rate for the electronic relaxation. Finally, the effects of site-selection, or 'hole burning,' are neglected in this model.

In order to simulate the spectral dynamics with this model, the absorption spectrum of each species in the model must be known. The absorption spectrum of the equilibrated ground-state electron $e^-_{s\text{-state}}$ is well known. The excited *p*-state absorption spectrum was an adjustable parameter, varied to match the experimental transients. The spectroscopic character of the desolvated and/or hot electron, $e^{-*}_{s\text{-state}}$, is somewhat arbitrary. Both transient desolvation and local heating

produce a red-shift in the absorption maximum relative to the equilibrated ground-state. Consequently we group these two effects together and characterize the electron as having an effective temperature T after the internal conversion to the ground state which cools exponentially with a time constant τ_s:

$$T(t, t') = T_e + \Delta T \exp[(t - t')/\tau_s]$$

where ΔT is the effective temperature increase immediately after electronic relaxation and T_e is the equilibrium temperature. An electron with an effective temperature T is assumed to have the same absorption spectrum as an electron in water with an equilibrium temperature T. The absorption spectrum of the aqueous electron at various temperatures has been tabulated (Jou and Freeman, 1979).

The nine absorption transients shown in Fig. 2 were globally fit to this model. The values of the excited state lifetime, τ_s, and ΔT were globally used for all nine transients, while the excited state extinction coefficient was independently varied at each wavelength. The excited state lifetime was 310 ± 80 fs, in agreement with previously measured values of 240 fs (Migus et al., 1987) and 540 ± 50 fs (Long et al., 1990). The value of the ground state solvation and cooling time, τ_s, was 1.1 ± 0.2 ps. This time constant is on the order of the timescale for thermal dissociation of hydrogen bonds in water ($\sim 0{,}5$ ps) and is comparable to the population relaxation time of vibrationally excited water with excitation in the $-$OH stretching mode (0.5-8 ps). The effective local temperature increase, ΔT, was determined as 34 ± 10 K. The resulting excited state absorption spectrum is strongly red-shifted relative to the ground state absorption, peaking at wavelengths longer than 1060 nm.

It should be mentioned that the results of this model are also consistent with an ultrafast (< 50 fs) electronic relaxation followed by fast ground state solvation and cooling on a 310 fs timescale. This interpretation would account for our observed lack of a theoretically predicted isotope effect since the electronic radiationless transition would not be observable with our instrumental resolution.

V. Comparison with Previous Work

The measured vibrational relaxation times of I_2^- at the bottom of the well are ~ 3 ps and ~ 4 ps for water and ethanol, respectively. These times are much faster than the relaxation times of typical neutral species. As a benchmark, vibrational relaxation of neutral I_2 in the ground electronic state occurs with a time constant of 50-200 ps in non-polar molecular solvents, with vibrational relaxation in the excited state being faster (Harris et al., 1988).

For the excess electron, both adiabatic and non-adiabatic MD simulations predict that after internal conversion, the ground state energy and corresponding spectral dynamics should evolve on two timescales — a fast inertial component, and a slower, 200-500 fs component (Barnett et al., 1989; Murphrey and

Rossky, 1993; Rossky and Schnitker, 1988; Webster et al., 1991). We are likely observing the slower timescale ground state transient solvation. The discrepancy of the measured 1.1 ± 0.2 ps time constant for ground state relaxation and both these MD simulations and the solvation time of water reflects the fact that cooling of the locally hot solvent is also occurring on a similar timescale, making separation of these two effects difficult.

The role of solvation and local heating in the observed spectral dynamics is a notable discrepancy between our three pulse, IR-pump data and the previous two pulse, UV-pump experiments. The data from the previous UV-pump work can be quantitatively modeled using a strictly two-state model. Conversely, our IR-pump transients cannot be successfully modeled without including the effects of ground state transient solvation and local heating. In the UV-pump studies, signal levels are governed by the magnitude of the extinction coefficient of the ground and excited states at the probe wavelength. Thus, the spectral manifestations of ground state solvation and local heating would be observed as small changes in optical density on top of a large signal due to ground state absorption, and are of minor importance. In the three pulse, IR-pump experiments presented here, the signal levels are governed by the *difference* in extinction coefficients between the ground and excited states. Thus, in the spectral region where the ground and excited states have similar absorption intensities (850-900 nm) the overall signal levels due to the two-state electronic relaxation are small, and would be zero in a rigorously two-state model. In this spectral region, processes which cause a breakdown in the two-state model become very noticeable.

Thus our IR-pump transients and the previous UV-pump experiments provide complementary information. The UV-pump experiments are sensitive to both the trapping and localization of electrons in the conduction band and to recombination of the electron-hole pair, two important processes of which our data provide no information. Conversely, our IR-pump experiments are very sensitive to ground state dynamics following electronic relaxation and can probe the transient solvation and cooling of locally hot solvent molecules after the internal conversion. Thus the IR-pump data presented here combined with previous UV-pump experiments and MD simulations can work together toward a global picture of the dynamics of excess electrons.

Acknowledgments

We acknowledge the support of the NSF. Y.K. and P.F.B. acknowledge Prof. N. Hirota for his support.

References

Banin, U., and Ruhman, S., Ultrafast Photodissociation of I_3^- : Coherent Photochemistry in Solution. In: *J. Chem. Phys.* **98**, 4391-4403, 1993.

Barnett, R.B., Landman, U., and Nitzan, A., Relaxation Dynamics Following Transitions of Solvated Electrons. In: *J. Chem. Phys.* **90**, 4413-4422, 1989.

Benjamin, I, and Whitnell, R.M., Vibrational Relaxation of I_2^- in Water and Ethanol: Molecular Dynamics Simulation. In: *Chem. Phys. Lett.* **204**, 45-52, 1993.

Harris, A.L., Brown, J.K., and Harris, C.B., The Nature of Simple Photodissociation Reactions in Liquids on Ultrafast Timescales. In: *Ann. Rev. Phys. Chem.* **39**, 341-366, 1988.

Jou, F., and Freeman, G.R., Temperature and Isotope Effects on the Shape of Absorption Spectrum of Solvated Electrons in Water. In: *J. Phys. Chem.* **83**, 2383-2387, 1979.

Kliner, D.A.V., Alfano, J.C., and Barbara, P.F., Photodissociation and Vibrational Relaxation of I_2^- in Ethanol. In: *J. Chem. Phys.* **98**, 5375-5389, 1993.

Li, M., Owrutsky, J., Sarisky, M., Culver, J. P., Yodh, Y., and Hochstrasser, R.M., Vibrational and Rotational Relaxation Times of Solvated Molecular Ions. In: *J. Chem. Phys.* **98**, 5499-5507, 1993.

Long, F., Lu, H., and Eisenthal, K.B., Femtosecond Studies of the Presolvated Electron: an Excited State of the Solvated Electron. In: *Phys. Rev. Lett.* **64**, 1469-1472, 1990.

Migus, A, Gaudel, Y., Martin, J.L., and Antonetti, A., Excess Electrons in Liquid Water: First Evidence of a Prehydrated State with Femtosecond Lifetime. In: *Phys. Rev. Lett.* **58**, 1559-1562, 1987.

Murphrey, T.H., and Rossky, P.J., The Role of Solvent Intramolecular Modes in Excess Electron Dynamics. In: *J. Chem. Phys.*, submitted, 1993.

Neria, E., Nitzan, A., Barnett, R.B., and Landman, U., Quantum Dynamical Simulations of Nonadiabatic Process: Solvation Dynamics of the Hydrated Electron. In: *Phys. Rev. Lett.* **67**, 1011-1014.

Papanikolas, J.M., Vorsa, V., Nadal, M.E., Campagnola, P.J., Gord, J.R., and Lineberger, W.C., I_2^- Photofragmentation/Recombination Dynamics in Size-Selected $I_2^-(CO_2)$ cluster ions: Observation of Coherent I-I Vibrational Motion. In: *J. Chem. Phys.* **97**, 7002-7005, 1992.

Rossky, P.J. and Schnitker, J., The Hydrated Electron: Quantum Simulation of Structure, Spectroscopy, and Dynamics. In: *J. Phys. Chem.* **92**, 4277-4285, 1988.

Salin, F., Squier, J., Mourou, G., and Vaillancourt, G., Multikilohertz $Ti:Al_2O_3$ Amplifier for High-Power Femtosecond Pulses. In: *Optics Letters* **16**, 1964-1966, 1991.

Webster, F.J., Schnitker, J., Friedrichs, M.S., and Friesner, R.A., Solvation Dynamics of the Hydrated Electron: A Nonadiabatic Quantum Simulation. In: *Phys. Rev. Lett.* **66**, 3172-3175, 1991.

Whitnell, R.M., Wilson, K.R., and Hynes, J.T., Vibrational Relaxation of a Dipolar Molecule in Water. In: *J. Chem. Phys.* **96**, 5354-5369, 1992.

Search for Vibrational Coherence Following the Photodissociation of Aromatic Disulfides in Solution

Abstract

The visible absorption band of photogenerated *p*-amino-phenyl thiyl radicals in methanol shifts in time. Time constants and temperature dependence are consistent with diffusive response of solvent polarization. An apparent oscillation of the absorption spectrum at early time may be an artifact.

Introduction

The photodissociation of bis(*p*-aminophenyl)disulfide in solution gives thiyl radical products on an ultrafast time scale:

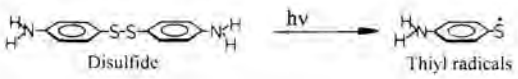

After photodissociation with ns UV pulses, the reaction products may be excited by a second photon, leading to intense red fluorescence (Morine and Kuntz, 1979) or even to stimulated emission (Ishizaka and Kotani, 1985). The efficiency of this radical dye laser depends strongly on the solvent. Also, the thiyl radicals have a ground-state dipole moment of 4.2 *D*, which is created in a weakly polarized solvent configuration. Therefore we had begun to examine the solvation of the *p*-aminophenyl thiyl radicals following ultrafast photodissociation (Ernsting, 1990). Here we report on more exact and quantitative measurements of spectral relaxation in methanol as solvent.

On the time scale from fs UV excitation of the parent disulfide to the ps range, one expects the following processes. Intramolecular dynamics of the dissociating excited parent molecule dominate the first 100 fs. This will be coupled to the inertial part in the solvent polarization response. For the following time window up to 500 fs, it is conceivable that the radical products may still possess vibrational coherence which should show up as an oscillation of the radical absorption band (given an appropriate excited-state potential). It was with this in mind that we reinvestigated the reaction — however unsuccessfully, as will be demon-

strated below. This report, then, by necessity concentrates on the longer time scale from 0.3 ps to 10 ps which is characterized by diffusive solvent dielectric relaxation.

Experimental

The sample (10^{-3} molar bis(*p*-aminophenyl)disulfide in methanol) was excited by a 120 fs pump pulse (FWHM) at 308 nm. After a variable time delay, the absorption spectrum of the radical products was measured in the range 400-720 nm using a white-light continuum. The latter was generated in 2.0 mm of water and quartz and imaged onto the sample using dispersion-free, anastigmatic optics. The overall pump-probe intensity cross correlation time at 570 nm was 230 fs (FWHM). This large value includes a significant contribution from the mismatch of group velocities between the UV pump pulse and the visible probe pulse in the sample interaction region (300 μm). Residual dispersion was measured by two-photon absorption in pure benzene (410-470 nm) and by the bleaching of malachit green (560-660 nm). The corresponding dispersion of time-zero, for various spectral components in the probe continuum, was found to be equivalent to that caused by 2.5 mm of quartz.

Results and Discussion

Fig. 1 gives a coarse representation of the spectral development over a time of two ps. A typical absorption spectrum is shown in Fig. 2. The following proce-

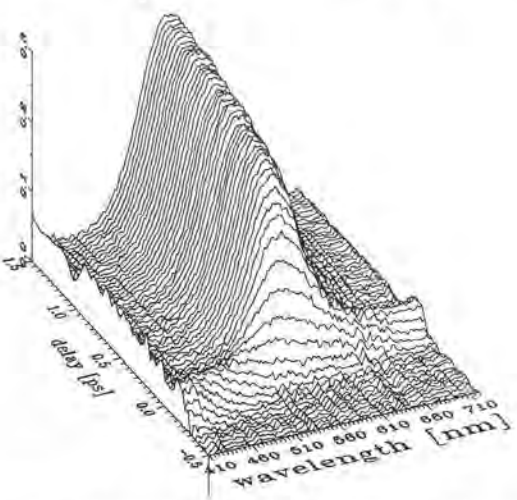

Fig. 1. Special evolution of the radical absorption band in methanol. (The method of representation introduces additional noise as compared to Fig. 2).

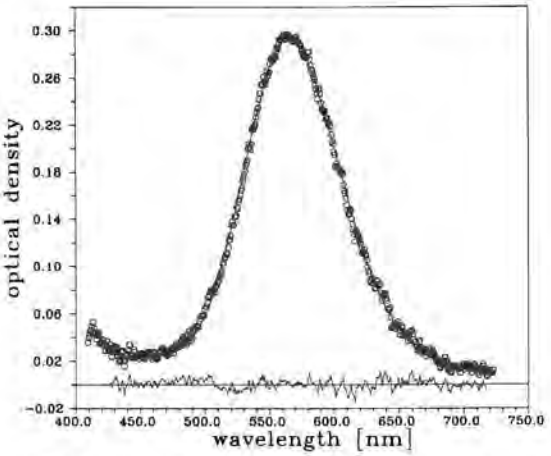

Fig. 2. Measured radical absorption band after 1.033 ps (dots) and 'log-normal' fit (line).

dure was used for evaluation. For each time delay, the measured transient spectrum was fitted with a 'log-normal' function of energy. From this fit the first moment, i.e. the effective spectral position of the band was determined. The spectral position was then plotted against time. A biexponential fit gave relaxation times as well as initial and final spectral position. Finally the shift of the spectral position from the position at infinite time was normalized to the total shift and the resultant $C(t)$ was plotted as a function of delay time. In the context of linear response theory $C(t)$ may be identified with the autocorrelation function for fluctuations in the electric field (Maroncelli and Fleming, 1988).

Fig. 3 shows $C(t)$ for methanol at several temperatures. Typically, a biexponential description is sufficient, with relaxation times in the range 0.5-1 ps and

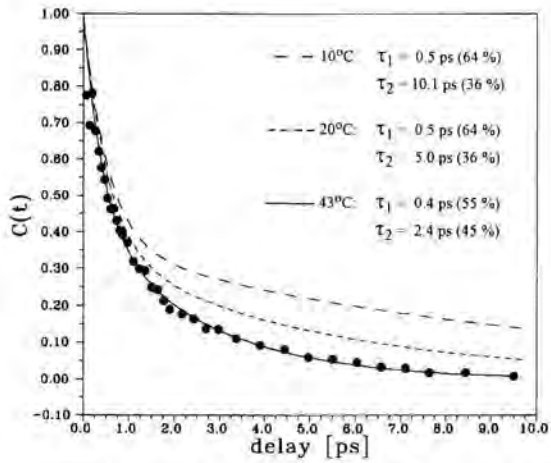

Fig. 3. Normalized spectral shift, in methanol at various temperatures.

5-10 ps. This was also found by observing the time-resolved dynamical Stokes shift of coumarin dyes in alcohol solutions (Maroncelli and Fleming, 1987). The latter process is primarily photo*physical*; the relaxation times may be interpreted as longitudinal relaxation times which are derived from a description of dielectric dispersion by Lorentzian terms with corresponding Debye relaxation times.

On the other hand, the spectral relaxation of the thiyl absorption band may in principle also be attributed to photo*chemical* processes, like the change in short- and long range interaction in the course of further separation of the two radicals. One would expect that the dynamics are governed by the internal energy only.

In this context it is instructive to consider the temperature dependence of the two time constants which are derived from $C(t)$. The fast component ($\tau \approx 0.5$ ps) is relatively unaffected by changes in temperature and should refer to the photochemical part of the dissociation. The slow component, on the other hand, shows a strong temperature dependence. The observed sensitivity is consistent with that of dielectric dispersion of bulk methanol.

Finally, the search for vibrational coherence in the photodissociation products: Fig. 4 shows the early part of the measured spectral shift $C(t)$ for the radical absorption band. A nearly overdamped oscillation is apparent and may be followed (with some reservations due to signal/noise) to 500 fs. Fourier transformation suggests a vibrational frequency around 170 cm^{-1} which was duly found in the fluorescence spectrum of isolated thiyl radicals in an argon matrix at 10 K (Mühlpfordt and Bultmann, 1992) and which may be associated with an inversion vibration of the amino group. However, we believe that the observed oscillation represents an artifact of measurement which is induced by the dispersion of time-zero mentioned earlier. Correction for this dispersion allows us to

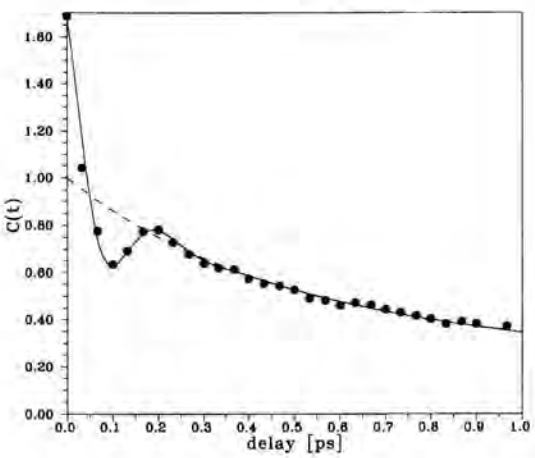

Fig. 4. Apparent oscillation of the spectral position (first moment of 'log-normal' fit) on a fs time scale.

remove the incipient, dominant part of the oscillation in Fig. 4. Yet the search for vibrational coherence in reaction products will be continued by us using smaller disulfides and inert solvents.

Acknowledgment

We are grateful to D. Bingemann and K. Kemeter for critical discussions, and to the Deutsche Forschungsgemeinschaft and the Fonds der Chemischen Industrie for financial support.

References

Ernsting, N.P., *Chem. Phys. Lett.* **166**, 221-226, 1990.
Ishizaka, S.-I., Kotani, M., *Chem. Phys. Lett.* **117**, 251-253, 1985.
Maroncelli, M., Fleming, G.R., *J. Chem. Phys.* **89**, 5044-5069, 1988.
Maroncelli, M., Fleming, G.R., *J. Chem. Phys.* **86**, 6221-6239, 1987.
Morine, G.H., Kuntz, R.R., *Chem. Phys. Lett.* **67**, 552-554, 1979.
Mühlpfordt, A., Bultmann, T., Unpublished results, 1992.

Authors' Address

Max-Planck Institut für Biophysikalische Chemie,
Postfach 2841,
D-3400 Göttingen, Germany

Excited-State Intramolecular Proton Transfer in 3-Hydroxyflavone: Comparison of Time- and Frequency-Domain Spectroscopy

Abstract

We report (I) the spectral evolution of transient absorption and gain for 3-hydroxyflavone (3-HF) in dry methyl cyclohexane, (II) the fluorescence excitation spectrum of the deuterated compound isolated in a supersonic jet. A comparison suggests that jet spectroscopy interrogates a metastable isomer of 3-HF in the electronic ground state. Semiempirical calculations support this hypothesis.

Introduction

Ever since Sengupta and Kasha (1979) reported dual fluorescence from 3-hydroxyflavone, this compound has kept spectroscopists busy — and often frustrated — by its rich pathology. The characteristic photochemical reaction following optical $\pi\pi^*$ excitation of 3-HF is excited-state intramolecular proton transfer (ESIPT) in the singlet manifold (cf. Fig. 1), after which green fluores-

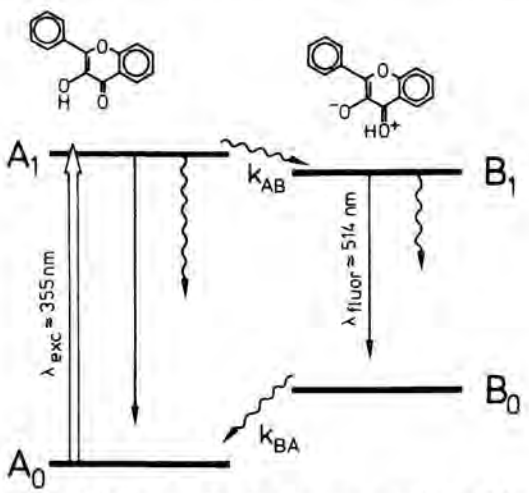

Fig. 1. Förster cycle for intramolecular proton transfer in 3-hydroxyflavone.

cence may be observed. A large part of previous work was aimed at establishing whether a barrier to this reaction exists. The pathology which has emerged so far may be grouped into two areas: extreme sensitivity to solvent perturbation (Mc Morrow and Kasha, 1984), and even to jet conditions (Ito et al., 1992), and a low-lying triplet state for the proton-transferred tautomer (Chou, 1990; Dick, 1989). Here we add a third: the hypothesis that the normal form of isolated 3-HF in its electronic ground-state possesses an isomer in which the hydroxyl group is oriented towards the phenyl ring. This hypothesis will be developed here in order to account for completely different behaviour of the isolated compound, as compared to a solution in dry, aliphatic solvents.

Transient Absorption in Solution

The latest time-resolved measurement of ESIPT in 3-HF was reported by Harris and coworkers (Schwartz et al., 1992; they also summarize the extensive earlier work). At room temperature in methyl cyclohexane, three kinetic contributions were observed. A time constant of 240 fs was attributed to the intrinsic process and a component with 80 fs could clearly be assigned to a cyclic monosolvate with hydroxyl-containing impurities. A long kinetic component, with time constant of 10.5 ps, was attributed to 3-HF which is H-bonded to at least two hydroxylic impurities in an external fashion without a cyclic structure.

We have repeated the transient absorption measurement, however with an extremely dry sample solution (solvent repeatedly dried over K/Na, transferred and used in a sealed quartz line) using broadband detection. Fig. 2 shows some of the transient absorption spectra at various delay times. They consist predominantly of excited-state absorption onto which the tautomer gain has been overlaid. At later times, there is net gain at 500 nm which has been used for stimulated emission (Chou and Aartsma, 1986; Parthenopoulus and Kasha, 1988). The time resolution of our experiments is limited by an optical path length of 1 mm (needed to achieve sample flow by using a closed gravity-flow system). The rise of absorption at 603 nm is shown in Fig. 3. It contains two kinetic components, with time constants of 160 fs and 10.5 ps. The observed short risetime is consistent with the earlier report (Schwartz et al., 1992) for internally H-bonded 3-HF, given an experimental error in determining time-zero for our setup. It is interesting to compare the spectral shape of the transient spectra at $t < 1$ ps and $t > 5$ ps in Fig. 2. One observes the slow rise of excited-state absorption around 610 nm (with time constant of 10.5 ps, as mentioned above) and some change in the shape of the gain band. Now the slow rise component can no longer be attributed to externally H-bonded 3-HF because of our stringent sample purity. We conclude that intramolecular vibrational redistribution and relaxation of excess vibrational energy must be responsible for the slow rise of absorption near 610 nm. This observation already points to a capacious potential energy surface for 3-HF in the S_1-state.

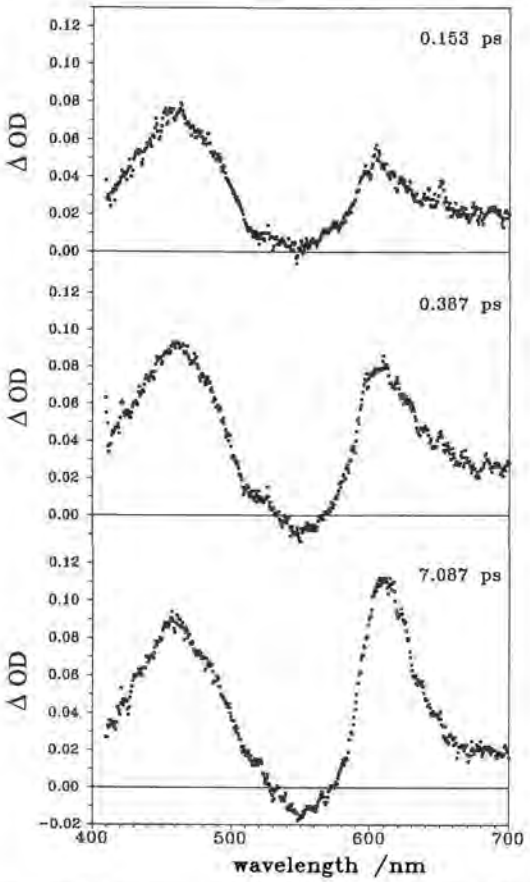

Fig. 2. Transient absorption spectra of 3-HF in dry methyl cyclohexane.

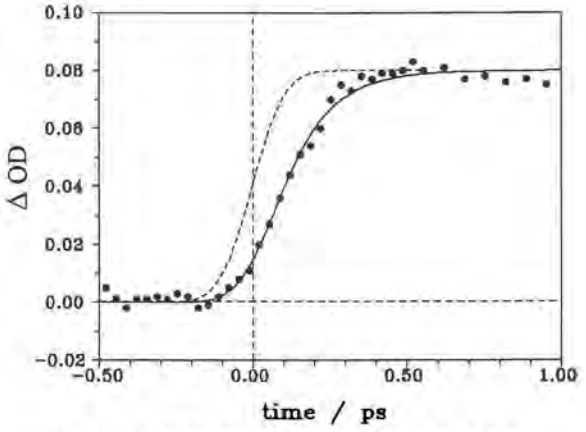

Fig. 3. Rise of transient absorption at 616 nm.

Lineshape- and Deuteration Studies of Jet-Cooled 3-HF

Isolated, jet-cooled 3-HF (cf. Fig. 4a) has an observed vibronic origin band at 28080.3 cm^{-1} (Ernsting and Dick, 1989); a vibrational progression in a 44 cm^{-1} mode can be assigned to phenyl torsion. The vibronic bands have Lorentzian lineshape with FWHM in the range 3.7-4.5 cm^{-1}, corresponding to lifetimes (because of the absence of pure dephasing) around 1.5 ps. The most striking feature of the jet spectroscopy of 3-HF, however, is the existence of a broad background for fluorescence excitation which also appears to depend on cooling conditions. It has been customary to ignore this background and to concentrate on spectral structure.

Fig. 4b shows the fluorescence excitation spectrum of deuterated 3-DF, the composition of which was checked by MS and NMR. Upon deuteration one obtains a more complicated spectrum, as was already mentioned by Ito et al.

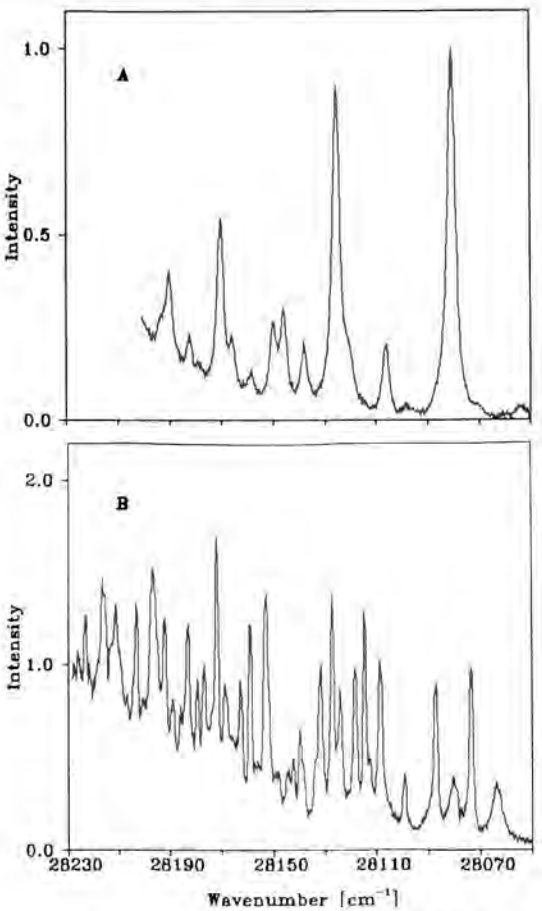

Fig. 4. Fluorescence excitation spectra of jet-cooled 3-HF (a) and 3-DF (b).

(1992). For every original band there appear at least three bands in the 3-DF spectra. Prominent bands have their linewidth reduced to 1.8 cm^{-1}, while other broad bands emerge from the background.

One may ask whether the spectral complication upon H/D exchange arises from inhomogeneity in the electronic ground state, or from complications in the excited state. We performed saturation experiments which allow an assignment of the various narrow bands in Fig. 4b to at least three different spectra, each of which is a replica of the spectrum for original 3-HF but shifted by different amounts. We conclude that deuteration leads to inhomogeneous broadening: the ground state vibrational level structure rearranges at thermal energies. The affected normal modes in the electronic ground state must contain strong contributions from positional changes in the hydroxyl hydrogen atom. We surmise that out-of-plane modes of a skeletal nature may be involved, with double-minimum potentials the existence of which may not matter for 3-HF but which become influential for 3-DF.

Semiempirical Calculations

With MNDO/AM1 + CI calculations, the phenyl torsion (angle π) and the torsion of the hydroxyl group (angle ϕ) were simultaneously investigated. Fig. 5 summarises the results for phenyl torsion for the S_0 and S_1 states. In the ground state in its internally H-bonded form, the phenyl group is predicted to be twisted by 28.3° from planarity, while the excited state should be planar. These findings are consistent with crystal structure data (Etter et al., 1986). As a consequence, one expects a Franck-Condon progression for the torsional mode which is red-degraded over a large spectral range. Instead we find a blue-degraded short progression in the torsional mode (Fig. 4a).

There remains the possibility that the observed line spectrum belongs to some metastable conformer in the ground state while the background (which is dominant in terms of integrated band strength) belongs to 3-HF in its normal form. Therefore we have twisted the hydroxyl group further away from planarity towards the transform (with respect to the carbonyl group) while relaxing the phenyl torsional angle π. A relative minimum was found at $\phi = 159.7°$, $\pi = -44°$, with an electronic potential energy 1091 cm^{-1} above the normal form. At the conditions of the jet expansion, about 10% of the sample should exist in this trans-configuration.

In conclusion, the following hypothesis is presented:

The spectral background for isolated 3-HF is assigned to the normal form. Its ESIPT reaction has a characteristic time constant of 160-240 fs. The lack of spectral structure is caused by the corresponding linewidth of 27 cm^{-1} in combination with spectral congestion.

The line spectrum for isolated 3-HF is tentatively assigned to a trans-like conformer. The vibronic lifetime of 1.4 ps reflects trans/cis isomerisation of the

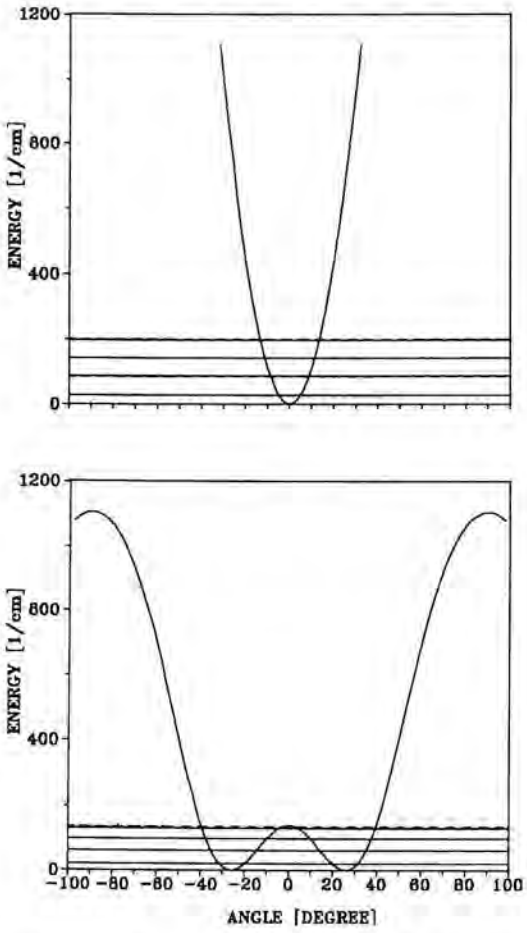

Fig. 5. Torsional potentials and eigen energies for 3-HF in its normal form.

hydroxyl group in the excited state rather than proton transfer. In addition, the PES should be complex with double minima along a normal coordinate which involves the motion of the hydroxyl proton.

Acknowledgment

We are grateful to K.H. Grellmann for critical discussions and for the sample preparation, and to the Deutsche Forschungsgemeinschaft and the Fonds der Chemischen Industrie for financial support.

References

Chou, P.T., and Aartsma, T.J., *J. Phys. Chem.* **90**, 721-723, 1986.
Chou, P.T., Martinez, M.L., and Studer, S.L., *J. Am. Chem. Soc.* **112**, 2427-2429, 1990.
Dick, B., *Phys. Chem.* **94**, 5752-5756, 1989.
Ernsting, N.P., and Dick, B., *Chem. Phys.* **136**, 181-186, 1989.
Etter, M.C., Urbanczyk-Lipkowsaka, Z., Baer, S., and Barbara, P.F., *J. Mol. Struc.* **144**, 155-167, 1986.
Ito, A., Fujiwara, Y., and Itoh, M., *J. Chem. Phys.* **96**, 7474-7482, 1992.
Mc Morrow, D., and Kasha, M., *J. Phys. Chem.* **88**, 2235-2243, 1984.
Parthenopoulus, D.A., and Kasha, M., *Chem. Phys. Lett.* **146**, 77-82, 1988.
Schwartz, B.J., Peteanu, L.A., and Harris, C.B., *J. Phys. Chem.* **96**, 3591-3598, 1992.

Authors' Addresses

A. Mühlpfordt, T. Bultmann, and N.P. Ernsting; Max-Planck Institut für biophysikalische Chemie, Postfach 2841, D-37077 Göttingen, Germany.
B. Dick; Institut für Physikalische und Theoretische Chemie, Universität Regensburg, D-93040 Regensburg, Germany.

Moshe Shapiro and Janet R. Waldeck

Transient Flux and Vibrational Coherence in Predissociation with Short Laser Pulses

Abstract

In this paper we examine how vector properties of photodissociation with a coherent laser pulse evolve in time during and after the excitation process. In particular, we define and explore the *transient* anisotropy parameter, $\beta(t)$. We apply our formulation to the case of the predissociation of the NaI molecule. We predict that under certain conditions $\beta(t)$ displays a *beating* phenomenon, in which the system oscillates periodically between a parallel-type and a perpendicular-type angular distribution. Depending on the excitation pulse, this 'vectorial' beating may be accompanied by a faster beating similar to the 'scalar' vibrational beating observed in the past in the NaI system. It is shown that the transient anisotropy beating may be used to obtain experimentally the time-dependent average interfragment separation, and that different J states are characterized by different interfragment separation curves.

I. Introduction

Molecular photodissociation is one of the few primary chemical processes in which it is possible to define clearly the initial state of the system. With ultrashort laser pulses much progress in mapping out the complete time evolution of the system from photon-absorption to separated fragments has been made. This includes the very ambitious task of looking at the very early stages of the process, when the fragments are still within range of one another, with the so-called 'femtosecond transition-state spectroscopy' - FTS - technique [Zewail 1988].

In the past, pulsed photodissociation experiments have focussed primarily on scalar properties, such as the transient populations at a certain distance between the departing fragments [Zewail 1989, Zewail 1991]. It is clear, however, that the observed signal may also yield information about *vector* properties arising, for example, from coherences between simultaneously excited rotational quantum states.

As in the scalar case, in order to extract information about the *molecule*, it is necessary to account precisely [Williams 1988, Krause 1991] for the manner in which the molecular system is prepared by the pulsed photoabsorption process.

This is done in the present study by using a *time-independent* based approach [Shapiro 1991, Shapiro 1993] for describing the time-dependent pulsed photodissociation dynamics. This approach is comprised of first-order perturbation theory in the light field and exact scattering theory for the response of the material part. An important feature of the theory is the proper convolution of the laser profile into the time-dependent material wavefunction, which leads in a very natural way to the definition of transient vector properties, such as $\beta(t)$ - the *transient* anisotropy parameter.

Contrary to the CW case, we show that the transient anisotropy oscillates between the parallel-type $\beta = 2$ angular distribution [Zare 1963, Zare 1967, Zare 1972, Balint-Kurti 1981] and the perpendicular-type $\beta = -1$ distribution. We illustrate the usefulness our theory by applying it to the predissociation of NaI. This system is of considerable interest because measurements of scalar properties, such as the transient populations during the photodissociation process, have been conducted for NaI by the FTS technique [Zewail 1989, Zewail 1991] and extensively analyzed theoretically [Engel 1988, Engel 1989, Choi 1989, Marcus 1988, Lin 1989, Lee 1989, Shapiro 1991a, Shapiro 1991b].

The organization of this paper is as follows: In Section II we derive expressions for $\beta(t)$ of diatomic and polyatomic molecules and in Sections III we present our results for the NaI system. As shown below, the co-existence between different time scales makes NaI an especially interesting system for studying transient vector properties.

II. Photodissociation Transients

In order to explore photodissociation transients we need to consider explicitly the temporal evolution of the system under the action of the time-dependent Hamiltonian, $H(t)$:

$$H(t) = H_0 + V(t). \tag{1}$$

In the above, H_0 represents the full material Hamiltonian and $V(t)$ - the light-matter interaction,

$$V(t) = -\mu_\varepsilon \varepsilon(t). \tag{2}$$

Here, μ_ε is the component of the electric dipole-operator along the direction of $\vec{\varepsilon}(t)$ - the light's electric-field vector.

Assuming that the pulse propagates in the x-direction, we can write the magnitude of its electric field as,

$$\varepsilon(x, t) = \int_{-\infty}^{\infty} d\omega \varepsilon(\omega) \exp(i\omega x/c - i\omega t) = \int_{-\infty}^{\infty} d\omega \bar{\varepsilon}(\omega) \exp(-i\omega t), \tag{3}$$

where, $\bar{\varepsilon}(\omega) \equiv \varepsilon(\omega) \exp(i\omega x/c)$, and the field at negative frequencies is defined, because of the reality of the pulse, as $\varepsilon(-\omega) \equiv \varepsilon^*(\omega)$.

The molecule, upon absorbing radiation, is excited from ψ_i - a bound eigenstate of H_0, to a linear combination of $\psi^-(E, \hat{\mathbf{k}}, n)$ - the continuum eigenstates of the same Hamiltonian:

$$H_0\psi^-(E, \hat{\mathbf{k}}, n) = E\psi^-(E, \hat{\mathbf{k}}, n). \tag{4}$$

Each $\psi^-(E, \hat{\mathbf{k}}, n)$ state correlates to a *single* product of a free translational state $|\boldsymbol{k}\rangle$, where $\mathbf{k}$ is the asymptotic wave-vector of the freely moving fragments, and an internal state $|n\rangle$, where n denotes a collection of (vibrational, rotational, etc...) fragment quantum numbers. The minus sign means that $\psi^-(E, \hat{\mathbf{k}}, n)$ evolves to the above state in the *distant future.*

The effects of the perturbation of the light pulse can be accounted for by expanding the total molecular wavefunction, $\Psi(t)$, as:

$$\Psi(t) = b_i(t)\,\psi_i \exp(-iE_i t/\hbar) + \sum_n \int d\hat{\mathbf{k}} \int dE\, b_{E,n,\hat{\mathbf{k}}}(t)\,\psi^-(E, \hat{\mathbf{k}}, n) \exp(-iEt/\hbar). \tag{5}$$

The continuum expansion coefficients, $b_{E,n,\hat{\mathbf{k}}}(t)$, are given in first-order perturbation theory [Shapiro 1991, Shapiro 1993, Saphiro 1973] as:

$$b_{E,n,\hat{\mathbf{k}}}(t) = \frac{\mathrm{i}}{\hbar} \langle \psi^-(E, \hat{\mathbf{k}}, n) \mid \mu_\varepsilon \mid \psi_i \rangle\, \tilde{\varepsilon}(\omega_{E,i})\, c_E(t), \tag{6}$$

where $\omega_{E,i} \equiv (E - E_i)/\hbar$ are the transition frequencies to the set of continuum states. The $c_E(t)$ coefficients are related to the finite-time Fourier transform of the pulse [Shapiro 1991, Shapiro 1993],

$$\begin{aligned} c_E(t) &\equiv \frac{1}{\tilde{\varepsilon}(\omega_{E,i})} \int_{-\infty}^{t} dt' \varepsilon(t') \exp(i\omega_{E,i} t') \\ &= \frac{1}{\tilde{\varepsilon}(\omega_{E,i})} \int d\omega\, \tilde{\varepsilon}(\omega) \frac{\exp[i(\omega_{E,i} - w)\, t]}{i(\omega_{E,i} - \omega)}. \end{aligned} \tag{7}$$

The $c_E(t)$ coefficients contain no molecular attribute except for the transition frequencies, $\omega_{E,i}$.

The asymptotic behavior of the molecular wavefunction is dictated by its continuum component, given, using Eq. (6) as

$$\begin{aligned} \Psi_c(t) = \frac{i}{\hbar} \sum_n \int d\hat{\mathbf{k}} \int dE' \, \langle \psi^-(E', \hat{\mathbf{k}}, n) \mid \mu_\varepsilon \mid \psi_i \rangle \\ \times \tilde{\varepsilon}(\omega_{E',i})\, c_{E'}(t)\, \psi^-(E', \hat{\mathbf{k}}, n) \exp(-iE't/\hbar). \end{aligned} \tag{8}$$

If we choose a single mode $\varepsilon(t)$, i.e., substitute,

$$\varepsilon(\omega) = \varepsilon_E \delta(\omega - \omega_{E,i}), \tag{9}$$

into Eq. (8), and choose $\varepsilon_E = 1$ we obtain a CW analogue of Eq. (8),

$$\Psi^{CW}(E)\exp(-iEt/\hbar) = \frac{2\mu i}{\hbar}\sum_n \int d\hat{\mathbf{k}}\, \langle \psi^-(E, \hat{\mathbf{k}}, n) \mid \mu_\varepsilon \mid \psi_i \rangle \times \psi^-(E, \hat{\mathbf{k}}, n)\exp(-iEt/\hbar). \tag{10}$$

$\Psi^{CW}(E)$ is thus a linear combination of degenerate energy eigenstates specific to the photo-excitation process of interest. Using Eq. (8) and Eq. (10) it is possible to express the time-dependent wavefunction as a transform of $\Psi^{CW}(E)$,

$$\Psi_c(t) = \frac{1}{2\pi}\int dE\tilde{\varepsilon}(\omega_{E,i})\, c_E(t)\exp(-iEt/\hbar)\, \Psi^{CW}(E). \tag{11}$$

The transition from the *CW* to the pulsed case is therefore accomplished by $O(t \leftarrow E)$ - a linear (integral) operator - given as,

$$O(t \leftarrow E)\cdot\psi^-(E, \hat{\mathbf{k}}, n) = \frac{1}{2\pi}\int dE\tilde{\varepsilon}(\omega_{E,i})\, c_E(t)\exp(-iEt/\hbar)\cdot\psi^-(E, \hat{\mathbf{k}}, n). \tag{12}$$

Any quantity containing *CW* amplitudes can be transformed to its transient analogue by applying $O(t \leftarrow E)$ to it. For example, we can transform the *angular photodissociation amplitude*, which plays a central role in the theory of photodissociation processes [Shapiro 1973, Balint-Kurti 1981, Schinke 1992]. It is given as,

$$f(E, \hat{\mathbf{k}}, n \mid i) \equiv \frac{2\pi i w_{E,i}^{1/2}}{\hbar}\langle \psi^-(E, \hat{\mathbf{k}}, n) \mid \mu_\varepsilon \mid \psi_i \rangle. \tag{13}$$

Its square is proportional to the state-specific photodissociation cross-section,

$$\sigma(E, \hat{\mathbf{k}}, n \mid i) = \frac{4\pi^2}{c}\, |f(E, \hat{\mathbf{k}}, n \mid i)|^2. \tag{14}$$

When we apply $O(t \leftarrow E)$ of Eq. (12) to Eq. (13), we obtain the *transient* angular photodissociation amplitude,

$$f(t, \hat{\mathbf{k}}, n \mid i) = \frac{i}{\hbar}\int dE\tilde{\varepsilon}^*(\omega_{E,i})\, c_E^*(t)\exp(iEt/\hbar)\, \omega_{E,i}^{1/2}\langle \psi^-(E, \hat{\mathbf{k}}, n) \mid \mu_\varepsilon \mid \psi_i \rangle. \tag{15}$$

In a similar fashion we can obtain the transient *partial-wave* amplitudes. Their *CW* counter-parts are used in the body-fixed partial-wave expansion [Balint-Kurti 1981] of the *CW* angular photodissociation amplitude,

$$f(E, \hat{\mathbf{k}}, vjm_j \mid E_i J_i p) = \sum_{J,\lambda} (2J+1)^{1/2}\, D^J_{\lambda, M_i}(\phi_k, \theta_k, 0)\, D^J_{-\lambda, -m_j}(\phi_k, \theta_k, 0) \times \begin{pmatrix} J & 1 & J_i \\ -M_i & 0 & -M_i \end{pmatrix} \tau(E, J, vj\lambda \mid E_i J_i p). \tag{16}$$

For a triatomic molecule the internal index n above is used to denote $\{v, j, m_j\}$ - the vibrational- rotational- and magnetic quantum numbers of the photo-fragments, respectively, with J, M, λ, p denoting respectively the total angular momentum, its space-fixed and body-fixed projections and the parity quantum numbers. $\tau(E, J, vj\lambda \mid E_i J_i p)$ are *reduced* partial amplitudes [Balint-Kurti 1981], related to the M_i-dependent partial amplitudes as,

$$\tau(E, J, vj\lambda \mid E_i J_i p) = \frac{2\pi i \omega_{E,i}^{1/2}}{\hbar} \langle \psi^-(E, J, vj\lambda) \mid \mu_c \mid \psi_i \rangle \Big/ \begin{pmatrix} J & 1 & J_i \\ -M_i & 0 & -M_i \end{pmatrix}. \quad (17)$$

The reduced amplitudes can be used to calculate the m_j-summed M_i-averaged cross-section [Balint-Kurti 1981],

$$\begin{aligned} \langle \sigma(\hat{\mathbf{k}}, E, vj \mid E_i J_i p) \rangle &\equiv \frac{1}{2J_i + 1} \sum_{M_i} \sum_{m_j} \sigma(\hat{\mathbf{k}}, E, vjm_j \mid E_i J_i M_i p) \\ &= \frac{4\pi^2}{c} \sum_{J, J', \lambda} [(2J+1)(2J'+1)]^{1/2} \\ &\quad \times (-1)^{\lambda + J + J'} \sum_{\mu = 0, 2} (2\mu + 1) P_\mu(\cos\theta) \\ &\quad \times \begin{pmatrix} J & J' & \mu \\ \lambda & -\lambda & 0 \end{pmatrix} \begin{pmatrix} 1 & 1 & \mu \\ 0 & 0 & 0 \end{pmatrix} \begin{Bmatrix} 1 & 1 & \mu \\ J & J' & J_i \end{Bmatrix} \\ &\quad \times \tau(E, J, vj\lambda \mid E_i J_i p)\, \tau^*(E, J', vj\lambda \mid E_i J_i p) \end{aligned} \quad (18)$$

where $(\theta, \phi) \equiv \hat{\mathbf{k}}$.

For pulse experiments the concept of a cross-section must be replaced by the more fundamental unnormalized *fluxes*). This does not change the definition or measurement of *relative* quantities such as the β anisotropy parameter. This quantity is defined as the ratio of the term multiplying $P_2(\cos\theta)$ in the above expression to the isotropic part. In the CW case, $\beta(E, vj \mid E_i J_i p)$ is obtained [Balint-Kurti 1981] by equating the following expression,

$$\langle \sigma(\hat{\mathbf{k}}, E, vj \mid E_i J_i p) \rangle = \sigma_0(E, vj \mid E_i J_i p) \{1 + \beta(E, vj \mid E_i J_i p) P_2(\cos\theta)\} \quad (19)$$

with Eq. (18), where $\sigma_0(E, vj \mid E_i J_i p)$ is the isotropic part of Eq. (18). We obtain that,

$$\begin{aligned} \beta(E, vj \mid E_i J_i p) &= (30)^{1/2} \sum_{J, J', \lambda} [(2J+1)(2J'+1)]^{1/2} (-1)^{\lambda + J + J' + J_i} \begin{pmatrix} J & J' & 2 \\ \lambda & -\lambda & 0 \end{pmatrix} \\ &\quad \times \begin{Bmatrix} 1 & 1 & 2 \\ J & J' & J_i \end{Bmatrix} \tau(E, J, \lambda)\, \tau^*(E, J', \lambda) \Big/ \sum_{J, \lambda} |\tau(E, J, \lambda)|^2, \end{aligned} \quad (20)$$

where $\tau(E, J, \lambda)$ is a short-hand notation for $\tau(E, J, vj\lambda \mid E_i J_i p)$.

The *transient* fluxes and transient anisotropy associated with it are obtained by simply substituting the time-dependent reduced amplitudes, given as,

$$\tau(t, J, vj\lambda \mid E_i J_i p) = \frac{1}{2\pi} \int dE \bar{\varepsilon}^*(\omega_{E,i})\, c_E^*(t) \exp(iEt/\hbar)\, \tau(E, J, vj\lambda \mid E_i J_i p), \qquad (21)$$

into expressions, analogous to Eq. (18), for the flux. We obtain that the transients fluxes are,

$$F(\hat{\mathbf{k}}, t, vj \mid E_i J_i p) = F_0(t, vj \mid E_i J_i p)\, \{1 + \beta(t, vj \mid E_i J_i p)\, P_2(\cos\theta)\} \qquad (22)$$

where, $F_0(t, vj \mid E_i J_i p)$ - the isotropic flux - is given as,

$$F_0(t, vj \mid E_i J_i p) = 2\pi \sum_{J,\lambda} |\tau(t, J, \lambda)|^2. \qquad (23)$$

and the transient anisotropy is given as,

$$\beta(t, vj \mid E_i J_i p) = (30)^{1/2} \sum_{J, J'\lambda} [(2J+1)(2J'+1)]^{1/2} (-1)^{\lambda + J + J' + J_i} \begin{pmatrix} J & J' & 2 \\ \lambda & -\lambda & 0 \end{pmatrix}$$

$$\times \begin{Bmatrix} 1 & 1 & 2 \\ J & J' & J_i \end{Bmatrix} \tau(t, J, \lambda)\, (\tau^*(t, J', \lambda)/F_0(t), \qquad (24)$$

where $\tau(t, J, \lambda)$ is short-hand for $\tau(E, J, vj\lambda \mid E_i J_i p)$ and $F_0(t)$ is short-hand for $F_0(t, vj \mid E_i J_i p)$.

These expressions simplify considerably for diatomic molecules correlating to a *single* fragment's electronic-state. In this case $\tau(E, J, vj\lambda \mid E_i J_i p)$ becomes [Levy 1988],

$$\tau(E, J, \lambda \mid E_i J_i p) = (-1)^{\lambda}\, t_\lambda [(2J+1)(2J_i+1)]^{1/2} \begin{pmatrix} J & 1 & J_i \\ -\lambda & \lambda & 0 \end{pmatrix}$$

$$\times [1 + p(-1)^{J+1+J_i}]\, T(E, J, \lambda \mid E_i J_i p). \qquad (25)$$

λ now denotes the (absolute value of the) projection of the electronic angular momentum on the internuclear distance. In the above, $t_\lambda \equiv 1/2$ for $\lambda = 0$ and $t_\lambda \equiv 1/\sqrt{2}$ for $\lambda > 0$. $T(E, J, \lambda \mid E_i J_i p)$ are radial bound-free integrals [Zare 1963, Zare 1967, Zare 1972],

$$T(E, J, \lambda \mid E_i J_i p) = \frac{2\pi i \omega_{E,i}^{1/2}}{\hbar} \int dR \psi^{R, J, \lambda -}(R)\, \mu_{\lambda,0}(R)\, \psi^{E_i J_i}(R). \qquad (26)$$

The $T(t, J, \lambda \mid E_i J_i p)$, transient radial integrals are obtained by applying $\mathbf{O}(t \leftarrow E)$ to Eq. (26).

For greater clarity, we now give explicit expressions for a parallel-type tran-

sition, i.e., the $\lambda = 0$ case. In this case the 3-j coefficients of Eq. (24) are zero except when $J = J_i \pm 1$ [Zare 1988]. We obtain that,

$$\beta_{\parallel}(t \mid J_i) = \{|T(t, J_i+1)|^2 (J_i+1)(J_i+2) + |T(t, J_i-1)|^2 J_i(J_i-1) + \frac{2R_e[T^*(t, J_i+1)\, T(t, J_i-1)]\, 3J_i(J_i+1)\}}{(2J_i+1)[|T(t, J_i+1)|^2 (J_i+1) + |T(t, J_i-1)|^2 J_i]}, \tag{27}$$

where, $T(t, J)$ is a short hand notation for $T(t, J, \lambda = 0 \mid E_i J_i p)$.

It is instructive to write the above result as,

$$2 - \beta_{\parallel}(t \mid J_i) = \frac{3J_i(J_i+1)}{2J_i+1} \cdot \frac{|\, T(t, J_i+1) - T(t, J_i-1)\,|^2}{|T(t, J_i+1)|^2 (J_i+1) + |T(t, J_i-1)|^2 J_i}. \tag{28}$$

It is clear from this expression that, as in the energy domain, when $T(t, J_i+1) = T(t, J_i+1)$ $\beta_{\parallel}(t) = 2$, i.e.,

$$F(\hat{\mathbf{k}}, t \mid J_i) = 3F_0(t \mid J_i) \cos^2 \theta. \tag{29}$$

This is the temporal *axial recoil* limit [Zare 1972, Greene 1982].

When $T(t, J_i-1) \ll T(t, J_i+1)$,

$$\beta_{\parallel}(t \mid J_i) = 2 - \frac{3J_i}{2J_i+1} \xrightarrow{J_i \to \infty} 1/2. \tag{30}$$

Likewise, when $T(t, J_i-1) \gg T(t, J_i+1)$,

$$\beta_{\parallel}(t \mid J_i) = 2 - \frac{3J_i+1}{2J_i+1} \xrightarrow{J_i \to \infty} 1/2. \tag{31}$$

The last two cases correspond to the R and P branches being well separated from one another in energy space. Such separation occurs if the continuous spectrum is composed of narrow resonances whose widths are smaller than the P to R spacings. A result of Eq. (31) is that in this case the full angular distribution assumes the shape,

$$F(\hat{\mathbf{k}}, t \mid J_i) = \frac{3}{4} F_0(t \mid J_i)(1 + \cos^2 \theta) \tag{32}$$

Finally when $T(t, J_i-1) = -T(t, J_i+1)$,

$$\beta_{\parallel}(t \mid J_i) = -1 + \frac{3}{(2J_i+1)^2} \xrightarrow{J_i \to \infty} -1, \tag{33}$$

and

$$F(\hat{\mathbf{k}}, t \mid J_i) = \tfrac{3}{2} F_0(t \mid J_i) \sin^2 \theta. \tag{34}$$

This is the temporal *transverse recoil* limit.

III. Computations of Vector Transients

We now apply the above formulation to a detailed study of the transient fluxes and transient anisotropy in predissociating NaI. Of interest is the motion of NaI on the $\Omega = 0^+$ excited state, which predissociates (due to nonadiabatic couplings) to the ground state. As shown in Fig. 1, the two states display an (avoided) ionic/covalent crossing. At short distances the excited state is covalent and the ground state is ionic; at longer distances the nature of the states is reversed.

Scalar transients, displaying vibrational recurrences, were measured by Zewail and coworkers [Zewail 1989, Zewail 1991] using the FTS technique. In these experiments a short ($\approx$ 40-125 fsec) 'pump' pulse in the $\approx 32000 - 33300\ \mathrm{cm}^{-1}$ frequency range, was used to excite a wavepacket comprised of a number of resonances belonging to the $\Omega = 0^+$ manifold. (In addition to exciting the $\Omega = 0^+$ resonances, the pulse also excites the $\Omega = 1$ continuum [van Veen 1981]. However, following Refs. [Engel 1988, Shapiro 1991b, Shapiro 1991], we neglect the $\Omega = 1$ contribution because the very fast transients of that state are assumed to vanish well before the first recurrence of the $\Omega = 0^+$ transients).

The part of the wavepacket which 'starts' its life on the repulsive branch of the $\Omega = 0^+$ state, moves back and forth on that state while 'leaking' into the ground state as it passes near the avoided crossing region. In Zewail's experiments [Zewail 1989], a second ('probe') pulse is frequency-tuned to excite the molecule to a second excited state, yielding Na* + I atoms. This is assumed to occur only when the wavepacket passes through a specified range of Na-I distances, fixed by the center-frequency of the probe pulse. Obviously, the assumption of the existence of a one-to-one correspondence between the Na-I range of distances and the center-frequency of the probe is the *raison d'être* of the experiment.

The response of the system as a function of the delay between the probe and pump pulses, gauged by the amount of Na* fluorescence, enables one to determine the time (measured from the 'moment of inception') it takes the wavepacket to pass through the range of Na-I distances susceptible to the action of

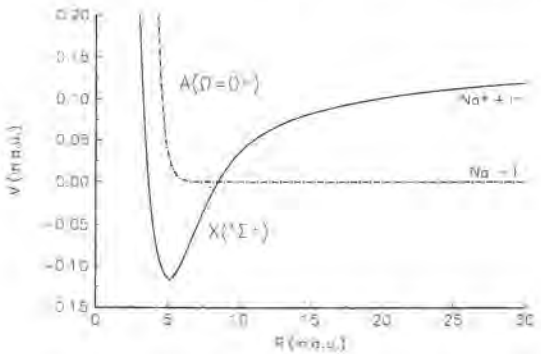

Fig. 1. The NaI ionic ($X\ ^1\Sigma^+$) and covalent ($\Omega = 0^+$) diabatic potential curves.

the probe pulse. In this way one can track down the motion of populations in the excited state and the degree of 'leakage' to the ground state at every passage.

Fig. 1 shows the ionic and covalent potential curves for NaI in the diabatic representation. These curves, taken from Ref. [Shapiro 1991], were parametrized using spectroscopic information derived from Refs. [Berry, 1979] and [Grice 1974].

Due to the parallel nature of the dipole moment associated with the NaI ($0^+ \leftarrow {}^1\Sigma^+$) transition, two rotational states arising from the $J_i - 1 \leftarrow J_i$ (P-type) and $J_i + 1 \leftarrow J_i$ (R-type) transitions are excited during photoabsorption. The energy-resolved vector properties of the system are therefore a result of interference between two, coherently excited, $\tau(E, J_i \pm 1, \lambda \mid E_i J_i p)$ amplitudes. Likewise the transient vector properties are a result of interference between two $\tau(t, J_i \pm 1, \lambda \mid E_i J_i p)$ amplitudes.

The computations of $\tau(E, J, \lambda \mid E_i J_i p)$ reported below (from which by applying $\mathbf{O}(t \leftarrow E)$ we obtain also the transient amplitudes) were carried out by solving a set of 'coupled-channels' equations [Bernstein 1979], based on the potentials shown in Fig. 1, using the artificial-channel method [Shapiro 1972, Shapiro 1982].

Energy Resolved Properties

We present first (in Figs. 2a and 2b) the computed $J_i = 40$ P and R energy-resolved partial photodissociation cross-sections,

$$\sigma(E, J_i \pm 1 \mid E_i J_i) = \frac{4\pi^2}{c} \mid \tau(E, J_i \pm 1, \lambda = 0 \mid E_i J_i p) \mid^2. \tag{35}$$

As in the rotationless case [Shapiro 1991, Shapiro 1993], both the P and R partial cross-sections show a series of narrow Fano-type [Fano 1961] resonances whose shape is due to transitions to a linear combination of the discrete spectrum of the $\Omega = 0^+$ state and the continuum of the ground state. As the frequency is changed, the resonance profiles vary in width and shape.

The energy-resolved anisotropy parameter, $\beta_\parallel(E)$, is (see Eq. (20)) a function of the same $\tau(E, J_i \pm 1, \lambda = 0 \mid E_i J_i p)$ amplitudes which determine the P- and R-partial cross-sections of Eq. (35). $\beta_\parallel(E)$, corresponding to the spectra in Figs. 2a and 2b, is shown in Fig. 2c. Its dependence on the resonance width can be understood in terms of the contribution of the individual P and R radial amplitudes.

As pointed out in the context of Eq. (27), an equality between these amplitudes implies that $\beta_\parallel(E) \to 2$. This is the case for the wider resonances, where the P and R cross-sections at any given energy are almost the same. This is in perfect accord with the classical interpretation [Bersohn 1969, Yang 1974, Jonah 1971] of $\beta_\parallel(E) \to 2$ as signifying a short lifetime, since by the Uncertainty Principle, broader resonances imply shorter lifetimes. Note, however, that $\beta_\parallel(E)$ often falls short of its maximal value of 2 due to a difference in the *phase* between the $T(E, J_i - 1)$ and $T(E, J_i + 1)$ amplitudes.

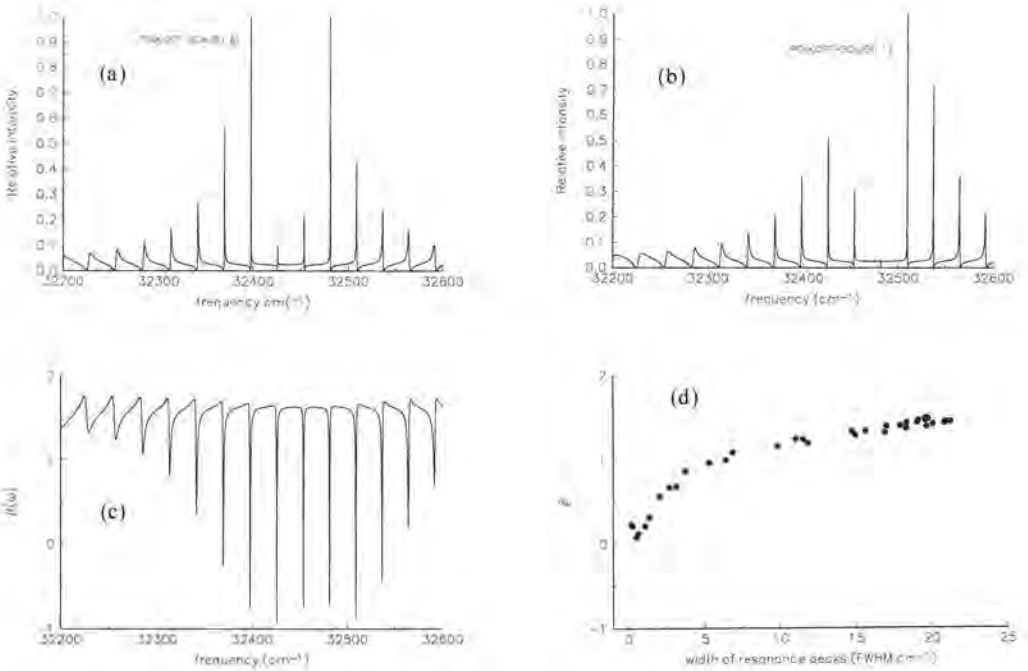

Fig. 2. Energy-dependent photodissociation cross-sections of NaI in the 32200-32600 cm^{-1} range: (a) $J=39 \leftarrow J_i=40$ (P-type transition), (b) $J=41 \leftarrow J_i=40$ (R-type transition), (c) the corresponding anisotropy parameter $\beta_\parallel(E)$ and (d) $\beta_\parallel(E)$ plotted as a function of the half-width of the shape-resonance peaks.

For narrow resonances a large variation in $\beta_\parallel(E)$ was found. This arises whenever the spacing between the P- and R-resonances is larger than their widths. In this case, according to Eq. (30) and Eq. (31), $\beta_\parallel(E) \to 1/2$.

In Fig. 2d, we plot $\beta_\parallel(E)$ as a function of the individual resonance-widths. The anticipated [Bersohn 1969, Yang 1974, Jonah 1971] correlation between the resonance widths and the magnitude of $\beta_\parallel(E)$ is to a large extent realized. We see that $\beta_\parallel(E)$ approaches asymptotically the value of 2 as the resonance widths become larger. However, as discussed above, $\beta_\parallel(E) \to 0.5$, rather than 0, as the resonance widths $\to 0$. It is true that for some resonances $\beta_\parallel(E)$ actually hits 0, yielding a completely isotropic distribution, but this is in fact due to some special relations between the P and R amplitudes of some long-lived resonances. In general, the low values of $\beta_\parallel(E)$ for narrow resonances do conform with our classical expectations [Bersohn 1969, Yang 1974, Jonah 1971] of a nearly isotropic distribution for long lifetimes, due to substantial rotation during the dissociation.

In order to set the stage for the discussion of $\beta_\parallel(t)$, we examine in Fig. 3a only a single P- and a single R-resonance, by concentrating on an energy segment lying between 32396 cm^{-1} and 32401 cm^{-1}. The corresponding anisotropy para-

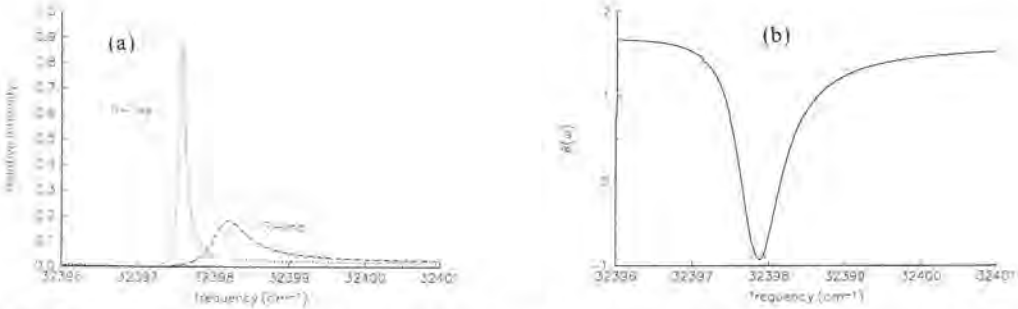

Fig. 3. (a) Energy-dependent P- (dotted line) and R-type (dot-dashed line) cross-sections in the region of a single resonance peak, (b) the corresponding $\beta_{\parallel}(E)$.

meter is shown in Fig. 3b. We see that across the resonance the angular distribution varies from a nearly parallel ($\beta_{\parallel}(E) \approx 2$) to a nearly perpendicular ($\beta_{\parallel}(E) \approx -1$) type distribution. It can be shown that it is the variation in the P/R relative phase, rather than the relative magnitude, that is primarily responsible for the variation in $\beta_{\parallel}(E)$.

Transient Fluxes

We now examine the transient fluxes under pulsed excitation conditions by operating with $\mathbf{O}(t \leftarrow E)$ of Eq. (12) on the above expressions. We first look at the *partial* P and R transient predissociation-fluxes which are proportional to $|\tau(t, J_i \pm 1, \lambda = 0 \mid E_i J_i p)|^2$. We consider a Gaussian pulse peaking at $t = 0$ lasting roughly 1 psec (corresponding to a spectral width of 10 cm^{-1}) whose central frequency is 32397.88 cm^{-1}. The results are shown in Fig. 4a. We see that the P-transient is longer-lived, with a half-life ($t_{1/2}$) of ≈ 39 psec than the R-tran-

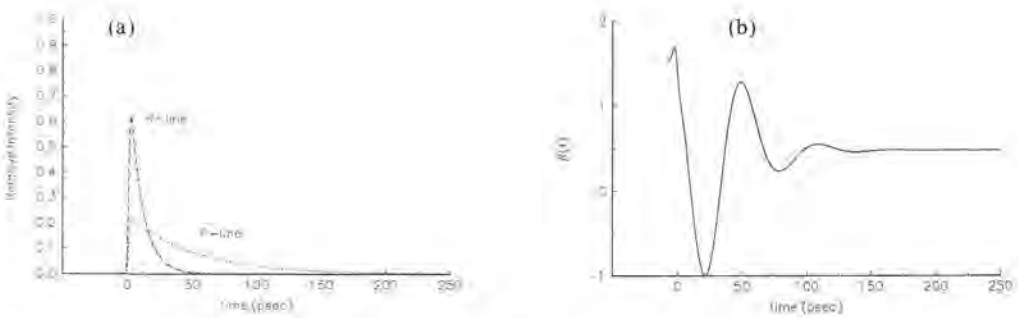

Fig. 4. (a) transient P- (dotted line) and R-type (dot-dashed line) photodissociation-rates corresponding to excitation of the transition shown in Fig. 3 by a laser pulse of 10 cm^{-1} FWHM centered at 32397 cm^{-1}, (b) the corresponding $\beta_{\parallel}(t)$.

sient whose $t_{1/2} \approx 10$ psec. This is in keeping with the corresponding energy resolved quantities, shown in Fig. 3a: the resonance width of the *P*-line, whose FWHM is $\approx 0.11\ \text{cm}^{-1}$, is smaller than that of the *R*-line, with FWHM of $0.64\ \text{cm}^{-1}$.

The corresponding transient anisotropy parameter, $\beta_{\parallel}(t)$, calculated via Eq. (27), is shown in Fig. 4b. It is seen to *oscillate* in time between the parallel and perpendicular limits: The molecule starts its life with a parallel-type $\cos^2\theta$ distribution, later this distribution breaks up and reassembles as a perpendicular-type $\sin^2\theta$ distribution, which then breaks up to reassemble with a less parallel distribution. The process repeats over and over again with an ever diminishing $\beta_{\parallel}(t)$-amplitude, until the anisotropy parameter converges asymptotically to the value of 0.5. As discussed above, in the high-J limit, this asymptotic value is the expected one when the process is dominated by either the *R*-line or the *P*-line. Indeed, as shown in Fig. 4a, the longer-lived *P*-line becomes the dominant one at times greater than 50 psec.

We have described here a (rotational) *beating* phenomenon. It is caused by the coherent excitation of two wavepackets, each belonging to a different J quantum number. In order to better appreciate this phenomenon we present in Figs. 5a-c a series of snapshots displaying the evolution of the transient fluxes of Eq. (22) as a function of time for the same psec pulse of Figs. 4. In these plots the magnitude of the radius-vector is proportional to the flux at a given direction.

We see that while the pulse builds up the predissociation flux the cloud of fragments formed is indeed of the $\cos^2\theta$ shape. However, once the pulse is completely over (at ≈ 3 psec), the distribution begins to change: As the fluxes decrease in magnitude, they are seen to undergo a smooth transition from a $\cos^2\theta$ angular shape to a $\sin^2\theta$ shape (at 20 psec). As Fig. 4b shows, $\beta_{\parallel}(t)$ actually oscillates several times after that, but the magnitude of the flux, shown in Fig. 5c, is, at this stage, quite small, making the additional oscillations less important.

The phenomenon of rotational beating strongly depends on the magnitude of the rotational quantum numbers involved. We show this by repeating the computations for other J_i values ($J_i = 2$, 10 as well as 40), while keeping the pulse parameters the same as in the above. As shown in Figs. 6a-c transitions originating from a smaller J_i quantum number yield $\beta_{\parallel}(t)$ which varies more slowly in time than transitions of higher partial waves. This phenomenon can be traced to the difference in centrifugal potentials which control $T(t, J_i \pm 1, \lambda \mid E_i J_i p)$ - the *P* and *R* radial bound-free integrals. We expect that as J_i increases so will the difference-centrifugal-potential and also the beating frequency.

A way of checking this idea in a quantitative manner is to express the time in units of t_{beat} - a rotational period associated with the difference centrifugal-potential,

$$\Delta V_{cent} = \frac{\hbar^2 J_i}{\mu R^2}. \tag{36}$$

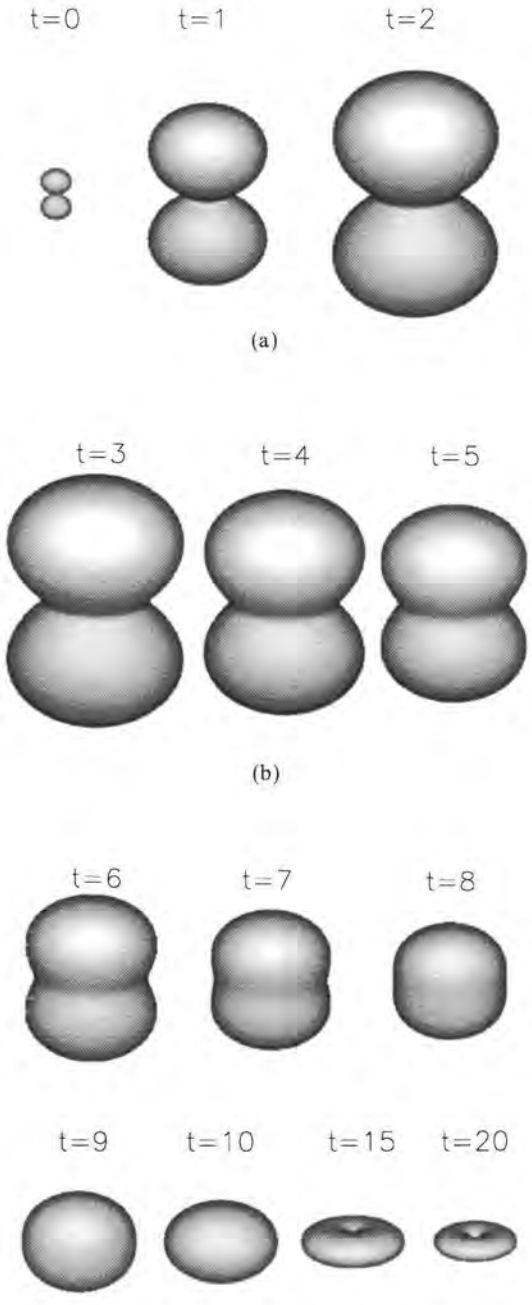

Fig. 5. Snapshots of transient predissociation fluxes for the pulse of Fig. 4. The time in psec is marked on the upper r.h.s. corner of each snapshot. a) Growth of the flux during the pulse. b) The predissociation flux immediately after the pulse. c) The flux at later times.

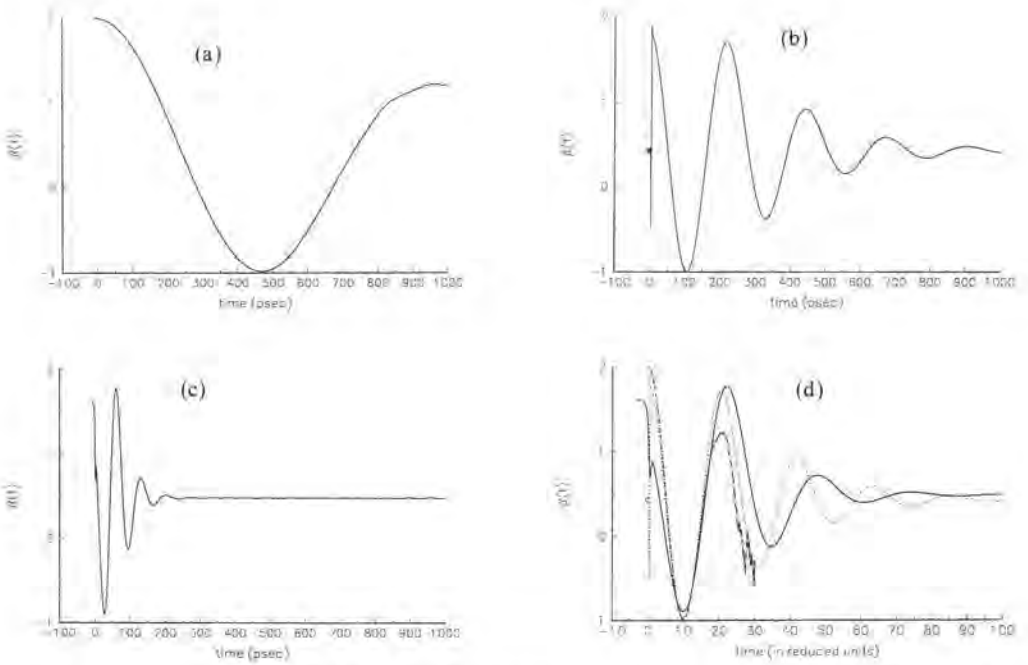

Fig. 6. $\beta_{\parallel}(t)$ for a laser profile of 10 cm^{-1} FWHM, centered at (a) $\lambda_{laser} = 232640.400$ cm^{-1} for $J_i = 2$, (b) 32630.300 cm^{-1} for $J_i = 10$ and (c) 33124.5 cm^{-1} for $J_i = 40$, and (d) the results of (a)-(c) replotted as a function of $t_{red} = t(\hbar J_i/\mu R_{eq}^2)$ for $J_i = 2$ (solid line), $J_i = 10$ (dotted line) and $J_i = 40$ (dot-dashed line).

given as,

$$t_{beat} \equiv \frac{\hbar}{\Delta V_{cent}} = \frac{\mu R^2}{\hbar J_i}. \tag{37}$$

As a first try we estimate t_{beat} by approximating R by a constant R_{eq}, chosen here to be 5.9 Å. Using the rescaled time ($t_{red} \equiv t/t_{beat}$), where $t_{beat} = 53.3$ psec for $J_i = 2$, 10.7 psec for $J_i = 10$ and 2.67 psec for $J_i = 40$, the results of Fig. 6a-c are overlapped in Fig. 6d. We see that now the initial fall-off of $\beta_{\parallel}(t)$ coincides for all J_i values. However, the plots begin to deviate from one another after about half a period. Obviously the estimate of the difference centrifugal-potential as being due to a fixed R_{eq} value is wrong. As the molecule breaks apart the difference centrifugal potential decreases, hence the inadequacy of the above t_{beat} at longer times.

We can use the beating of $\beta_{\parallel}(t)$ to *invert* the relation and deduce the *time-dependent* effective interfragment distance, $R(t)$ in a predissociation process. In Fig. 7a we plot the relative $R(t)$ thus extracted for $J_i = 10$ and $J_i = 40$. As a check, the transient anisotropies of all three J_i-levels plotted against $t_{red} = t$-

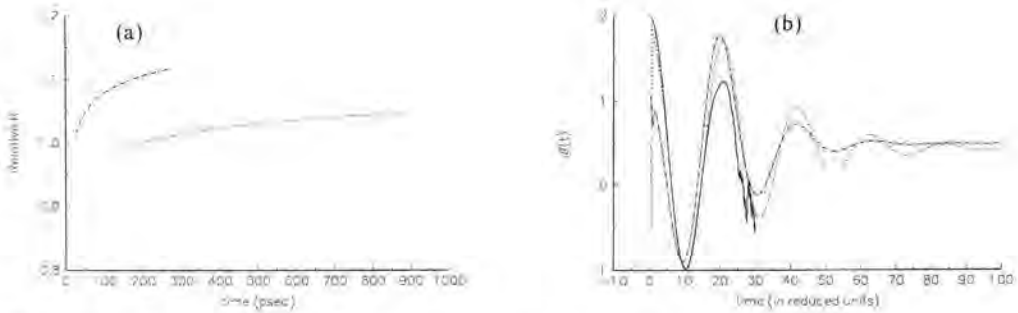

Fig. 7. (a) The relative time-dependent internuclear separation, $R(t)$, as determined from the beating in $\beta_{\parallel}(t)$ for $J_i = 10$ (dotted line) and $J_i = 40$ (dot-dashed line). (b) $\beta_{\parallel}(t)$, as in Fig. 6(d), replotted using the reduced time $t_{red} = t(\hbar J_i/\mu R(t)^2)$.

$(\hbar J_i/\mu R(t)^2)$ are shown in Fig. 7b. We see that the periodicities of all three anisotropies now neatly coincide.

The $R(t)$ extracted in Fig. 7a are seen to depend on J_i as the higher J_i values correspond to more elongated $R(t)$. From Figs. 7a and 6a-c, it is also clear that due to the shortening of the beat periodicity with J_i, information extracted from higher rotational levels pertains to earlier times.

We conclude that measurements of the changing beat frequency as a function of time would allow one to experimentally extract $R(t)$ for a *single resonance*. As discussed in the next section the $R(t)$ thus extracted should be viewed as a result of time-averaging over faster motions, if such exist. This is in fact the case when more than one resonance is excited by the laser pulse.

Vibrational Beating

As we increase the laser band-width, more than one (P or R) resonance may be excited. When this is done, we encounter *vibrational beating* type phenomena which also exist for the rotationless models of NaI [Engel 1988, Engel 1989, Choi 1989, Marcus 1988, Lin 1989, Lee 1989, Shapiro 1991a, Shapiro 1991b]. Of particular interest are the consequences of the considerable variation in the size and width of the predissociative NaI resonances [Cong 1990, Shapiro 1991b, Chapman 1991].

$\beta_{\parallel}(t)$ is also expected to be affected by the incorporation of an increasing number of resonances of differing widths. Fig. 8 shows the computed absorption spectrum of NaI superimposed with laser profiles of various band-widths, all centered at $\lambda_{laser} = 32397.88\ \text{cm}^{-1}$. As pointed out above, the laser profile of $10\ \text{cm}^{-1}$ FWHM spectral width (≈ 1 psec duration) coincides with only a single resonance while the profiles of the $30\ \text{cm}^{-1}$ FWHM and broader pulses overlap a number of peaks.

As a start, the P and R photodissociation-rates are plotted in Fig. 9a and Fig. 9b, respectively, for the 10 and $30\ \text{cm}^{-1}$-wide pulses. Those resulting from

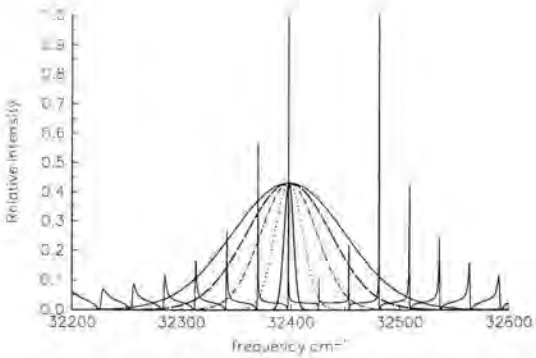

Fig. 8. The NaI spectrum in the 32200-32600 cm^{-1} range, superimposed by laser spectral profiles having widths of 10 cm^{-1} (solid line), 30 cm^{-1} (dotted line), 60 cm^{-1} (dot-dashed line), 90 cm^{-1} (dashed line) and 120 cm^{-1} FWHM (solid line).

excitation by the broader pulse rise initially more quickly and are superimposed by local oscillations of ≈ 1.2 psec time period. These oscillations arise from *vibrational beating* - the quantum recurrences of wavepackets composed of a number of coherently excited resonances. Hence the fast oscillations are not present when only a single resonance is excited (e.g. the case of the 10 cm^{-1}-wide pulse).

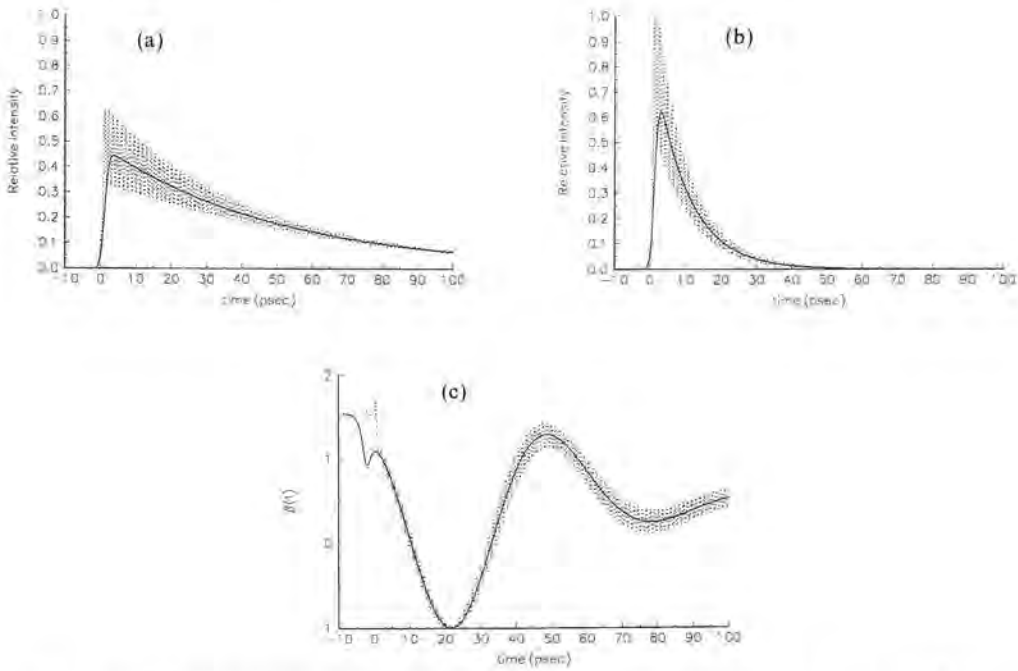

Fig. 9. A comparison of the (a) *P*-type, (b) *R*-type transient rates and (c) the corresponding $\beta_{\parallel}(t)$, calculated over 100 psec using the spectra and laser profiles of 10 cm^{-1} (solid line) and 30 cm^{-1} (dotted line) shown in Fig. 8.

The anisotropy parameter, $\beta_{\parallel}(t)$, corresponding to the P and R rates of Figs. 9a, b is shown in Fig. 9c. The anisotropy parameter corresponding to the wider ($30\,cm^{-1}$) pulse is seen to display *fast* oscillations, of ≈ 1.2 psec time period, superimposed on slow undulations. The slow undulations (common also to the $10\,cm^{-1}$ pulse) are recognizable as the rotational beating discussed in the previous section. The fast oscillations have the same origin as the vibrational beating discussed above which were first observed by Zewail et al. for the *scalar* properties [Zewail, 1989]. Indeed their periodicity, which is dictated by the inter-resonance spacing, is in good agreement with these experiments.

The magnitude of the fast oscillations become more pronounced for wider laser pulses. This effect is shown in Figs. 10a-c where we display the transient P-type rate, the R-type rate and the corresponding $\beta_{\parallel}(t)$, for the five laser profiles shown in Fig. 8. This effect is due to constructive interference between resonances. As more resonances with similar spacings are excited coherently the amplitude of the fast recurrences increases. Note that although $\beta_{\parallel}(t)$ converges, at a rate commensurate with the lifetime of the state, to the value of 0.5, the local oscillations about this value persist strongly even when there is little P- and R-transition amplitude.

The use of very broad (e.g., $>100\,cm^{-1}$) laser pulses happens to involve one additional coherent effect which alters significantly the vibrational beating. In the NaI system a broad enough laser pulse may overlap several groups of resonances, differing from one another by their relative energy spacings. As a result, the vibrational beating is expected to display several periodicities [Chapman 1991, Shapiro 1991b]. In Fig. 11a, where the NaI absorption spectrum ($J=39 \leftarrow J_i=40$) is displayed over a wide energy range, three 'families' of resonances are apparent: the first occurring at an energy $<31800\,cm^{-1}$, the second within the range 31800-32400 cm^{-1}, and the third at an energy $>32400\,cm^{-1}$. Centering a laser pulse of $240\,cm^{-1}$ FWHM at $32200\,cm^{-1}$ causes excitation of a single 'family' of resonances. As shown in Fig. 11b, the resulting vibrational beating is singly periodic. In contrast, when the same laser

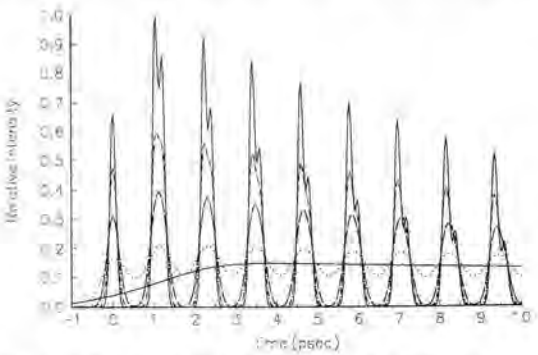

Fig. 10. The same as in Fig. 9 for the first 10 psec using the spectra and laser profiles of $10\,cm^{-1}$ (solid line), $30\,cm^{-1}$ (dotted line), $60\,cm^{-1}$ (dashed line), $90\,cm^{-1}$ (dot-dashed line) and $120\,cm^{-1}$ FWHM (solid line) shown in Fig. 8.

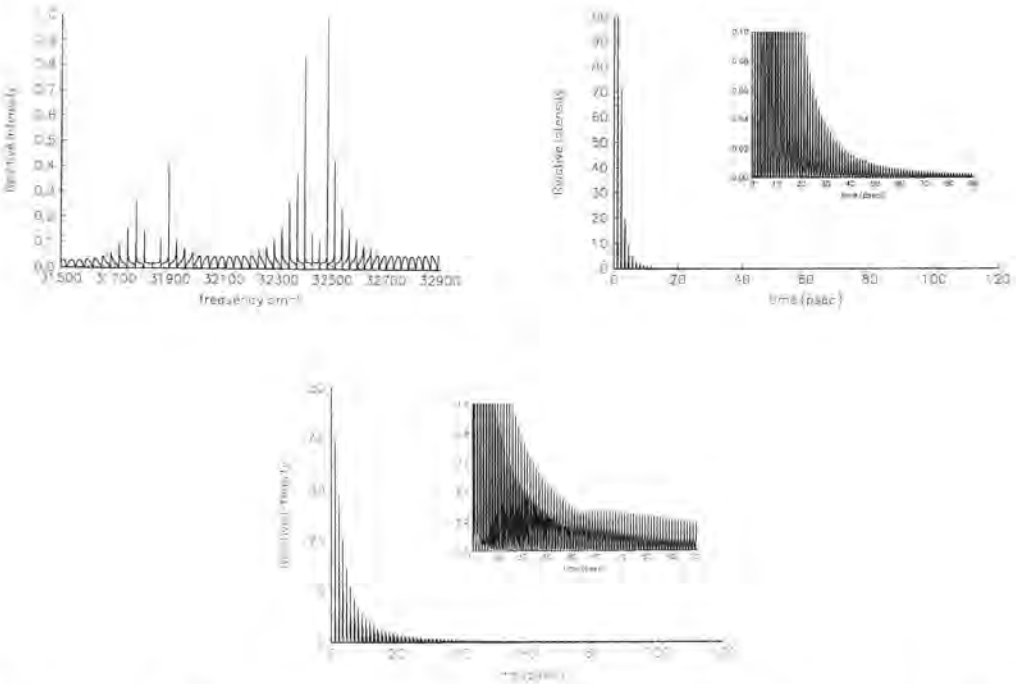

Fig. 11. (a) The NaI spectrum, for a *P*-type transition, in the 31500-32900 cm^{-1} range. (b) The transient photodissociation rates corresponds to excitation with a laser pulse of 240 cm^{-1} FWHM centered at 32200.00 cm^{-1}. (c) The same as (b) for a laser pulse centered at 32397.88 cm^{-1}.

pulse is centered at 32497.88 cm^{-1}, thus overlapping with two 'families' of resonances (see Fig. 11c), two trains of vibrational beating with slightly different periods are visible. When the two trains of beating coincide in phase (at around 60 psec) they interfere constructively (see the inset to Fig. 11c). A similar phenomenon was observed experimentally [Cong 1990] and analyzed semiclassically by Chapman and Child [Chapman 1991].

IV. Conclusions

In this paper we have introduced the concept of transient anisotropy and studied it for a predissociating system. We have shown that the transient anisotropy undergoes two types of oscillations: a slow rotational beating, which is unique to this vectorial property, and a fast quantum recurrence occurring when a number of resonances are excited simultaneously by a broad-band laser pulse, which is also observable for scalar quantities.

The rotational beating phenomenon consists of periodic oscillations between

a parallel-type and a perpendicular-type angular distribution. We have shown that the periodicity of this beating is very sensitive to the rotational state and to the time-dependent average interfragment separation.

Because of the existence of many ways of detecting the vector correlations in photodissociation [Chamberlain 1975, Docker 1987, Simons 1987, Hall 1986, Houston 1987, Hall 1989, Dixon 1986, Chandler 1987] the detection of the time-dependent anisotropy may prove to be a very powerful method of following 'real-time' dynamics. This can be achieved in a number of pump-dump scenarios. Of particular interest in the present context is the use of transient coherent polarization spectroscopy [Shen 1984, Chen 1992]. The depolarization associated with those experiments are closely connected to the initial fall-off in the rotational beating pattern discussed here.

As is the case for the scalar quantities [Krause 1991] the vectorial transients have been shown to depend sensitively on the laser pulse parameters. In fact, the energy → time transform used here already incorporates in it the pulse shape. One may, if one wishes, deconvolute the laser pulse from the observed signal. However we prefer to work with the observables themselves.

References

Balint-Kurti, G.G., and Shapiro, M., *Chem. Phys.* **61**, 137, 1981.

See, Bernstein, R.B., *Atom-Molecule Collision Theory — A Guide for the Experimentalist* (Plenum, N.Y.), pp. 239-255; 265-298, 1979.

Berry, R.S., in *Alkali Halide Vapors*, edited by Davidovitz, P., McFadden, P.L., (Academic, New York), 1979.

Bersohn, R., and Lin, S.H., *Adv. Chem. Phys.* **16**, 67, 1969.

Chamberlain, G.A., and Simons, J.P., *Chem. Phys. Lett.* **32**, 355, 1975.

Chapman, S., and Child, M.S., *J. Phys. Chem.* **95**, 578, 1991.

Chandler, D.W., and Houston, P.L., *J. Chem. Phys.* **87**, 1445, 1987.

Chen, Y. , Hunziker, L., Ludowise, P., and Morgan, M., *J. Chem. Phys.* **97**, 2149, 1992.

Choi, S.E., and Light, J.C., *J. Chem. Phys.* **90**, 2593, 1989.

Cong, P., Mokhtari A., and Zewail, A.H., *Chem. Phys. Lett.* **172**, 109, 1990.

Dixon, R.N., *J. Phys. Chem.* **85**, 1866, 1986.

Docker, M.P., Hodgson, A., and Simons, J.P., *Chem. Phys. Lett.* **128**, 264, 1987.

Dubs, M., Brülmann, U., and Huber, J.R., *J. Chem. Phys.* **84**, 3106, 1986.

Engel, V., Metiu, H., Almeida, R., Marcus R., and Zewail, A.H., *Chem. Phys. Lett.* **152**, 1, 1988.

Engel, V., and Metiu, H., *J. Chem. Phys.* **90**, 6116, 1989.

Fano, U., *Phys. Rev.* **124**, 1866, 1961.

Greene C.H., and Zare, R.N., *Ann. Rev. Phys. Chem.* **33**, 119.

Grice, R., and Herschbach, D.R., *Mol. Phys.* **27**, 159.

Hall, G.E., Sivakumar, N., and Houston, P.L., Burak, I., *Phys. Rev. Lett.* **56**, 1671, 1986.

Hall, G.E., and Houston, P.L., *Ann. Rev. Phys. Chem.* **40**, 375, 1989.
Herzberg, G., *Molecular Spectra Molecular Structure* (*I. Spectra of Diatomic Molecules*, (Van Nostrand Reinhold Co., New York), 1950.
Houston, P.L., *J. Phys. Chem.* **91**, 5388, 1987.
Jonah, C., *J. Chem. Phys.* **55**, 1915, 1971.
Krause, J.L., Shapiro, M., and Bersohn, R., *J. Chem. Phys.* **94**, 5499, 1991.
Lee, S.Y., Pollard, W.T., and Mathies, R.A., *J. Chem. Phys.* **90**, 6146, 1989.
Levy, I., and Shapiro, M., *J. Chem. Phys.* **89**, 2900, 1988.
Lin, S.H., and Fain, B., *Chem. Phys. Lett.* **155**, 216, 1989.
Marcus, R.A., *Chem. Phys. Lett.* **152**, 8, 1988.
Rittner, E.S., *J. Chem. Phys.* **19**, 1030, 1951.
Schinke, R., *Photodissociation Dynamics* (Cambridge University, Cambridge), 1992.
Shapiro, M., *J. Chem. Phys.* **56**, 2582, 1972.
Shapiro, M., *Isr. J. Chem.* **11**, 691, 1973.
Shapiro, M., and Bersohn, R., *Ann. Rev. Phys. Chem.* **33**, 409, 1982.
Shapiro, M., *Isr. J. Chem.* **31**, 323, 1991.
Shapiro, M., in *Mode-Selective Chemistry*, edited by J. Jortner, R.D. Levine, B. Pullman, (Kluwer Academic, The Netherlands) p. 283, 1991a.
Shapiro, M., *Faraday Disc. Chem. Soc.* **91**, 352, 1991b.
Shapiro, M., *J. Phys. Chem.* **97**, 7396, 1993.
Shen, Y.R., *The Principles of Nonlinear Optics* (John Wiley, New York), 1984.
Simons, J.P., *J. Phys. Chem.* **91**, 5378, 1987.
van Veen, N.J.A., de Vries, M.S., Sokol, J.D., Baller T., and de Vries, A. E., *Chem. Phys.* **56**, 81, 1981.
Williams, S.O., and Imre, D.G., *J. Phys. Chem.* **92**, 6648, 1988.
Yang, S., and Bersohn, R., *J. Chem. Phys.* **61**, 4400, 1974.
Zare, R.N., and Hershbach, D.R., *Proc. IEEE* **51**, 173, 1963.
Zare, R.N., *J. Chem. Phys.* **47**, 204, 1967.
Zare, R.N., *Mol. Photochem.*, **4**, 1, 1972.
Zare, R.N., *Angular Momentum* (John Wiley Sons Inc., New York), 1988.
(a) Zewail, A.H., *Science* **242**, 1645; (b) Zewail, A.H., and Bernstein, R.B., *Chem. Eng. News* **66**, 451988; (c) Rosker, M.J., Rose, T.S., and Zewail, A.H., *Chem. Phys. Lett.* **146**, 175; (d) Rose, T.S., Rosker, M.J., and Zewail, A.H., *J. Chem. Phys.* **88**, 6672, 1988.
Rose, T.S., Rosker M.J., and Zewail, A.H., *J. Chem. Phys.* **91**, 7415, 1989.
Zewail, A.H., *Faraday Disc. Chem. Soc.* **91**, 207, 1991.

W. Wang, L. Dhar, J. Fourkas, K.A. Nelson, L. Xiao and D.F. Coker

Femtosecond Spectroscopy of Reaction Dynamics in Condensed Phases

Abstract

Molecular dynamics simulation of solvent cage effect on photodissociation has been described. The results show that in low temperature solid matrices photoexcitation of a diatomic molecule to its gas phase repulsive excited state could lead to oscillatory quasibound motion. This type of motion should be observable with femtosecond time resolved spectroscopy. Single shot femtosecond spectroscopic methods have been demonstrated. These methods will play important roles in studying photoreaction dynamics in solid state samples.

I. Introduction

Solvent cage effects on photodissociation have been studied at length both experimentally and theoretically. Much of the experimental effort to date has been directed at events immediately following photodissociation, especially geminate recombination and vibrational relaxation. For example, seminal work on molecular iodine dissociation and recombination in liquids [Harris et al.] helped to establish I_2 as a prototype reaction for studying cage effects. The natural next step toward a more complete understanding of the cage effects is to probe solvent influence on the elementary chemical event, that is on dissociation itself, in addition to the subsequent events which may follow it. This includes the dynamics of molecular motion on the repulsive potential energy surface and nonadiabatic transitions between different potential surfaces. Recent steps in this direction have been reported. [Zewail, et al.; Scherer, et al.].

On the theoretical side, the dynamical interplay between a reacting species and its liquid-state environment has been treated primarily through a generalized Langevin equation (GLE) approach [Hynes]. In the adiabatic limit, in which the solvent (whose dynamics are 'fast') is able to follow completely the ('slow') motion toward reaction, the effective mean solvent forces on the reacting species can be calculated at any point along the reaction path. In the opposite limit, the solvent can be treated to first order as a rigid cage whose structure does not relax on the ('fast') time scale of dissociation or other motion along a

reaction path. This limit can be treated naturally through a molecular-time-scale generalized Langevin equation (MTGLE) approach [Adelman] which is mathematically equivalent to the regular GLE method but which emphasizes the dynamics on time scales faster than those of solvent relaxation. The theory reflects the fact that solvent cage effects on reactions can be separated temporally into instantaneous and delayed contributions. This is because the energy dissipation and local solvent structural rearrangement occur on a finite time scale. At the very early stage of a photodissociation reaction, the solvent environment around the reactant may not have time to adjust itself to follow the motion of the separating solute fragments. The fragments will collide with the cage which will relaxe from its initial configuration. In this case the instantaneous cage force is much stronger than the effective mean solvent forces experienced by the reactant when perfect (adiabatic) following of the solvent configuration is allowed. The delayed process corresponds to the energy flow from solute to solvent and the relaxation of the solvent structure. The complete cage effect is an interplay of these two processes. This interplay could result in reaction dynamics ranging from diffusion-like motion in the weak cage limit to oscillatory motion in the rigid cage limit.

Here we ask two questions concerning elementary liquid-state photodissociation dynamics. First, under what solvent conditions do reaction dynamics show oscillatory character due to collisions between incipient photofragments and solvent molecules? To be specific, we consider dissociation of a diatomic molecule in an unstable electronic excited state potential energy surface and we ask at what point motion in the unstable state becomes oscillatory due to trajectory-reversing collisions with neighboring molecules. This behavior should occur when the instantaneous cage forces restraining photofragment separation are sufficiently strong and the cage relaxation dynamics are slower than the time required for substantial molecular stretching along the dissociation path. Second, what are the prospects for direct experimental observation of this type of oscillatory behavior in a system which still can undergo reaction? Such observations would be of great interest not only for elucidation of solvent effects on reactions but also to provide information on the structural relaxation dynamics of solvents themselves. However they are made difficult by the extent of inhomogeneity in the liquid, reflected in a wide range of local environments encountered by photoexcited molecules. Some molecules may dissociate with little resistance, while others may undergo excited-state oscillations of varying number and frequency before dissociation or relaxation back to the molecular ground state. In addition to this inhomogeneous dephasing of intermolecular vibrational motion, fluctuations in the local environments will yield an additional (homogeneous) contribution. Thus in any experiment which averages over many excited molecules, it is not clear that oscillatory signals will be observed under any conditions. Experiments in ordinary (nonviscous) liquids are not encouraging in this regard [Joly and Nelson, Ernsting]. Results from more highly ordered media such as crystalline solids [Tokizaki, et al.], ordered van der Waals clusters [Papanikolas, et al.], and even some proteins [Vos, et al.] are more encourag-

ing, although the oscillations observed are not believed to be due to vibrations of molecules in unstable electronic excited states.

In order to reach answers to these two questions, both experimental and theoretical efforts have been undertaken. On the theoretical side, we have performed molecular dynamics simulations on a model system of a diatomic molecule (modeled after I_2) in xenon solution. Molecular dynamics simulations of I_2 in condensed phases have been carried out by many groups [Bunker and Jacobsen; Brown, et al.; Yan, et al.]. We have chosen this system in our initial study because the relevent parameters are few and well characterized. However, it is worth noting that this system may not be optimal for observation of coherent motion of unstable species within solvent cages since the solvent atoms interact only through van der Waals forces. Our main objective is to assess the likelihood of observing reactant-solvent 'collisions' (as evidenced by oscillations of the trapped fragments). This study opens the door to examination of trends as the magnitude and type of solvent forces are varied. In the current study, the density and temperature were varied.

Experimentally, the major challenge is posed by the nature of the samples most likely to show the behavior we seek. Good candidates might be liquids at evelated pressures and/or reduced temperatures and viscous liquids with strong intermolecular interactions. None of these samples can be flowed easily, and so the usual experimental approach of collecting data from a single irradiated region of the sample with excitation and variably delayed probe pulses is not viable. Since the sample must be irradiated many times by excitation pulses and variably delayed probe pulses, with the temporal information collected 'point by point' along the time axis as the probe pulse delay is varied, the buildup of reaction product in the irradiated region would interfere with the measurements. Our approach to circumvent these problems has been to develop single-shot or limited-shot femtosecond spectroscopy techniques through which the temporal evolution of the reacting species may be monitored in real time after irradiation by an excitation pulse.

II. Molecular Dynamics Simulations

Model and Method

The model system used in this study consists of one I_2 molecule embedded in a solution of 254 xenon atoms. The simulation box is cubic, and periodic boundary conditions are used for solvent-solvent and solvent-solute interactions. The box size is about 25 Å for the highest density which is big enough to accomodate the largest I-I separation in our simulations. The xenon-xenon and iodine-xenon interactions were described by Lennard-Jones potentials and calculated out to a cutoff of $2.5\sigma_{Xe}$. The iodine ground state potential was a Morse potential fitted to the RKR potential of LeRoy [LeRoy]. The excited state potential for I_2 used was that of the repulsive $^1\Pi_u$ state of form $c^{-9.5}$ [Brown, et al.]. The actual

dynamics of I_2 includes both predissociation from its bound B state and curve crossing to other states at the asymptotic region. For our goal of seeking oscillatory behavior under a range of conditions, we have ignored these effects and considered only the $^1\Pi_u$ state with no curve crossing. The parameters used in this study are listed in Table 1.

Newton's equations of motion were propogated with 1 fs step size using the velocity Verlet algorithm [Swope, et al.]. First a set of solvent configurations was generated, starting from a FCC lattice of 256 xenon atoms at a specified density and at 1000 K. After 1000 steps with temperature scaling, we integrated the system for 5 to 6 ps before we started to save configurations of the system at 5 ps intervals. A total of 1,024 configurations at each specified density were saved. The radial distribution functions were examined, and confirmed that the liquid state was reached for each density. Next we used the set of 1,024 configurations to generate the initial solution configurations. Two adjacent xenon atoms were removed from the center of the simulation box in each solvent configuration, and an I_2 molecule was inserted in their place. The iodine center of mass and orientation matched those of the two removed xenon atoms. The system was then allowed to run at 1000 K for 5 to 6 ps, with velocity scaling for the first picosecond. The final temperature was reached by quenching the system from 1000 K down to the chosen temperature and letting the system equilibrate for 8 to 10 ps. At this point, the simulation of photodissociation began. Photoexcitation was simulated by swithing the I_2 potential from the ground to the excited state for all trajectories. This corresponds to excitation by a δ-pulse. The evolution of the system was then monitored for 2 picoseconds and relevent quantities were saved for analysis.

Several solvent reduced densities were used. Here we report results from a liquid solution with reduced density of 0.7 at temperature 250 K. We also report

Table 1. Potential parameters

Xe-Xe	$4\varepsilon[(\sigma/r)^{12}-(\sigma/r)^6]$ $\sigma = 4.055$ Å $\varepsilon = 229$ K
I-Xe	$4\varepsilon[(\sigma/r)^{12}-(\sigma/r)^6]$ $\sigma = 3.94$ Å $\varepsilon = 328.6$ K
I-I (ground state)	$D\{\exp[-2\beta(r-r_e)]-$ $2\exp[-\beta(r-r_e)]\}$ $D = 18044.61$ (K) $\beta = 1.867$ (Å^{-1}) $r_e = 2.668$ (Å)
I-I (excited state)	$cr^{-9.5}$, $c = 5.755 \times 10^7$ (K)

results at a solvent reduced density of 1.1 and a temperture of 40 K to simulate rigid cage limit. This corresponds to a low-temperature solid solution. Our results show that the solvent radial distribution function for the solid solution is similar to those reported earlier [Abraham; Rahman, et al.] for amorphous Lennard-Jones solids with a split second peak. This solid is different from crystalline xenon which obtains at the specified density and temperature. However, since our primary interest is to investigate the possibility of observing coherent oscillatory motion of unstable molecules in solvent cages with inhomogeneous environments, amorphous solids should be more suitable. A more detailed report on a range of solid and liquid densities will be presented subsequently [Wang, et al.].

The pure solvent runs were performed on SGI workstations. All runs with I_2 were carried out on the Thinking Machines Corp. CM5 at Boston University. Since our problem was intrinsically parallel, linear speedup can be achieved. The CM5 we used was a 64-node distributed memory parallel machine partitioned into one 32-node and two 16-node partitions. Each processing node includes one RISC microprocessor, with 32 Mbytes of memory divided into 4 banks each of which is attached to a vector unit (VU). Each VU was optimally suited for a vector of length 8, and so with the 32-node machine we were able to run all 1,024 trajectories simultaneously. On a 16-node machine longer processing times were needed to run 1,024 trajectories. With our system of 256 particles and 1,024 trajectories, about 2 seconds per step were required on the 32-node machine and about 4 seconds per step on the 16-node machine.

Results and Discussion

Figure 1 shows the major results for the high-density, low-temperature solution. The first panel shows the averaged internuclear distance between the two iodine atoms as a function of time. Oscillatory motion in the unstable electronic excited state is clearly seen. The second panel shows the force autocorrelation function $\langle \mathbf{F}(0) \cdot \mathbf{F}(t) \rangle$ and orientational autocorrelation function $\langle P_2[\cos \theta(t)] \rangle$ of the I-I pair. The quasibound motion of the I-I pair is again demonstrated. The last two panels show the probability of finding the I-I separation within a predefined window on the potential surface. This quantity was used to estimate the results of a femtosecond transient absorption experiment. A precise calculation would require detailed potential energy surfaces for both the initial and final states involved in the probing process and the transition dipole moment for the probe wavelength and spectral bandwidth. The goal in the present work was simply to assess whether the oscillatory dynamics might be observed with realistic averaging over an ensemble of trajectories. We used a window of width 0.2 Å centered at positions (I-I separations) of 3.3 Å and 3.9 Å. These values represent probing at the inner and outer (cage) potential wall respectively. At the inner wall, we see first a sharp peak corresponding to the initial passage of the trajectories through the probing region. Then there is a slower rise due to the rebound off

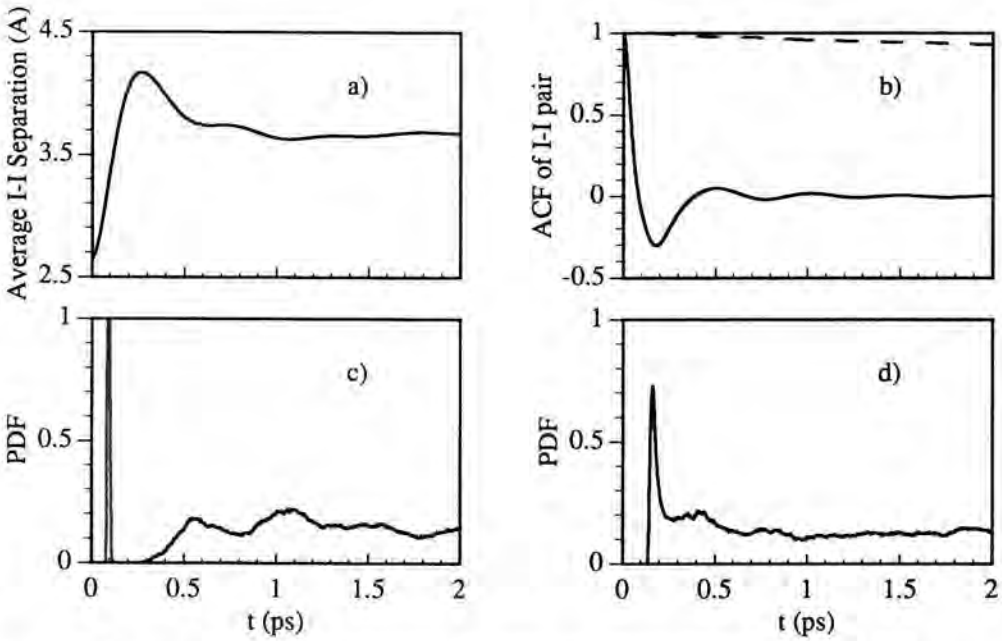

Fig. 1. MD simulation results for model I_2 in xenon of reduced density 1.1 and at 40 K. a) average I-I internuclear separation; b) force (full line) and orientation (dashed line) autocorrelation functions; c) probability of finding I-I in a 0.2 A window centered at 3.3 A on potential surface; d) same as in panel c) except the window is centered at 3.9 A.

of the solvent cage. Superimposed on this rise is an oscillation which reflects coherent oscillation in the excited-state PES which would be unbound except for the cage forces which restrain fragment separation. This explanation is supported by comparing the oscillation period with the force autocorrelation function. The oscillation peaks match precisely to the positive peaks in the force autocorrelation function. The same picture can be seen at the outer probing window as well. In this case, two oscillations are seen. They match the negative peaks of the force autocorrelation function. An additional interesting feature associated with the outer probing region is the splitting of the first peak. This corresponds to the swarm of trajectories moving in and out of the probing region. This effect has been observed [Mokhtari, et al.] in gas phase NaI, and provided information about the intramolecular potential energy surfaces. Our results suggest that the observations can be extended to condensed phases and will provide information about the dynamical cage forces. The period of the oscillation is about 500 fs which implies a cage period of about 1 ps. More detailed discussion will be presented elsewhere.

Figure 2 shows the simulation results for the low density and high temperature solution. Since the general behavior is almost the same for all probing positions along the potential surface, we present here only one probability distribution function. The window width was set to 0.2 Å and the center of the window

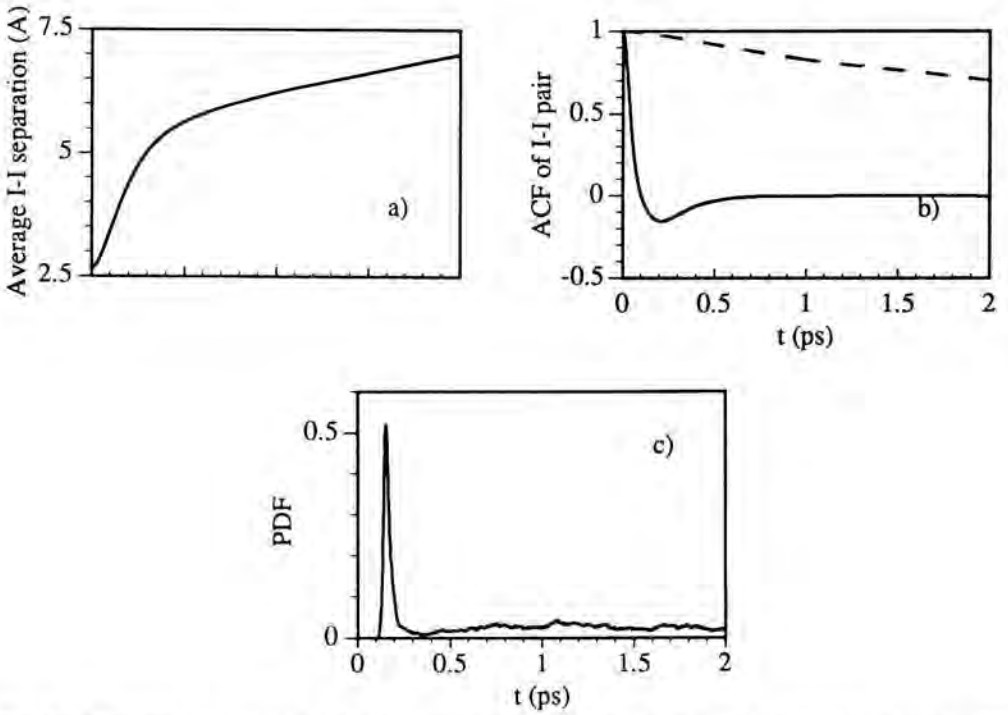

Fig. 2. MD simulation results of I_2 in xenon of reduced density 0.7 and at 250 K. a) average I-I separation; b) force (full line) and orientation (dashed line) autocorrelation function; c) probability distribution for a window centered at 3.5 A and 0.2 A wide.

was at 3.5 Å. No oscillatory motion is observed. From the force autocorrelation function, we can see that although there is a hard first collision with the solvent cage, relaxation of the cage is fast in this case. The average I-I separation increases monotonically (top sweep) with no oscillations as observed at higher density.

The preliminary results reported here are encouraging in that they suggest that conditions needed for observation of oscillatory motion in unstable potential energy surfaces may be obtained in some materials at realistic pressures and temperatures. As mentioned above, there may be many systems with greater propensity toward showing this behavior than iodine in xenon.

III. Femtosecond Single Shot Methodologies

As mentioned in the introduction, it is likely that systems in which the oscillations we are studying can be observed may involve elevated pressures, high viscocities, or other samples not conducive to flowing and removal of reaction products. Efforts are underway to develop methods for single-shot femtosecond

spectroscopy. The laser system used to conduct these preliminary single shot experiments has been described in detail in earlier publications [T.P. Dougherty, et al.]. Briefly, an antiresonant ring dye laser is synchronously pumped by the frequency-doubled output of a cw modelocked Nd:YAG laser. The output, centered at 620 nm, is passed through a three-stage amplifier which is pumped by the frequency-doubled output of a Q-switched, modelocked, and cavity-dumped Nd:YLF laser. The Nd:YAG and Nd:YLF pump lasers are synchronized through the use of a common RF source which drives both of their modelockers. The synchronously amplified output consists of 80 fs, 10 μJ, 620 nm pulses at a 500 Hz repetition rate.

Multiple Probe Pulse Method

We have constructed a single-shot femtosecond spectrometer consisting of a series of partial reflectors, delay lines, and other optics such that a single probe pulse is split into sixteen pulses whose arrival times at the sample are controlled independently. The setup is illustrated in Fig. 3. The apparatus includes several sets of four reflectors whose reflectivities at the probe wavelength are 25%, 33%, 50%, and 100%. This insures reasonably equal intensities of all sixteen probe pulses. The probe pulses are overlapped spatially with the excitation pulse at the sample. The transmitted probe pulses are incident on different regions of a CCD detector and their intensities are measured. The CCD detector is equipped with software designed to locate separate 'regions of interest' (i.e. separate laser spots) and to carry out simple manipulations of the intensities recorded at pixels within each region.

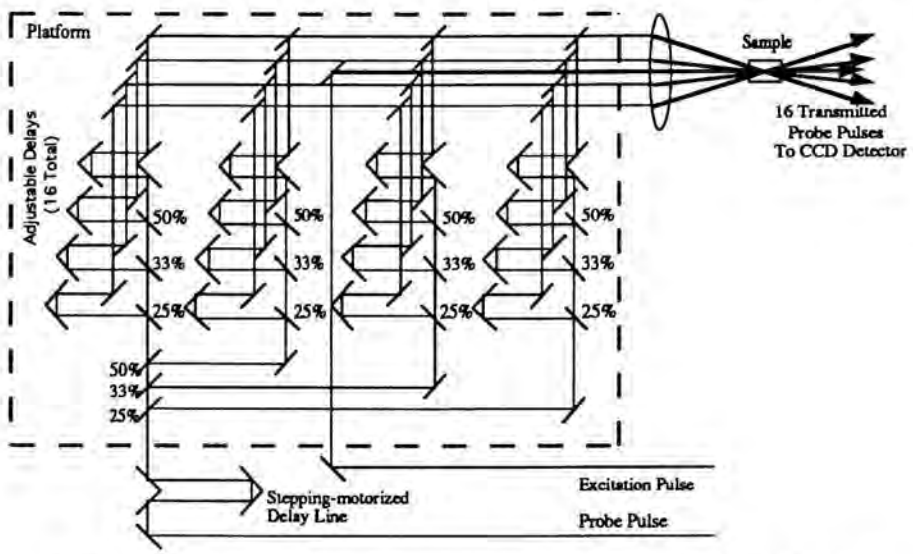

Fig. 3. Schematic illustration of pump-probe experiment with 16 probe pulses.

In the preliminary multiple probe pulse experiments, transient birefringence (i.e. optical Kerr effect or OKE) or transient absorption was measured. In the former case, the excitation pulse was linearly polarized at 45° from vertical (V). The probe pulses were V polarized, and a horizontal (H) polarizer was placed in front of the CCD detector. In the latter case, the excitation polarization was varied and there was no polarizer after the sample. Note that in addition to the individual delay lines for each probe pulse, there is an overall delay line which changes the timing of all the probe pulses relative to the excitation pulses but not relative to each other. Data were recorded with several choices of overall delay to check for internal consistency. In addition, data were recorded over periods of several hours to check for drift in the spatial alignment of the pulses in the sample or at the CCD detector.

The first one-shot data were optical Kerr effect measurements on carbon disulphide liquid in a 2 mm thick cuvette. Typical data are shown in Fig. 4, along with data recorded in the conventional manner (many shots, with a variably delayed probe pulse). These data were recorded before the CCD detector was equipped with the software to do automatic analysis on multiple regions of interest (ROI's). The integrated intensity readings at each laser spot were recorded by repeating ROI analysis for each spot manually to determine the intensity of the corresponding pulse. Differences in probe pulse intensities or in the degrees of overlap between different probe pulses and the excitation pulse were not accounted for. Thus the data show considerable scatter. Nevertheless, the overall temporal response of the sample is represented. The data were reproducible, as illustrated in Fig. 5 which shows an additional one-shot scan recorded with a slightly different 'overall' delay relative to the excitation pulse but with no changes in the relative delays. The response (including scatter, which is primarily due to systematic errors described above) is the same except for the small

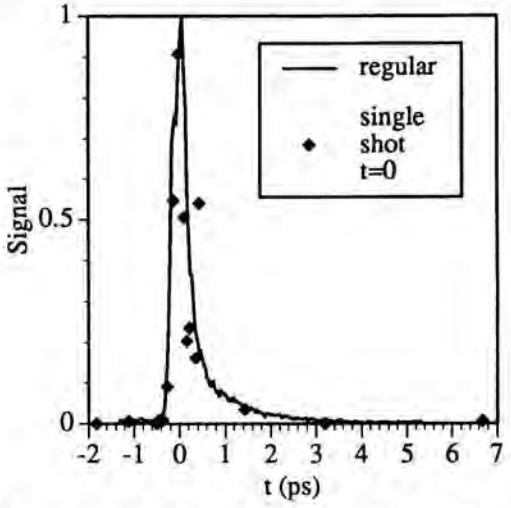

Fig. 4. Single shot optical Kerr effect in CS_2.

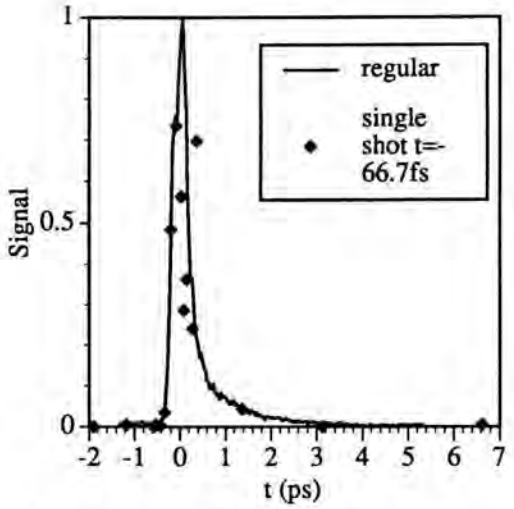

Fig. 5. Same as in Fig. 4 except an overall delay of the pump pulse against the probe pulses.

changes in overall timing. These and other data were recorded over a period of several hours, with no apparent deterioration due to changing spatial overlap of the seventeen pulses.

Transient absorption measurements were recorded on an approximately 10^{-3} M solution of malachite green in ethanol in a 2 mm cuvette. The CCD detector was equipped with the software described earlier, and differences in probe pulse intensities were accounted for in the analysis. Differences in the extent of overlap between different probe pulses and the excitation pulse were partially accounted for by measuring the transient absorption of each probe

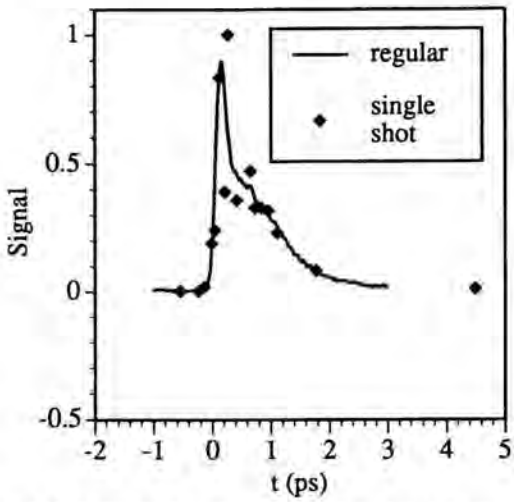

Fig. 6. Single shot pump-probe experiment in malachite green in methonal.

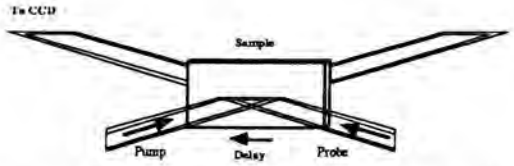

Fig. 7. Geometry of the large angle single shot pump-probe experiment.

pulse at zero delay time, and normalizing the data appropriately. Typical data are shown in Fig. 6. Remaining systematic error may be reduced with the use of a different excitation wavelength, which eliminates excitation scatter and coherent coupling of varying amounts into the probe spots on the CCD. Additional data recorded from malachite green over periods of several hours and with different 'overall' timing were consistent with that shown.

Large-angle Method

An alternate approach to single-shot ultrafast spectroscopy is to spatially encode temporal information onto a single probe beam. An example of such a technique is shown in Fig. 7. In this pump/probe setup, both the pump and probe beams are cylindrically focussed onto a thin sample. The direction of the pump beam propagation makes an angle θ with the surface normal, and the direction of the probe beam makes an angle of $-\theta$. Thus, the pump beam hits the left side of the sample first and the right side of the sample last, whereas the probe beam hits the right side of the sample first and the left side of the sample last. This acts to encode a delay time into the spatial profile of the probe beam, i.e., the rightmost part of the probe beam experiences the shortest interpulse delays, while the

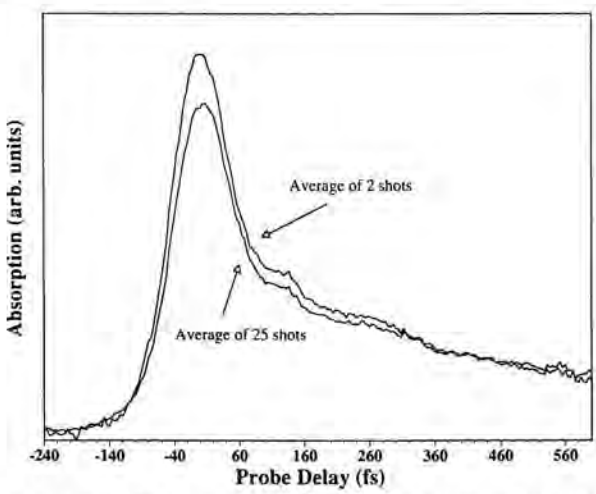

Fig. 8. Single shot pump-probe data taken in malachite green with the large angle method.

leftmost part experiences the longest delay. Using an array detector, the spatial intensity profile of the probe beam can be monitored in a single laser shot. This technique is related to single-shot autocorrelation methods that have been demonstrated. [Kane and Trebino].

Shown in Fig. 8 is an example of preliminary data recorded with this technique. The sample was a 100 μm-thick cell of ethyl violet in methanol. The top curve is result of averaging only two laser shots while the bottom curve is the average of twenty-five shots.

IV. Summary

Molecular dynamics simulations have been carried which indicate that in a condensed-phase environment that offers sufficient resistance against molecular photofragmentation, phase-coherent vibrational oscillations of the photoexcited species can be observed. Experimental realization of this possibility would yield valuable insight into the strengths of solvent forces exerted on reactive species and on the effects of local solvent relaxation on solute reaction dynamics and yield. The simulation results indicate that elevated pressure (or perhaps highly viscous solvents) are necessary to provide a sufficiently strong force. In this case continuous flow of the sample is not possible and a buildup of reaction product may occur during time-resolved measurements involving repeat irradiation of a sample volume with the excitation pulse. Preliminary demonstrations of two single-shot femtosecond spectroscopy methods that avoid product buildup problems have been presented.

Acknowledgments

The authors thank Robert Putnam of Thinking Machines Corp. for help on CM5. W.W., L.D., J.F., and K.A.N. were supported in part by ONR Grant No. N00014-90-J-4070 and by NSF grant no. CHE-8901722. L.X. and D.F.C. were supported in part by NSF grant no. CHE-8913780 and CHE-9058348.

References

Abraham, F.F., *J. Chem. Phys.* **72**, 359, 1980.
Adelman, S.A., a) *Adv. Chem. Phys.* **53**, 61, 1983; b) *J. Stat. Phys.* **42**, 37, 1986.
Brown, J.K., Harris, C.B., and Tully, J.C., *J. Chem. Phys.* **89**, 6687 (1988).
Bunker, D.L., and Jacobsen, B.S., *J. Amer. Chem. Soc.* **94**, 1843 (1972).
Dougherty, T.P., Wiedderecht, G.P., and Nelson, K.A., *Science* **258**, 770, 1992.
Ernsting, N.P., *Ultrafast Phenomena VIII* (Springer-Verlag, Berlin, 1993), p. 638.
Harris, A.L., Brown, J.K., and Harris, C.B., *Ann. Rev. Phys. Chem.* **39**, 341, 1988, and the references therein.

Hynes, J.T., in Theory of Chemical Reaction Dynamics IV, M. Baer (Ed.), CRC Press, 1985.
Joly, A.G., and Nelson, K.A., *Chem. Phys.* **152**, 69, 1991.
Kane, D.J., and Trebino, R., *Opt. Lett.* **18**, 823, 1993.
Khundkar, L.R., and Zewail, A.H., *Ann. Rev. Phys. Chem.* **41**, 15, 1990.
LeRoy, R.J., *J. Chem. Phys.* **52**, 2683, 1970.
Mokhtari, A., Cong, P.J., Herek, L., and Zewail, A.H., *Nature*, **348**, 225, 1990.
Papanikolas, J.M., Vorsa, V., Nadal, M.E., Campagnola, P.J., Gord, J.R., and Lineberger, W.C., *J. Chem. Phys.* **97**, 7002, 1992.
Rahman, A., Mandell, M.J., and McTague, J.P., *J. Chem. Phys.* **64**, 1564, 1976.
Swope, W.C., Anderson, H.C., Berens, P.H., and Wilson, K.R., *J. Chem. Phys.* **76**, 637, 1982.
Tokizaki, T., Makinura, T., Akiyama, H., Nakumara, A., Tanimura, K., and Itoh, N., *Phys. Rev. Lett.* **67**, 2701, 1991.
Vos, M.H., Lambry, J.-C., Robles, S.J., Youvan, D.C., Breton, J., and Martin, J.-L., *Proc. Natl. Acan Sci. USA* **88**, 8885, 1992.
Wang, W., Nelson, K.A., Xiao, L., and Coker, D.F., in preparation.
Yan, Y., Whitnell, R.M., Wilson, K.R., and Zewail, A.H., *Chem. Phys. Lett.* **193**, 402, 1992.
Zewail, A.H., Dantus, M., Bowman, R.M., and Mokhtari, A., *J. Photochem. Photobiol.* **A62**, 301, 1992.

Authors' addresses

W. Wang, L. Dhar, J. Fourkas, and K.A. Nelson: Department of Chemistry, Massachusetts Institute of Technology, Cambridge, MA 02139, USA
L. Xiao and D.F. Coker: Department of Chemistry, Boston University, Boston, MA 02215, USA

Charles V. Shank, Robert W. Schoenlein, Chris J. Bardeen,
and Daniel M. Mittleman

Femtosecond Photon Echoes

Abstract

The advent of femtosecond optical pulse technology has permitted the application of photon echo spectroscopic techniques to optical transitions in condensed matter that have previously been inaccessible owing to a lack of sufficient time resolution. Often transitions which dephase on a femtosecond time scale involve a complex manifold of levels. A mode cancellation technique has been developed to suppress the apparent dephasing effects of a dominant vibrational mode. Applications to molecules in solution and semiconductor nanocrystals will be described.

Introduction

The nature of spectral broadening of electronic transitions in condensed matter systems has recently been the subject of considerable interest. Several nonlinear optical techniques, including coherent and incoherent transients (Becker et al., 1989; Bigot et al.,1991; Weiner et al., 1985; De Silvestri et al., 1984, Nibbering et al., 1991; Moshary et al., 1991), hole burning (Brito Cruz et al., 1986), and resonance Raman spectroscopy have been used to measure the contributions of various processes and timescales.

The two pulse photon echo technique or time resolved four wave mixing (Kurnit et al, 1964) is the most general technique for measuring dephasing of an optical transition. A two pulse optical sequence is used to excite the transition under study. The first pulse excites the electronic transition, creating a macroscopic polarization in the medium; a second optical pulse delayed in time scatters off of the polarization in the momentum phase-matched direction ($2\mathbf{k}_2 - \mathbf{k}_1$). For an inhomogeneously broadened transition the scattered wave is an echo, which is an optical pulse delayed in time by an amount corresponding to the spacing of the exciting pulse sequence. The energy of the echo pulse decays as the delay of the exciting pulses becomes comparable to the dephasing time of the optical polarization. For a homogeneously broadened transition an echo is not produced; the scattered wave is not a pulse but a polarization free decay.

The above description is complete for a photon echo in a simple two level

system. However, most real experimental systems possess a manifold of levels which greatly complicates the interpretation of the echo. For a molecule each of the Franck Condon connected levels produces an echo. Since all of the echoes are coherent, they interfere giving rise to quantum beats. These quantum beats can give the appearance of rapid dephasing.

A scheme for reducing the effects of quantum beats involves the addition of a third optical pulse to the excitation sequence. In this case a three pulse (3PE) or stimulated echo is detected in the phase matched direction $(-\mathbf{k}_1+\mathbf{k}_2+\mathbf{k}_3)$. The energy of the 3PE is measured as a function of the time delay between the first and second pulse $\mathbf{t}_{12}$ or as a function of the delay between the first and third pulse $\mathbf{t}_{13}$. Since the arrival of the third pulse determines when the echo is formed, it is possible to generate the echo at a specific phase of the quantum beat by adjusting $\mathbf{t}_{13}$. In particular, if the third pulse is delayed by exactly one vibrational period, then the nuclei have returned to their original positions and the quantum-beat modulation of the echo is suppressed. In contrast, if the arrival of the third pulse is out of phase with the vibrational motion, then the nuclei are maximally displaced and the echo decay is strongly modulated by the quantum beat.

The concept of quantum-beat suppression was initially described as a means of suppressing modulations due to hyperfine splitting in electron-spin echo experiments (Mims, 1972). For an inhomogeneously broadened system, delta function pulses, and a single harmonic mode at a frequency w, the 3PE echo signal

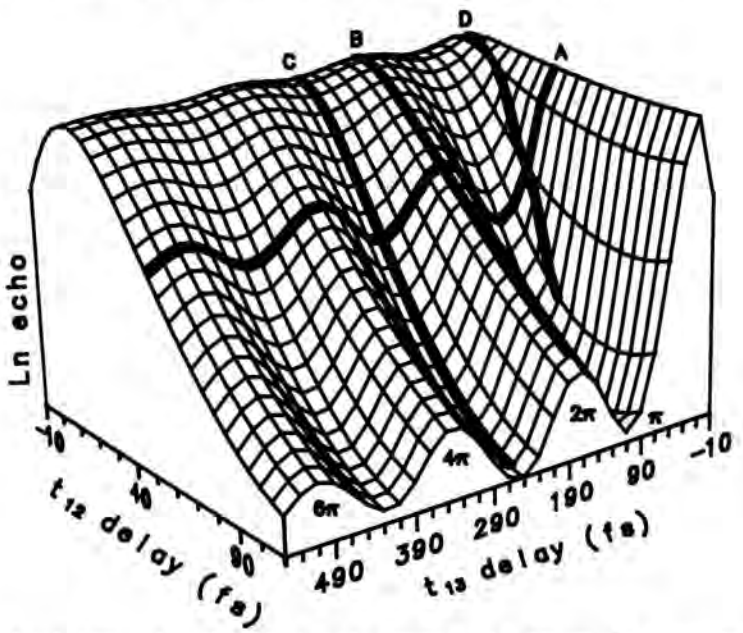

Fig. 1. Calculated three-pulse echo signal in the presence of a 200 cm^{-1} photon mode as a function of delay between pulse one and two (t_{12}) and between pulse one and three (t_{13}). Solid line D corresponds to the two-pulse echo in which $t_{12}=t_{13}$.

in the $-\mathbf{k}_1+\mathbf{k}_2+\mathbf{k}_3$ direction is given by (Heller, 1975; Yan and Mukamel, 1988; Yan and Mukamel, 1991)

$$S(\mathbf{t}_{12}, \mathbf{t}_{13}) \sim \exp[-4\Delta^2(1-\cos\omega\mathbf{t}_{12})\,(1-\cos\omega\mathbf{t}_{13})]\exp[-4\mathbf{t}_{12}/T_2]$$

where T_2 is the electronic dephasing time and Δ is the electron-phonon coupling parameter (dimensionless nuclear displacement). The modulation of the echo response corresponds to the harmonic displacement of the nuclei, $\delta x \sim \Delta[1-\cos(\omega t)]$, where $\delta x = 0$ refers to the equilibrium position of the nuclei in the ground state (i.e. prior to excitation). Clearly, the quantum-beat modulation of the echo is strongest for $\mathbf{t}_{13} = \pi/\omega$ ($\delta x =$ maximum) and the modulation is completely suppressed for $\mathbf{t}_{13} = 2\pi/\omega$ ($\delta x = 0$).

Fig. 1 shows the predicted three-pulse photon echo response ($-\mathbf{k}_1+\mathbf{k}_2+\mathbf{k}_3$ direction) in the presence of quantum beats, as a function of the delay between the first and second pulse $\mathbf{t}_{12}$ and between the first and third pulse $\mathbf{t}_{13}$. This illustrative calculation includes a dephasing time of 80 fs, as well as the (damped) vibrational dynamics of a 205 cm^{-1} mode. The solid line (A) represents the expected echo response for a fixed delay of the second pulse ($\mathbf{t}_{12} = 50$ fs) as a function of the third pulse delay. The oscillations in (A) result from the vibrational coherence of the mode.

Experiment

The first application of the quantum beat suppressed photon echo technique has been the study of electronic dephasing in CdSe nanocrystals (Schoenlein et al, 1993). These crystals which range in size from 20 to 80 Angstroms have very interesting properties. These crystals exhibit a number of novel properties resulting from three-dimensional confinement because they are small compared to the size of a bulk exciton. In such crystals, the quasi-continuum of electronic states in the bulk is reduced to a series of discrete electronic transitions. This change in density of states gives rise to large optical nonlinearities and a blue-shift of the excitonic absorption peak. Due to the strong dependence of the band gap on size (Alivisatos et al, 1989), even highly monodisperse samples are substantially inhomogeneously broadened. The photon echo technique is ideally suited to measuring dephasing in these crystals.

These photon echo measurements were performed with a laser system (Schoenlein et al., 1990) consisting of a colliding pulse modelocked laser (CPM) with two multipass dye amplifiers pumped at 400 Hz by a XeF excimer laser. Microjoule pulses from the first amplifier (50 fs, 620 nm) are used to generate a white-light continuum in a jet of ethylene glycol, and the blue green (484-507 nm) portion of the continuum is re-amplified in the second amplifier. A sequence of gratings and prisms are used to directly compress the amplified continuum, resulting in nearly transform-limited pulses of 15 fs duration.

Initial measurements of electronic dephasing in 22 Angstrom CdSe nanocrystals were performed with the two pulse echo technique. The echo decay times (t_{echo}) observed ranged from ~ 9 fs at 30 K to ~ 6 fs at 235 K. The extremely rapid decay and the temperature dependence suggests that the polarization response measured by the two-pulse echo is strongly modulated by the vibrational modes of the system as described in the introduction. This result corresponds to line D in Figure 1.

Next, experiments were performed using the three pulse photon echo technique. The experimental result corresponding to the prediction of Fig. 1 line (A) is shown in Fig. 2. In this measurement of the echo signal as a function of $\mathbf{t}_{13}$ (with $\mathbf{t}_{12} = 33$ fs), oscillations are observed resulting from the coherent vibrational excitation, and the measured period is consistent with the 205 cm^{-1} LO phonon mode. In addition the phonon oscillations are damped on a time scale of a picosecond. This damping is likely due to the decay of optic phonons into low frequency vibrational modes, and is in good agreement with the measured 15 cm^{-1} Raman line width (Alivisatos et al., 1989).

In order to directly investigate electronic dephasing the results of Fig. 2 are used to determine the optimal delay for the third pulse. By positioning the third pulse at exactly one LO phonon period ($\mathbf{t}_{13} = 2\pi/\omega$) and scanning the delay of

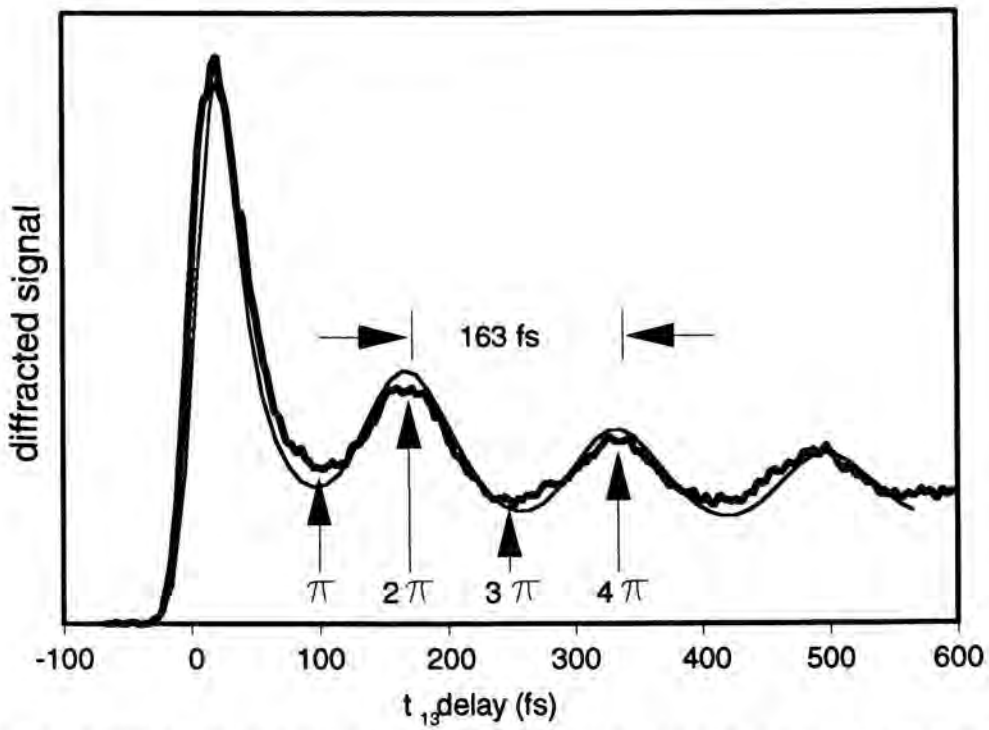

Fig. 2. Detected signal for setting $\mathbf{t}_{12}$ to zero and scanning $\mathbf{t}_{13}$, the delay of the third pulse. The thick line is experimental and the thin line is a theoretical fit with one phonon mode at 205 cm^{-1}.

pulse two (t_{12}) the effects of the vibrational dynamics can be effectively suppressed (Fig. 1 curve B). Conversely, if the third pulse is positioned out of phase with the LO phonon ($t_{13} = 3\pi/\omega$), then the decay will be strongly modulated by the quantum beat (Fig. 1 curve C). The corresponding experimental measurements are shown in Fig. 3. With the third pulse in the 2π position ($t_{13} = 163$ fs) an echo decay time of 20 fs is measured. With the third pulse in the 3π position ($t_{13} = 245$ fs), the echo is strongly modulated by the quantum beat, and the decay time is much faster (9 fs).

The mode suppressed photon echo technique can also be used to study the nature of spectral broadening of electronic transitions of large molecules in solution. A dye molecule often has a large manifold of vibronic levels which can rapidly damp a photon echo signal. Previous three pulse photon echo experiments on large molecules in solution have not addressed the complexity of multilevel interactions (Bigot et al., 1991, Becker et al., 1989).

Typically a large molecule such as the oxazine molecule LD690 has a system mode with a strong Franck-Condon overlap. In an oxazine molecule, a ring breathing mode at about 590 cm^{-1} is dominant. This mode will strongly modulate the polarization induced in the sample by a femtosecond pulse, and will therefore complicate the interpretation of echo experiments. The strength of this modulation is evident in Fig. 4, in which the 3PE signal for LD690 dissolved in ethylene glycol is shown as a function of the third pulse delay t_{13} (Bardeen and Shank, 1993). An oscillation with a period of roughly 60 fs is clearly observed.

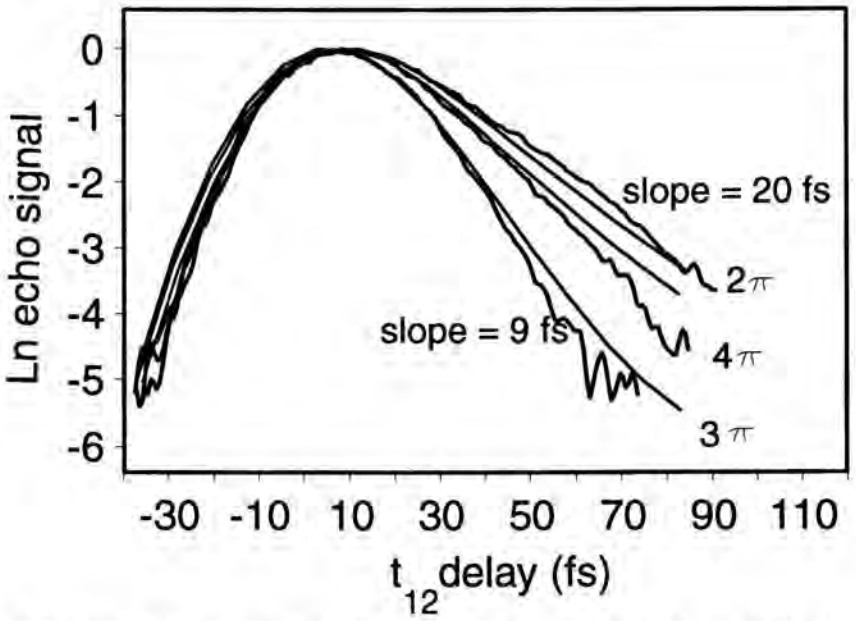

Fig. 3. Three-pulse echo (22 Angstrom particles, 15 K) as a function of t_{12}, with the third pulse in phase for curves labeled 2π and 4π, and out of phase for the curve labeled 3π, with quantum beat of 163 fs. The thin lines are calculated fits.

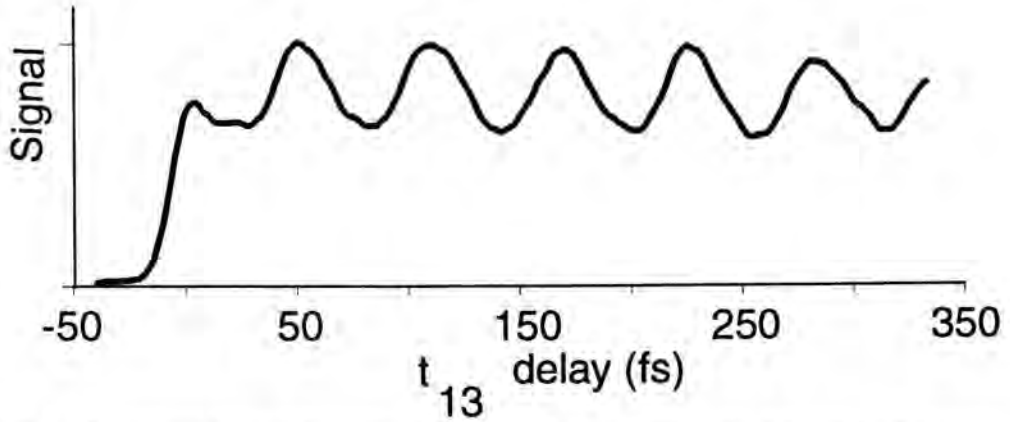

Fig. 4. Experimental signal for setting t_{12} to zero and scanning t_{13}, the delay of the third pulse, showing the population dynamics of LD690.

Using the 3PE, the effects of this vibration can be suppressed. Fig. 5 shows measured (thick lines) and calculated (thin lines) 3PE signals in LD690 as a function of the second pulse delay t_{12}. The upper lines are for a delay of $t_{13} =$ 60 fs and the lower lines are for $t_{13} = 90$ fs. The measurement at 60 fs delay is in phase with the vibration and is clearly asymmetric and shifted in time with a slower decay than the 90 fs measurement. The difference between the two measu-

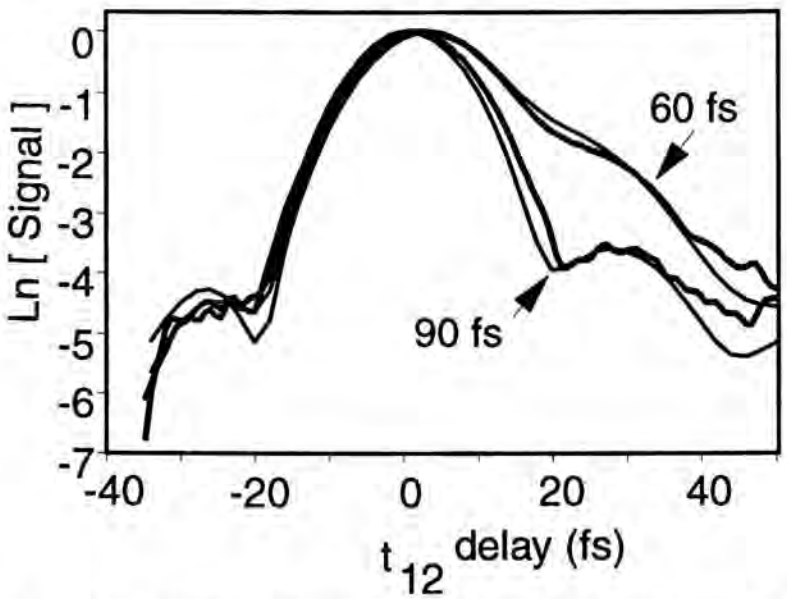

Fig. 5. Experimental (thick) and calculated (thin) three pulse echo signals, scanning the second pulse, for $t_{13} = 60$ fs and $t_{13} = 90$ fs in the molecule LD690. For the calculated signal a T_2 of 30 fs and an inhomogeneous linewidth of 295 cm^{-1} have been assumed.

rements clearly illustrates the influence of the 590 cm^{-1} mode on the observed decay and shows that it must be taken into account in any quantitative interpretation of the echo signal. In addition the asymmetry in the echo is indicative of inhomogeneous broadening on the time scale of the measurement.

To calculate the observed echo signals in the perturbation limit it is necessary to evaluate four-time correlation functions for a multilevel system that result from solving the optical Bloch equations (Yan and Mukamel, 1988; Yan and Mukamel 1991). A semi-classical Liouville space formalism was used and the resulting integrals were evaluated numerically. Since detailed mode data was not available for LD690, an approximate model that fits the linear absorption was used for the calculation. A value of the dephasing time $T_2 = 30$ fs was used in a fit to the data. Since only a small number of Franck-Condon connected modes were included in the calculation, much of the damping has to come from this short dephasing time. A more realistic model would probably include more modes and result in a proportionately longer T_2; consequently, a T_2 of 30 fs is most likely a lower bound. A complete description of the Franck-Condon allowed transitions must be available to accurately model the echo decay and separate multilevel effects from that of pure dephasing, which contains information on the time scale of the solvent-chromophore interaction.

In conclusion we have demonstrated the utility of the mode suppression three pulse echo technique for studying dephasing in complex optical transitions. This technique should prove valuable in the study of femtosecond dynamics of systems which exhibit multilevel structure.

References

Alivisatos, A.P., Harris, T.D., Carroll, P.J. Steigerwald, M.L., and Brus, L.E., *J. Chem. Phys.* **90**, 3463, 1989.

Bardeen, C.J., and Shank, C.V., *Chem. Phys. Lett.* **45**, 234, 1993.

Becker, P.C., Fragnito, H.L., Bigot, J.Y., Brito Cruz, C.H., Fork, R.L., and Shank, C.V., *Phys. Rev. Lett.* **63**, 505, 1989.

Bigot, J.Y., Portella, M.T., Schoenlein, R.W., Bardeen, C.J., Migus, A., and Shank, C.V., *Phys. Rev. Lett.* **66**, 1138, 1991.

Brito Cruz, C.H., Fork, R.L., Knox, W.H., and Shank, C.V., *Chem. Phys. Lett.* **132**, 341, 1986.

De Silvestri, S., Weiner, A.M., Fujimoto, J.G., and Ippen, E.P., *Chem. Phys. Lett.* **112**, 195, 1984.

Heller, E.J., *J. Chem. Phys.* **62**, 1544, 1975.

Kurnit, N.A., Abella, I.D., and Hartmann, S.R., *Phys. Rev. Lett.* **43**, 567, 1979.

Mims, W.B., *Phys. Rev. B* **6**, 3543, 1972.

Moshary, F., Arend, M., Friedberg, R., and Hartmann, S.R., *Phys. Rev. A.* **46**, R33, 1992.

Nibbering, E.T.J., Wiersma, D. and Duppen, K., *Phys. Rev. Lett.* **66**, 2465, 1991.

Schoenlein, R.W., Bigot, J.Y., Portella, M.T., and Shank, C.V., *Appl. Phys. Lett.* **58**, 801, 1990.
Schoenlein, R.W., Mittleman, D.M., Shiang, J.J., Alivisatos, A.P., and Shank, C.V., *Phys. Rev. Lett.* **70**, 1014, 1993.
Weiner, A.M., De Silvestri, S. and Ippen, E.P., *J.O.S.A. B* **2**, 654, 1985.
Yan, Y.J., and Mukamel, S., *J. Chem. Phys. Lett.* **89**, 5160, 1988.
Yan, Y.Y. and Mukamel, S., *J. Chem. Phys.* **94**, 179, 1991.

D.M. Jonas, S.E. Bradforth, S.A. Passino and G.R. Fleming

Ground State Wavepackets in Pump-Probe Spectroscopy

Abstract

We discuss the pump-probe signals expected from ground state wavepackets. The concept of a 'pure hole' is examined. The temporal form of the signals can be qualitatively predicted from the pump and probe wavelengths and pulse durations using the classical Franck principle. Temperature is found to play an important role. These considerations are illustrated with quantum mechanical calculations of the iodine ground state transient dichroism signal.

Introduction

Femtosecond pump pulses typically launch wavepackets on both ground and excited electronic states. Pump-probe spectroscopies [e.g., differential absorption (Pollard and Mathies, 1992), transient dichroism in the diffusive reorientation limit (Scherer et al., 1993)] detect the difference between the probe beam after the sample with and without the pump. This is a combined signal from *both* wavepackets, which must somehow be disentangled. The pump interactions shown in Fig. 1 illustrate how a short, vibrationally abrupt pump pulse excites coherent vibrations on both the ground and excited electronic states. Unfortunately, signals from vibrational wavepackets on the ground vibrational state depend strongly on temperature and the characteristics (e.g. wavelength and pulse duration) of both the pump and probe pulses. In particular, the wavepacket recurrence frequencies need not equal a molecular vibrational frequency.

For simplicity, quantum density matrix treatments of pump-probe signals have usually considered only two vibrational levels in each electronic state (Chesnoy and Mokhtari, 1988; Walmsley et al., 1988), which yields the oversimplified result that cosinusoidal beats are expected at each vibrational frequency difference. Similarly, the importance of temperature does not seem to be widely appreciated. The behaviour for coherent excitation of many vibrational levels is complex and not easily understood by viewing the signals as multi-level quantum beats. Heller and coworkers have emphasized the conceptual and computational advantages of classical mechanics for understanding short time quantum dynamics e.g. wavepacket motion (Heller, 1981) and low resolution spectra

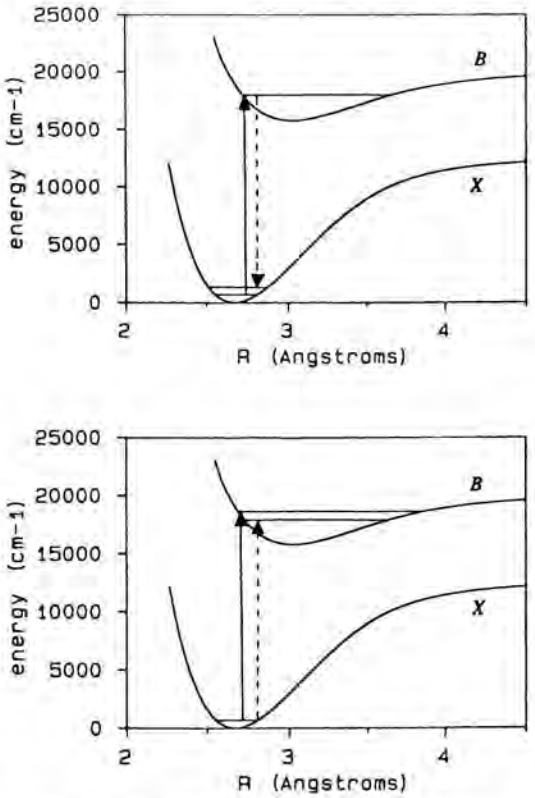

Fig. 1. Illustration of coherent wavepacket preparation on the ground (X) and excited (B) states of iodine by a 580 nm pump pulse. For this pump wavelength, the outer turning points of the ground state vibrational levels overlap the excited state. Stimulated Raman scattering by the pump excites a coherent superposition of the ground state levels which is initially located near the outer classical turning point of the termally populated X-state levels (Fig. 1 (top)). The excited state wavepacket is initially located near the inner classical turning point of the B-state and is composed of roughly $v' = 15$-19, as diagrammed in Fig. 1 (bottom). (Level spacings have been exaggerated for clarity.)

(Reimers et al., 1983; Bergsma et al., 1984). We have found the classical mechanical behaviour of a thermal ensemble is relatively easy to visualize and use to understand pump probe signals. Classical mechanics is only numerically accurate in the high temperature limit, $\hbar\omega \ll kT$.

Classical Wavepacket Dynamics

The classical Franck principle states that nuclei do not have time to move or change velocity during a sudden electronic transition (Franck, 1925). This implies conservation of nuclear kinetic energy during electronic transitions. The classical transition energy is therefore given by the potential energy difference,

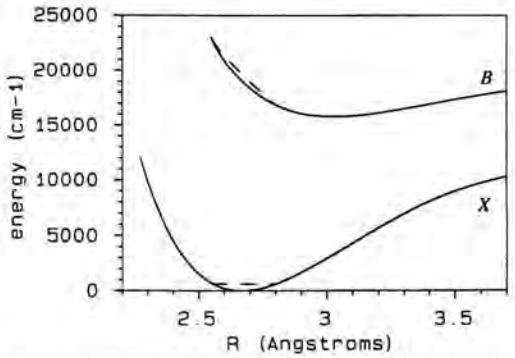

Fig. 2. Mulliken difference potential for $B \leftarrow X$ absorption by the oscillating wavepacket prepared by the pump pulse. From the classical Franck principle, as the wavepacket passes through a given internuclear distance, absorption occurs at the wavelength which conserves nuclear kinetic energy during the electronic transition. In Fig. 2, the kinetic energy of one trajectory in the ground state wavepacket is superposed (dashed lines) on the B and X state potentials (solid lines). For each value of R, absorption from the X state can occur classically for photon energies equal to the vertical difference between the two dashed lines (Mulliken difference potential.)

which is a function of the nuclear coordinates. Mulliken difference potentials (Tellinghuisen, 1985) are used to illustrate this point for the I_2 $B \leftarrow X$ transition in Fig. 2. The Franck-Condon principle has sometimes been incorrectly interpreted as implying absorption and emission only from the vicinity of the classical turning points. Note that time averaging, which biases the transition probability towards local extrema of the difference potential in a frequency resolved experiment, is irrelevant for time resolved spectroscopy with pulses fast compared to vibrational motion. In femtosecond experiments, one is quite likely to probe the wavepacket when it has high momentum as it crosses the middle of the well.

Consider an ensemble of classical molecules with energy given by the horizontal dashed line on the potential labelled X in Fig. 2. A resonant pump pulse which is short compared to half the vibrational period yet spectrally narrow compared to the allowed range of transition energies will only electronically excite those molecules which pass through a small range of internuclear distances during the pump pulse. This launches a group of molecules ('wavepacket') on the excited state and leaves a complementary 'hole' in the ground state ensemble, both of which can modify a subsequent probe pulse.[1] The internuclear distance at which a wavepacket is probed by a given wavelength can be approxima-

[1] Classically, the Fourier transform limit for an electromagnetic wave implies an optimum pulse duration for producing a narrow hole: if the frequency spread is made smaller to excite a smaller range of internuclear distances then the pulse is necessarily longer and molecules travel in and out of the pumped region during the pulse; conversely a shorter pulse has a broader spectrum and excites a larger range of internuclear distances. The optimum pulse duration for a narrow ground state hole is not necessarily the same as that for a narrow wavepacket on the excited state.

tely calculated from the Mulliken difference potential by the classical Franck principle. The absorption frequency at which a particular internuclear distance is probed should not be expected to be accurate to better than a vibrational quantum.

By probing with different wavelengths, we can follow the excited state wavepacket and ground state hole as they move back and forth (Bernstein and Zewail, 1989; Scherer et al., 1993). Consider the wavepacket prepared on the lower electronic state in Fig. 1. Classical mechanics allows one to understand that the ground state wavepacket interacts with a probe pulse as an oscillating 'hole' which is probed each time it passes through th range of internuclear distances dictated by the probe center wavelength. For instance, as one tunes the probe to the blue of the 580 nm pump in Fig. 1, one probes the ground state wavepacket at smaller R. In the middle of the well, a green probe beam will interact with the hole twice per vibrational period after an initial delay of roughly a quarter vibrational period. At the inner wall, a blue probe will interact with the hole once per vibrational period after an initial delay of about half a vibrational period.

Raman processes in which molecules are transferred to the excited state, move on the excited state potential, and then returned to the ground state by the pump also occur. These non-abrupt processes only occur to the extent that vibrational motion is possible during the pump pulse, but if they are sufficiently rapid and the temperature is low, they can cause excess population at some internuclear distances even though the net population of the ground electronic state has been depleted. The relevant vibrational timescale for these non-abrupt Raman processes depends on the excess kinetic energy acquired in the excited state (determined by the difference potential) before the molecule moves outside the range of internuclear distances sampled by the pump spectrum. Non-abrupt Raman processes are therefore less important for a pump Franck-Condon region near the classical turning point (where molecules move slowly) than a pump Franck-Condon region near the ground state equilibrium geometry.

If $\rho(R, t)$ is the probability distribution for internuclear distance, R, in given classical ensemble at time t, then the absorption cross section is given by [Bergsma et al., (1984) Eq. 2.13]

$$\sigma(\omega) = \frac{4\pi^2\omega}{\hbar cn} \int \mu(\omega : R)\, \rho(R, t)\, \mu(R : \omega)\, dR. \tag{1}$$

We write $\mu(R : \omega)$ to emphasize that absorption of light with frequency ω can only take place when the molecule is at the internuclear distance R determined by the classical Franck principle. The number of photons absorbed is proportional to

$$A \propto \int \int E(\omega, t)\, \sigma(\omega)\, E(\omega, t)\, d\omega\, dt \tag{2}$$

Photon detected pump-probe signals,[2] S, are proportional to $A - A_{EQ}$, where A_{EQ} is the equilibrium probe absorption, and thus depend on $\delta\rho(t) = \rho(R, t) - \rho_{EQ}(R)$. For an electronically excited state, $\delta\rho_e(t)$ is always positive for all R, since ρ_{EQ} is zero, i.e. we have a pure wavepacket. Since only the squares of μ and E enter into Eq. (1) and (2), this fixes the sign of each excited state pump-probe signal[3] so that the pump-probe signal never passes through zero. For the ground state, ρ_{EQ} is not zero and $\delta\rho_g(t)$ need not be negative for all R. In this case, the ground state pump-probe signal does not have a definite sign. If non-abrupt Raman processes which require nuclear motion during the pulse can be neglected, $\delta\rho_g$ is negative $[\delta\rho_g(0) \approx -\delta\rho_e(0)]$, i.e. we have a pure hole and the ground state pump-probe signal is signed.

Quantum Correspondence

It is helpful to view pump-probe signals as periodic absorption and/or emission by oscillating wavepackets on the ground and excited states. The appropriate formulas analogous to Eq. (1) and (2) involve the density matrix, ρ. The quantum analogue of Eq. (2) is

$$A \propto \frac{4\pi^2\omega}{\hbar cn} Tr(E\mu\rho\mu^* E^*) \tag{3}$$

(the integrals over ω and t have been suppressed for clarity). The pump probe signal is determined by $\delta\rho(t) = \rho(t) - \rho_{EQ}$, where $\rho(t)$ is the density matrix of the system after interaction with the pump and ρ_{EQ} is the equilibrium density matrix. For the excited electronic state, $\delta\rho(t) = \rho_e(t)$, the vibrational density matrix of the excited state, therefore the excited state pump-probe signal is signed (i.e., cannot pass through zero) by the density matrix inequality $\xi^* \rho \xi \geqslant 0$ for an arbitrary vector ξ (Landau and Lifschitz, 1977). We refer to a coherent state where $\delta\rho$ is 'positive' as a 'pure particle.'

The ground state pump-probe signal is more complicated. Clearly, coherent vibration on the ground electronic state arises from stimulated Raman scattering. For the ground state, the diagonal elements of $\delta\rho(t) = \rho_g(t) - \rho_{EQ}$ in the eigenstate basis need not all be negative when Raman processes are considered. For a non-resonant pump pulse, some of the diagonal elements of $\delta\rho(t)$ are positive and some are negative (ground state population is redistributed but not

[2] Experiments which detect changes in total photon number do not detect stimulated Raman scattering of the probe beam, since this simply exchanges red and blue probe photons without changing the total probe photon number. The experiments discussed by Pollard and Mathies (1992), in which the probe beam is spectrally dispersed, do detect such exchanges between red and blue probe photons and hence are sensitive to stimulated Raman scattering of the probe.

[3] It is sometimes possible to probe more than one electronic transition with a single wavelength. In this case, the pump-probe signal for each electronic transition is signed, but the total signal may not be.

removed) so that $\delta\rho$ is not 'negative' (Hoffman and Kunze, 1971) and the pump-probe signal can oscillate between positive and negative values. The classical theory suggests that for impulsive resonant excitation, $\delta\rho_g(0) \approx -\delta\rho_e(0)$. When $\delta\rho$ is 'negative,' we have an inequality $\xi^* \delta\rho \xi \leqslant 0$ for an arbitrary vector ξ and refer to the coherent vibrational state as a 'pure hole,' *All* pump-probe signals from a 'pure hole' are signed, which simplifies the interpretation immensely.[4]

The signal for a pure hole is a quantum beat,[5] e.g.

$$S = Ae^{-t/T_1} + \sum_i B_i \cos(\omega_i t + \phi_i)\, e^{-t/T_2} \tag{4}$$

where A and B_i have the same sign and obey inequalities which may be formally derived from the density matrix inequality given above. Similarly, $T_1 \geqslant T_2$ by the density matrix inequality $|\rho_{ij}| \leqslant \sqrt{\rho_{ii}\rho_{jj}}$ (Landau and Lifschitz, 1977). The interpretation of any fit to Eq. 4 must assure that the terms attributed to each electronic transition obey the above inequalities.

Whether the coherent vibration on the ground electronic surface approximates a 'pure hole' or not depends on the temperature and the characteristics of the pump. For simplicity, we restrict our discussion to the case where the transition dipole is independent of nuclear coordinates. For a δ-function pump pulse, there is no time to move on the excited state potential and we have a uniform depletion of all vibrational levels (Tanimura and Mukamel, 1993). This is a boring pure hole because it doesn't move, but it seems reasonable to expect that shorter pulses will excite coherent vibrations that better approximate a pure hole. For real pulses, in order to have a pure hole, it is necessary to depopulate higher lying levels faster than population is transferred into them from lower levels by resonant impulsive Raman scattering. This should be possible if the Franck-Condon factors increase faster than the Bolzmann factors drop: i.e. Franck-Condon factor times Boltzmann factor increasing with vibrational excitation. This criterion can be approximately met when the vibrational displacement is large, the spectrum at the pump wavelength is dominated by hot bands, and the temperature is sufficiently high relative to the vibrational frequency. These circumstances seem closely related to the classical situation discussed in the last section, but hold only approximately for our example of molecular iodine at room temperature.

Examples

We shall illustrate the points discussed above with transient dichroism results reported for a solution of iodine in hexane at room temperature by Scherer,

[4] Note that a signed pump-probe signal does not imply the coherent vibration is a pure hole. We have not yet examined the matrix $\delta\rho$ to determine how accurately the examples shown below approximate pure holes.

[5] Eq. 4 assumes that all vibrational levels have identical population (T_1) and coherence (T_2) lifetimes.

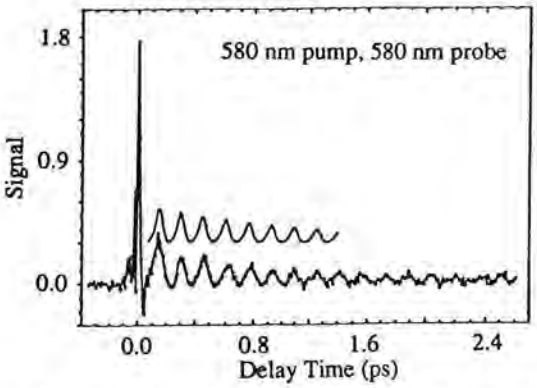

Fig. 3. Calculated ground state pump-probe signal and observed transient dichroism signal for 580/580 pump/probe wavelengths. The observed signal is the sum of a positive transient dichroic response from $B \leftarrow X$ absorption (analysis recovers a large damped cosine at 220 cm^{-1}, a smaller damped cosine at 420 cm^{-1}, and a positive 1500 fs exponential decay) and a negative response from absorption by the B-state wavepacket. The ground state signal is attributed to probing the X-state wavepacket hole near the outer turning point once per vibrational period, as expected for this probe wavelength from the classical Franck principle and the Mulliken difference potential. The calculated pump-probe signal has been multiplied by a 1200 fs exponential decay and displaced upwards for comparison.

Jonas and Fleming (1993) and new calculations of the ground state pump-probe signal using the gas-phase iodine potentials. The iodine ground state vibrational frequency is 211 cm^{-1} (which approximately equals kT at room temperature) in both hexane and the gas phase. One simplyfying aspect of the iodine examples shown here is that the difference potential for $B \leftarrow X$ absorption (Fig. 2) decreases monotonically with increasing R. Therefore, each probe wavelength accesses only one value of R.

The quantum calculations are carried out to demonstrate the correspondence between classical and quantum description of the ground state behavior laid out above. The potential used here are cubic spline interpolated RKR potentials.[6] The first four vibrational eigenstates of the ground potential surface, i.e. those with any significant Boltzmann weight, are found numerically by an algorithm based on the Numerov-Cooley method (Cooley, 1961) with the simplification introduced by Ross (1983). For each ground vibrational eigenstate a propagation is carried out for the ground and excited state wavepackets created by interaction of the iodine molecule with the pump pulse. This coupled calculation, which carries the molecule-field interaction to infinite order in the electric field, is performed by solving the time dependent Schrodinger equation (see for example equation 4.29 of Scherer et al., 1991). The time propagator is approximated by the second order differencing method and the nuclear kinetic energy is eval-

[6] The X-state potential is from LeRoy (1970). The B-state potential is from Barrow and Yee (1973) [note the typographical error for $G(v=46)$ which should read $G(v) = 3892.86$ cm^{-1}] and Tellinghuisen (1973).

uated by fast Fourier transform. (Kosloff, 1988) In the calculation the coupling is given by $\mu E_0 \cos(\omega t) \exp(-t^2/\tau^2)$. Both pump and probe pulses are chosen to be Gaussian with FWHM of 15 fs and $\mu E_0 = 0.001$ atomic units; the variation of the electronic transition moment with R (Koffend et al., 1979) has been neglected.

Stimulated Raman processes lead to motion of the ground state quantum wavepacket. The interaction of the probe pulse with the ground state wavepacket is subsequently calculated, once again by explicit coupled propagation, as a function of pump-probe delay time. Prior to initiating the probe pulse the excited state amplitude is removed, so as to eliminate any interference effects (in contrast to the phase locked pulse pair signal of Scherer et al., 1991). The $B \leftarrow X$ transition probability, evaluated at the end of the probe pulse, is stored at each delay. From equation (3), the pump-probe signal is evaluated as a difference of the pump attenuated $B \leftarrow X$ transition probability. The ground state transient dichroism signal (which is the *negative* of the pump-probe signal) is shown in all figures.

The signals due to each initial ground eigenstate are summed after weighting by the appropriate Boltzmann factor. Simulations have been performed for two probe wavelengths with a 580 nm pump. 580 nm probes the outer turning point (see Figure 1) whereas a 526 nm probe wavelength interrogates the ground state wavepacket as it passes through the center of the well (this can be deduced from the Mulliken difference potential in Fig. 2).

The 580 nm pump/580 nm probe (580/580) dichroic signal is shown along with the calculated pump-probe signal in Fig. 3. According to Fig. 2, we expect $B \leftarrow X$ absorption with zero phase shift at the X-state vibrational frequency from the outer turning point of the X-state. This is essentially the observed result,

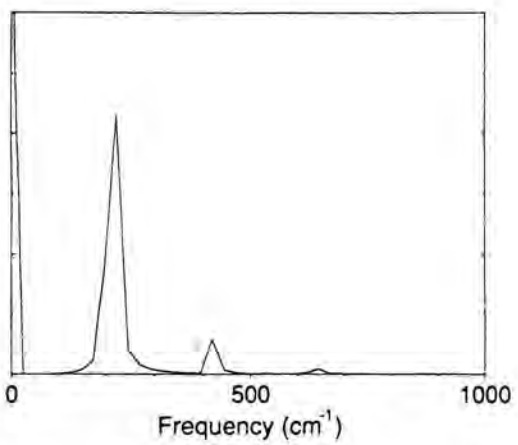

Fig. 4. Fast Fourier Transform (FFT) of the calculated 580/580 pump-probe signal. The first harmonic dominates both the experimental and calculated pump-probe signals, but the second harmonic, which sharpens the peaks, cannot be neglected.

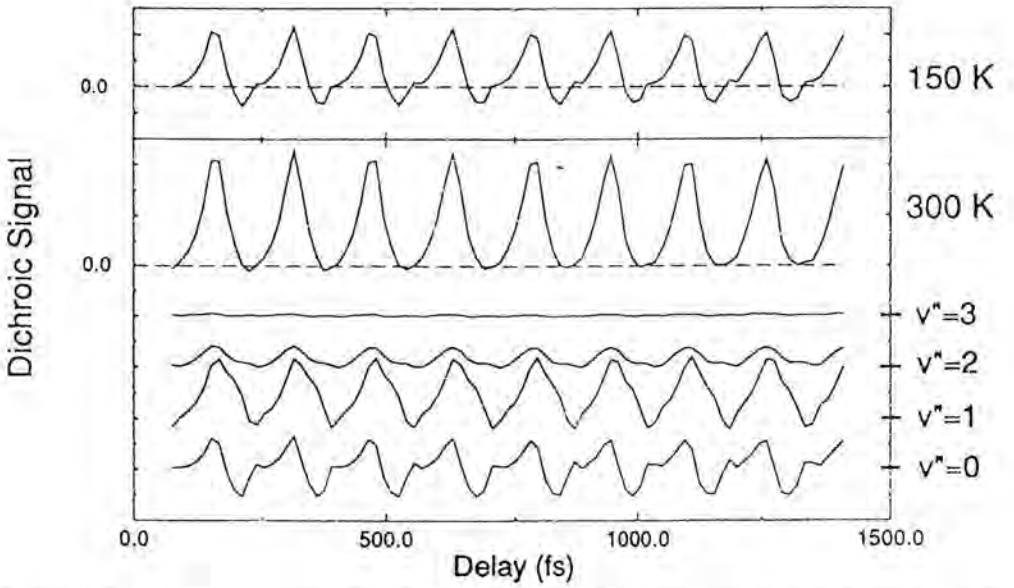

Fig. 5. Effect of temperature and breakdown of the calculated 580/580 pump-probe signal by initial vibrational eigenstates. The top panel shows the signal at $T = 150$ K, which oscillates through zero (dashed line) and does not have a definite sign. The bottom panel displays the nearly signed signal at $T = 300$ K and breaks that signal down into contributions from thermally populated initial eigenstates. The signal from each initial state is displaced in the plot, with zero for each trace indicated by the respective tick mark adjacent to the labeled initial vibrational quantum number. Note that the signal for $T = 0$ K, which would arise entirely from $v'' = 0$, is much more complicated than the signed total signal at $T = 300$ K.

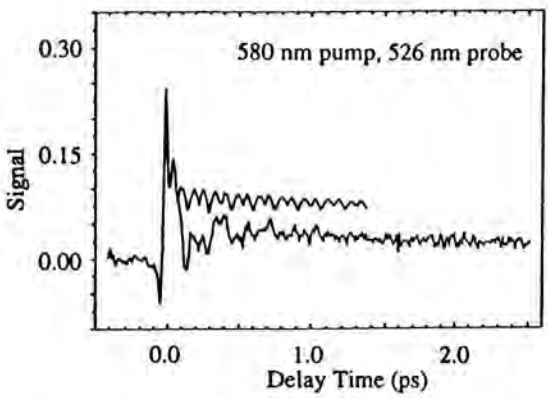

Fig. 6. 580/526 transient dichroic response and calculated ground state pump-probe signal. Analysis of the transient dichroism signal revealed five terms, including a 423 cm^{-1} damped cosine and a positive exponential. The 423 cm^{-1} damped cosine and positive exponential have been attributed to probing the X-state 'hole' as it passes through the center of the well *twice* per vibrational period (hence the doubled frequency). The calculated pump-probe signal has been multiplied by a 1200 fs exponenial decay and displaced for comparison (see text).

which also agrees well with our calculations. The Fourier transform of the calculated 580/580 pump-probe signal (Fig. 4) recovers both the fundamental and the second harmonic of the vibrational frequency because the pump-probe peaks are more sharply modulated than a cosine. The second harmonic was also detected in the analysis of the experimental signal.

Fig. 5 illustrates the temperature dependence of the 580/580 signal and displays the signal calculated for each initial vibrational eigenstate. It is clear from Fig. 5 that the concept of a pure hole is useless for a single eigenstate but helpful for a thermal ensemble. Whether the ground state signal is signed or not clearly depends strongly on the temperature.

The 580/526 data is reproduced in Fig. 6. This data set was difficult to interpret, perhaps because the signal to noise is low and analysis recovered five components. From Fig. 2, we expect to probe the wavepacket as it moves across the middle of the X-state well. The ground state vibrational coherence signal was experimentally assigned by the 423 cm^{-1} frequency, (roughly double the ground state vibrational frequency) and the decay time, which is essentially the same as that recovered for the ground state from the 580/580 data. The doubled frequency results from probing the wavepacket as it crosses the middle of the X-state potential twice per vibrational period - a result that is borne out by the calculated signal. A comparison between the experimental and calculated signals suggests that the actual time zero occurs about 20 fs after the maximum experimental cross-correlation (not shown) and 40 fs before the maximum electronic response. The calculated pump-probe signal in Fig. 6 has been shifted accordingly. The agreement between experiment and calculation is gratifying. The FFT of the calculated 580/526 pump-probe signal (Fig. 7) shows that the second harmonic of the ground state vibrational frequency is more prominent than the fundamental, as expected from the classical theory. Fig. 8 shows the breakdown of the 580/526 pump-probe signal by eigenstate. The signal is dominated by $v'' = 0$, and thus depends less strongly on temperature than the 580/580 signal. Note the slight asymmetry of the double peaks.

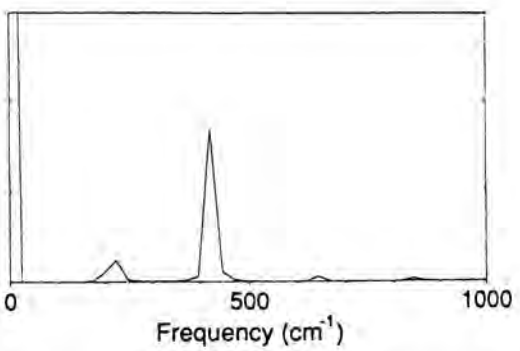

Fig. 7. FFT of the calculated 580/526 pump-probe signal. The second harmonic dominates but there is still some amplitude at the first harmonic.

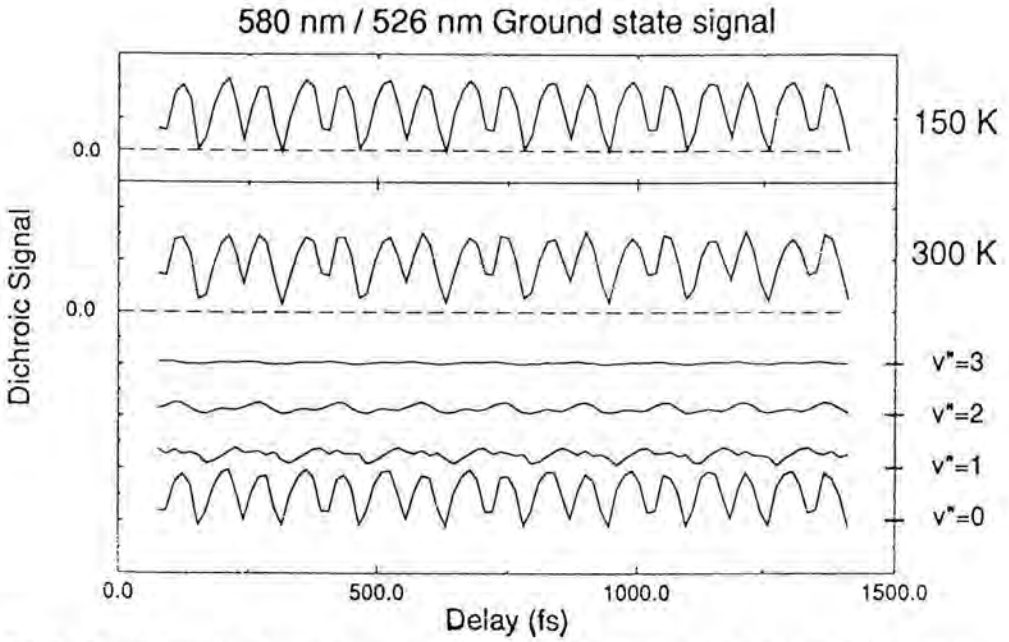

Fig. 8. Breakdown by eigenstates and effect of temperature on the calculated 580/526 pump-probe signal.

Concluding Remarks

We mention a simple example that illustrates how a 'hole' produced by abrupt optical excitation can be viewed as caused by either stimulated Raman scattering or absorption, depending on the states used for calculations. Both viewpoints are equally correct. The model system consists of an electronic ground state with a symmetric double well and an electronically excited state with a single, nearly identical well on the left side only. We take the temperature such that the lowest symmetric, $|s\rangle$, and antisymmetric, $|a\rangle$, ground vibrational states are essentially equally populated, but all other levels are essentially unpopulated. The density matrix for a system having equal probability to be in either of the localized non-stationary states $|L\rangle = (|s\rangle + |a\rangle)/\sqrt{2}$ and $|R\rangle = (|s\rangle - |a\rangle)/\sqrt{2}$ is identical to that for a system having equal probability to be in either of the two eigenstates $|a\rangle$ and $|s\rangle$. It is therefore equally correct to view the system as being in eigenstates or in non-stationary states, since any two systems with the same density matrix are indistinguishable (Von Neumann, 1955).

If we calculate to second order the effect of a short pulse (compared to the inverse tunneling frequency) resonant with the excited electronic state in either set of states, we deplete only $|L\rangle$ and are left with a coherent 'hole' which oscillates back and forth between the two equivalent wells. For the eigenstates, this depletion is calculated as stimulated Raman scattering by $|a\rangle$ and $|s\rangle$, but

the view that this coherent 'hole' arises from absorption of $|L\rangle$ only is equally correct. If we consider quantum harmonic oscillators at high temperature, randomly phased coherent harmonic oscillator states (Cohen-Tannoudji et al., 1977) are very similar to the classical picture. In the coherent harmonic oscillator basis, the neglect of non-abrupt Raman processes which change $\langle x \rangle$ or $\langle p \rangle$ yields a pure hole in the ground state. In the general case, it may be helpful to think of the thermal population on the ground electronic state as distributed over randomly phased coherently vibrating states rather than eigenstates.

A simple classical theory based on the Franck principle is very helpful for gaining an intuitive understanding of the vibrational wavepacket modulation of the individual pump-probe signals, and has been used to qualitatively predict the iodine $B \leftarrow X$ transient dichroism as a function of probe wavelength. Preliminary calculations indicate that the interpretation of ground state signals with the classical Franck principle is essentially correct. For a qualitative understanding necessary to begin fitting data, it may be advantageous to perform pump-probe experiments in the limit where the ground state wavepacket is a pure hole. In the future, we hope to subtract the calculated ground state contribution to the pump-probe signals, form a model for the excited state signals with the classical Franck principle, and then fit the data quantitatively to reveal finer features of the excited state dynamics. The concept of a ground state 'hole' seems to be very useful for understanding pump probe signals.

The authors are with the Department of Chemistry and James Franck Institute, the University of Chicago, Chicago, IL 60637, USA. This work was funded by the NSF. DMJ thanks the NSF for a postdoctoral fellowship. We thank Prof. J.A. Cina for helpful discussions.

References

Barrow, R.F., and Yee, K.K., *J. Chem. Soc.*, Faraday Trans. II **69**, 684-700, 1973.

Bergsma, J.P., Berens, P.H., Wilson, K.R., Fredkin, D.R., and Heller, E.J., *J. Phys. Chem.* **88**, 612-619, 1984.

Bernstein, R.B., and Zewail, A.H., *J. Chem. Phys.* **90**, 829-842, 1989.

Chesnoy, J., and Mokhtari, A., *Phys. Rev. A* **38**, 3566-3576, 1988.

Cohen-Tannoudji, C., Diu, B., Laloë, F., *Quantum Mechanics* (Wiley-Interscience, New York), 1977.

Cooley, J.W., *Math. Comp.* **15**, 363-374, 1961.

Franck, J., *Trans. Far. Soc.* **21**, 536-542, 1925.

Heller, E.J., *J. Chem. Phys.* **62**, 1544-1555, 1975.

Heller, E.J., *Acc. Chem. Res.* **14**, 368-375, 1981.

Hoffman, K., and Kunze, R., *Linear Algebra, second edition*, (Prentice-Hall, Englewood Cliffs, NJ) Sec. 9.3., 1971.

Koffend, J.B., Bacis, R., and Field, R.W., *J. Chem. Phys.* **70**, 2366-2372, 1979.
Kosloff, R., *J. Phys. Chem.* **92**, 2087-2100, 1988.
Landau, L.D., and Lifschitz, E.M., *Quantum Mechanics, third edition*, (Pergamon Press, New York) Sec. 14, 1977.
LeRoy, R.J., *J. Chem. Phys.* **52**, 2683-2689, 1970.
Pollard, W.T., and Mathies, R.A., *Ann. Rev. Phys. Chem.* **43**, 497-523, 1992.
Reimers, J.R., Wilson, K.R., and Heller, E.J., *J. Chem. Phys.* **79**, 4749-4757, 1983.
Ross, S.C., Ph. D. thesis, Carleton University, 1983.
Scherer, N.F., Carlson, R.J., Matro, A., Du, M., Ruggiero, A.J., Romero-Rochin, V., Cina, J.A., Fleming, G.R., and Rice, S.A., *J. Chem. Phys.* **95**, 1487-1511, 1991.
Scherer, N.F., Jonas, D.M., and Fleming, G.R., *J. Chem. Phys.* **99**, 153-168, 1993.
Tanimura, Y., and Mukamel, S., *J. Opt. Soc. Am. B.* **10**, 2263-2268, 1993.
Tellinghuisen, J., *J. Chem. Phys.* **58**, 2821-2834, 1973.
Tellinghuisen, J., *Adv. Chem. Phys.* **60**, 299-369, 1985.
Von Neumann, J., *Mathematical Foundations of Quantum Mechanics*, (Princeton University Press, Princeton, NJ), 1955.
Walmsley, I.A., Mitsunaga, M., and Tang, C.L., *Phys. Rev. A* **38**, 4681-4689, 1988.

M.D. Fayer

Dynamics in Complex Liquids: Optical Nonlinear Experiments

Abstract

Transient grating optical Kerr effect measurements of orientational relaxation over 6 decades in time (fsec to nsec) and 12 decades of amplitude on the isotropic phase of liquid crystals, on the side groups of polymers as melts and in solution, and on a common organic liquid, are reported. Orientational relaxation in all of these systems displays non-hydrodynamic behavior in that it is viscosity and temperature independent over wide ranges of viscosity and temperature.

Introduction

Orientational relaxation is commonly discussed in terms of hydrodynamic theory (Debye, 1929; Kivelson, 1987). A molecule is assumed to undergo orientational diffusion in a featureless continuous medium. The rate of orientational diffusion (decay of the orientational correlation function) is described by the Debye-Stokes-Einstein equation (Kivelson, 1987; Berne, 1976). The orientational correlation function decay is exponential with a decay constant, τ, which is proportional to the molecular volume and viscosity and inversely proportional to the temperature. Since the viscosity usually decreases exponentially with increasing temperature, τ decreases rapidly as the temperature is raised.

The hydrodynamic continuum model does not consider anisotropic intermolecular interactions which can give rise to local structures in liquids. For example, it is known from neutron scattering that in both benzene and naphthalene neat liquids, the molecules reside in crooked T shaped structures (Misawa, 1990). These structures are not stable but exist on a time scale that is short compared to the time for rotational diffusion. Recent experiments have demonstrated that in liquids having significant local structure, fast orientational relaxation can be unrelated to hydrodynamic motions (Deeg, 1990; Greenfield, 1992; Greenfield, 1993; Sengupta, 1992; Sengupta, 1993). In fact, dynamics in a variety of types of systems are observed to be viscosity/temperature (η/T) independent over wide ranges of η/T. These experimental results are explained in terms of a model that states the orientational relaxation dynamics arise from relaxation on the free energy potential surface that is responsible for the formation of the local

structures rather than rotational diffusion. A perturbation, either optical or thermal, moves the system away from the local potential minimum. Then, the system relaxes back to the minimum, regenerating the original local structure. On a longer time scale, the system will undergo rotational diffusion which randomizes the local structure. However, on a time scale short compared to rotational diffusion, orientational relaxation is non-hydrodynamic and is decoupled from the bulk viscosity.

Experimental Method

The Transient Grating Optical Kerr Effect (TG-OKE) method (Deeg, 1990; Greenfield, 1992; Greenfield, 1993; Sengupta, 1992; Sengupta, 1993) and Dynamic Light Scattering (DLS) (Berne, 1976) experiments give direct access to the orientational correlation function (or its Fourier transform). DLS has been used to measure rotational dynamics in a very wide variety of systems, but in practice it is limited in time resolution. In a DLS experiment, the fast dynamics can appear as a very broad, low amplitude frequency distribution making it difficult to observe fast processes in the presence of slower relaxations. The transient grating approach to measure the OKE, first applied by Eyring and Fayer (Eyring, 1984), is the time domain analog of the DLS experiment (Yan, 1987a; Yan, 1987b). The time resolution of TG-OKE is limited only by the pulse width of the laser. In the time domain it is possible to separate fast and slow contributions to the signal more readily than in the frequency domain, and the time domain experiments provide increased dynamics range, making it possible to observe the full scope of dynamics in a complex system. In the TG-OKE experiment, two optical pulses are overlapped in time and space, creating an optical interference pattern. The interference pattern, through the OKE, creates a spatially varying orientational anisotropy in the sample. This spatially periodic anisotropy acts as a Bragg diffraction grating. If the pulses are much faster than the material's response, the material reacts with the impulse response function $G(t)$. By diffracting a variably delayed third pulse, the probe, from the grating induced in the sample, the decay of the anisotropy induced by the excitation pulses can be observed. The diffracted intensity is given by:

$$I(t) \propto |\chi^{(3)}(t)|^2 \propto |\delta\varepsilon(t)|^2 \propto |G^{\varepsilon\varepsilon}(t)|^2 \tag{1}$$

Here $\chi^{(3)}$ is the third order nonlinear susceptibility, $\delta\varepsilon$ is the grating's peaknull difference of the dielectric constant, and $G^{\varepsilon\varepsilon}$ is the impulse response function of the dielectric constant.

It has been shown by Etchepare and co-workers (1987) and extended by Deeg and Fayer (1989a) that it is possible to select out specific elements of the $\chi^{(3)}$ tensor by controlling the polarizations of each excitation beam, the probe beam, and polarization of observation of the signal beam. With a macroscopically isotropic sample, the electronic OKE (instantaneous polarization of the electrons)

and the nuclear OKE (orientational anisotropy) can be separated. Acoustic response of the sample can be eliminated by using a polarization grating (Eyring, 1984; Deeg, 1989b).

Results and Discussion

Fig. 1 displays TG-OKE data taken on the isotropic phase of the liquid crystal methoxy Benzylidene butylidene butyl aniline (MBBA) at 68.3 °C. In panel (a), the electronic optical Kerr effect and the nuclear optical Kerr effect data are shown (Deeg, 1990; Deeg, 1989a). The electronic trace is centered at $t=0$ and gives the instrument response of the experimental apparatus. The nuclear curve (molecular orientational dynamics) shows a small but real displacement from the electronic curve. The very fast rise and decay, out to approximately 1 psec, are caused by the librational dynamics (Deeg, 1989b). All of the data sets begin with this very fast feature. The data from 1 to 4 psec is blown up by the factor of 20. After 2 psec the decay is almost flat in this plot. In panel (b), the very fast decay is the continuation of the data that appear flat in panel (a). The data becomes almost flat after ~ 100 psec. In panel (c), the steep part of the data at short time is the almost flat data displayed in (b). Clearly this data is highly non-exponential. It spans a very wide range of time (tens of fsec to tens of nsec) and spans a very broad dynamic range of signal intensity.

The data can be divided into three time ranges. At very short time (< 1 psec), the data reflects the librational dynamics. The very short time behavior will not be considered further. The intermediate time scale data (~ 1 psec to ~ 1 nsec) represents the intradomain dynamics of the pseudo-nematic domains which exist in the isotropic phase of liquid crystals near the nematic phase transition temperature, and the long time scale data (> 1 nsec) results from the randomization of the pseudo-nematic domains that can be discussed in terms of the Landau-de Gennes (LdG) theory (Deeg, 1990; Standus, 1993; Stankus, 1992; de Gennes, 1974; de Gennes, 1969).

The long time scale dynamics were fit to a squared exponential, since the observable is the square of the response function (see Eq. 1) (Eyring, 1984; Yan, 1987a; Yan, 1987b). To analyze the faster dynamics, the square root of the data was taken to eliminate cross terms in Eq. 1. The slow LdG exponential decay is subtracted from the full data set, leaving the faster data.

Fig. 2 shows a log-log plot of four data sets taken at 52.6, 60.8, 68.5, and 78.2 °C. Within experimental error, all of the data sets display identical highly non-exponential decays. The decays are viscosity/temperature independent. The fast dynamics become temperature dependent at ~ 90 °C. This is the same temperature range where the slow dynamics begin to deviate from LdG theory, i.e., the temperature range in which the correlation length becomes so small that pseudo-nematic domains no longer exist. This behavior is identical to that which was observed in the isotropic phase of the liquid crystal, pentylcyanobiphenyl (5CB) (Deeg, 1990). As long as the correlation length is sufficiently long for

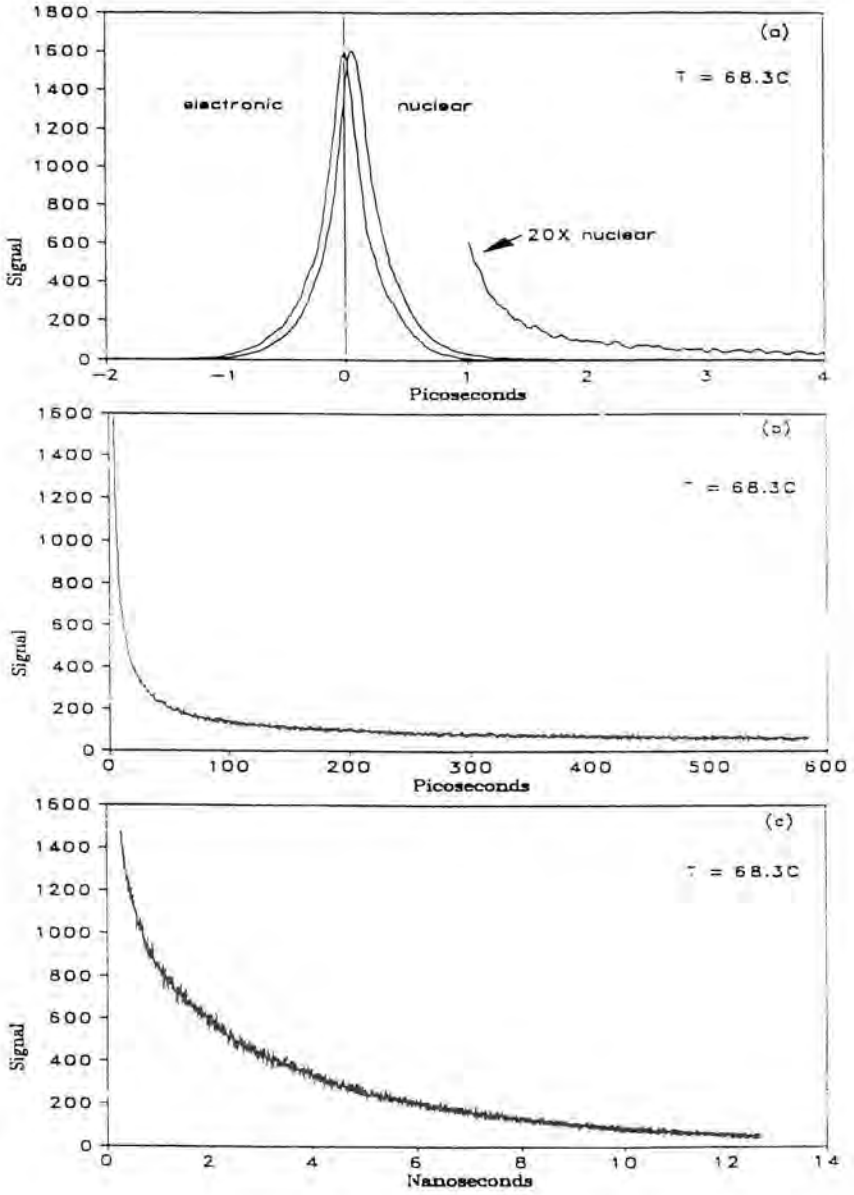

Fig. 1. Transient Grating Optical Kerr Effect datafor MBBA at 68.3 °C. (a) Electronic and nuclear optical Kerr effect. The electronic effect, centered at $t = 0$, give the instrument response. The nuclear effect arises from the orientational dynamics of the MBBA. The short time behavior reflects librational dynamics. For $t > \sim 1$ psec the data is multiplied by 20. This is the beginning of the orientational relaxation. (b) The time scale is expanded. The steep part of the decay is the almost flat part (> 2 psec) in panel a. (c) The time scale is expanded. The steep part of the decay is the almost flat part (> 30 psec) in b. The data is non-exponential and spans a very broad range of time scales and a very broad range of signal amplitude.

pseudo-nematic domains to exist, as demonstrated by the slow dynamics obeying the LdG theory, the fast intradomain dynamics are viscosity/temperature independent. Thus, the fast, intradomain dynamics are not hydrodynamic.

As can be seen in Fig. 2, for times shorter than 1 nsec, the data fall on a straight line, corresponding to a power law decay.

$$G(t) = G_0 t^{-\alpha} \tag{2}$$

From the data, α is 0.63 ± 0.03. The fast dynamics in 5CB (Stankus, 1993) are also a power law with $\alpha = 0.63 \pm 0.02$. Thus, qualitatively and quantitatively, the orientational relaxation dynamics in the isotropic phase of both liquid crystals, MBBA and 5CB, are strikingly similar. In both systems, the slow dynamics are accurately described by the LdG theory until the correlation length falls just below $3\xi_0$. At higher temperatures, deviation from the LdG theory is observed. The fast intradomain dynamics are viscosity/temperature independent from the nematic-isotropic phase transition to the temperature at which the correlation length falls below $3\xi_0$. When the correlation length becomes less than $3\xi_0$, the fast dynamics become temperature dependent. In the temperature independent range, the fast dynamics decay as a power law, $t^{-\alpha}$, with α equal to 0.63 for both systems. These identical features of the two systems may suggest that there is universal, fundamental dynamical behavior of the isotropic phase of liquid crystals.

As demonstrated above, MBBA, like 5CB, displays temperature independent dynamics over a broad time range and a sizable temperature span. Recently, several polymers in solutions and melts (Sengupta, 1992; Sengupta; 1993) have been observed to have viscosity/temperature independent orientational relaxation of side groups on a psec time scale. An example is shown in Fig. 3. The system is the polymer poly(2-vinylnaphtalene) (P2VN) in CCl_4 solution. Fol-

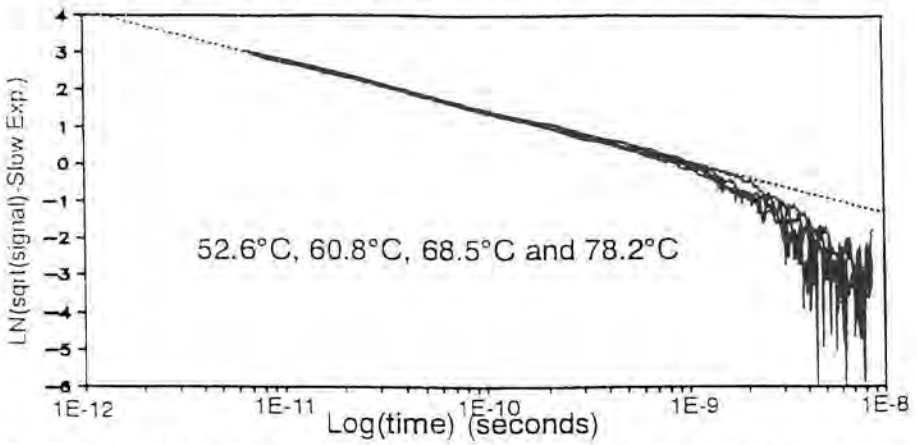

Fig. 2. Data sets at four temperatures (52.6 °C → 78.2 °C) are plotted vs time on a log-log plot. The decays are superimposable, showing that the fast MBBA dynamics are viscosity/temperature independent. The dotted line is a straight line through the data showing that the decays obey a power law ($t^{-\alpha}$) with $\alpha = 0.63 \pm 0.03$.

lowing the decay of the librational dynamics, P2VN displays a bi-exponential decay. The naphthalene side groups are highly polarizable and have a large anisotropy in their polarizability. The signal comes from the side groups (Sengupta, 1993). Fig. 3 shows the η/T dependence over a range in which η/T changes by more than a factor of twenty. It is seen that the orientational relaxation dynamics are unchanged. This is in contrast to 2-ethylnaphthalene (the mono-

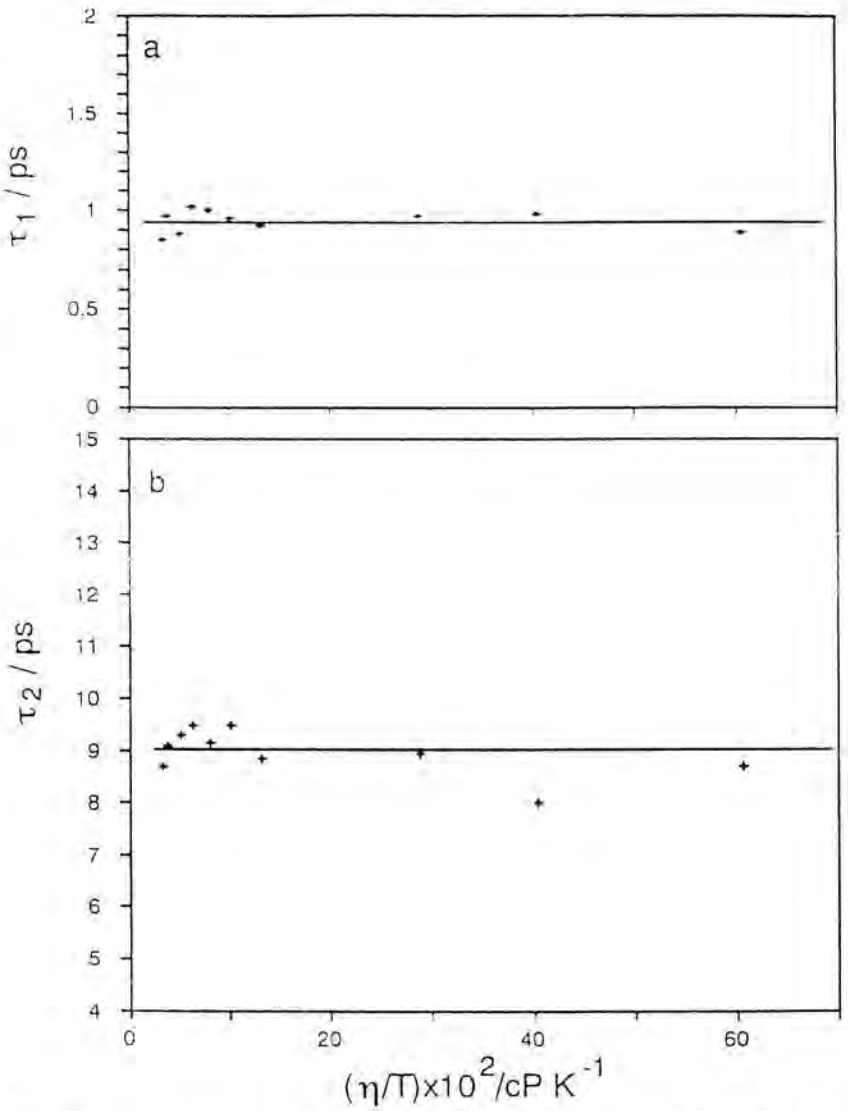

Fig. 3. Viscosity/temperature dependence of the naphthyl side groups of the polymer poly(2-vinylnaphthalene) in CCl4 solution. The orientational relaxation of the side groups displays no viscosity/temperature.

mer of P2VN) in CCl_4 solution at low concentration, which displays hydrodynamic behavior. However, the pure molecular liquid, 2-ethylnaphthalene (Greenfield, 1992), also displays a fast orientational relaxation component that is viscosity/temperature independent.

All of these liquids have in common significant local structure caused either by strong anisotropic intermolecular interactions or backbone structure and side group steric interactions. These local structures exist for a time scale long compared to the time scale of the temperature independent orientational relaxation. The fast dynamics of the two liquid crystals and 2-ethylnaphthalene become temperature dependent at sufficiently high temperature such that the time scale for slower hydrodynamics processes that destroy the local structures becomes comparable to the that of the fast dynamics. In the polymers studied, the motions of the backbone that will modify the local side group configurations are so slow that the psec side group orientational dynamics were not observed to be viscosity/temperature dependent even though η/kT was change by a factor of 20 to 40 in the systems studied.

The above considerations indicate that local structures are responsible for the temperature independent dynamics. As long as the local structure lasts for a time longer than the structural relaxation, the dynamics are temperature independent. Consider MBBA as an example. The MBBA sample is isotropic prior to excitation. The order parameter, S, is zero. Application of the E field induces an anisotropy. This is illustrated in Fig. 4 for the macroscopic system. The system begins

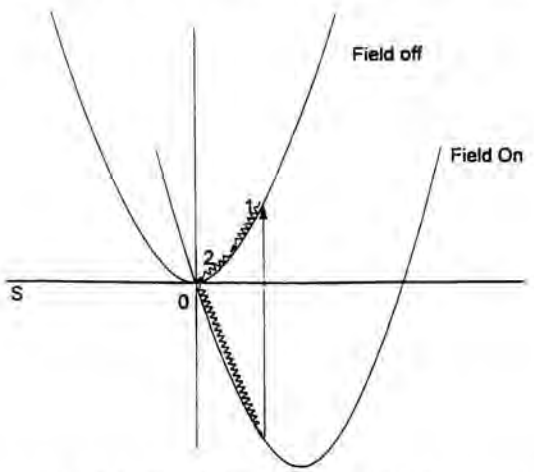

Fig. 4. Schematic illustration of the TG-OKE experiment for the macroscopic sample. Initially, the order parameter, $S=0$, the minimum of the free energy surface (field off). When the field is applied, the potential surface shifts (field on); the system wants to align under the influence of the field. During the pulse, the system evolves downward along the new surface. When the field is removed, the potential returns to the field off surface. This leaves the system with $S \neq 0$, not at the bottom of the well. Application of the E field induces an anisotropy. Evolution will now occur on the surface to reestablish $S=0$. Relaxation of the induced anisotropy has two components: 1. intradomain relaxation giving rise to the fast dynamics, 2. domain randomization giving rise to the slow dynamics as described by Landau-de Gennes theory.

at $S=0$, the minimum of the free energy surface. When the field is applied, the potential surface shifts; the system wants to align under the influence of the field. During the pulse, the system evolves downward along the new surface. When the field is removed, the potential returns to the field free surface. This leaves the system with $S \neq 0$, not at the bottom of the well. Evolution will now occur on the surface to reestablish $S=0$. The arrow labeled 1 on the figure represents the structural relaxation. This relaxation is viscosity/temperature independent. Following the structural relaxation, there may still exist an anisotropy in the sample. This will decay by hydrodynamic orientational diffusion on a time scale much longer than the relaxation back to the original local structure. This has been observed in the MBBA, 5CB, and pure 2-ethylnaphthalene systems.

Concluding Remarks

Using the TG-OKE experimental method, we have been able to examine the fast orientational dynamics of liquids over 6 decades of time ($\sim$ 100 fsec to 100 nsec) and more than 12 decades of signal decay. A fundamentally new picture of orientational relaxation is evolving from these measurements. In systems that display local structure in the liquid, orientational dynamics can be viscosity/temperature independent over wide broad ranges of viscosity and temperature. The dynamics are controled by the local potential surface that gives rise to the local structure. A perturbation of the local structure, optical or thermal, is followed by relaxation back to the potential minimum, not orientational diffusion. This will occur as long as the time scale for the relaxation on the potential surface is fast compared to the time scale for loss of the local structure. On long time scales or in very simple liquids in which there is no significant local structure, hydrodynamic orientational diffusion will occur.

The isotropic phase of liquid crystals display particularly striking behavior. The most remarkable observations are the complete lack of temperature dependence of the fast (1 psec $< t <$ 1 nsec) orientational dynamics over a range of temperatures in which the viscosity undergoes a large change and the slow dynamics change decay rates by well over an order of magnitude. The temperature independent fast dynamics are associated with molecular motions in the pseudo-nematic domains that exist in the isotropic phase near the nematic phase transition. The fast dynamics remain temperature independent until the domain correlation length falls slightly below $3\xi_0$, the same correlation length (and temperature) at which the Landau-de Gennes theory ceases to hold for the slower dynamics.

The MBBA and 5CB results are remarkably similar. The slow dynamics exhibited by both systems obey the Landau-de Gennes theory over a wide range of temperatures. The slow dynamics involve the orientational randomization of the domains. Deviation from the LdG theory begins when the correlation length becomes slightly less than $3\xi_0$. Within experimental error, the deviation begins at the identical correlation length for the two samples. This may suggest a fun-

damental minimum correlation length for the existence of local nematic behavior in the isotropic phase. Both MBBA and 5CB exhibit a power law decay, $t^{-\alpha}$, for the fast dynamics. It is note worthy that in both sampels, α is measured to be 0.63.

The lack of temperature dependence of the fast dynamics is described in terms of the local pseudo-nematic structure that exists in the domains. The onset of temperature dependence coincides with the correlation length becoming so small that the domains cease to exist. The radiation field (or a thermal fluctuation) changes the local order parameter associated with a domain. This moves the system away from the minimum of the local free energy surface that exists on a time scale short compared to the domain randomization time. The system then relaxes back to the minimum. An increase in temperature reduces the domain size. However, as long as it is sufficiently large, ($> 3\xi_0$) there is a well defined local structure and a well defined free energy surface. Since the relaxation dynamics depend on the slope of the potential, the dynamics are temperature independent until a temperature is reached at which the time scale for domain randomization is equal to the time scale for intradomain structural relaxation.

Several other liquid state systems have recently been observed to display fast orientation dynamics that are temperature independent (Greenfield, 1992; Greenfield, 1993; Sengupta, 1992; Sengupta, 1993). All of these system have in common well defined local structures. When these structures are perturbed, they relax to the local potential minimum and reform the local structure. On longer time scales than the relaxation, hydrodynamic randomization occurs. The temperature independent relaxation should be common to many structured liquids and other molecular materials.

Acknowledgment

This work was supported by the National Science Foundation Division of Materials Research (DMR90-22675).

References

Berne, B.J., and Pecora, R., Dynamic Light Scattering Wiley, New York, 1976.

de Gennes, P.G., The Physics of Liquid Crystals Clarendon, Oxford, 1974.

de Gennes, P.G., Phenomenology of short-range-order effects in the isotropic phase of nematic materials. In: *Phys. Lett.* **30A**, 454-456, 1969.

Debye, P., Polar Molecules, Dover, 1929.

Deeg, F.W., and Fayer, M.D., Analysis of complex molecular dynamics in an organic liquid by polarization selective subpicosecond transient grating experiments. In: *J. Chem. Phys.* **91**, 2269-2279, 1989a.

Deeg, F.W., Stankus, J.J., Greenfield, S.R., Newell, V.J., and Frayer, M.D., Anisotropic reorientational relaxation of biphenyl: transient grating optical Kerr effect measurements. In: *J. Chem. Phys.* **90**, 6893-6902, 1989b.

Deeg, F.W., Greenfield, S.R., Stankus, J.J., Newell, V.J., and Fayer, M.D., Non-hydrodynamic molecular motions in a complex liquid: temperature dependent dynamics in pentylcyanobiphenyl. In: *J. Chem. Phys.* **93**, 3503-3514, 1990.

Etchepare, J., Grillon, G., Chambaret, J.P., Hamoniaux, G., and Orszag, A., Polarization selectivity in time-resolved transient phase grating. In: *Optics Comm.* **63**, 329-334, 1987.

Eyring, G., and Fayer, M.D., A picosecond holographic grating approach to molecular dynamics in oriented liquid crystal films. In: *J. Chem. Phys.* **81**, 4314-4321, 1984.

Greenfield, S.R., Sengupta, A., Stankus, J.J., and Fayer, M.D., Local structure dynamics in Liquids: non-hydrodynamic orientational relaxation of 2-ethyl naphthalene. In: *Chem. Phys. Lett.* **193**, 49-54, 1992.

Greenfield, S.R., Stankus, J.J., Sengupta, A., Terazima, M., and Fayer, M.D., Effects of local liquid structure on orientational relaxation: 2-ethylnaphthalene, neat and in solution. In: *J. Phys. Chem.* submitted, 1993.

Kivelson, D., Rotational dynamics of small and macromolecules. eds. T. Dorfmüller and R. Pecora, Springer, Berlin, 1987.

Misawa, M., and Fukunaga, T., Structure of liquid benzone and naphthalenes studied by pulsed neutron total scattering. In: *J. Chem. Phys.* **93**, 3495-3502, 1990.

Sengupta, A., Terazima, M., and Fayer, M.D., Ultrafast side group motions of polymers. In: *J. Phys. Chem.* **96**, 8619-8626, 1992.

Sengupta, A., and Fayer, M.D., Ultrafast side group dynamics in polymer melts: viscosity/temperature independent orientational relaxation. In: *J. Chem. Phys.* submitted, 1993.

Stankus, J.J., Torre, R., Marshall, C.D., Greenfield, S.R., Sengupta, A., Tokmakoff, A., and Fayer, M.D., Nanosecond time scale dynamics of pseudo-nematic domains in the isotropic phase of liquid crystals. In: *Chem. Phys. Lett.* **194**, 213-216, 1992.

Stankus, J.J., Torre, R., and Fayer, M.D., The influence of local liquid structure on orientational dynamics: the isotropic phase of liquid crystals. In: *J. Phys. Chem.* submitted, 1993.

Yan, Y., and Nelson, K.A., Impulsive Stimulated Light Scattering. I. General Theory. In: *J. Chem. Phys.* **87**, 6240-6256, 1987a.

Yan, Y., and Nelson, K.A., Impulsive Stimulated Light Scattering. II. Comparison to Frequency Domain Light-Scattering Spectroscopy. In: *Chem. Phys.* **87**, 6257-6265, 1987b.

Author's Address

Chemistry Department
Stanford University
Stanford, CA 94305
USA

Y. Tanimura and S. Mukamel

Nuclear Dynamics of Liquids; possible probe by 2D femtosecond off-resonant spectroscopy

Abstract

The nonlinear nuclear optical response of liquids subjected to a series of N off-resonant femtosecond laser pulses is calculated using the N'th order non-Condon response function for a multimode Brownian oscillator model. This multidimensional spectroscopy can be used to unveil the homogeneous or the inhomogeneous nature of the spectral density observed in impulsive Raman and birefringence measurements.

Introduction

Nuclear motions in liquids take place over a broad range of time scales. It is therefore not clear whether spectral lineshapes can be classified as either homogeneous or inhomogeneous. Even when such classification is possible by virtue of separation of timescales, it is not easy to firmly establish it experimentally. Early picosecond coherent Raman measurements were assumed to have the capacity of selectively eliminating inhomogeneous vibrational dephasing and revealing the homogeneous component. [Kaiser and Laubereau (1978); Zinth, et al. (1981); Oxtoby (1979); George et al., (1984)].

Loring and Mukamel (1985) have formulated the problem using a multitime correlation function approach and proved that this electronically off-resonant Raman technique, which contains only a single time variable is equivalent to linear absorption and is thus non selective in principle. They pointed out that only multitime techniques such as the Raman echo can address this issue. Several experiments have been subsequently carried out in order to measure the homogeneous vibrational linewidth [Vanden Bout, Muller, and Berg (1993); Muller, Wynne, and van Voorst (1988)]. These experiments were conducted on isolated intramolecular high frequency vibrations. In these applications the light pulses were longer than the vibrational periods. As such they did not have the time resolution to observe directly the vibrational motions. The decay of the signal with the delay between the excitation and the probe pulses then reflects vibrational dephasing.

Recent development of femtosecond techniques made it possible to probe

intermolecular vibrations in the frequency range 0-700[cm^{-1}] using an impulsive excitation with pulses short compared with the vibrational periods. Under these conditions the time resolved signal can show the coherent vibrations as well as their dephasing. It is tempting to analyze the spectral densities obtained [Nelson, et. al (1985-1990); McMorrow, et al. (1987, 1988, 1991); Cho, et al. (1993b)] in terms of instantaneous normal mode analysis of liquids [Keyes (1984); Chen and Stratt (1991)]. However, since impulsive birefringence and stimulant Raman techniques have only a single time variable, the limitations of the picosecond Raman measurements apply here as well; the homogeneous and the inhomogeneous nature of nuclear motions cannot be addressed.

In this article we present a closed form expression for the nuclear response function to third and fifth order in the field, using a harmonic model for nuclear motions with a nonlinear coupling to the radiation field (i.e. through the nonlinear dependence of the polarizability on nuclear coordinates).

This multimode Brownian oscillator model provides a convenient means for incorporating nuclear degrees of freedom in optical response functions. We have recently used a path integral approach to develop exact closed expressions for the nuclear wavepackets in phase space and for the nonlinear response functions for this model, including a coordinate dependent dipole interaction (non-Condon dipole interaction). Inhomogeneous broadening is incorporated by assuming a static distribution of the oscillator parameters (Fried and Mukamel, 1993). As an illustration, we analyze the possible application of a 5-pulse ($P^{(5)}$) measurement to a model liquid with a typical optical birefringence spectral density.

Off-Resonant Non-Condon Response Functions

We consider off-resonant spectroscopy of liquids in which all optical frequencies and their combinations are far detuned off any electronic excitation.

The external field consists of a train of N pairs of simultaneous pulses, followed by a final (probe) pulse,

$$E(\mathbf{r}, t) = \sum_{i=1}^{N} E_j(\mathbf{r}, t) + E_T(\mathbf{r}, t), \tag{1}$$

where

$$E_j(\mathbf{r}, t) = E_j(t) \{\exp[i(\Omega_j t - \mathbf{k}_j \mathbf{r})] + \exp[i(\Omega'_T t - \mathbf{k}_T \mathbf{r})]\} + c.c., \tag{2}$$

and

$$E_T(\mathbf{r}, t) = E_T(t) \exp[i(\Omega_T t - \mathbf{k}_T \mathbf{r})] + c.c.. \tag{3}$$

Here $E_j(t)$ denotes the temporal profile of the j'th pulse. We assume that the pulse pairs are well separated in time. We further assume that the system is initially in thermal equilibrium in the ground electronic state.

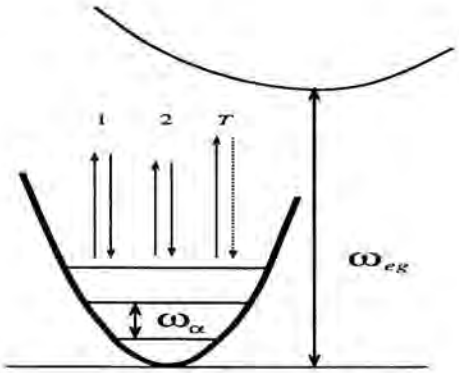

Fig. 1. The potential surfaces of the ground state and the first excited state for an α'th Brownian oscillator. Shown also in the pulse interaction scheme for a $P^{(5)}$ ($N=2$) process. Two off-resonant pairs of the pulses labeled 1 and 2 perturb the nuclear motion in the ground state. The fifth pulse labeled T then creates the polarization and generates the signal. This experiment has two time intervals and can therefore distinguish between inhomogeneous and homogeneous spectral densities.

Off resonant measurements have the following attractive characteristics. (i) Excited state populations are limited by the Heisenberg relation to very short times $\Delta t \approx 1/\Delta\omega$, where $\Delta\omega$ is the off-resonant detuning. As $\Delta\omega$ is increased, these populations become practically negligible and the measurements probe only ground state dynamics. (ii) The time the system spends in an electronic coherence is also limited by the same Heisenberg relation, and consequently nuclear dynamics can be neglected during the coherence periods. We can then perform time integrations over these periods and describe the interaction of the liquid with the laser fields by an effective Hamiltonian

$$H_{eff} = H_g(\mathbf{p}, \mathbf{q}) - \alpha(\mathbf{q})\, E(\mathbf{r}, t), \tag{4}$$

where $H_g(\mathbf{p}, \mathbf{q})$ is the ground state Hamiltonian and $\alpha(\mathbf{q})$ is the electronic polarizability that depends parametrically on the nuclear coordinates $\mathbf{q}$ (Hellwarths, 1977; Yan and Mukamel, 1991; and Tanimura and Mukamel, 1993). We assume the following model for the electronic polarizability,

$$\alpha(\mathbf{q}) = \exp\left(\sum_s A_s a q_s\right), \tag{5}$$

where A_s is the dipole coupling constant for the s'th oscillator. The dimension of A_s is chosen to be m^{-1}, therefore, a is a dimensionless coupling parameter. The coordinate q dependence of s may arise from the coordinate dependence of the dipole moment and of the electronic energies.

For off resonant excitation, the $2N+1$'th polarization is then expressed as

$$P^{(2N+1)}(t) = 2^{N+1} E_T(t) \exp(i\Omega_T t - i\mathbf{k}_T \mathbf{r}) \left\{ \prod_{j=1}^{N} \int_0^\infty d\tau_j E_j^2 \left(t - \sum_{k=j}^{N} \tau_k \right) \times \left[2\cos\left(\Delta\Omega_j \left(t - \sum_{k=j}^{N} \tau_k \right) - \Delta\mathbf{k}_j \mathbf{r} \right) + 1 \right] \right\} R^{(2N+1)}(\{\tau_j\}), \quad (6)$$

where $\Delta\mathbf{k}_j \equiv \mathbf{k}_j - \mathbf{k}'_j$, $\Delta\Omega_j \equiv \Omega_j - \Omega'_j$.

For H_g, we assume a multimode Brownian oscillator model.

$$H_g(\mathbf{p}, \mathbf{q}) = \sum_s \left\{ \frac{p_s^2}{2m_s} + \frac{m_s \omega_s^2 q_s^2}{2} + \sum_k \left[\frac{(p_k^s)^2}{2m_k^s} + \frac{m_k^s (\omega_k^s)^2}{2} \left(x_k^s - \frac{c_k^s q_s}{m_k^s (\omega_k^s)^2} \right)^2 \right] \right\}. \quad (7)$$

Here, x_k^s, p_k^s, m_k^s, and ω_k^s, are the coordinate, the momentum, the mass and the frequency of the k'th bath oscillator for s'th mode, respectively. We assumed that the optically active vibrations are linearly coupled to a heat bath. The heat-bath system may represent optically inactive vibrational modes, phonons, solvent modes, etc.

We can think of the system in terms of a few Brownian oscillators q_s, or an infinite number of harmonic oscillators (with no damping). The two pictures are mathematically equivalent. The former may provide a better physical insight regarding the relevant collective nuclear motions.

Expanding in powers of a^2, the lowest term in the third order response function is given by

$$R^{(3)}(\tau_1) = \frac{2}{\hbar} a^2 \int d\Gamma\, S(\Gamma)\, C''(\tau_1; \Gamma), \quad (8)$$

where

$$C''(t; \Gamma) = \int d\omega\, J(\omega; \Gamma) \sin(\omega t). \quad (9)$$

Here, we introduce the spectral distribution function

$$J(\omega; \Gamma) = \sum_s \eta_s f(\omega; \omega_s, \gamma_s), \quad (10)$$

where $\Gamma \equiv \{\eta_s, \omega_s, \gamma_s\}$ represents the parameters of the model namely the strength of the interaction (η_s), the frequency (ω_s), and the relaxation rate (γ_s) of the s'th mode and

$$f(\omega; \omega_s, \gamma_s) = \frac{1}{2\pi} \frac{\omega\gamma_s}{(\omega_s^2 - \omega^2)^2 + \omega^2\gamma_s^2}. \quad (11)$$

The effect of the heat bath is expressed by the spectral distribution, $\gamma_s(\omega)$ will represents the friction induced by the bath on the s'th oscillator,

$$\gamma_s(\omega) \equiv \sum_k \frac{(c_k^s)^2}{2m_k^s(\omega_k^s)^2}\,\delta(\omega-\omega_k^s). \tag{12}$$

In this study we assume a frequency-independent friction $\gamma_s(\omega)=\gamma_s$, which represents a Gaussian-white noise on the nuclear system. The coupling strength is given by

$$\eta_s \equiv \frac{\hbar A_s^2}{m_s}. \tag{13}$$

This model can be used to represent specific coordinates, whether local (e.g. intramolecular) or collective in nature. Even if we do not have a clear idea of the nature of the modes of the system, it can be used as a convenient parameterization. In the liquid phase, the distribution of the values of $\{\eta_s, \omega_s, \gamma_s\}$ may reflect different slowly interconverting local environments. Similar problems of inhomogeneity are of current interest in the studies of dissipative kinetics observed in charge transfer in the photosynthetic reaction center (Walker, et.al. 1992, 1993).

Consider the following form for the birefringence (Kerr) amplitude

$$R^{(3)}(\tau_1) = \frac{2}{\hbar}a^2 \int d\Gamma\, S(\Gamma) \int d\omega\, J(\omega;\Gamma)\sin(\omega\tau_1), \tag{14}$$

where

$$\begin{aligned} R^{(3)}(\omega) &\equiv \int d\tau_1 e^{i\omega\tau_1} R^{(3)}(\tau_1) \\ &= \frac{\omega A_1 C_1}{2\pi[(B_1^2-\omega^2)^2+\omega^2 C_1^2]} + \frac{\omega A_2 C_2}{2\pi[(B_2^2-\omega^2)^2+\omega^2-C_2^2]}. \end{aligned} \tag{15}$$

Here A_1, B_1, C_1, etc. are chosen to represent the experimental birefringence spectral density of CH_3CN of these parameters (in $[cm^{-1}]$) are given by (Cho et.al, 1993b)

$$A_1 = 0.01,\ B_1 = 50,\ C_1 = 100,\ A_2 = 0.04,\ B_2 = 350,\ C_2 = 25. \tag{16}$$

$R^{(3)}$ depends on the homogeneous J and inhomogeneous S components only through the combination

$$\int d\Gamma\, S(\Gamma)\, J(\omega;\Gamma). \tag{17}$$

There are therefore infinite number of choices of inhomogeneous distribution

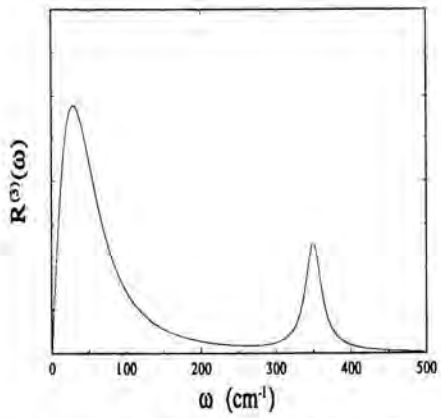

Fig. 2. The spectral density $R^{(3)}(\omega)$ of CH_3CN obtained from the optical Kerr experiment (Cho et al., 1993).

$S(\Gamma_s)$ and homogeneous spectral distribution $J(\omega; \Gamma_s)$, that gives the same optical Kerr signal,

$$I^{(3)}(T_1) = |R^{(3)}(T_1)|^2, \tag{18}$$

where $R^{(3)}$ is given by Eq. (15). Hereafter we adopt the two extreme choices; (i) a purely homogeneous two oscillator case, where spectral density is attributed to the two oscillator modes

$$S(\Gamma_1, \Gamma_2) = \prod_{\alpha=1}^{2} \delta(\eta_\alpha - A_\alpha)\, \delta(\omega_\alpha - B_\alpha)\, \delta(\gamma_\alpha - C_\alpha), \tag{19}$$

$$J(\omega; \Gamma_1, \Gamma_2) = \eta_1 f(\omega; \omega_1, \gamma_1) + \eta_2 f(\omega; \omega_2, \gamma_2) \tag{20}$$

(ii) purely inhomogeneous one oscillator case, where a single harmonic frequency is inhomogeniously distributed

$$S(\Gamma_1) = \lim_{\varepsilon \to 0} \delta(\eta_1 - 1)\, \delta(\gamma_1 + \varepsilon)[A_1 f(\omega_1; \beta_1, C_1) + A_2 f(\omega_1; B_2, C_2)], \tag{21}$$

$$J(\omega; \Gamma_1) = \eta_1 f(\omega; \omega_1, \gamma_1). \tag{22}$$

As can be seen from Eq. (14), the third order signal, which corresponds to the optical Kerr (birefringence) experiments, is identical for the two models. This is in agreement with our previous analysis to the effect that we cannot distinguish between homogeneous and inhomogeneous contributions from experiments based on the third order response function.

Let us consider now the fifth order signal. The 5'th order off-resonant response function is given by

$$R^{(5)}(\tau_2, \tau_1) = \frac{4a^4}{\hbar^2} \int d\Gamma\, S(\Gamma)\, C''(\tau_2; \Gamma)\, [C''(\tau_1; \Gamma) + C''(\tau_1 + \tau_2; \Gamma)], \tag{23}$$

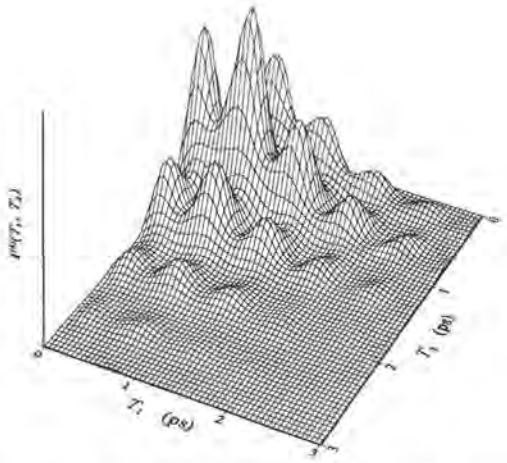

Fig. 3. The time domain 2D signal $I^{(5)}(T_1, T_2)$ for the pure homogeneous case (i) using the spectral distribution of Fig. 2.

or alternatively,

$$R^{(5)}(\tau_2, \tau_1) = \frac{4}{\hbar^2} a^4 \int d\Gamma\, S(\Gamma) \left[\int d\omega\, J(\omega; \Gamma) \sin(\omega\tau_2) \right] \times \left\{ \int d\omega\, J(\omega; \Gamma)\, [\sin(\omega\tau_1) + \sin(\omega(\tau_1 + \tau_2)] \right\}. \tag{24}$$

For impulsive pump probe experiments, such that $E_T(t) = \delta(t - T_1 - T_2)$,

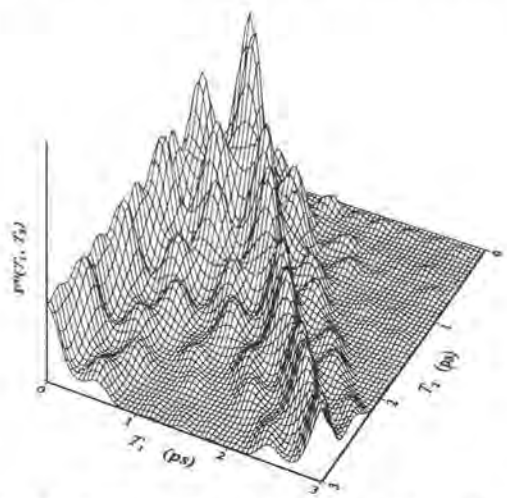

Fig. 4. The time domain 2D signal $I^{(5)}(T_1, T_2)$ for the pure inhomogeneous case (ii) using the spectral distribution of Fig. 2.

$E_1(t) = \delta(t)$, and $E_2(t) = \delta(t - T_1)$ for the 5'th order, we can perform the time integrations over τ_j. Then the total signal intensity related the square of the polarization is given by (up to a proportionality constant)

$$I^{(5)}(T_1, T_2) = |R^{(5)}(T_2, T_1)|^2. \tag{25}$$

$R^{(5)}$ depends on $J(\omega; \Gamma)$ and $S(\Gamma)$ separately and not merely through the combination Eq. (17). This opens up the possibility of observing the difference between the homogeneous and the inhomogeneous contributions to the spectral density obtained from birefringence $R^{(3)}$ experiments (Figs. 3-6). The two models Eq. (19) together with Eq. (20) or Eq. (21) together with Eq. (22) have dramatically different predictions for $R^{(5)}$. This is illustrated in the following numerical calculations. For (i) the pure homogeneous and (ii) the pure inhomogeneous cases. As seen from the figures, the fifth order (3-pulse) signal is very different for the two cases. The $I^{(5)}$ signal constitutes a two-dimensional spectroscopy with a two independent time periods during which the nuclear coherence evolves.

A different perspective on these results can be obtained by performing two-dimensional ($2D$) Fourier transformation, as follows,

$$I(\omega_2, \omega_1) = \left| \int_0^\infty dT_1 \int_0^\infty dT_2 e^{i\omega_1 T_1 + i\omega_2 T_2} I(T_2, T_1) \right|^2. \tag{26}$$

Calculations were made using a two-dimensional fast Fourier transform (FFT) routine on a 256 by 256 grid. Figs. 7 and 8 show, respectively, the 2D Fourier

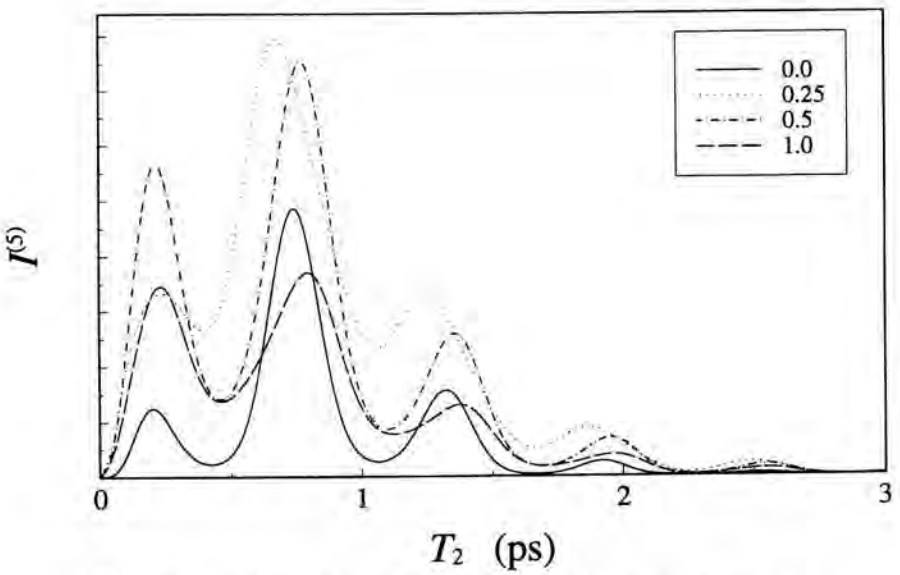

Fig. 5. Sections of Fig. 3 for different value of T_1 as indicated (in ps).

transform of (i) the pure homogeneous (Figs. 3 and 5) and (ii) the pure inhomogeneous cases (Figs. 4 and 6). In Fig. 7, we observe peaks whose positions are determined by the products $[\sin(\omega_a T_2)+\sin(\omega_b T_2)][\sin(\omega_a T_1)+\sin(\omega_b T_1)]$ and $[\sin(\omega_a T_2)+\sin(\omega_b T_2)]\{\sin[\omega_a(T_1+T_2)]+\sin[\omega_b(T_1+T_2)]\}$, however, since their spectral width at $(\omega_1, \omega_2)=(\pm 50, \pm 50)$ $[\mathrm{cm}^{-1}]$ are broad ($\gamma_a = 100$ $[\mathrm{cm}^{-1}]$), we cannot distinguish them from the zero frequency peak at $(\omega_1, \omega_2)=(0, 0)$. In the purely homogeneous case, one can observe coherent modes of the ground states as shown in this Figure.

Fig. 8 represents the pure inhomogeneous case, where we can rewrite the response function as

$$R^{(5)}(T_2, T_1)=\int d\omega_1 [A_1 f(\omega_1; B_1, C_1)+A_2 f(\omega_1; B_2, C_2)] \times \{\cos[\omega_1(T_1-T_2)]+\cos[\omega_1 T_1] -\cos[\omega_1(T_1+T_2)]-\cos[\omega_1(T_1+2T_2)]\}. \quad (27)$$

Thus, the response function consists of functions of the form $f(T_1-T_2)$, $g(T_1+T_2)$, $j(T_1+T_2)$ and $k(T_1)$. Since we performed the Fourier transformation over T_1, $T_2 \geqslant 0$, the contributions of $f(T_1-T_2)$ and $k(T_1)$ are large compared with the contribution from $g(T_1+T_2)$ and $j(T_1+2T_2)$ and show maxima along the lines $\omega_1=-\omega_2$ and $\omega_2=0$. The distribution of the ground state mode frequency can be observed on these lines as the peaks at $(\omega_1, \omega_2)=(\pm\omega_b, 0)$ and $(\omega_1, \omega_2)=\pm(\omega_b, -\omega_b)$. The functions $g(T_1+T_2)$ and $j(T_1+2T_2)$ also

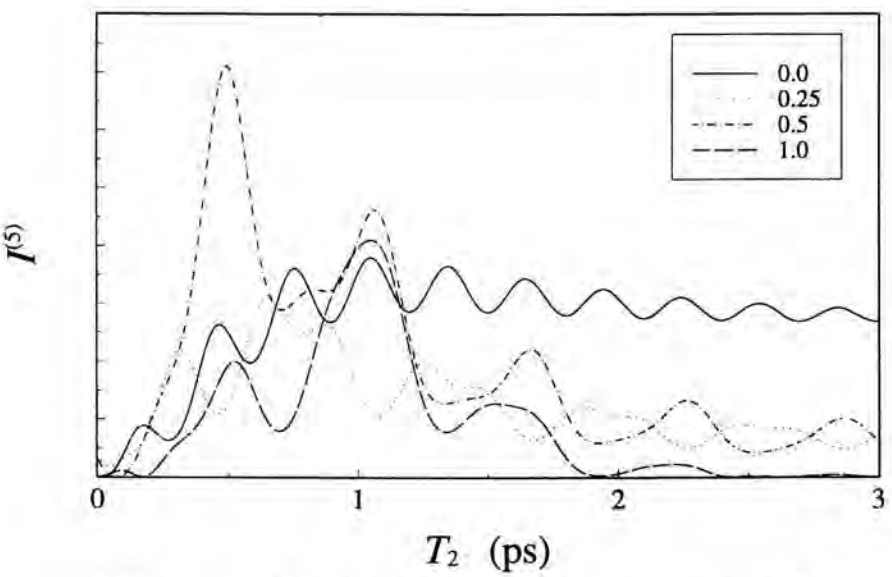

Fig. 6. Sections of Fig. 4 for different value of T_1 as indicated (in ps).

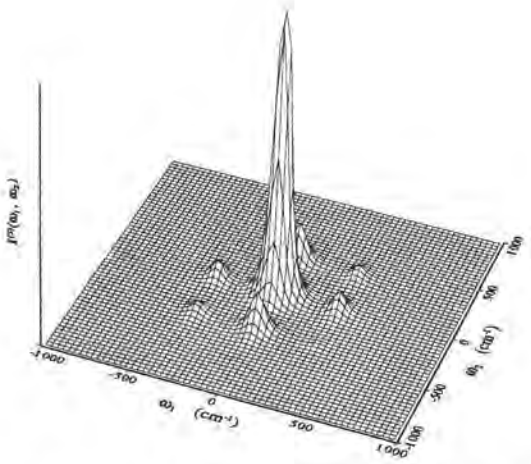

Fig. 7. The frequency domain 2*D* signal $I^{(5)}(\omega_1, \omega_2)$ corresponding to Figs. 3 and 5.

show small peaks at $(\omega_1, \omega_2) = \pm(\omega_b, \omega_b)$ and $(\omega_1, \omega_2) = \pm(\omega_b, 2\omega_b)$, however, the contribution from ω_a cannot be distinguished from the central peak.

n conclusion, the two models, which have an identical 1*D* (birefringence) spectrum clearly show very different 2*D* spectra. Realistic situations of the liquid spectral density are expected to be intermediate between these purely homogeneous and inhomogeneous cases. Separately of $J(\omega; \Gamma)$ and $S(\Gamma_s)$ may thus be probed by performing higher order measurements in addition to the optical Kerr experiment.

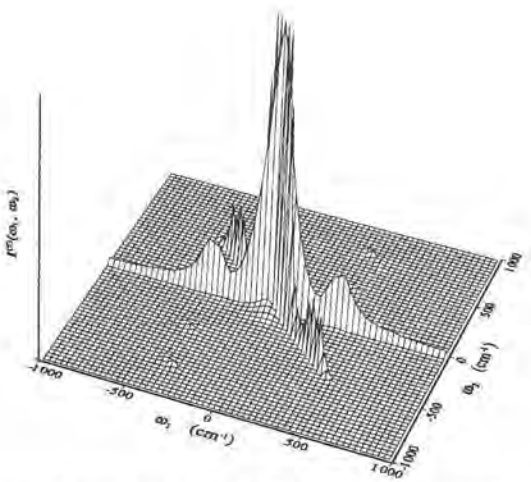

Fig. 8. The frequency domain 2*D* signal $I^{(5)}(\omega_1, \omega_2)$ corresponding to Figs. 4 and 6.

Acknowledgements

We wish to thank J. Buontempo, S. Palese, and D. Miller, V. Chernyak, M. Cho and G. Fleming for most useful discussions. The support of the National Scientific Foundation and the Air Force Office of Scientific Research is gratefully acknowledged.

References

Chen, A., and Stratt, R.M., *J. Chem. Phys.* **95**, 2669, 1991.
Cho. M., Fleming, G.R., and Mukamel, S.J, *Chem. Phys.* **98**, 5314, 1993a; Cho, M., Du, M., Scherer, N.F., Fleming, G.R., and Mukamel, S., submitted to *J. Chem. Phys.*, 1993b.
Egelstaff, P.A., An ntroduction to the Liquid State (Academic, New York), 1967.
Ernst, R.R., Bodenhausen, G., and Wokaun, Principles of nuclear magnetic resonance in one and two dimensions, (Clarenson press, Oxford, 1987), 1987.
Fried, L.E. and Mukamel, S., *Adv. Chem. Phys.* **84**, 435, 1993.
Fayer, M.D.
George, S.M., Harris, A.M., Berg, M., and Harris, C.B., *J. Chem. Phys.* **73**, 5573, 1984.
Hallwarth, R.W., *Prog. Quant. Electr.* **5**, 1, 1977.
Keyes, T., and Ladanyi, B.M., *Adv. Chem. Phys.* **56**, 411, 1984.
Laubereau, A., and Kaiser, W., *Rev. Mod. Phys.* **50**, 607, 1978.
Loring, R.F., and Mukamel, S., *J. Chem. Phys.* **83**, 2116, 1985.
Muller, L.J., Vavid, D., and Berg, M., submitted to *J. Chem. Phys.*, 1993.
Muller, M., Wynne, K., and van Voorst, J.D.W., *Chem. Phys.* **128**, 549, 1988.
MacMorrow., D., Kalpouzos, and C. Kenney-Wallace, G.A, *Chem. Phys. Lett.* **137**, 323, 1987; MacMorrow, D., Lotshaw, W.T., Kenney-Wallace, G.A., *IEEE J. Quantum Electron* **QE24**, 443, 1988; Lotshaw, W.T. McMorrow, D., and Lotshaw, W.T., *J. Phys. Chem.* **95**, 10395, 1991.
Nelson, K.A. and Ippen, E.F., *Adv. Chem. Phys.* **75**, 1, 1989; Weiner, A.M., Leaird, D.E., Wiederrecht, G.P., and Nelson, K.A., *Science* **247**, 1317, 1990; Yan, Y.X., Gamble, E.B., and Nelson, K.A., *J. Chem. Phys.* **83**, 5391, 1985; Ruhman, S., Joly, A.G., Kohler, B., Nelson, K.A., and Williams, L.R., *Rev. De. Phys.* **22**, 1717, 1978; Ruhman, S., Joly, A.G., Kohler, B., Nelson, K.A., and Williams, L.R., *J. Phys. Chem.* **91**, 2237, 1987.
Noda, I., *J. Am. Chem. Soc.* **111**, 8116, 1989; Noda, ., *Appl. Spectrosc.* **44**, 550, 1990.
Oxtoby, D.W., *Adv. Chem. Phys.* **40**, 1, 1979.
Scherer, N.F., Ziegler L.D., and Fleming, G.R., *J. Chem. Phys.* **96**, 5544, 1992.
Tanimura, Y., and Mukamel, S., *Phys. Rev.* **E47**, 118, 1993a; *ibid*: to be published in *J. Opt. Soc. Am.* **B**, 1993b; *ibid.* submitted to *J. Chem. Phys.*, 1993c.
Yan Y.J., Mukamel, S., *J. Chem. Phys.* **94**, 997, 1991.
Vanden Bout, D., Muller, L.J., and Berg, M., *Phys. Rev. Lett.* **67**, 3700, 1991.

Walker, G.C., Akesson, E., Johnson, A.E., Levinger N.E., and Barbara, P.F.; *J. Phys. Chem.* **90**, 3128, 1992; Tominaga, K., Kliner, D.A.V., Johnson, A.E., Levinger, N.E., and Barbara, P.F., *J. Chem. Phys.* **98**, 1228, 1992.
Zinth, W., Polland, H.-J., Laubereau, A., and Kaiser, W., *Appl. Phys.* **B26**, 77, 1981; Zinth, W., Leonhardt, R., Holzapfel, H., and Kaiser, W., *IEEE J. Quantum Electron.* **24**, 455, 1988.

Author's address

Department of Chemistry
University of Rochester
Rochester, New York 14627
USA

Boris A. Grishanin, Andrei Yu. Chikishev, Nikolai I. Koroteev,
Valentin D. Vachev and Victor N. Zadkov

Fast (Pico- and Femtosecond) Reaction Dynamics in the Excited States of Large Molecules: Fluorescence Studies and Computer Simulations

Abstract

In the *First part* the results are presented of the investigation of firefly luciferase which catalyzes bioluminescent oxidation of luciferin to oxyluciferin. The methods were applied of fluorescence intensity and anisotropy decay analysis and fluorescence spectrochronography. Fluorescence lifetimes and rotational correlation times were determined of luciferin, methoxyluciferin and of luciferase tryptophan along with the intramolecular relaxation time of luciferase. A possibility is discussed of the light induced enzyme conformational changes. In the next two chapters a computer simulation procedure is developed for modeling ultrafast photoinduced intramolecular dynamics in polyatomic molecules. Electronic-vibrational excitation by ultrashort laser pulses (20 fs ÷ 1 ps) is treated explicitly using quantum theory in harmonic approximation. MD simulation is used for studying the excited state dynamics. *Second part* of the paper is devoted to the modeling of photoinduced isomerization of stilbene molecule. Model potential energy surfaces (PES) for the ground and first excited singlet states are obtained using experimental absorption spectra in supersonic jet. Using a symmetry along the torsional coordinate PES, it is shown that *cis*-stilbene undergoes the first stage of the isomerization reaction, i. e. transition to the twisted configuration, much faster than *trans*-stilbene, only due to the specific conformational properties. *Third part* is focused on modeling of dissociation dynamics of ethylene molecule in the ground electronic state excited by short IR laser pulse.

Part I. Luciferin-luciferase System: Model for Light-induced Protein Conformational Dynamics Study

Introduction

Firefly luciferase catalyzes luciferin oxidation in the presence of ATP and magnesium bicathions. The product of the reaction is oxyluciferin in the singlet electronic excited state and its deactivation is accompanied by the yellow-green

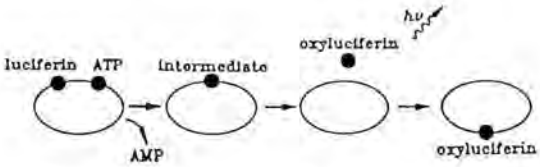

Fig. 1. The simplified scheme of the bioluminescent reaction.

bioluminescence ($\lambda_{max} = 560 - 570$ nm) (McElroy et al., 1974). The simplified reaction scheme is presented in Fig. 1.

Earlier a dissociative mechanism of oxyluciferin deactivation was suggested (Gandelman, 1990), which presumes that the excited molecule leaves the protein globule and emits light quantum in solution. One may consider luciferin-luciferase system to be a good model for studying light-induced transformations in enzyme-substrate system. Bioluminescence reaction only takes place in the presence of two substrates: luciferin and ATP. Hence the complex of the enzyme with only one of them is rather stable and suitable for the studies of both protein and substrate properties. Unfortunately up to now there are no X-ray data on the luciferase structure. But the primary sequence is known already and it is shown that there is only one tryptophan residue in this molecule (Kutuzova, 1992), which makes it suitable for the kinetic fluorescence study, for tryptophan is known to be very sensitive probe of both static and dynamic properties of the protein matrix (Lackovicz, 1983). The stationary fluorescence spectrum of luciferase displays maximum at 336 nm indicating the unpolar environment of the tryptophan residue. Luciferin may exist in solution in protonated or deprotonated forms. The equilibrium constant is 8.7 for the molecule in the ground state, hence at neutral pH's luciferin is almost completely protonated. These two different forms of the molecule possess completely different fluorescence and absorption spectra. For the protonated molecule absorption and fluorescence maxima are at 330 and 440 nm, respectively, whereas for the deprotonated one they are shifted to 380 and 540 nm, respectively. Extinction coefficients of the two forms are practically equal at 350 nm. Methoxyluciferin is a structural analog of the reaction substrate, but as it is unionizable it has only one absorption and one fluorescence maximum at 326 and 427 nm respectively.

Experimental

Luciferase was purified by the method of Philippova et al. (1984). In the experiments we used luciferase solutions in 0.1 M tris-acetate buffer (pH = 7.8) at concentration 10^{-6} M. Luciferin was synthesized by the method of A. Schogolev et al. (1983). 6'-methoxyluciferin was synthesized as described by White et al. (1965). Aqueous solutions of luciferin and methoxyluciferin were prepared in 0.1 M tris-acetate buffer (pH = 7.8). Time-resolved fluorescence measurements were carried out on the spectrometer described elsewhere (Kamalov, 1987). Fluorescence was excited by single pulses of Q-switched, mode-locked Nd:YAG

laser third harmonic radiation $\lambda_{ex} = 355$ nm, $\tau_{pulse} = 50$ ps (luciferin and methoxyluciferin) or forth harmonic radiation $\lambda_{ex} = 266$ nm, $\tau_{pulse} = 50$ ps (tryptophan). In all the measurements, except that of the anisotropy decay, registration polarizer was set at the magic angle relative to the polarization of the excitation beam. Time-correlated single photon counting technique was used for registration. Spectral resolution of the registration system was ≈ 1 nm. Kinetic data were processed with an original program of multiexponential fit which did not require preliminary setting of the number of exponentials in the fitting procedure.

Luciferin fluorescence in solution and in complex with luciferase.

The decay curves of luciferin aqueous solution and enzyme-substrate complex are practically identical at 540 nm (deprotonated luciferin) and are different at 440 nm (protonated luciferin). The quantitative comparison of the last two evolves from the fluorescence lifetimes estimation, the results of which are presented in Fig. 2.

The component at appr. 4 ns may be neglected as belonging to the residual input of the deprotonated molecules fluorescence. Thus the difference between the free substrate in solution and in complex with the enzyme is in the relative decrease of the fast component amplitude and in the appearance of the new component with the lifetime of 1.06 ns. It may be explained by the change in the chromophore environment in the complex with the enzyme resulting in the diminishing of the fluorescence quenching. It was also interesting to examine the behavior of the fluorescence anisotropy in this case. However luciferin-luciferase system does not seem to be the best for such experiments because of the relatively fast fluorescence decay at the magic angle, which leaves rather poor chances to observe relatively slow rotations in case the substrate is immobile in the complex with enzyme. That is why we carried out the fluorescence anisotropy measurements using methoxyluciferin instead of luciferin both in solution and in complex with luciferase, firstly because of its longer fluorescence decay and secondly because its stationary fluorescence is similar to that of the protonated

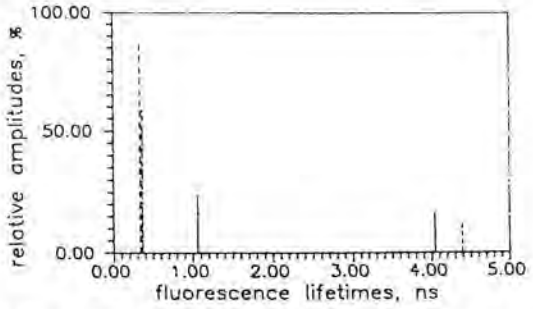

Fig. 2. Fluorescence lifetimes distributions of luciferin aqueous solution (dashed line) and enzyme-substrate complex (solid line), $\lambda_{fl} = 440$ nm.

luciferin. The fluorescence decay curves measured with parallel (perpendicular) excitation and registration polarizers appeared to be practically identical for methoxyluciferin aqueous solution and for methoxyluciferin-luciferase complex, which presumes free rotation for the substrate analog in both systems. The parameters of the fluorescence anisotropy decay were estimated to be: initial anisotropy $r_0 = 0.30$, rotational correlation time $\varphi = 410$ ps. The linear size of the molecule was estimated to be about 7 Angstroms which is in good agreement with the real size of the methoxyluciferin molecule. All the data presented indicate that the excited luciferin molecule has rather weak contacts with the protein. The latter is in good agreement with the idea of dissociative behaviour of the emitter in the bioluminescent reaction.

Luciferase intramolecular dynamics

It is well known that tryptophan may be used as a fluorescence probe of both static and dynamic properties of the protein matrix (Lackovicz, 1983). In case of only one tryptophan residue per protein molecule and in the absence of the energy transfer processes it is possible to study protein intramolecular dynamics by means of tryptophan fluorescence spectrochronography. This method implies the study of the evolution of fluorescence spectra in time after pulse excitation. Both direct measurements of the time-resolved fluorescence spectra (TRFS) and their reconstruction from the fluorescence decay curves are possible (Lackovicz, 1983). In our studies we used the method of TRFS reconstruction. Luciferase aqueous solution tryptophan fluorescence decay curves were measured at 24 wavelengths from 310 to 380 nm with the step of 3 nm which covers tryptophan stationary fluorescence spectrum. After the multiexponential approximation average fluorescence lifetimes were obtained (Fig. 3).

The increase of the average fluorescence lifetime at the longwavelength part of the spectrum is quite natural for the relaxation process. All the decay curves

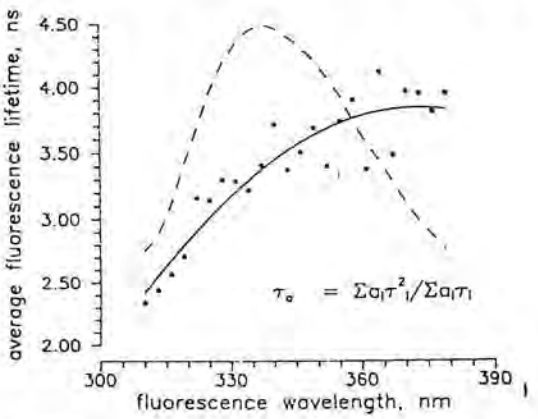

Fig. 3. Average luciferase tryptophan fluorescence lifetime dependence on the fluorescence wavelength (dashed line - luciferase stationary fluorescence spectrum).

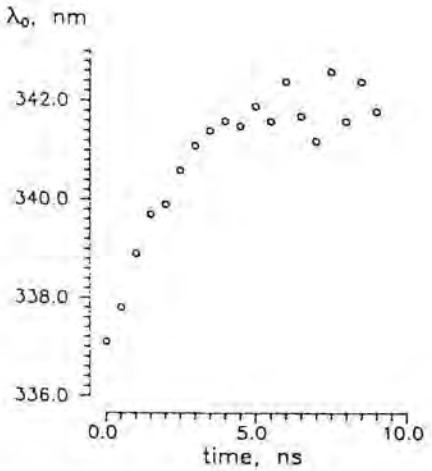

Fig. 4. Log-normal approximation of luciferase TRFS at different delays after excitation pulse.

were scaled in amplitude with the scaling factors depending on the stationary fluorescence intensity at the given wavelength. After that the TRFS were reconstructed by integrating fluorescence decay curves at all wavelengths within narrow (0.5 ns) time gate at different delays. The TRFS were then approximated with log-normal function to determine accurately the positions of the maximum, right and left half-maxima. The results of TRFS reconstruction along with the evolution of their position in time are presented in Figs. 4, 5.

The characteristic time of the TRFS red-shift and hence, according to the assumption, the relaxation time of the protein matrix was estimated to be 2.5 ns.

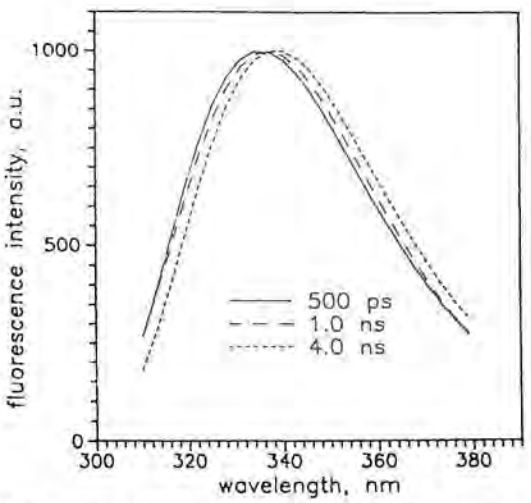

Fig. 5. Luciferase TRFS shift vs delay time after excitation pulse ($\lambda_0 = 1/\nu_0$, ν_0 — TRFS log-normal approximation maximum frequency).

We also carried tryptophan fluorescence anisotropy measurements. The decay curves measured at 340 nm with parallel and crossed polarizers in excitation and registration were synchronously processed with multiexponential approximation for fluorescence decay and monoexponential approximation for anisotropy decay. Within this approximation the initial anisotropy was estimated to be $r_0 = 0.184$ and the rotational correlation time - $\varphi = 21.2$ ns. It is clear that such a long correlation time may correspond only to the rotation of the globule as a whole. The attempt of introducing additional components to the anisotropy approximation failed, indicating that the long component is undoubtedly dominating. However it is still probable that there are faster rotations in this system. To prove that let us analyze the behavior of two decay curves: one of them is measured at the magic angle and corresponds to the total fluorescence intensity (I_{tot}) and the other one is calculated as a difference between the two decay curves measured with parallel and crossed excitation and registration polarizers respectively ($I_{diff} = I_{par} - I_{ort}$) and is equal to anisotropy multiplied by total intensity: $I_{diff} = r(t) * I_{tot}$. Hence the decay time(s) of I_{diff} must be faster than both the fluorescence decay time(s) and rotational correlation time(s), because $\tau_{diff}^{-1} = \tau_{tot}^{-1} + \varphi^{-1}$. The distribution of the decay times for I_{tot} and I_{diff} is presented in Fig. 6.

The rotational correlation time estimated from the shortening of the longest fluorescence decay time (6.65 ns) is 19 ns which is in good agreement with the above mentioned direct estimation. However the same time estimated from the shortening of the fastest component (0.99 ns) is only 2.98 ns, which is only possible in case of the rotation not of the globule as a whole but of only a part of it. Of course, further more precise measurements are necessary to prove the existence of this fast rotation, corresponding, possibly, to the intraglobular motions.

Luciferase conformation changes upon luciferin binding

It was demonstrated in the previous stationary fluorescence measurements that luciferase tryptophan fluorescence is strongly quenched by luciferin (Brovko,

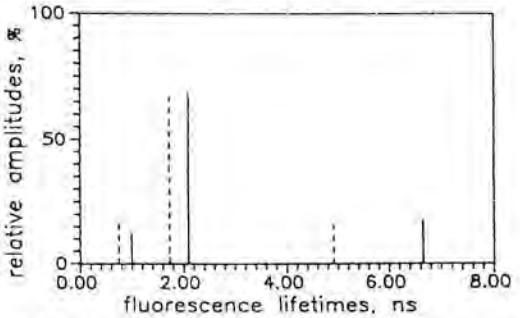

Fig. 6. The distribution of the decay times for I_{tot} (solid line) and I_{diff} (dashed line) (see text) of luciferase tryptophan fluorescence, $\lambda_{fl} = 340$ nm.

1986). In Fig. 7 tryptophan fluorescence decay curves are presented of free luciferase and the sample where 50% of the enzyme molecules formed complex with the substrate.

The fluorescence intensity of the last sample is about 20% lower compared to the first one, but the fluorescence decay curves are almost identical. The same was observed for the samples with different percentage of the complex. The stability of the fluorescence lifetime of the chromophore being quenched indicates that the fluorescence quenching is of stationary type, i.e. the chromophore forms nonfluorescing complex with some adjacent molecule(s). In our case one may suppose that tryptophan is quenched due to the change of enzyme conformation after substrate binding. It is not clear if luciferin directly quenches tryptophan fluorescence. However it comes from the fluorescence and anisotropy measurements of the luciferin itself that it is more likely that substrate binding site is situated close to the enzyme surface and that substrate binding is rather flexible. On the other hand tryptophan is most probably located inside protein globule in its hydrophobic area (according to the stationary fluorescence data presented here above). All this may indicate that tryptophan is quenched not directly by luciferin but by the adjacent amino-acids after the conformational change. Assuming dissociative behaviour of the excited substrate/product in the system considered and the protein conformation changes upon substrate binding we may suggest a model of the light-induced protein conformational changes. (Ultra)short light pulse brings the ligand molecule to the excited state which induces ligand- enzyme complex dissociation. This dissociation (may be considered as a mechanical shock) leads to the conformational changes in the protein, which may be detected by methods of ultrafast laser spectroscopy.

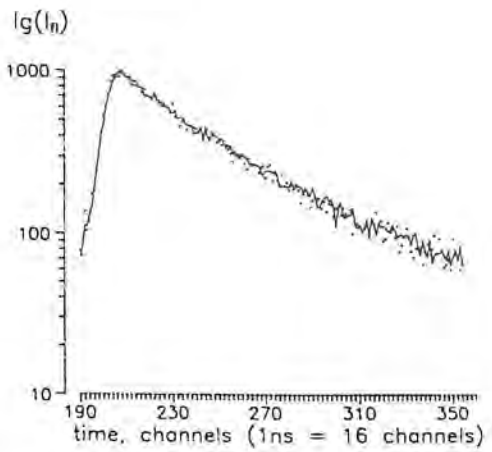

Fig. 7. Tryptophan fluorescence decay curves of the sample in which 50% of the enzyme molecules formed complex with the substrate (dots) and of free enzyme (solid line), $\lambda_0 = 340$ nm.

The results obtained for luciferin- luciferase complex and their comparison with that for luciferin solution allow us to suggest that substrate binding changes enzyme conformation. Luciferase intramolecular dynamics is detected and relaxation time is estimated by the method of spectrochronography; luciferase tryptophan fluorescence data may indicate that luciferase intramolecular segment motility is possible.

Part II. MD Investigations of Photoinduced Transformations in Organic Molecules

1. *Introduction*

Many important processes in polyatomic molecules take place in excited electronic states or use them as transition states. Between these are photoinduced isomerization of retinal systems and photosynthetic bacteria, electron transfer in biological, interfacial, or electrochemical systems, vibrational relaxation in liquids, and photodissociation. These processes occur typically on pico- and subpicosecond timescales, and recent advances in generation of ultrashort and broadly tunable laser pulses are highly promising for experimental studies of the basic mechanisms realized in Nature (Akhmanov 1992, Dexheimer 1992, Mathies 1988, Shoenlein 1991). Such investigations are important also in the search of new materials for nonlinear optics, electro-optics and molecular electronics.

The complexity of the objects under consideration, however, makes difficult a direct interpretation of the data obtained from different laser spectroscopy methods in both time and frequency domains. Thus, appropriate approximations and computer simulation methods are necessary.

Molecular Dynamics (MD) is a computer-based technique for modeling gases, liquids and solids on microscopic scales of distance and time, and is therefore an ideal technique for studying molecular behavior in many physical processes (*Computer Simulation* ... 1990, Levine 1987, *Molecular Dynamics* ... 1986). The method is based on the assumption that atomic motions are governed by classical mechanics provided some appropriate multidimensional force-field is used. Limitations of the method are well known. A fundamental one results from the basic assumptions of the method, namely, quantum-mechanical behavior is neglected and a single potential energy surface is assumed to govern the motion. The quantum nature of vibrational and electronic motion, however, is important and must generally be accounted for. Other problems are connected with practical difficulties in constructing accurate force-field, including large number of atoms, integrating over long times, or achieving accurate statistical sampling. All of these depend on the efficiency of the computational procedure and models used.

A general formulation of the problem and the approach used can be understood from Fig. 1. A molecule being initially in a ground electronic state $|1\rangle$ after irradiation is excited to an upper electronic level $|2\rangle$. The initial state of the molecule after excitation depends on the two potential energy surfaces (PES) and laser pulse characteristics such as laser frequency, time duration and coherence length. The laser pulse duration τ_p should be compared with the vibrational period τ_v of the molecule. For instance, ultrashort laser pulse, $\tau_p \ll \tau_v$, would bring the molecule to the excited electronic state without sufficient changes in the nuclei configuration (Franck-Condon transition). In the quasi-stationary case a long laser pulse with sufficient coherence length would excite (under appropriate conditions) a single vibrational level (SVL). Actually a 15 ps laser pulse may be long enough for a SVL excitation (Felker 1988). In the intermediate case of comparable τ_p and τ_v the excited state is determined by a complex interference between vibrational movements in the two electronic states.

Most often the experimental situation corresponds to the intermediate case with vibrational frequencies in the range of $20\ \mathrm{cm}^{-1} \div 3500\ \mathrm{cm}^{-1}$ and excitation by laser pulse in the range of $20\ \mathrm{fs} \div 1$ ps. Elsewhere (Grishanin 1991, Grishanin 1992), we have considered this intermediate case and presented a quantum harmonic theory of the one-photon electronic-vibrational excitation. The basic results of this previous study are as follows. The transition probability is given by

$$P(\omega_L) = (\Omega_L^2/4) \int f_p(\tau) \exp[i(\omega_L - \omega_{12})\,\tau]\, \chi(\tau)\, d\tau, \qquad (1)$$

where $f_p(\tau) = \int u_p(s-\tau/2)\, u_p^*(s+\tau/2)\, ds$ is the laser pulse autocorrelation function, $\Omega = E_L d_{12}/\hbar$ is the Rabi frequency, ω_{12} is the frequency of the electronic transition; $\chi(\tau)$ is analytical function of the frequency matrices ω_1 and ω_2, the deviations Δ of the energy minima along each vibrational coordinate, and temperature (see Eqs. (5–6) in (Grishanin 1992)).

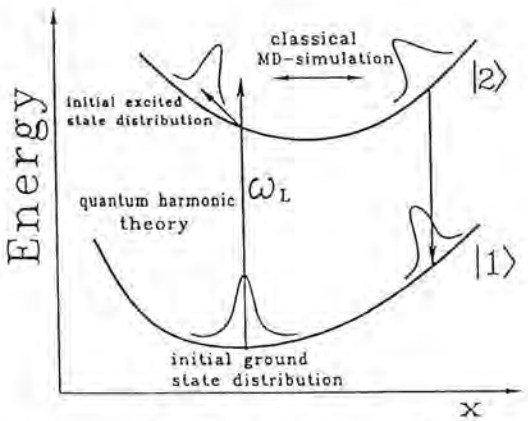

Fig. 1. MD simulation of electronically excited polyatomic molecules. The excitation by ultrashort laser pulses is treated explicitly, using quantum harmonic theory. MD simulation is used for modeling the excited state dynamics.

After averaging the displacements of nuclei coordinates over the laser pulse one obtains

$$x_q = x_2 + \int p(\tau)\, \Delta x(\tau)\, d\tau / P(\omega_L), \tag{2}$$

where x_q is a $3N$-dimensional vector of the averaged coordinates after excitation; x_2 is $3N$-coordinate vector of the energy minima point of $|2\rangle$, $p(\tau)$ is the time density of transition probability $dP(\omega_L)/d\tau$ (see Eq. (1)), $\Delta x(\tau)$ is the displacement relative to x_2 at the moment of time τ (see Eqs. (7–8) in (Grishanin 1992)). For the average momenta we have $p_q = 0$.

The absorption (excitation) spectrum or 0^0 dispersed fluorescence spectrum (0^0 denotes the vibrationless excited electronic state) are calculated using Eq. (1), in which the integration is carried over a time period larger than all vibrational periods. In Sec. 2 we use the available absorption spectrum of stilbene molecule obtained in supersonic jets for precise determination of characteristics of 12 active normal modes (we use only modes well identified in the experimental spectrum). In doing so the PES are determined in harmonic approximation which may be useful in applications such as ultrafast excitation or early stage dynamics.

In Sec. 3 the PES are determined in a more general way by Molecular Mechanics (MM) potential energy functions. The correspondent parameters are calculated so as to ensure good agreement between calculated and experimental spectra. In Sec. 4 MD simulation results on the excited state PES (in the full $3N$-dimensional coordinate space) are reported. Using Eq. (2), MD trajectories are calculated with initial conditions given by the centers of weight of the wave packet. The dynamical behavior of *trans*- and *cis*-stilbene are compared.

2. *Spectra Calculation and Normal Modes Characteristics*

In harmonic approximation the molecule is considered as a set of $3N-6$ independent harmonic oscillators or normal modes (N is the number of atoms). If one neglects anharmonicities and Dushinski rotation each vibrational degree of freedom can be described by its frequencies in the ground and excited state, and by the displacement Δ between the minima of the two states. Actually, in the absorption spectrum only a small number of modes with sufficient values of Δ appear with sufficient intensity and are usually called optically active modes.

Using Eq. (1), Eqs. (5-6) in (Grishanin 1992) and the developed computer procedure we simulate *trans*-stilbene supersonic jet absorption spectrum using the characteristics of 12 optically active normal modes. Their frequencies in the ground and first excited singlet state are known from supersonic-jets experimental spectra (see Tables 2 and 3 in (Syage 1984)). The simulation consists in varying the displacements along each mode until the relevant calculated intensities agree well with the experimentally obtained ones. The final result is presented in Fig. 2. The simulation is straightforward, not surprisingly as the normal modes are independent, and the precision of the calculated characteristics is mainly

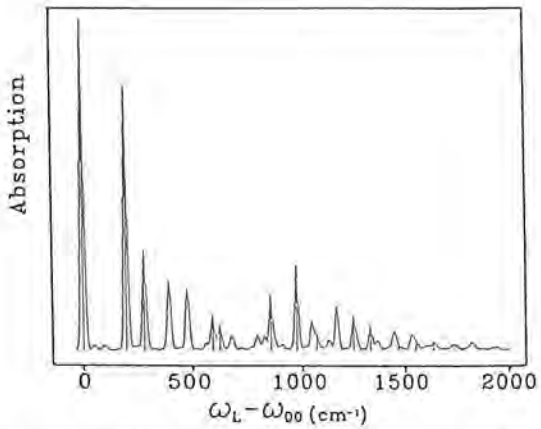

Fig. 2. The absorption spectrum of jet-cooled *trans*-stilbene molecule calculated using 12 active modes. The calculation was made using Eq. (1) (see Eqs. (5-6) in (Grishanin 1992)).

determined by the precision of the experimental spectrum. This is also due to the effectiveness of the computational procedure allowing for a large number of iterations. A spectrum calculation takes of about 4 min with spectral resolution of 1 cm^{-1} on a 33 MHz i486-based computer. This is $3N-6$ dimensional calculation ($N=26$), though for only 12 modes $\Delta \neq 0$. In a similar calculation Shan et al. (1987) determined the characteristics of 17 anthracene mode, using a more general but not so efficient computational procedure.

The obtained normal mode characteristics may be used for constructing the molecular Hamiltonian in applications where the harmonic approximation is valid, for instance in consideration of ultrashort pulsed laser excitation and early stage dynamics.

3. *Using of Molecular Mechanics Method for Calculation of the Ground and Excited States' Potential Energy Surfaces*

In many applications harmonic approximation is not adequate and a more general determination of the PES is necessary. As an example, in this section we determine the PES of the ground and the electronically excited states of stilbene molecule by means of the Molecular Mechanics (MM) potential energy functions. MM functions have been developed and parameterized on the basis of structural and thermodynamic experimental data. In this work, with the example of stilbene molecule, we parameterize our force field using the absorption spectrum obtained in supersonic jet experiments (Syage 1984).

We use the following MM potential energy functions (Vinter 1987):

$$U(r_1, \ldots, r_N) = U_b + U_{va} + U_{tor} + U_{vw}, \tag{3}$$

where U_b, U_{va}, and U_{tor} are contributions due to deviations of chemical bonds

lengths, valence and torsional (dihedral) angles from their equilibrium values, respectively, U_{vw} being the contribution due to Van-der-Waals interactions.

All the equilibrium bond lengths, valence angles and Van-der-Waals radii are well known (Vinter 1987) and may be used directly. The transferability of the force constants has been proved for a large number of molecules. For dynamic investigations, however, the force constants should be adjusted additionally, as well as the equilibrium bond lengths and valence angles of the excited molecule. Using the standard technique we calculate the frequency matrix of the ground state and vary the force constants of the MM PES (4-7) until a good fit to the available experimental data is obtained. As a result we can characterize entirely the ground PES and with the finally accepted parameters the calculated frequencies correspond to the experimental values (see Tables 1-3 in (Syage 1984)) with deviations less than $10\,cm^{-1}$.

For the excited state we accept the same potential energy functions as that for the ground state and look for the changes of the parameters accounting for the absorption and 0^0 dispersed fluorescence spectrum. Spectra are calculated using Eq. (1). The main features of the spectra are determined by the normal modes deviations of the two terms $\Delta = (x_2 - x_1)$ and the differences of the frequency matrices ω_1 and ω_2 or, correspondingly, by the changes of the parameters of the MM PES. Spectra are most sensitive to changes in the equilibrium bond lengths. As a rule, bond lengths increase in an excited state. However, in stilbene, delocalization of the double bond results in stretching of the ethylene bond $C_e{=}C_e$ and compression of C_e–*phenyl* bond in the excited state compared to their lengths in the ground state. In our calculations we also find out that changes in bond lengths larger then 0.01 Å lead to highly congested unresolved spectra, while it is known from the experiment that the spectra consist of well-resolved lines. Consequently, we used an iterative procedure for calculating the parameters of the excited PES, varying their values in thus obtained limits.

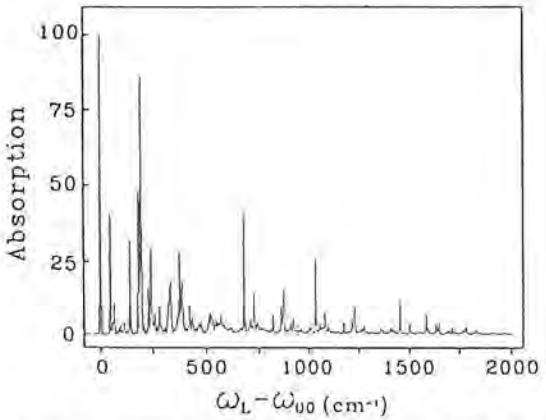

Fig. 3. The calculated absorption spectrum of jet-cooled *trans*-stilbene. The calculation was made using Eq. (1) and potential energy surfaces determined by Molecular Mechanics method using Eqs. (4-7) and parameters obtained here; ω_{00} is the vibrationless electronic transition frequency.

The finally accepted parameters were used for calculation of spectrum that is shown in Fig. 3. It fits well the experimental data from (Syage 1984), showing the same trends for the dominant peaks and a similar background.

4. *MD Simulations of Excited State Dynamics*

4.1. *General scheme*

A general scheme of the computer experiments which are possible with the developed simulation programs is presented in Fig. 4.

Using a standard MM program or self-made minimization procedure and the expression for the force field one obtains the equilibrium molecular structure. Then, as it has been described in Sec. 3, using Eq. (1) it is possible to calculate the force field parameters in accordance with the available experimental data. We note, however, that the computer simulation is not straightforward. The spectrum is determined by the characteristics of the normal modes (see Sec. 2) while in the simulation one varies the force field parameters. For a certain force field it may be not possible to obtain appropriate parameters.

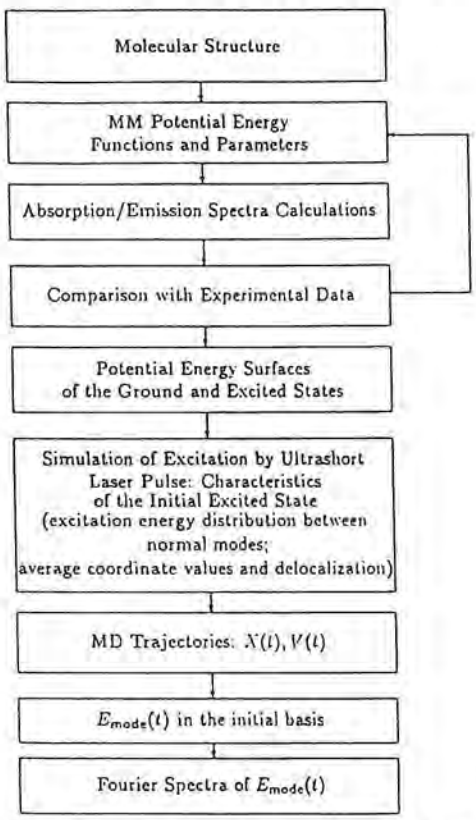

Fig. 4. General scheme of computer experiments on photoinduced excited state dynamics.

Having determined the PES of the ground and excited states one uses the standard technique for obtaining the eigenvalues and vectors for the matrices of the potential energy second derivatives. The eigenvalues determine the frequency matrices, while the eigen vectors determine the basis for transformation of Cartesian coordinates to normal coordinates. Using this initial basis and calculated MD trajectories it is possible to monitor the time evolution of the energy in all vibrational modes. The Fourier spectra of these time-dependencies reveal the typical frequencies of the energy exchange between the normal modes. For calculating MD trajectories in the excited state the initial coordinates should be determined by using the calculated average (over the excitation pulse duration) coordinates (Eq. (2)) and their delocalization Δx (Eq. (8) in (Grishanin 1992)).

We have used this procedure for modeling ultrashort pulsed laser excitation (a number of modes with sufficient Δ-s excited simultaneously) or SVL excitation and study of the processes of intramolecular vibrational energy redistribution (IVR) in anthracene ($C_{14}H_{10}$) and p-difluorobenzene ($C_6F_2H_4$) (Vachev 1992).

4.2. *MD study of the photoinduced stilbene isomerization*

Stilbene (1,2-diphenylethylene) has been studied extensively as a model system for isomerization dynamics. The two conformers, *trans* and *cis*, are divided by a 46 kcal $\times$ mol^{-1} potential barrier in the ground electronic state. In the first excited singlet state, however, only a small barrier of about 3.3 kcal $\times$ mol^{-1} is known to exist (as found from supersonic jet experiments), not far away along the torsional coordinate. Ground state equilibrium geometries of the two conformers are shown in Fig. 5, and the torsional dependences for the ground and excited states are shown in Fig. 6.

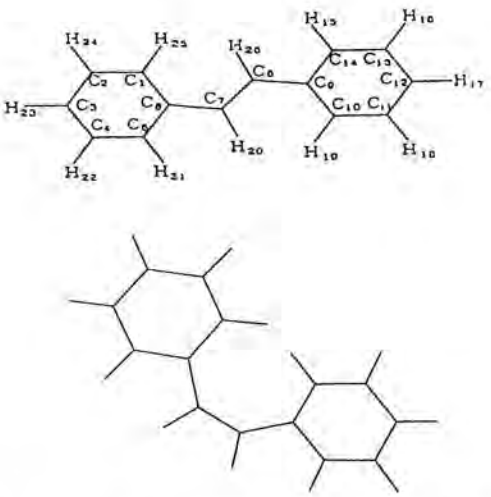

Fig. 5. Ground state equilibrium geometries of *trans*- (above) and *cis*-stilbene (below).

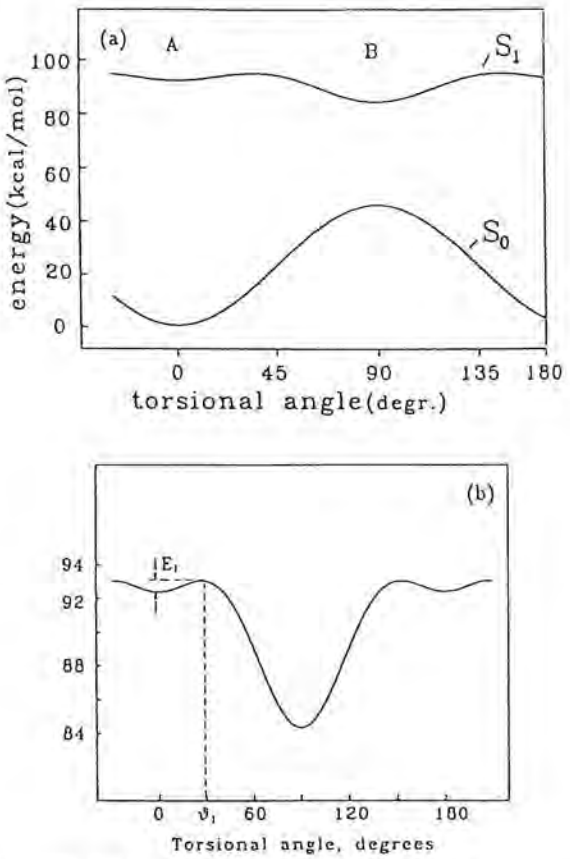

Fig. 6. The potential energy surfaces for the ground and excited electronic states of stilbene as a function of ethylene torsional coordinate (a) and the torsional potential for the excited state (b, see Eq. (8)). The local barrier E_l and its position θ_l along the torsional angle are determined by parameters V_1 and V_2 in Eq. (8).

Typical isomerization times vary from ~ 200 ps to ~ 10 ps in vapors and different solvents, depending, also, on the excitation wavelength. The times of *cis*-stilbene isomerization are much less (of about $1 \div 2$ ps) and using of a barrierless PES or very small barrier to isomerization is accepted (Abrash 1990, Frederick 1991, Petek 1990, Todd 1990). The information deduced from experiments is, however, related to an effective PES, because after a certain amount of energy is transferred to the molecule, the latter undergoes the transition.

Here we will use the MM PES determined in Sec. 3. The torsional dependence (see Eq. (6)) along the $C_6C_7C_8C_9$ torsional angle in this model would coincide with a quantum chemical calculation in which only this angle is varied, all other parameters being constant. Performing the calculation described in Sec. 3 we ensure that the harmonic part of our PES is in accordance with the experimental data. The anharmonic part of the potentials may be proved only by means of

explicit dynamic calculations. We point out, however, that the anharmonic part of the potential is not determined only by Eqs. (6-7). Although, the other two potentials, Eqs. (4-5) are a harmonic approximation with respect to internal coordinates, they contribute to anharmonic terms due to the nonlinear relation between internal and normal coordinates. An estimation using 3-th and 4-th order derivation matrices shows a reasonable anharmonic part of the potentials. In previous studies (Vachev 1991) we found that in the isomerization reaction only small changes of the bond lengths (less than 5%) and of the valence angles (less than 8%) occur. Consequently, a reasonable model is to use the calculated parameters for the whole time of the reaction and to determine additionally only

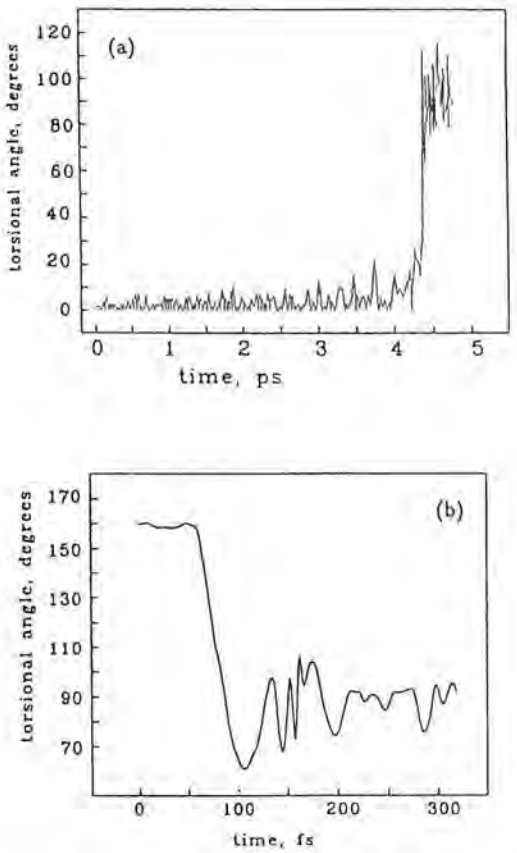

Fig. 7. Typical dependences on time of the torsional angle $C_6C_7C_8C_9$ (see Fig. 5), calculated along MD trajectories for *trans*-stilbene (a) and *cis*-stilbene (b). The potential energy surfaces are determined by Eqs. (3-8). In Eq. (8) $V_1 = 2.9$ kcal $\times$ mol^{-1}, $V_2 = 8$ kcal $\times$ mol^{-1}. The initial coordinates for MD trajectories are calculated using Eq. (2), simulating molecule excitation by 40 fs Gaussian laser pulse with excess vibrational energy $E_v = 3000$ cm^{-1}.

the energy dependence on the torsional coordinate. We used the following expression for ethylenic bond contribution in the excited PES (see Fig. 6):

$$U_{eth} = V_1 \sin^2(2\theta) - V_2 \cos^2(\theta - \theta_0), \quad (4)$$

where θ is the torsional angle corresponding to twisting of the molecule around the double ethylenic bond, and $\theta_0 = 90°$. Parameters V_1 and V_2 determine the local barrier of isomerization (region A in Fig. 6) and the deeper potential well around the twisted geometry (region B in Fig. 6). We use $V_2 = 8$ kcal $\times$ mol^{-1} and different values of V_1 in this way modeling different values of the local barrier E_l and its position along the torsional coordinate θ_l (see Fig. 6b). This simple analytical function enables for modeling of a barrierless potential (with $V_1 = 0$), a flat local potential (for instance, with $V_1 = 2$ kcal $\times$ mol^{-1} the potential is flat with accuracy of 0.001 kcal $\times$ mol^{-1} over 8°), and with small local barrier (see Fig. 6b).

To perform a MD study of the excited state dynamics we simulate molecule excitation by ultrashort 40 fs laser pulse with frequency exceeding the frequency of the vibrationless transition by 3000 cm^{-1}. Using Eq. (2) we calculated the coordinates averaged over the time of excitation and use them as a starting point for the MD trajectory. For integration of the equations of motion we use 4-th order Runge-Kutta algorithm with adaptive stepsize control ensuring conservation of the total energy within an accuracy of 2%. Along the obtained MD-trajectories we calculate the torsional angle ($C_6C_7C_8C_9$). Typical dependencies of the torsional angle on time are shown in Fig. 7 for the two conformers. One and the same PES determined by Eqs. (3-8) was used, under one and the same excitation. Nevertheless, the dynamic behavior of the two conformers is different. The *cis*-stilbene molecule undergoes transition to the twisted conformation much faster than *trans*-stilbene. The results for different values of the local barrier and its position along the torsional coordinate are shown in Table 1.

Table 1. *Trans*- and *cis*-stilbene dynamics on the excited PES (3*N*-dimensional). The time for reaching the twisted conformation depends on the parameters of the ethylene torsional potential (see Eq. (8)). Units: V_1, V_2, E_1 –kcal/mol, θ_1 –degr and τ_{90} –fs.

Torsion. potent. param.				stilbene	
				trans	*cis*
V_1	V_2	θ_1	E_1	τ_{90}	τ_{90}
0	8	0.000	0.00	112	37
2	8	8.667	0.00	302	52
2.5	8	20.00	0.10	1087	65
2.8	8	23.33	0.23	3282	78
2.9	8	24.67	0.28	4221	86
3.1	8	26.00	0.39	6889	102
3.3	8	27.33	0.51	10554	189
3.5	8	28.67	0.64	15318	1889

Most likely, the different dynamic behavior is due to the strong Van-der-Waals interactions between atoms C_6, C_{14}, H_{15}, and H_{21} in *cis*-stilbene (see Figure 5).

Conclusion to Part II

Frequency- and time-resolved absorption/emission spectra recorded in supersonic jets contain a large amount of information about the potential energy surfaces of the ground and electronically excited states, and about the purely intramolecular photoinduced dynamics. Previously, using the first order perturbation theory for the quantum density matrix and local quadratic approximation of the PES near the ground state equilibrium coordinates we have found out exact expression for the one-photon quantum transition probability $P(\omega)$, giving its dependence on the frequency matrices and the normal modes' displacements of the both electronic terms (see Eq. (1)). If, then, one uses any appropriate way of determining the PES, spectra calculation based on these equations can be used for adjusting the parameters of the PES. Otherwise, if only experimental spectra are available, the frequency matrices are determined to some extent and the dimensionless normal modes displacements can be calculated in a computer simulation (Sec. 3). We determined the PES by means of the MM potential energy functions. They are relatively simple and widely used in structural studies of organic molecules. We have shown that the MM potential energy functions can also be used successfully for dynamical studies and some of the parameters can be determined.

After the PES or equivalently (in harmonic approximation) the frequency matrices and the dimensionless displacements of normal modes are determined, some characteristics of the excited state can be calculated and used for an accurate MD or wave packet analysis of the molecule's dynamics after excitation. As a first guess, the coordinates x_q averaged over the pulse duration (see Eq. (2)) may be used as initial conditions for the equations of motion. For a more precise quantitative results, a statistical averaging of the delocalization Δx during the excitation should be done.

We have presented a general scheme of the computer experiments, which can made with the developed molecular simulation packages (see Sec. 4.1). Our results on the excited state dynamics of stilbene show that the different dynamic behavior of the *trans*- and *cis*-stilbene can be accounted for by the specific conformational interactions rather than by an asymmetry of the PES along the torsional coordinate.

Part III. Computer Modeling of Photoinduced Dissociation of Ethylene Molecule by Short IR Laser Pulse

1. *Introduction*

How to excite a molecule to a selected vibronic state? How to control over an excitation of a molecule? These questions are of great importance for molecular

spectroscopy and laser chemistry (Letokhov 1983). A way to control over molecular excitation by IR laser pulse is to use frequency-swept (chirped) pulses. The idea of such an excitation discussed over the past few decades (Chelkovski 1990, Grishanin 1992a, Letokhov 1983) is illustrated in Fig. 1.

In order to excite a harmonic oscillator, one should fit the excitation frequency to that of the oscillator. By contrast, for anharmonic oscillator the efficiency of such an excitation will be much lower due to the anharmonicity. To overcome this difficulty, the pulse frequency should follow the vibrational level spacing $\omega_k = \omega_{k+1} - \omega_k$ (see Fig. 1). As a result the efficiency of the excitation will be enhanced. In addition, frequency sweeping is a powerful tool for control over the vibrational mode's energy exchange, because of its phase sensitivity.

There is a limited number of experimental works on this problem. Enhanced population transfer from the lowest level to the highest level in the three-state ladder $5s \rightarrow 5p \rightarrow 5d$ of rubidium atom by chirped ultrashort laser pulses was experimentally observed in (Broers) (see also the references therein). The excitation of C_2H_4 molecule by chirped ultrashort IR laser pulses was investigated in (Gordienko 1992).

The theoretical investigation of the dynamics of an excited molecule based on running the wave packets' dynamics or on solving the Shrödinger equation is

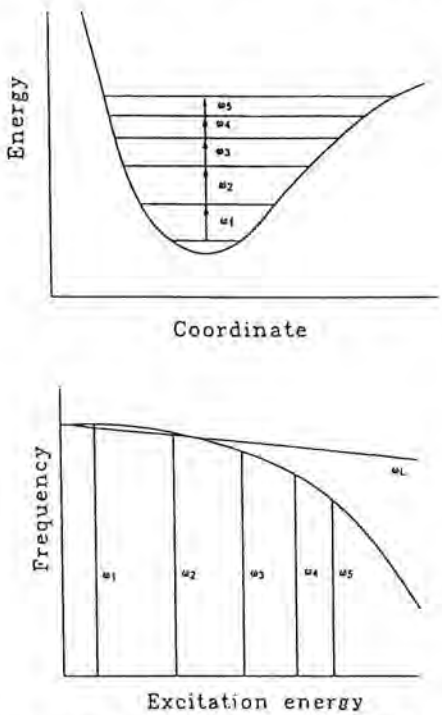

Fig. 1. The potential energy function of an anharmonic oscillator (above) and the frequency-sweep dependence (below) such that the frequency ω_L follows the vibrational level spacing; ω_k are the vibrational frequencies.

bounded in practise by the case of diatomic molecules (Chelkovski 1990, Grishanin 1992a). Here we present a theoretical model which is suitable for running the Molecular Dynamics of multiatomic molecules excited by a laser pulse. Using this model, we revealed the features of the chirped pulsed laser excitation of C_2H_4 molecule.

There are some qualitative considerations (Grishanin 1992a) which prove the validity of using the method of classical Molecular Dynamics (MD) for describing the dynamics of a multiatomic molecule under the conditions where quasistochastic quasiclassical contribution to the Liouville operator is much greater than the quantum contribution due to anharmonicity. In any case, to prove the validity of classical MD, it is necessary to run a computer modeling and to compare its results with the experimental data.

We present here the results of MD simulation of the dynamics of ethylene molecule (C_2H_4) excited by picosecond IR laser pulse. The parameters of the potential energy surface described by the Molecular Mechanics (MM) method (Burkert) were determined using fitting method described in (Grishanin 1992b). With the parameters, the molecule's dynamics, the temporal dependence of its total energy, and its power emission spectrum were calculated.

2. *Computer Simulation Results*

We describe the molecule's dynamics using the classical Hamiltonian equations for nuclei coordinates and momenta, with the potential function (Grishanin 1992b) which is supplemented with the Hamiltonian of interaction of the molecule with the laser field

$$\mathscr{H}_I = -\sum e_k \vec{r}_k \vec{E}_L(t).$$

Charge distribution is introduced here by the set of effective charges e_k which correspond to separate atoms. The initial conditions for $\vec{r}_k, \vec{p}_k$ are represented by pseudorandom numbers, which simulate fluctuations produced by the quantum thermal equilibrium distribution at temperature T. To simulate this distribution, we introduce the set of Gaussian random values for the fluctuations of coordinates and momenta of normal modes λ, so that their energies are equal to energies predicted by Plank formula

$$\varepsilon_\lambda = \hbar\omega_\lambda / [\exp(\hbar\omega_\lambda / kT) - 1].$$

These fluctuations are the fluctuations of the center of the wave packet which describes the molecule in terms of quantum theory, when the packet is disturbed by the equilibrium temperature fluctuations. These fluctuations produce the corresponding incoherent thermal radiation of the molecule. This radiation is included in the calculated spectral characteristics of individual molecule, in addition to the coherent response to the external field. In order to separate the coherent component of the molecule's radiation, one should simulate not a single

molecule but the proper ensemble of molecules. The rotational fluctuations must be taken into account by introducing fluctuations of the total angular momentum resulting in the corresponding fluctuations of momenta $\delta\check{p}_k$. In the majority of our calculations the temperature is taken to be zero, to make more clear the dependencies due to the processes of intramolecular energy exchange.

The equilibrium configuration of ethylene molecule is represented in Fig. 2. Laser field is described by a Gaussian pulse with the duration $\tau_p = 1\text{-}10$ ps and the frequency assumed to be linear function of time t:

$$\check{E}_L(t) = E_0\vec{e}\cos\varphi(t)\exp[-4(t-t_c)^2/\tau_p^2],$$
$$\varphi(t) = \omega_{L0}t + (1/2)(d\omega_L/dt)\,t^2.$$

Here ω_{L0} is the initial laser frequency, t_c is the moment of time when the field intensity is equal to its maximum value. The field intensities are chosen in the interval $I = 10^9 - 10^{13}$ W/cm^2. The polarization $\vec{e}$ is orthohonal to the plane of molecule, i.e., it is parallel to the vector of dipole moment of the out-of-plane vibration (along z-axis).

The first step of computer modeling is the determination of MM parameters of a molecule using the available data (Grishanin 1992b). The next step is calculating of time dependencies of coordinates $\vec{r}_k(t)$ and the total energy $E(t)$. With the help of two-dimensional computer visualization of $\vec{r}_k(t)$, $E(t)$ and of three-dimensional dynamics of the molecule, it is possible to investigate the qualitative dependencies between the characteristics of molecular excitation and parameters of the pulse.

There are two regions of laser intensities that has been investigated in this work:

—The region of moderate fields with $I \leqslant 10^{11}$ W/cm^2, where a molecule does not dissociate and its motion is relatively regular;

—The region of strong fields with $I \geqslant 10^{12}$ W/cm^2, where molecules undergo quasistochastic motion and can dissociate into two or several fragments.

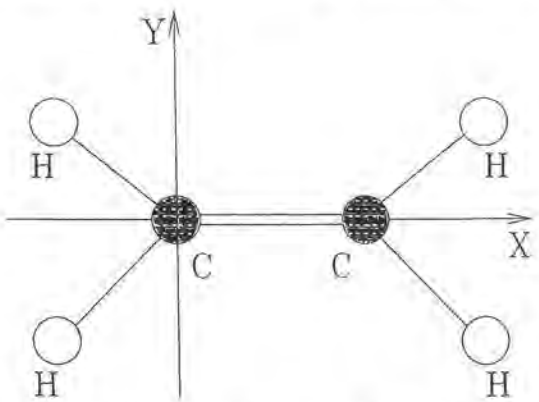

Fig. 2. The equilibrium configuration of an ethylene molecule.

In Fig. 3 the dependence of total energy $E(t)$ normalized to its maximum is represented for the chirp-free pulse with $\tau_p = 6$ ps and the temperature $T = 0$ K. Similar dependencies for the pulse with positive linear chirp and for the pulse with the negative chirp, with the same frequency deviation of about 1%, are represented for the intensities $I = 10^9$, 10^{10}, and 10^{11} W/cm^2. The maximum value of the field amplitude is achieved at $t_c = 6$ ps.

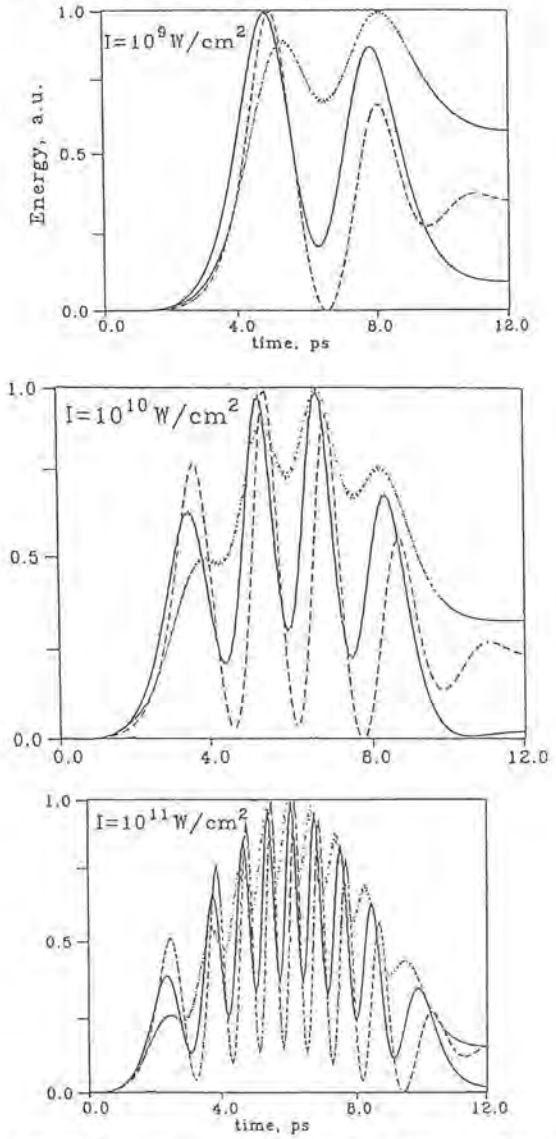

Fig. 3. Total energy of C_2H_4 molecule under excitation at $I = 10^9$, 10^{10}, and 10^{11} W/cm^2. Pulse duration is equal to 6 ps; chirp is equal to 0% (solid line), +1% (dashed line) or −1% (points) of vibrational frequency.

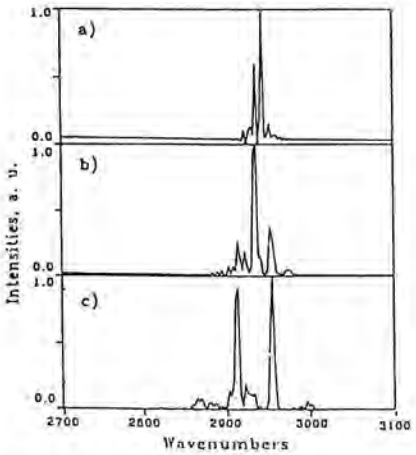

Fig. 4. Fluorescence spectrum of the third harmonic at $I = 10^9$ (a), 10^{10} (b), and 10^{11} W/cm^2 (c).

In the case of chirp-free pulse one can see the oscillations of the total energy of a molecule, despite the exact resonance of laser frequency with the out-of-plane mode oscillations of C_2H_4 molecule.

The more intense is the field, the faster are the molecular oscillations. At the end of the pulse the molecule preserves a significant part of its maximum energy only at minimum intensity $I = 10^9$ W/cm^2. Such a behavior is explained by changing of the eigenfrequency of the excited mode due to its anharmonicity. For a harmonic oscillator the total energy should grow steadily and be a quadratic function of time for a square pulse.

Chirping enlarges the amount of a total energy preserved in a molecule after the pulse is over, as soon as the conserved energy dependence on field intensity remains the same. The ratio of the total energy preserved in a molecule to its

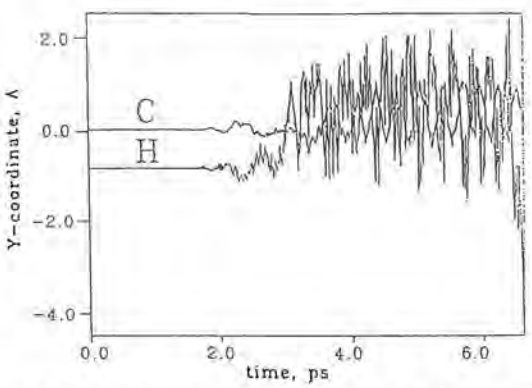

Fig. 5. $C_2H_4 \rightarrow C_2H_3 + H$ dissociation reaction of C_2H_4 molecule excited by IR laser pulse with linear positive chirp of about 15% to laser frequency. Pulse duration is equal to 4.4 ps, energy density is equal to 40 J/cm^2.

maximum value for the chirp-free pulse yields the value $E_+/E_0 = 3.2$ at $I = 10^9$ W/cm^2. For the case of a pulse with a negative chirp this value yields $E_-/E_0 = 6.5$. Therefore, a negative chirp is more consistent with the form of potential surface of ethylene molecule. Nevertheless, both types of chirping are effective. Hence, the effective force constant for the out-of-plane mode varies non-steadily as a function of the excitation rate.

The spectral distributions of the third harmonic in the spectrum of fluorescence for $I = 10^9 - 10^{11}$ W/cm^2 are shown in Fig. 4 for the chirp-free excitation. The general qualitative rule is enriching of spectra with the increase in intensity. This fact can be accounted for by increasing of intermode exchange with the increase of excitation rate of a molecule. For moderate fields the major part of the molecule's energy is stored in the resonant mode, and the processes of intermode exchange are relatively small. In the case of strong fields the molecule dissociates. During the excitation the nuclear motion becomes chaotic resulting, in particular, in spontaneous breaking down of initial symmetry of the molecule (the vibrations of different H-atoms and C-atoms are not identical, though at $T = 0$ and $\vec{e} \parallel z$ they should be identical). Nevertheless, the pulse parameters still affect the reaction dynamics due to both the initial non-chaotic stage of the excitation process and the details of interaction of the chaotic molecular vibrations with the external field. At lower intensities the main reaction channel is the breaking of one hydrogen bond. In this case, using of chirp allows one to reduce the dissociation threshold (Fig. 5). At higher intensities all the other channels are possible. As an example, the reaction $C_2H_4 \rightarrow CH_2 + CH_2$ is shown in Fig. 6. Hence, one can control the reaction channel by varying the chirp parameters. There is only one difficulty, that is, there is no simple recipe for choosing the optimal parameters.

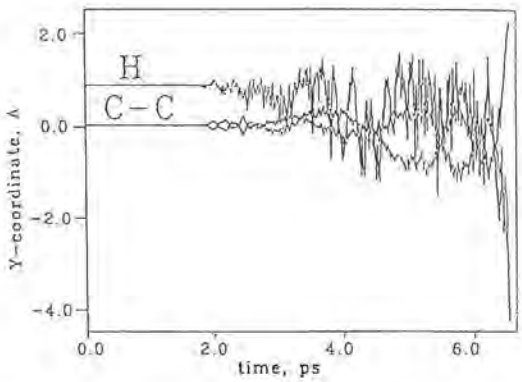

Fig. 6. $C_2H_4 \rightarrow CH_2 + CH_2$ dissociation reaction of C_2H_4 molecule excited by IR laser pulse. Pulse duration is equal to 4.4 ps, energy density is equal to 44 J/cm^2. Laser frequency is in resonance with the mode 949 cm^{-1}.

Acknowledgements

We wish to express our gratitude to the late Professor Sergei Akhmanov who initiated this work, for his support and valuable discussions. We are also grateful to Dr. A. Makarov for many helpful and stimulating discussions. The authors are indebted to Drs. L.Yu. Brovko, O.A. Gandelman, A.P. Shkurinov for their help in the experimental work and for stimulating discussions. The research was supported by the Russian Programs 'Physics of Lasers and Laser Systems' and 'Engineering Enzymology', grant No.1-250.

References

Part I

Brovko, L.Yu., Dementyeva, E.I., and Ugarova, N.N., Biochemistry (a translation of Biokhimija) **51**, 111-119, 1986.

Gandelman, O.A., Brovko, L.Yu., Ugarova, N.N., and Shchegolev, A.A., Biochemistry (a translation of Biokhimija) **55**, 785-789, 1990.

Kamalov, V.F., Razzhivin, A.P., Toleutaev, B.N., Chikishev, A.Yu., and Shkurinov, A.P., *Sov. J. Quant. Electr.* **14**, 1303-1308, 1987.

Kutuzova, G.D., Dementyeva, E.I., Boldwin, T.O., and Ugarova, N.N., Biotekhnologia (in press), 1992.

Lackovicz, J.R., Principles of Fluorescence Spectroscopy, Plenum Press, New York, 1983.

McElroy, W.D., and DeLuca, M., in: Cormier M.J., Hercules D.M. and Lee J. (Eds.), Chemiluminescence and Bioluminescence, Plenum, New York, p. 285, 1974.

Philippova, N.Yu., Dukhovich, A.F., Bukatina, V.A., and Ugarova, N.N., *Biokhimija* **49**, 1965-1971 (in Russian), 1984.

Talebarovskaya, I.K., Catcova, V.A., Rizhova, V.V., Schogolev, A.A., and Berezin, I.V., Russian Patent No. 1192324, 1983.

White, E.H., Worther, H., Field, G.E. and McElroy, W.D., *J. Org. Chem.* **30**, 2344-2353, 1965.

Part II

Abrash, S., Repinec, S., Hochstrasser, R.M., 'The viscosity dependence and reaction coordinate for isomerization of *cis*-stilbene', *J. Chem. Phys.*, **93**, pp. 1041-1053, 1990.

Akhmanov, S.A., Vysloukh, V.A., and Chirkin, A.S., *Optics of femtosecond laser pulses*, AIP, 1992.

Computer simulation studies in Condensed Matter Physics, Landau D.P., Mon K.K., and Schutter H.B. (Editors), Springer, 1990.
Dexheimer, S.L., Wang, Q., Peteanu, L.A., Pollard, W.T., Mathies, R.A., and Shank, C.V., 'Femtosecond impulsive excitation on nonstationary vibrational states in bacteriorhodopsin', *Chem. Phys. Lett.* **188**, pp. 61–66, 1992.
Felker, P.M., and Zewail, A.H., 'Picosecond time-resolved dynamics of vibrational energy redistribution and coherence in beam-isolated molecules', *Adv. Chem. Phys.* **70**, pp. 265–364, 1988.
Frederick, J.H., Fujiwara, Y., Pen, J.H., Yoshihara, K., and Petek, H., 'Models for stilbene photoisomerization: experimental and theoretical studies of the excited state dynamics of 1,2-diphenylcycloalkenes', *J. Phys. Chem.* **95**, pp. 2845-2858, 1991.
Grishanin, B.A., Vachev, V.D., and Zadkov, V.N., 'On the theory and MD simulation of one-photon electronic excitation of polyatomic molecules', *Proc. SPIE*, **1402**, pp. 44-52, 1991.
Grishanin, B.A., Vachev, V.D., Zadkov, V.N., 'Computer simulation of the conformational switching induced by ultra short laser pulse', *Nonlinear Optics*, **3**, pp. 375-386, 1992.
Levine, R.D., and Bernstein, R.B., *Molecular reaction dynamics and chemical reactivity*, Oxford Univ. Press, 1987.
Mathies, R.A., Cruz, C.H.B., Pollard, W.T., and Shank, C.V., 'Direct observation of the femtosecond excited state *cis-trans* isomerization in rhodopsin', Science, **240**, pp. 777-780, 1988.
Petek, H., Yoshihara, K., Fujiwara, Y., and Frey, J.G., 'Isomerization of *cis*-stilbene in rare-gas clusters: direct measurements of *trans*-stilbene formation rates on a picosecond time scale', *J. Opt. Soc. Am.* B, **7**, pp. 1540-1544, 1990.
Schoenlein, A.M., Peteanu, L.A., Mathies, R.A., and Shank, C.V., *Science*, **254**, p. 3412, 1991. *Molecular dynamics simulations of statistical mechanical systems*, N. Holland, Amsterdam, 1986.
Shan, K., Yan, Y.J., and Mukamel, S., 'Intra-molecular dephasing and vibrational redistribution in the dispersed fluorescence of ultracold molecules: application to anthracene', *J. Chem. Phys.*, **87**, pp. 2021-2035, 1987.
Syage, J.A., Feller, P.M., and Zewail, A.H., 'Picosecond dynamics and photoisomerization of stilbene in supersonic beams. I. Spectra and modes assignments', *J. Chem. Phys.* **81**, pp. 4685-4705, 1984.
Todd, D., Jean, J., Rosenthal, S., Ruggiero, A.J., Yang, D., and Fleming, G., 'Fluorescence upconversion study of *cis*-stilbene isomerization', *J. Chem. Phys.* **93**, pp. 8658-8668, 1990.
Vachev, V.D., Grishanin, B.A., and Zadkov, V.N., 'MD study of pulsed laser excitation of electronic transitions in polyatomic molecules', *Izv. Akad. Nauk, Ser. Fiz.* **56**, pp. 16-26, 1992.
Vachev, V.D., and Zadkov, V.N., 'Molecular Dynamics of stilbene molecule under laser excitation', *Proc. SPIE* **1403**, pp. 487-496, 1991.
Vinter, J., Davis, A., and Saunders, M., 'Strategic approaches to drug design', *J. Comp. Aided Mol. Design* **1**, pp. 31-51, 1987.

Broers, B., van Linden-van den Heuvel, H.B., and Noordam, L.D., 'Efficient population in a Three-Level Ladder System by Frequency-Swept Ultrashort Laser Pulses' (to be published).

Burkert, U., and Allinger, N.L., Molecular Mechanics, Washington, *ACS* **177**.

Chelkovski, S., Bandrauk, A.D., and Corcum, P.B., *Phys. Rev. Lett.* **65**, p. 2355, 1990.

Gordienko, V.M., Biglov, Z.A., Danilov, E.O., and Slobodyanyuk, V.A., 'Resonance interactions of 10 μm picosecond pulses with polyatomic molecules', In: *Inst. Phys. Conf. Ser.* No. 126, IOP, p. 477, 1992.

Grishanin, B.A., Vachev, V.D., and Zadkov, V.N., 'Analysis of molecular dissociation by chirped infrared laser pulse', In: *Inst. Phys. Conf. Ser.* No. 126, IOP, p. 571, 1992.

Grishanin, B.A., Vachev, V.D., and Zadkov, V.N., 'Computer Simulation the Conformational Switching Induced an Ultrashort Laser Pulse', *Nonlinear Optics* **3**, pp. 375-386, 1992.

Letokhov, V.S., Nonlinear Selective Photoprocesses in Atoms and Molecules, "Nauka" Publishers, Moscow, 1983 (In Russian).

Physics Department and International Laser Center, Moscow State University, 119899 Moscow, Russia

Koos Duppen, Erik T.J. Nibbering and Douwe A. Wiersma

Solvent Dynamics probed by Photon Echo

Abstract

Solvent dynamics, which lies at the heart of 'femtochemistry' in solution, has been studied by femto-second photon echo and chirped four-wave mixing. A single Brownian oscillator is shown to provide an excellent description of the optical dynamics in the case of resorufin in dimethylsulphoxide. For pinacyanol in ethylene glycol at least three Brownian oscillators are needed to simulate the spectral and dynamical data. The different solvent behaviour is ascribed to hydrogen bonding effects in the case of ethylene glycol.

Introduction

The grasp of solvent dynamics is at the heart of the understanding of solution chemistry and henceforth much work has been devoted to this subject both experimentally and theoretically. In the past, liquid state dynamics has been accessed by coherent resonance Rayleigh mixing [Yajima et al., 1978], polarization spectroscopy [Song et al., 1978], resonance Raman scattering [Brafman et al., 1984; Nibbering et al., 1990], time-resolved hole burning [Brito-Cruz et al., 1986], optical Kerr effect measurements [McMorrow et al., 1988], and, more recently, by femtosecond photon echo [Becker et al., 1989; Bigot et al., 1991; Nibbering et al., 1991] and time-dependent Stokes shift measurements [Rosenthal et al., 1991]. The conclusion of all these experiments is that solvent dynamics has a component that proceeds on a femtosecond time scale. The same conclusion was drawn from molecular dynamics simulations of liquids [Maroncelli and Fleming, 1989]. For a better grip on 'femtochemistry' in solution detailed study of these ultrafast motions is therefore essential.

While the outcome of molecular dynamics simulations depends on knowledge of the intermolecular potentials, the conclusions drawn from experiments depend heavily on the dynamical model used to analyze the data. Recently it has been realized [Nibbering et al., 1990] that the optical dynamics, which is used as a probe for solvent dynamics, cannot be modelled using the optical analog of the Bloch equations. The fundamental reason is that in liquids there is not a clear separation of time scales, between bath fluctuations and optical coherence decay. A model that allows for dynamics in this regime is the so-called stochastic

modulation model. It has recently been applied successfully to the case of resorufin in dimethylsulphoxide [Nibbering et al., 1991]. Here the dynamics on all time scales -as expressed in the optical lineshape- were linked with the solvent dynamics on a femtosecond time scale, as probed by the two-pulse photon echo. However, this model does not account for the response of the solvent on optical excitation of the probe molecule. This solvation effect occurs on all time scales, but most notably at a sub 100 fs time scale [Rosenthal et al., 1991]. A model that does account for this effect is the so-called multimode Brownian oscillator (MBO) model. In this model the solvent motions that determine the dynamics are treated separately (projected out) from the solvent motions that have little effect on the optical dynamics. These Brownian oscillators are then used to 'dress' the electronic two-level system. Nuclear motion takes place on harmonic potential surfaces which are linearly displaced on optical excitation.

Fig. (1) shows how a displaced Brownian oscillator affects the optical response. Due to the fluctuations (damping) of the oscillatory movement, the width of the electronic transition increases. Due to the displacement of the potential surfaces, a nonequilibrium situation is created upon excitation with respect to the nuclear coordinate, which leads to a red or a blue shift of the electronic transition frequency, depending on the position of the 'particle' and 'hole' relative to the equilibrium minimum of the potential wells.

In this paper we will present and discuss some of our recent results of femtosecond photon echo and chirped four-wave mixing experiments on resorufin in dimethylsulphoxide (DMSO) and pinacyanol in ethylene glycol. We will show that the MBO model provides an excellent fit to all experiments in the case of resorufin. The first results on pinacyanol indicate that the solvent dynamics in this case are more complex and that therefore more than one oscillator is needed to model the dynamics. We further conclude that the dynamics for protic and aprotic solvents are different.

Prior to presenting our data the basic relaxation function will be discussed that emerges from the MBO theory. Further details on the MBO theory can be found, for instance, in a paper by Yan and Mukamel [1988].

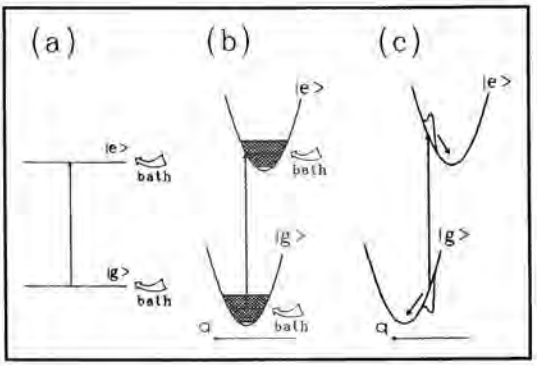

Fig. 1. Modelling of non-Markovian two-level dynamics by the Brownian oscillator model.

Brownian Oscillator Model

A Brownian oscillator is characterized by three parameters: frequency ω, damping $\gamma(t)$, and displacement d. A particular two-level system may be dressed with any number of oscillators, each with different parameters. Depending on whether $\gamma(t)$ is much larger or smaller than ω the Brownian oscillator is overdamped or underdamped. The underdamped modes are responsible for the vibrational structure in the optical spectra, while the overdamped modes dominate the dynamics. When it is further assumed that the solvent dynamics are fast compared to the oscillator dynamics the so-called Markovian limit of the MBO model is obtained. For this case a very simple expression for the correlation function of the strongly overdamped Brownian oscillator can be derived:

$$M_j(t) = \exp(-\Lambda_j t) \tag{1}$$

Here Λ_j is the inverse correlation time of the oscillator's correlation function, and defined by $\Lambda_j = \omega_j^2/\gamma_j$.

The various kinds of (non)linear optical responses that are probed in the different experiments are most conveniently expressed in terms of an overall line broadening function $g(t)$ [Yan and Mukamel, 1990; Mukamel, 1990], which consists of contributions from different Brownian oscillators $g_j(t)$. We are particularly interested in the form of this function in the case of strongly overdamped modes, because especially these modes contribute to line broadening and other dynamical effects. The line broadening function of an overdamped oscillator can be written as :

$$g_j(t) = i\frac{\lambda_j}{\Lambda_j}[1 - \exp(-\Lambda_j t)] + \frac{\Delta_j^2}{\Lambda_j^2}[\exp(-\Lambda_j t) + \Lambda_j t - 1] \tag{2}$$

λ_j is the reorganisation parameter, which is given by $\lambda_j = \omega_j d_j^2/2$. Δ is related to the frequency ω and displacement d of the oscillator by the relation: $\Delta_j^2 = \omega_j^2 d_j^2 [n(\omega) + 1/2]$. In the high temperature limit ($kT \gg \hbar\omega_j$) this relation becomes $\Delta_j^2 \approx 2kT\lambda_j/\hbar$, thus relating Δ_j an λ_j directly. Therefore in the high temperature limit these strongly overdamped modes (SOMs) are characterized by only two parameters (Δ_j and Λ_j).

For further details on how to arrive at Eqs. (1) and (2) we refer to [Duppen et al., 1993].

It should be noted that when the imaginary part in Eq. (2) is ignored the line broadening function of the stochastic model is recovered [Nibbering et al., 1991]. As mentioned, in this model solvation is not accounted for.

Liquid state optical dynamics

We will present results of a number of linear and nonlinear optical experiments on the system resorufin in dimethylsulphoxide (DMSO). These results will be

discussed in the context of the multi-mode Brownian oscillator (MBO) model in its simplest form: a single, overdamped oscillator will be used to mimic the solvent dynamics. For pinacyanol some preliminary stimulated photon echo measurements will be shown. Here at least three Brownian oscillators are needed to simulate the liquid state dynamics.

Two-pulse photon echo experiments

The fastest experiment is a two-pulse photon echo. In this experiment two short optical pulses with wavevectors $\mathbf{k}_1$ and $\mathbf{k}_2$ excite the system in an impulsive way. Conventionally the rephasing of the polarization leading to echo formation is supposed to arise from a static distribution of transition frequencies (inhomogeneous broadening). Homogeneous broadening causes a decay of the echo amplitude when the pulse separation τ is increased. In a liquid the presence of inhomogeneous broadening is not crucial for a photon echo to be generated. Instead, the correlation function Eq. (1) provides the necessary phase memory, but only for a time corresponding to the correlation time Λ^{-1}. Rephasing and echo formation will thus be possible for pulse separations up to this time.

The experimental decay of the echo intensity is shown for resorufin in DMSO in Fig. 2. These signals were measured with a beam geometry shown in the inset. The two optical pulses were generated with a Colliding-Pulse Mode-Locked (CPM) laser and amplified with a copper-vapor laser, which gave transform-limited 50 fs pulses with a repetition-rate of 8.3 kHz. These pulses were subsequently chirped in a single-mode optical fiber to a duration of 1.2 ps with a center wavelength of 620 nm and a bandwidth of 3000 cm^{-1}, and subsequently compressed to a duration of about 9 fs using a combination of two gratings and four prisms [Nibbering et al., 1991]. The pulses were crossed at an angle of about 4.5° in a 60 μm thick jet of the dye solution (10^{-3} M). The nonlinear signals in the phase-matched direction $2\mathbf{k}_2 - \mathbf{k}_1$ were detected with a photomultiplier and a lock-in amplifier.

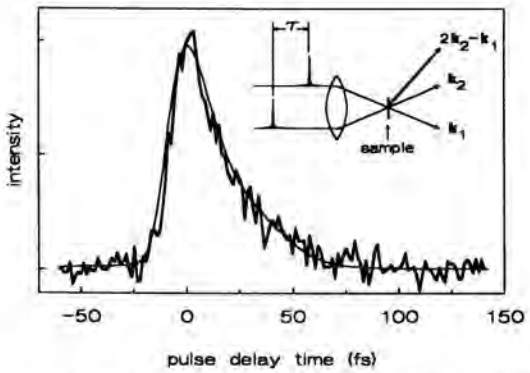

Fig. 2. Two pulse photon echo signal of resorufin in DMSO at room temperature as a function of relative pulse delay time τ (dotted line). The beam geometry is shown in the inset.

The notable asymmetry in the trace of Fig. (2) indicates that dephasing of resorufin in DMSO is not irreversible. Apparently partial rephasing occurs when pulse 2 interacts with the sample at a time τ after pulse 1, which makes it ligitimate to call these signals photon echoes.

It can be shown [Nibbering et al., 1991] that for delta pulse excitation the two-pulse echo intensity has the following expression:

$$I_{2PE}(t, \tau) \sim \exp[-2Re[2g(t) + 2g(\tau) - g(t+\tau)\}] \tag{3}$$

with the delay time τ defined to be positive (pulse $\mathbf{k}_2$ after pulse $\mathbf{k}_1$).

The result of Eq. (3) is remarkable, especially with regards to solvation. A possible time dependent shift of the system frequency is incorporated in the imaginary part of the lineshape function $g(t)$. Since Eq. (3) only involves the real part of $g(t)$, it follows that the photon echo signal is insensitive to net rearrangements of the solvent shells upon excitation of the probe molecule! The reason for this behaviour is that only coherent superposition states are involved in the generation of the echo signal, and that an inversion of phase occurs when the second pulse is applied. Only fluctuations (damping) are important for the decay of the signal. In the case of a strongly overdamped oscillator, the expression for $I_{2PE}(t, \tau)$ is identical to that of the stochastic model of optical dynamics [Nibbering et al., 1991; Duppen et al., 1993], since the line broadening function for the stochastic model is identical to the real part of an overdamped $g(t)$. So, when Eq. (2) is inserted in Eq. (3) the same expression is obtained that was used previously to analyze these data in the context of the stochastic model [Nibbering et al., 1991]:

$$I_{2PE}(t, \tau) \sim \exp\left[\frac{-2\Delta^2}{\Lambda^2} \times \{2e^{-\Lambda t} + 2e^{-\Lambda \tau} - e^{-\Lambda(t+\tau)} + \Lambda(t+\tau) - 3\}\right] \tag{4}$$

To compare this theoretical expression with experiment, the finite pulse width and the detector response have to be considered. The assumption of delta pulses that was made in Eq. (4) is an idealization of the actual pulse width of about 9 fs. However, as long as the pulses are short enough to ignore the system dynamics during the optical interaction, the impulsive treatment is still valid. The observed signal can then be calculated by convolving the calculated delay dependence with the experimental time resolution. Also, the detector integrates the echo signal that is generated after the interactions with both pulses over all times t. The experimental trace that was obtained for resorufin in DMSO therefore has to be compared to the following theoretical expression:

$$S_{2PE}(\tau) = \left\{\int_0^\infty dt\, I_{2PE}(t, \tau)\right\} \otimes T(\tau) \tag{5}$$

where $T(\tau)$ is a measure of the time resolution and $\otimes$ designates a convolution.

When Eq. (5) is fitted to the experiment on resorufin in DMSO, the smooth curve in Fig. (2) is obtained. The parameter values of the fit are: $\Delta = 41$ THz

(rad/sec) and $\Lambda = 27$ THz (sec^{-1}). In the MBO model Δ is a measure of the Franck-Condon allowed frequency range of the optical transition and is related to the reorganization parameter λ, while Λ is the inverse of the correlation time of the Brownian oscillator motion ($\tau_c = \Lambda^{-1} = 37$ fs). In the stochastic model, Δ is the root mean square amplitude and Λ the correlation time of the frequency fluctuations of the optical transition. Next to the electronic absorption at 595 nm only one vibronic transition at 576 nm was taken into account in the calculation of the signal of Fig. (2). This gives rise to a very weak beat in the observed decay. All other vibronic transitions are either too weak to contribute to the nonlinear signals, or they are outside the bandwidth of the optical pulses. The full vibronic structure of resorufin in DMSO will be discussed more extensively below.

Chirped four-wave mixing

In chirped four-wave mixing [Duppen et al., 1993] two or three chirped optical pulses interact in a sample to generate a nonlinear signal. These chirped pulses are strongly non-transform limited, but their optical phases are well-defined at all times. The carrier frequency is explicitly time dependent, which for a linearly chirped pulse can be written as:

$$\omega(t) = \omega_0 + bt \tag{6}$$

Here ω_0 (rad/sec) is an off-set frequency and b is the chirp rate (rad/sec^2). Typically, in chirped four-wave mixing the durations of the pulses are long compared to the dynamics. The time scale of the experiment is determined by the ratio of the width of the optical transition and the chirp rate, i.e. by the time it takes the optical field to sweep across the material resonance.

An experimental result of chirped four-wave mixing on resorufin in DMSO is shown in Fig. (3). In this experiment two pulses were used with a beam geometry shown in the inset. These pulses were generated with the same set-up that

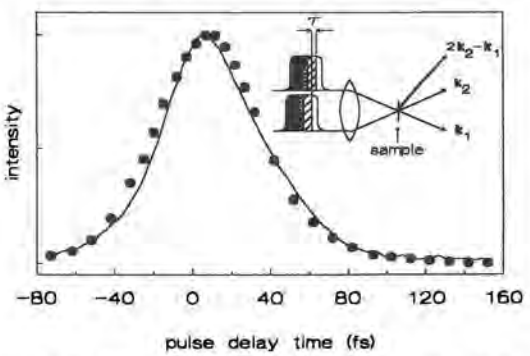

Fig. 3. Two pulse chirped four-wave mixing signal of resorufin in DMSO at room temperature as a function of relative pulse delay time τ (solid line). The beam geometry is shown in the inset; the different shades in the pulses indicate the frequency chirp.

was used for the photon echo experiment, only the compression stages were left out. This means that the pulse duration was about 1.2 ps with a spectral width of about 3000 cm^{-1}, while the chirp rate was 2.6 cm^{-1}/fs. As indicated in the inset of Fig. (3), a relative delay τ implies an instantaneous frequency difference between both beams of $\delta\omega = b\tau$ (Eq. 6). The solid dots in Fig. (3) present the result of a numerical calculation [Duppen et al., 1993] using the same parameters as in the fit to the photon echo. Except for the overall intensity of the signal there is no fitting parameter involved in the numerical calculation. Yet, the calculated and measured traces of Fig. (3) agree very well. It is precisely this consistency in the modelling of the ultrafast photon echo and the chirped four-wave mixing signals that substantiates our Brownian oscillator approach to optical dynamics.

Absorption and emission

It is straightforward to calculate the absorption and emission spectra of a two-level electronic system dressed with Brownian oscillators. The absorption spectrum $S_A(\omega)$ can be written as:

$$S_A(\omega) = 2\omega Re\left\{\int_0^\infty dt \exp[i(\omega - \omega_{eg})\, t] \exp[-g(t)]\right\} \tag{7}$$

were ω is the frequency of the absorbed light and ω_{eg} is the transition frequency of the electronic two-level system, which is centered in between the absorption and the emission maxima. The line broadening function $g(t)$ for an overdamped mode is given by Eq. (2). The steady state emission spectrum $S_F(\omega)$ is:

$$S_F(\omega) = 2(\omega)^3\, Re\left\{\int_0^\infty dt \exp[i(\omega - \omega_{eg})\, t] \exp[-g^*(t)]\right\} \tag{8}$$

where ω is the frequency of the emitted light and $g^*(t)$ is the complex conjugate of $g(t)$. By inspection of Eqs. (7) and (8) it is clear that the fluorescence spectrum $S_F(\omega)$ is practically the mirror image of $S_A(\omega)$ around the center frequency ω_{eg}.

In Fig. 4 the calculated absorption and emission spectra of resorufin in DMSO at room temperature are compared with the experimental results.

Again, just as in the calculation of the photon echo decay and the chirped four-wave mixing signal, a single overdamped oscillator was assumed to determine the optical response, with parameter values $\Delta = 41$ THz and $\Lambda = 27$ THz. The different vibronic components were considered as separate transitions, with absorption intensities as indicated by the structure underneath the spectra. Both the positions of these vibronic lines and their relative intensities are known from a report on resorufin in a glass [Van den Berg and Völker, 1988].

The enlarged part of Fig. (4) shows the origin region of the electronic transition of resorufin in DMSO. The one overdamped Brownian oscillator does not

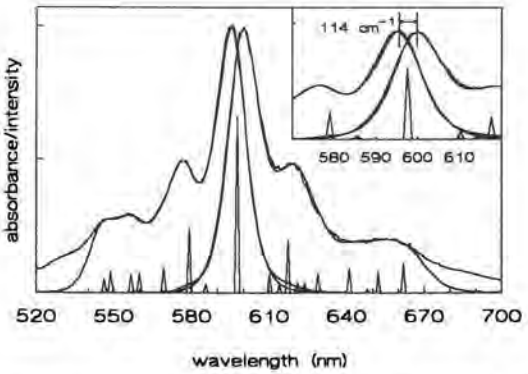

Fig. 4. Room temperature absorption and emission spectra of resorufin in DMSO. The fits are based on the level structure and transition moments shown below the curve. The enlarged view of the origin region clearly shows that the steady-state Stokes shift of 114 cm^{-1} is correctly predicted.

only describe the absorption and emission spectra very well, but also, within 10% accuracy, the steady-state Stokes shift. The Brownian oscillator model further predicts that the time-dependent Stokes shift occurs typically in about the correlation time Λ^{-1}. The time scale of solvation for resorufin in DMSO is therefore 37 fs. This fast reorientation of the solvent shells agrees with recent results of molecular dynamics simulations [Maroncelli, 1991].

Stimulated photon echo experiments

In the previous section we showed that a single Brownian solvent oscillator provides an excellent description of the optical dynamics on *all* time scales. Two-pulse photon echo and chirped four-wave mixing experiments on the system pinacyanol in ethylene glycol, however, showed that the dynamics in this solvent cannot be modelled by one Brownian oscillator. The question arises whether this different dynamical behaviour is due to hydrogen bonding effects in this solvent.

In order to obtain greater insight in this question we performed stimulated photon echo experiments.

Fig. 5 shows that the echo decay of pinacyanol in ethylene glycol extends over a couple of hundred femtoseconds with oscillatory structure superimposed on it. The very fast beating is due to coherent excitation of the vibronic structure in the absorption spectrum. The initial fast and slower decays must be due to different overdamped solvent oscillators. The observed low-frequency modulation may be due to a solvent librational mode. To analyze this complex echo decay we need an expression for the stimulated photon echo (3PSE). In the MBO model for the three pulse photon echo intensity the following expression is obtained:

$$I_{3PSE}(\tau, T) \propto \int_0^\infty |[R_1(t, T, \tau) + R_2(t, T, \tau)]|^2 \, dt$$

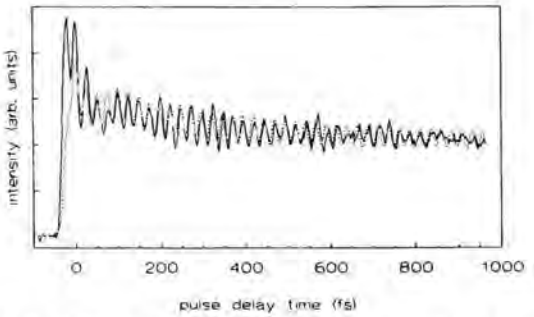

Fig. 5. Fits to a three pulse stimulated photon echo on pinacyanol in ethylene glycol using three Brownian solvent oscillators. The delay between beams 2 and 1 is 10 fs.

where the explicit forms of $R_1(t, T, \tau)$ and $R_2(t, T, \tau)$ are:

$$R_1(t, T, \tau) \equiv \exp[-g^*(t) - g^*(\tau) + g(T) - g(T+t) - g^*(\tau+T) + g^*(\tau+T+t)]$$

$$R_2(t, T, \tau) \equiv \exp[-g(t) - g^*(\tau) + g^*(T) - g^*(T+t) - g^*(\tau+T) + g^*(\tau+T+t)]$$

with $g(t) \equiv \sum_j g_j(t)$, and $g_j(t)$ is given by Eq. (2) for the overdamped modes.

To simulate the 3PSE echo decay for pinacyanol in ethylene glycol we took the following approach: first we determined from the absorption spectrum the high-frequency mode (1360 cm^{-1}) to fix the fast beating pattern; then the ultrafast component in the echo decay (tens of fs) was generated by varying the parameters Δ and Λ of one oscillator; in the third step we followed the same procedure to generate the long component (few hundred fs) in the echo decay; finally we made an educated guess about the underdamped solvent mode from the experimental echo trace. When all these independent simulations were judged to be satisfactorily, calculations were performed including all three Brownian oscillators. Our best result at this time is shown as the dotted curve in Fig. 5. While the simulated echo signal does not provide an excellent fit to the experimental

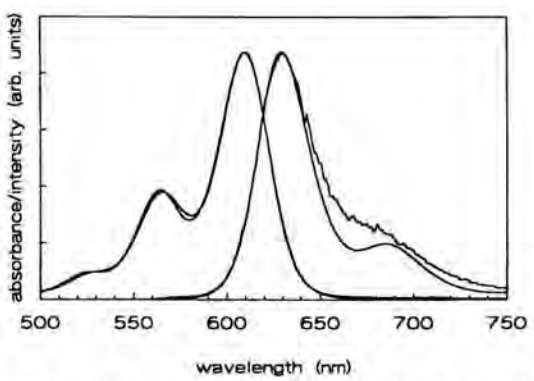

Fig. 6. Absorption and fluorescence spectra of pinacyanol chloride in ethylene glycol at room temperature. The smooth curves are fits using a set of three Brownian solvent oscillators.

decay yet, it seems that we have captured the gross features of the bath dynamics. (The discrepancy near zero delay time remains puzzling!) Of the three solvent Brownian oscillators needed to describe the echo decay two are strongly overdamped, while the third one is an underdamped mode with a frequency of about 220 cm^{-1}. We tentatively assign these oscillators to inertial, diffusive and librational solvent molecule motion, respectively. The librational and diffusive components in the dynamics may be due to hydrogen bonding because they are not significant in aprotic solvents. Further analysis of these echo decays, however, is necessary to substantiate these conjectures.

In Fig. 6 we show the absorption and emission spectra of pinacyanol chloride in ethylene glycol at room temperature. As can be seen, reasonable agreement is obtained for the lineshapes in absorption and emission, as well as for the Stokes shift. The noticable discrepancy between theory and experiment in case of the emission spectrum may be due to pinacyanol isomer emission. This is subject of further investigation.

Discussion

In the previous section it was shown that a number of different optical experiments on resorufin in DMSO can all be explained consistently in terms of a rather simple model, based on Brownian nuclear motion. The optical transition, which involves electronic degrees of freedom, is dressed with nuclear motion in harmonic potential wells. It turned out to be sufficient to consider a single overdamped mode for a quantitative explanation of all observed experimental features. Only two parameters are involved that are the same for all calculated (non-) linear optical responses, from the ultrafast photon echo and chirped four wave mixing results to the absorption and emission properties, including the magnitude of the solvation Stokes shift. The modulation strength of the electronic transition is $\Delta = 41$ THz (in angular frequency units), while the inverse correlation time is $\Lambda = 27$ THz ($\tau_c = 37$ fs). This indicates that the solute and solvent dynamics occur on similar time scales, and the optical dephasing therefore has a non-Markovian character.

For pinacyanol the situation is more complex; here we need at least three different Brownian solvent oscillators and the fits obtained, especially to the stimulated photon echo decay, are not very satisfactory. As stated, the reason for the different behaviour of the two solvents may be related to the occurrence of hydrogen bonding in ethylene glycol. Further coherent optical studies of different probe molecules in this and other similar solvents are called for.

What remains to be answered is the physical significance of the Brownian oscillator model; in what way should the overdamped mode be interpreted? One way to address this question is to relate the results presented here to recent molecular dynamics simulations of solvation dynamics [Maroncelli, 1991] and of two pulse photon echoes [Fried et al., 1992]. In these simulations it appears that the time dependence of solvation is mainly due to reorientational motions

of solvent molecules. However, the time scale for solvation-energy relaxation is much faster than the times normally associated with single-particle reorientations (typically in the order of pico- to subnanoseconds). The solvation relaxation process apparently is due to a collective effect of the solvent molecules surrounding the solute. Molecular dynamics simulations therefore strongly suggest that the overdamped Brownian oscillator in the case of resorufin describes the collective effect of the inertial motions of individual DMSO molecules around the solute molecules. While the Brownian oscillator is strongly overdamped (which predicts an unphysical exponential behavior of the oscillator at very short times), the underlying single molecule rotational motions could well be underdamped.

Acknowledgment

We thank F. de Haan for his help with formatting this paper and for his contribution to the numerical calculations of the chirped four-wave mixing signals. The investigations were supported by the Netherlands Foundation for Chemical Research (SON) and Physical Research (FOM) with financial aid from the Netherlands Organization for the Advancement of Science (NWO).

References

Becker, P.C., Fragnito, H.L., Bigot, J.-Y., Brito-Cruz, C.H., Fork, R.L., and Shank, C.V., *Phys. Rev. Lett.* **63**, 505, 1989.

Berg, R. van den, and Völker, S., *Chem. Phys.* **128**, 257, 1988.

Bigot, J.-Y., Portella, M.T., Schoenlein, R.W., Cunningham, J.E., and Shank, C.V., *Phys. Rev. Lett.* **67**, 636, 1991.

Brafman, O., Chan, C.K., Khodadoost, B., Page, J.B., and Walker, C.T., *J. Chem. Phys.* **80**, 5406, 1984.

Brito-Cruz, C.H., Fork, R.L., Knox, W.H., and Shank, C.V., *Chem. Phys. Lett.* **132**, 341, 1986.

Duppen, K., Nibbering, E.T.J., Haan F. de, and Wiersma, D.A., *Phys. Rev. A* **47**, 5120, 1993.

Fried, L.E., Bernstein, N., and Mukamel, S., *Phys. Rev. Lett.* **68**, 1842, 1992.

Maroncelli, M., and Fleming, G.R., *J. Chem. Phys.* **89**, 5044, 1989.

Maroncelli, M., *J. Chem. Phys.* **94**, 2084, 1991.

McMorrow, D., Lotshaw, W.T., and Kenney-Wallace, G.A., *IEEE J. Qu. El.* **QE-24**, 443, 1988.

Mukamel, S., *Annu. Rev. Phys. Chem.* **41**, 647, 1990.

Nibbering, E.T.J., Duppen, K., and Wiersma, D.A., *J. Chem. Phys.* **93**, 5477, 1990.

Nibbering, E.T.J., Wiersma, D.A., and Duppen, K., *Phys. Rev. Lett.* **66**, 2464, 1991.

Rosenthal, S.J., Xie, X., Du, M., and Fleming, G.R., *J. Chem. Phys.* **95**, 4715, 1991.
Song, J.J., Lee, J.H., and Levenson, M.D., *Phys. Rev. A* **17**, 1439, 1978.
Yajima, T., Souma H., and Ishida, Y., *Phys. Rev. A* **17**, 324, 1978.
Yan Y.J., and Mukamel, S., *J. Chem. Phys.* **89**, 5160, 1988.
Yan Y.J., and Mukamel, S., *Phys. Rev. A* **41**, 6485, 1990.

Authors' Address

Ultrafast Laser and Spectroscopy
Laboratory, Department of Chemistry, University of Groningen,
Nijenborgh 4, 9747 AG, Groningen,
The Netherlands

Bern Kohler, Jeffrey L. Krause, Ferenc Raksi, Christoph Rose-Petruck,
Robert M. Whitnell, Kent R. Wilson, Vladislav V. Yakovlev and YiJing Yan

Femtosecond Pulse Shaping for Molecular Control

Abstract

Recent theoretical progress allows the calculation of globally optimal light fields in the weak field limit for controlling wave packet dynamics of molecules. Using the optimal field for focussing a wave packet on the B state of I_2 as an example, we discuss the experimental pulse shaping techniques which can be used with the Ti:Sapphire femtosecond laser system we are currently constructing for performing quantum control experiments.

Introduction

We are constructing in our laboratory a femtosecond laser system with the goal of optically probing and controlling chemical reaction dynamics (Yan et al., 1992). First experiments are planned for gas-phase diatomic molecules for which the quantum dynamics can be readily computed. Recent theoretical progress in our group has yielded methods for efficiently calculating the required light fields which are globally optimal in the weak field limit (Yan et al., 1993; Krause et al., 1993). Our initial interest has been to calculate fields which produce wave packet focusing on the excited state surface of a diatomic molecule such as I_2 or Na_2. The calculated fields, or 'divine light waves', are globally optimal in the sense that no other weak field produces a molecular wavefunction at a selected time which better achieves a chosen target. Several theoretical examples of quantum control for realistic molecular systems have been described recently by us (Krause et al., 1993; Kohler et al., 1993). The computed fields are encouragingly simple, robust and are well approximated by pulses which are technically feasible.

After reviewing some of the theoretical equations for computing optimal weak fields, and discussing the optimal field for a particular control scenario which we have called the I_2 molecular refletron, we outline the requirements for a femtosecond light field synthesizer for quantum control. We describe our current amplified femtosecond laser system, and discuss the modifications we are currently completing in order to synthesize the required pulse shapes.

Focusing matter with light: The molecular reflectron

As described elsewhere in more detail (Krause et al., 1993), we have calculated the optimal field for controlling wavepacket focusing on the excited B state of I_2. In what we term the 'molecular reflectron' in analogy to a device for focusing charged particles, a bound, minimum-uncertainty wave packet is produced on the excited B state centered at an internuclear separation of 3.72 Å with a negative momentum (i.e., directed toward the molecular center of mass). The average final momentum was chosen to correspond to a kinetic energy of $p^2/2m = 0.05$ eV. The duration for control was restricted to a 550 fs time interval. The end of this interval defines a target time, $t_f = 550$ fs, at which maximum wavepacket focusing occurs. This control scenario is depicted schematically in Fig. 1.

The focused wave packet of the reflectron is produced at the target time by controlling the interference of the wavepacket which is reflected from the outer potential wall. It is important to note that wave packet focusing represents a significant departure from the 'natural' (uncontrolled) dynamics of the system. The wave packet created by an ultrashort pulse usually spreads rapidly due to the anharmonicity of the potential energy surface upon which it propagates.

In order to calculate the optimal field for the reflectron, we begin with a conventional wave packet propagation in the absence of the light field. We write the time-propagated wave packet on the excited state as,

$$|\psi_e^0(t)\rangle = \exp(-i[H_e - \varepsilon_{v''}]t/\hbar)\,|\psi_e^0(0)\rangle, \tag{1}$$

where H_e is the excited state Hamiltonian, and $\varepsilon_{v''}$ is the energy of the ground electronic state vibrational level $|v''\rangle$ which we take as our initial state, $|\psi_e^0(O)\rangle = \mu\,|v''\rangle$. Using the Condon approximation, the transition dipole moment, μ, is assumed constant. Using the time-evolved wave packet, $|\psi_e^O(t)\rangle$, we next calculate the molecular response function, M, for a desired target operator $\hat{A}$,

$$M(t_2, t_1) = \langle \psi_e^0(t_2) \mid \hat{A} \mid \psi_e^0(t_2 + t_1)\rangle. \tag{2}$$

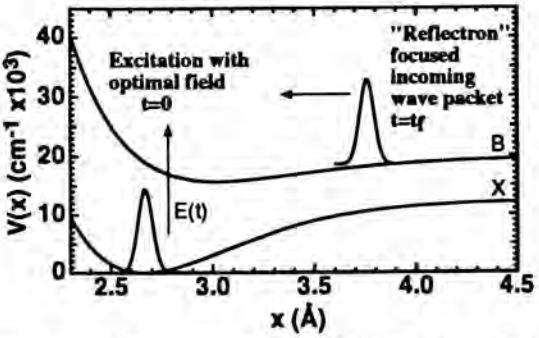

Fig. 1. Reflectron scenario: At $t = 0$ the optimal light field excites a wavepacket on the B state of I_2 which then focuses at time $t = t_f$.

For the reflectron and other examples which have been investigated, the target operator is simply a projection operator onto a target wave function which we have chosen to be a minimum uncertainty Gaussian centered at a particular position and momentum. The solution to the control problem is that electric field which excites a vibrational wave packet which best overlaps the target at the target time t_f. The solution is found by solving the eigenvalue equation,

$$\int_0^{t_f} d\tau' \, M^s(\tau, \tau') \, E(\tau') = \lambda E(\tau). \tag{3}$$

Here M^s is the Hermitian symmetrized form of the molecular response function M (Yan et al., 1993; Krause et al., 1993). The eigenvector, $E(\tau)$, associated with the largest eigenvalue is the globally optimal light field. This field excites a wave packet which best overlaps the target at the final time.

For the case of the I_2 molecular reflectron outlined above, we find that the globally optimal field is a single pulse with a smooth envelope and modest phase structure. We can write the field in complex form as,

$$E(t) = A(t) \, e^{-i\Phi(t)} \, e^{-i\omega_c t} \tag{4}$$

where ω_c is the carrier frequency, $A(t)$ is the pulse envelope, or instantaneous amplitude, and $\Phi(t)$ is the instantaneous phase minus $\omega_c t$.

In the lower two panels of Fig. 2, $A(t)$ and $\Phi(t)$ for the reflectron optimal field are indicated by the solid curves. The carrier frequency of the optimal field is 18557 cm^{-1}, corresponding to an excess energy of approximately 2800 cm^{-1} above the $0-0$ $X \leftarrow B$ transition energy. The derivative with respect to time of the total phase is the instantaneous frequency of the field, and is shown by the solid curve in Fig. 3. The mostly linear decrease of the instantaneous frequency during those times when the pulse has appreciable amplitude is indicative of nearly linear, frequency downchirp. The deviation from linearity is a signature of nonlinear frequency chirp. We write the Fourier transform of the pulse as,

$$\tilde{E}(\omega) = \int_{-\infty}^{\infty} dt \, e^{i\omega t} \, E(t) = a(\omega) \, e^{i\varphi(\omega)}, \tag{5}$$

where $a(\omega)$ and $\varphi(\omega)$ are the spectral amplitude and spectral phase, respectively. These quantities are shown for the reflectron optimal field by the solid curves in the upper panels of Fig. 2. Because the pulse shapes which can be readily synthesized in the laboratory are limited, we have fit the optimal field by a parameterized form. Previously, we fit the field in the time-domain by a Gaussian envelope and an instantaneous phase which we expressed as a cubic polynomial (Krause et al., 1993). Here, we describe the results when a fit is made to the optimal field in the frequency domain. The fitting function used for the spectral amplitude is,

$$a(\omega) = e^{-(\omega - \omega_c)^2/2\gamma^2}, \tag{6}$$

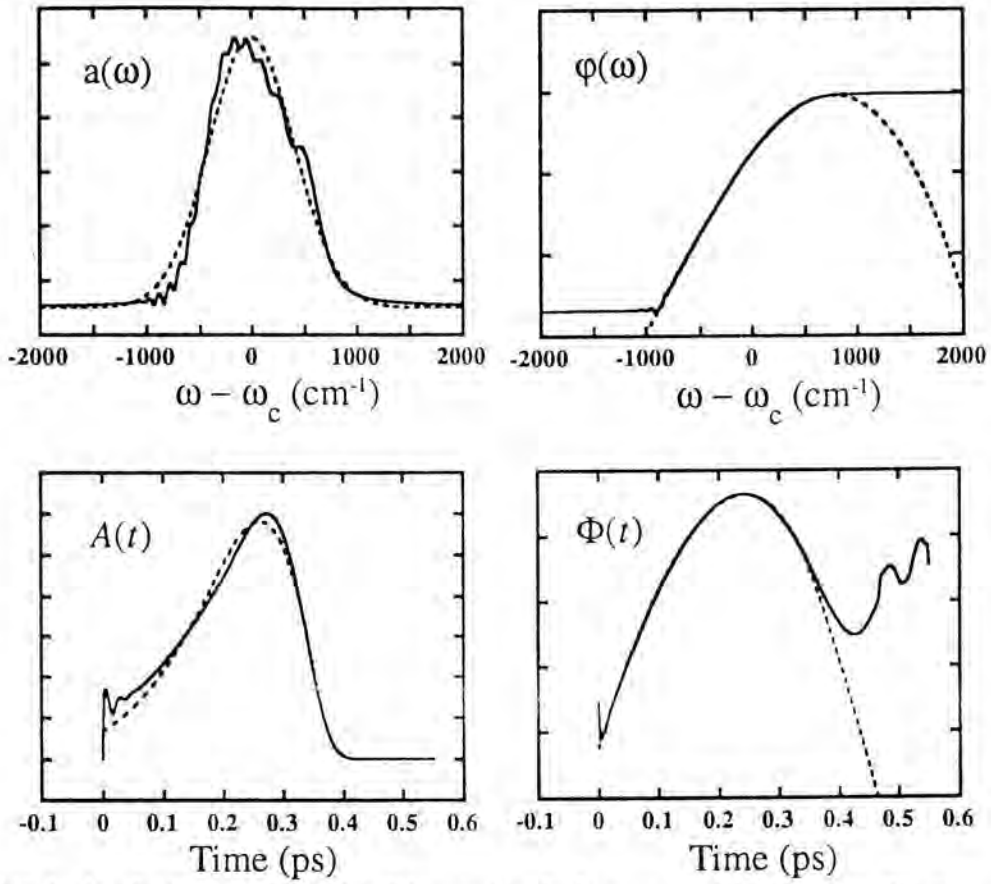

Fig. 2. I_2 reflectron optimal field (solid curves) in the frequency and time domains. The parameterized field obtained by fitting Eqns 6 and 7 to the optimal field are shown by the dashed curves. The lower panels are Fourier transforms of the upper ones.

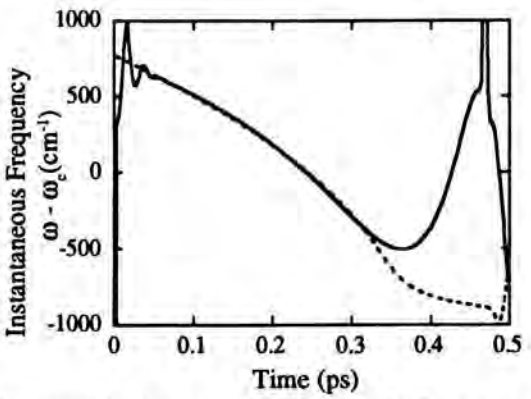

Fig. 3. Instantaneous frequency (minus carrier frequency) of reflectron optimal field (solid curve) and fit field (dashed curve).

Table 1. Best Fit Parameters for I_2 Reflectron Optimal Field.

ω_c	18557 cm^{-1}
γ	404 cm^{-1}
φ'	244 fs
φ''	-1206 fs^2
φ'''	-6210 fs^3

and the spectral phase is fit by a cubic polynomial,

$$\varphi(\omega) = \varphi_0 + \varphi'(\omega - \omega_c) + \tfrac{1}{2}\varphi''(\omega - \omega_c)^2 + \tfrac{1}{6}\varphi'''(\omega - \omega_c)^3. \quad (7)$$

The physical meaning of the coefficients in this truncated Taylor series expansion is as follows: φ_0 is a constant phase and is arbitrary for a field consisting of a single pulse, φ' is the group delay and simply shifts the arrival time of the pulse, φ'' and φ''' are responsible for linear and nonlinear frequency chirp, respectively. The light field calculated from the best fit parameters (summarized in Table 1) is shown in both the time and frequency domains by the dashed curves in Fig. 2. The parameterized field agrees excellently with the optimal field, even reproducing the asymmetry of the pulse temporal envelope.

We have calculated the achievement, or magnitude of the normalized overlap of the time-evolved wave packet on the excited state resulting from excitation of I_2 by parameterized fields, and investigated the effects of varying the parameters (Krause et al., 1993; Kohler et al., 1993). We note that the parameterized field obtained here by fitting in the frequency domain rather than the time domain, produces an achievement which is modestly higher. This is a reflection of the fact that the spectral envelope of the optimal field is more closely approximated by a Gaussian than is the more asymmetric temporal envelope.

The robustness of the achievement to variations in the field parameters is discussed elsewhere (Kohler et al., 1993). The results indicate that the success of the control depends mainly on the phase of the field. Changing the chirp of the pulse from negative to positive results in a substantial decrease in overlap. This is consistent with a physical picture in which the target wave packet is created by starting different frequency components at different times in such a way that after reflection from the outer wall of the potential they interfere at the target time to create a strongly localized wave packet in position and momentum. The achievement is relatively insensitive to changes in the pulse envelope and pulse bandwidth, which simplifies the task of synthesizing light fields for performing control, as discussed next.

Experimental Considerations

In planning the synthesis of ultrafast light fields, it is important to consider the requirements imposed by the spectral bandwidth. Given the short duration of

these fields, it is usually only possible to perform pulse shaping in the frequency-domain. Weiner and Heritage have demonstrated filters which change the spectral amplitudes and phases of a spectrally dispersed ultrafast pulse that are very effective for femtosecond pulse shaping (Weiner and Heritage, 1987). The output pulse of such a Fourier-plane filter is given by computing the inverse Fourier transform of the input pulse multiplied by the complex filter transmittance. Filters such as these are linear, and therefore cannot create energy at frequencies not present in the input pulse. Thus, if linear filtering is used to create a tailored light field, the quantity of interest is the maximum duration pulse which need be input to our pulse synthesizer, assuming that we start with a transform-limited pulse and conserve energy. Transform-limited, or approximately transform-limited pulses, are created by most laser oscillators and amplifiers. The best-fit reflectron light field, discussed above, has a Gaussian frequency spectrum, and therefore the transform-limited pulse duration is given by,

$$\tau = \frac{\ln 16}{\Delta\omega} = \frac{\sqrt{\ln 16}}{\gamma} \tag{8}$$

where $\Delta\omega$ is the FWHM of $|E(\omega)|^2$. For the reflectron best-fit field $\Delta\omega = 673\ \mathrm{cm}^{-1}$, corresponding to a transform-limited pulse with a temporal FWHM of 22 fs. Such a pulse, while experimentally challenging, is feasible using current laser technology.

Our concept is to produce the shortest femtosecond pulses possible with sufficient energy to enable conversion to other frequencies via nonlinear optical techniques, and then to shape the pulses using spectral pulse filtering. Our current experimental setup is shown in Fig. 4. The laser system we have selected as the engine for our molecular control spectrometer is a regeneratively amplified Ti:Sapphire (Ti:S) femtosecond laser, first demonstrated by Salin et al. (1991). The laser system produces several watts of femtosecond light, corresponding to

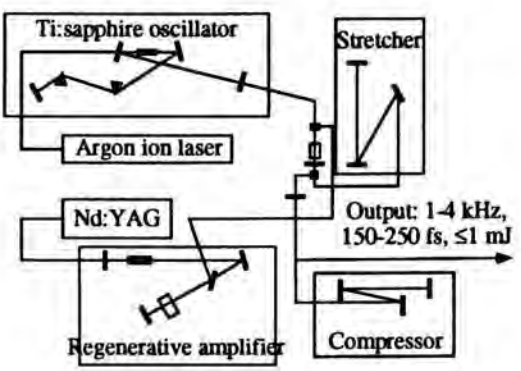

Fig. 4. Ti:Sapphire laser system incorporating chirped pulse amplification to produce several watts average power of femtosecond light.

millijoule energy pulses at kHz repetition rates. It is the highest average power amplified femtosecond light source currently available.

A Ti:S oscillator (Clark Instruments, Model NJA-4) produces 50 fs pulses which are tunable over the Ti:S gain bandwidth. Next, the oscillator pulses are linearly chirped with an all-reflective pulse stretcher to 200-300 ps, and are injected into a regenerative amplifier pumped by an intracavity-doubled Nd:YAG laser. The Nd:YAG laser (Clark-MXR, Model OCR-1000) produces 4-16 mJ pulses at a repetition rate of 1-5 kHz. The regenerative amplifier exhibits a slope efficiency of nearly 40%, resulting in very efficient amplification. Using two 1200 groove/mm gratings, the amplified pulses are compressed back down to approximately 75 fs. The through-put of the pulse compressor is 60%, and we have measured as much as 2.5 W of average power at 2 kHz repetition rate after our compressor. The high repetition rate of the laser system will enhance signal averaging, while the high pulse energy will permit frequency conversion via nonlinear optical methods. Recently, we have gained considerable experience in producing low-order optical harmonics using nonlinear optical crystals. Using BBO, we have obtained as much as 7 microjoules per pulse at 260 nm (via third harmonic generation).

While the pulse duration out of our amplifier is considerably longer than the 22 fs pulse required for the I_2 reflectron, we believe we will be able to produce <50 fs pulses soon, by upgrading our Ti:S oscillator to produce 20 fs pulses (Huang et al., 1992), and by minimizing dispersive phase errors in the stretcher/compressor combination (Lemoff, 1993).

Portions of the spectrum which are difficult to access with harmonics of the laser fundamental can be produced by continuum or white light generation (Alfano and Shapiro, 1970). The amount of energy per unit spectral bandwidth obtainable from white light is considerably lower than in the case of harmonic generation. Furthermore, an exponential decrease in spectral energy density with increasing frequency shift from the fundamental light is usually observed (Fork et al., 1983). Nevertheless, a one or two-stage dye amplifier pumped by doubled light derived from a portion of the amplified pulse can be used to increase the energy of the white light pulses to the microjoule level. Another issue with white light is the degree of spectral coherence, since this determines the ultimate duration of the pulses derived from the continuum. By selecting an intensity close to the threshold for generating white light, it has been demonstrated that portions of the white light spectrum can be compressed to as short as 16 fs (Raksi, 1992).

Assuming we have created a transform-limited pulse of sufficiently short duration, we must still create the frequency chirp required by the reflectron optimal field. Creating a negative chirp requires negative group velocity dispersion obtainable from a grating pair (Treacy, 1987), or from prisms (Fork et al., 1984). The spectral phase obtained from the parameterized field provides the necessary information for converting a transform-limited Gaussian pulse into the desired field. The spectral phase, $\varphi(\omega)$, obtained from the parameterized field indicates precisely what phase modulation is necessary to synthesize the desired field from a transform-limited Gaussian pulse. The phase modulation can be applied either

by using a liquid crystal modulator (Weiner and Heritage, 1987), or by propagating the pulse through a dispersive optical system which causes the pulse to accumulate the correct amount of frequency-dependent phase.

As already mentioned, pairs of gratings or prisms can be used, but bulk materials, interferometers, optical fibers, and other devices which provide the proper dispersion can be useful as well. The coefficients in the Taylor series expansion for the spectral phase acquired by a pulse which passes through such a pulse-shaping device are readily calculated, and can then be simply matched to the corresponding coefficients of the parameterized field.

As can be seen in Table 1, the I_2 reflectron requires $\varphi'' = -1206\,\text{fs}^2$ and $\varphi''' = -6210\,\text{fs}^3$. Such values are readily obtained experimentally. Since the cubic dispersion of a grating pair has the opposite sign of that of a prism pair, it should be possible to use both in combination to produce precisely this phase structure.

Finally, we note that positive chrips can readily be produced either by using a properly chosen length of bulk dispersive material such as a fiber (Grischkowsky and Balant, 1982), or using lenses or concave mirrors in combination with gratings or prisms as in the pulse stretcher of our chirped pulse amplifier (Martinez, 1987).

Summary

We have discussed an experimental instrument for synthesizing light fields for performing quantum control on molecules. Using the field necessary for obtaining wavepacket focusing on the *B* state of molecular iodine as an example, we have shown that the necessary experimental instrumentation for quantum control is readily available. The light field to achieve this control has been computed and is the globally optimal field in the weak field limit. This field has a simple structure and is described to a good approximation as a frequency-chirped, Gaussian pulse. We have discussed the steps we are taking to synthesize this and other tailored light fields using the Ti:S femtosecond laser based instrument we are currently constructing in our laboratory. We have outlined the upgrade path on which we are presently embarking to improve the capabilities of our current laser system and to produce the kinds of light fields which will be needed not only to probe, but ultimately to control the quantum dynamics of molecules.

References

Alfano, R.R., and Shapiro, S.L., *Phys. Rev. Lett.* **24**, 584, 1970.
Lemoff, B.E., and Barty, C.P.J., *Opt. Lett.* **18**, 1651, 1993.
Fork, R.L., Martinez, O.E., and Gordon, J.P., *Opt. Lett.* **9**, 150, 1984.
Fork, R.L., Shank, C.V., Hirlimann, C., and Yen, R., *Opt. Lett.* **8**, 1, 1983.
Grischkowsky, D., and Balant, A.C., *Appl. Phys. Lett.* **41**, 1, 1982.

Huang, C., Asaki, M., Backus, S., Murnane, M., Kapteyn, H., and Nathel, H., *Opt. Lett.* **17**, 1289, 1992.
Kohler, B., Krause, J.L., Raksi, F., Rose-Petruck, C., Whitnell, R.M., Wilson, K.R., Yakovlev, V.V., and Yan, Y.J., *J. Phys. Chem.* **97**, 12602, 1993.
Krause, J.L., Whitnell, R.M., Wilson, K.R., Yan, Y.J., and Mukamel, S., *J. Chem. Phys.* **99**, 6562, 1993.
Martinez, O.E., *IEEE J. of Quant. Electron.* **23**, 59, 1987.
Raksi, F., private communication, 1992.
Salin, F., Squier, J., Mourou, G., and Vaillancourt, G., *Opt. Lett.* **16**, 1964, 1991.
Treacy, E.B., *IEEE J. of Quant. Electron.* **5**, 454, 1969.
Weiner, A.M., and Heritage, J.P., *Revue de Phys. Appl.* **22**, 1619, 1987.
Yan, Y.J., Kohler, B.E., Gillilan, R.E., Whitnell, R.M., Wilson, K.R., and Mukamel, S., Ultrafast Phenomena VIII, Springer, Berlin, 1992.
Yan, Y.J., Gillilan, R.E., Whitnell, R.M., Wilson, K.R., and Mukamel, S., *J. Phys. Chem.* **97**, 2320, 1993.

Authors' Address:

Department of Chemistry
University of California, San Diego
La Jolla, CA 92093-0339, USA

R.M. Hochstrasser

Ultrafast Dynamics Seen Through the Vibrations

Abstract

Ultrafast processes in condensed phase are explored with transient vibrational spectroscopy. Examples include vibrational relaxation, chemical reactions, protein dynamics and energy transfer.

Introduction

Direct interrogation of molecular vibrations by infrared or Raman scattering is complementary to optical spectroscopic studies of ultrafast processes. The vibrational spectroscopies have some advantage in as much as the structurally important modes can be observed directly even when electronic transitions may be inaccessible. Although there are as yet no ultrashort pulse lasers in the structurally useful region of the infrared spectrum, say from 500 to 4000 cm^{-1} the recent advances in ultrafast technology in combination with advances in nonlinear materials, permit more effective generation of shorter time resolution. Free electron lasers may also help fill the gap. At time of writing the shortest IR pulse used in an experiment was 160 fs (Owrutsky et al. 1992). There appears to be no technological barrier in obtaining useable pulses of about one-half this width. It is therefore evident that ultrafast processes can be studied directly via the vibrations and the purpose of this talk is to summarize some of the recent results obtained in this laboratory using a variety of IR and finally Raman methods.

First a very brief summary of the current capabilities of transient IR methods will be given. The methods themselves have been adequately described in recent review articles (Anfinrud et al., 1992; Locke et al., 1993). There then follows an account of various areas of research in which these methods have been employed by us. For this talk, the following topics will be considered in more detail:

(1) Ultrafast population relaxations of simple ions in solution.

(2) Bimolecular abstraction reactions producing HCl or HCN in solution.

(3) Protein dynamics: Reaction center electron transfer reaction.

(4) Partial Dephasing in the Raman scattering of porphyrins related to the reaction center.

In the first example infrared pump/probe experiments are used to measure orientational and T_1 relaxation times. The use of IR in probing small molecules

whose electronic transitions are not accessible in solutions is the next example. The remainder of the talk is concerned with protein phenomena, the identification of both electronic and vibrational transitions in the IR and with dephasing dynamics of porphyrin-like molecules that occur in the reaction center.

Transient Infrared Spectroscopy

Important characteristics of ultrafast technologies include such features as the available time resolution, the repetition rate which is a critical feature in determining the ultimate signal-to-noise, the range of accessible IR frequencies and the available energy in the pump and probe pulses. Table I shows some of these parameters that are typical for the experiments reported here.

Parameters of IR Spectroscopy

Pulsewidth:	$\geqslant 150$ fs
Time resolution:	$\geqslant 100$ fs
Repetition rate:	$\leqslant 5$ kHz
Energy/IR pulse:	ca. 0.5 μJ (pump)
Probe range:	700-4000 cm^{-1}

Experiments have been performed with significantly more intense pulses than those in Table I but only at the expense of repetition rate. A very useful summary of work on developing higher intensity, mainly slower repetition rate infrared sources is given in the article by Laubereau (Laubereau, 1992). Our goal has been to minimize the incident pulse energy and maximize the rep rate. In this laboratory transient IR spectroscopy was used to study dynamics in hemoproteins (Moore et al., 1987; Anfinrud et al., 1989), photochemistry of metal carbonyls (Anfinrud et al., 1990), orientational dynamics in proteins (Hansen et al., 1989; Locke et al., 1991), relaxation of ions in water (Owrutsky et al., 1991; Li et al., 1993), heat transduction in proteins (Lian et al., 1992), free induction decay of molecules on metal surfaces (Owrutsky et al., 1992), dynamics and spectra associated with electron transfer in reaction centers (Maiti et al., 1993; Sension et al., 1993) and with Bacteriorhodopsin (Diller et al., 1992) and bimolecular chemical reactions in solutions (Raftery et al., 1993). These experiments have involved a variety of different laser configurations and methods of generating IR pulses for pumping and probing samples. The first method used by us, and one that is particularly useful for protein studies, involved gated detection of quasi-CW IR beams (Moore et al., 1987). In other experiments ultrashort IR pulses were generated in a conventional manner by means of difference frequency mixing.

Ultrafast Population Relaxation of Simple Ions in Solution

The observation that high frequency vibrational states of diatomic (Heilweil et al., 1982) and triatomic ions (Owrutsky et al., 1991; Li et al., 1993) relax on the

few picosecond timescale in hydroxyllic solvents demonstrates the importance of Coulomb forces in the coupling to the solvent. Infrared pump/probe experiments with tunable pulses have enabled measurements of T_1 relaxation and orientational relaxation (T_R) of a number of simple pseudo-halogen ions N_3^-, NCO^- and NCS^-. These ions have an asymmetric stretch mode near 2000 cm^{-1} which is studied in this work. The principal results were as follows:

- An inverse relation between T_1 and T_R was found:

  For $T_1 \ll T_R$ Vibrational relaxation occurs within a well-defined solvent structure - i.e. supermolecule relaxation.

  For $T_1 > T_R$ Vibrational relaxation averaged over a broad range of structures.

- The T_1 relaxation is charge related indicating importance of Coulombic forces. This may mean that not only the nearest neighbor solvent atoms are involved. Relaxation rates are roughly consistent with being proportional to $(\text{charge})^2$.
- The T_1 relaxation depends on the extent of motion of the end atoms in the asymmetric stretch coordinate.
- Hydrogen bonding is a crucial factor in ultrafast relaxation. In nonhydroxyllic solvents the rates are much slower.
- A possible role seen for internal modes of water is inferred from isotope effects (H_2O/D_2O) in the T_1 relaxation of N_3^-.
- caveat: No evidence was yet established for solvent induced anharmonic coupling of the asymmetric stretch with other modes. Such pathways of relaxation would have much larger solvent forces available since smaller amounts of internal energy loss are involved. It will be interesting to discover whether such solvent induced anharmonic paths can permit ultrafast relaxation and not show up in the IR spectrum as resonances.

Certainly ultrafast infrared methods will, in the future, allow measurements of this nature for wide classes of molecular ions. In bringing such measurements into relationship with theory not only will these specific ions be better understood but the broader goal of experimentally determining the relevant force correlation functions for simple liquids such as H20 will be advanced.

Bimolecular Hydrogen Abstraction Reactions

Here is an area where IR methods allow detection in the condensed phase of transiently generated small molecules that could not be sensed with current laser optical methods.

Experimentally, gas phase studies have relied on collisionless conditions that allow evaluation of product states long after the reaction has taken place. Recent experiments have shown that the vibrational relaxation in condensed phase is often slow (10's to 100's of picoseconds), so that evaluation of the vibrational states should indeed still be possible. Over the past several years, methods in transient IR spectroscopy have progressed to the point where the sensitivity and

time resolution are sufficient to probe these distributions before they thermalize and to measure reaction rates.

A prototype experiment for a bimolecular reaction, hydrogen abstraction by chlorine, is shown in the figure. A near UV photon excites a chlorine molecule from its ground state to a dissociative ($^1\Pi$) state. In the gas phase, photolyzing chlorine atoms at 355 nm would result in 11 kcal/M of translational energy per atom, which would easily be enough to surmount the small activation barrier to hydrogen abstraction from the reactant. However, the results of the experiment indicate that most of the reaction is thermal, and thus the chlorine atoms lose their kinetic energy before they react with the solvent.

Fig. 1 also shows the potential energy surface (dotted line) along the reaction coordinate (the hydrogen asymmetric stretch), as well as the Cl-H-R transition state. The activation barrier (exaggerated in the figure) is estimated to be 0.5 to 1 kcal/M in the gas phase, and the exoergicity is 8 ± 0.5 kcal/M. The dotted vertical line that separates the chlorine molecular potential from the reaction potential indicates the 'point of no return' for the chlorine atoms. At this atomic separation, of approximately 4.6 Å, chlorine atoms feel an attractive energy kT. Similar considerations apply to H abstraction from $CHCl_3$ by CN radicals except that in this case the HCN is born vibrationally hot (Raftery and Hochstrasser, 1993). Our results show that the majority of chlorine atoms or CN radicals in solution do not react during their first encounter with a solvent molecule. From kinematic considerations, after 3 collisions, occurring within a time of 1 ps, chlorine atoms would lose the 11 kcal/M of initial translational energy (imparted by the 355 nm photolysis pulse) and thus become thermalized quickly.

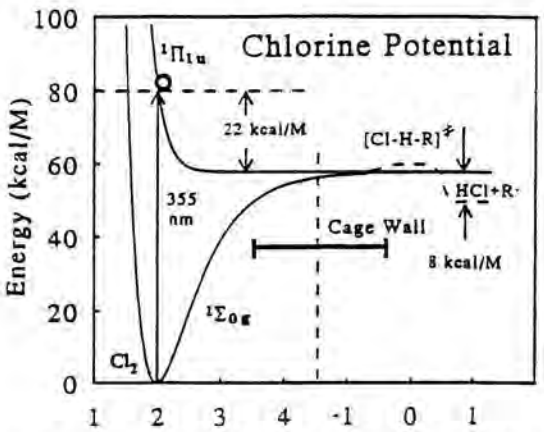

Fig. 1. Combined potential energy diagram of chlorine molecule and the reaction coordinate for hydrogen abstraction. The 355 nm transition is shown from the ground state to the dissociative $^1\Pi$ state with excess energy 11 kcal/M per Cl atom. The potential energy along the reaction coordinate (hydrogen asymmetric stretch) is indicated by the dotted line. The vertical dotted line marks the minimum necessary separation (4.6 Å) at which Cl atoms may go on to react with hydrogen. The approximate distance to the nearest solvent molecule is indicated by the heavy horizontal line labelled as 'Cage Wall.'

It is expected that the mean force potential for the bimolecular process will be modified from the gas phase potential by solvation. The resulting change in activation free energy will cause the rates in the gas and solution phase to be different. Therefore, the slow solution phase reaction rates could simply be caused by an increased activation barrier in solution. Although no direct measurement of the barrier has been reported for this reaction, there are several gas phase studies of the reaction of chlorine with cyclopentane that give an activation barrier of about 0.5 kcal/M (Kondratiev, 1972; Davis, 1970). A change in activation free energy of approximately 1.1 kcal/M would be required to account for the factor of 14 observed in the rates, assuming that chlorine is reacting thermally. One might expect the increased barrier height to be due to a larger (negative) free energy change of solvating the Cl atom compared to the solvation of the transition state. There is also information which could imply that part of the reduction in the rate is due to entropic factors caused by the solvent caging effect on Cl (Galiba, 1966).

In general, the influence of vibrational excitation on simple gas phase bimolecular reactions has been frequently considered both theoretically and experimentally (Steinfeld et al., 1989). In the condensed phase the effect of vibrational relaxation needs to be considered. In many cases the vibrational energy relaxation induced by the solvent forces will occur on timescales that are very long compared with the time for activation and passage through a transition state region. In this limit the medium induced relaxation should have little effect on a reaction product distribution. For example, we have observed HCN, generated in the reaction of CN with $CHCl_3$, in its $v=0$, 1 and 2 states in solution (Raftery and Hochstrasser, 1993). Perhaps of even greater importance is that it should be possible in this limit to prepare specific reactant vibrational states in solution that will live long enough to undergo reaction. For example, if the vibrational relaxation time of a mode is 100 ps, the molecule, having a radius of 3 Å will most probably diffuse a distance of about 10 Å before the vibrational excitation is lost in a liquid having a viscosity of 0.1 cp. This situation leaves the vibrationally excited molecule with plenty of opportunity to undergo a bimolecular reaction. However much work, both theoretical and experimental, remains to be accomplished before a broad understanding of the solvent effects on transition state dynamics is achieved.

Protein Dynamics

Proteins exhibit IR transitions that are characteristic of structure in the amide regions where vibrations of the peptide backbone occur. Transitions in this region (1400-1800 cm^{-1}) have relatively small cross sections so high sensitivity methods are needed to detect changes. Cofactors also have characteristic IR transitions such as the strong FeCO absorption in heme proteins and the carbonyl sidechains of chlorophylls.

It is well-known from optical studies that the early steps of electron transfer in photosynthetic reaction centers are very fast (Breton et al., 1986): An electron

moves from the excited chlorophyll dimer, $BChl_2^*$, to the bacteriopheophytin PPh in about 3 ps. The first quinone, Q, is reduced by BPh^- in about 200 ps. Thus the protein states $BChl_2^*:BPh:Q$, $BChl_2^+:BPh^-:Q$ and $BChl_2^+:BPh:Q^-$ are all interceptable by the current IR technology. If the protein or cofactor sidechains undergo changes in their IR spectra during these transformations it will be possible to characterize them and relate them to structural alterations.

We first studied the changes in the vibrational transitions of the protein and redox cofactors of the photosynthetic reaction center by picosecond infrared spectroscopy (Maiti et al., 1993). The spectra in the vibrational mid-infrared region (1800-1550 cm^{-1}) of hydrated and partially dehydrated reaction centers were investigated from 50 ps to 4 ns after photoinitiation of the electron transfer. Features in the infrared difference spectra were identified with both protein and redox cofactor vibrational mode *s* and correlated with electron transfer events whose kinetics were measured in the infrared and visible regions. The observed protein response is confined to a few amide I transitions (1644 cm^{-1}, 1661 cm^{-1}, 1665 cm^{-1}) and carboxylic residues (1727 cm^{-1}). About 85% of the observed signal corresponded to alterations in the cofactor associated ester and keto-carbonyls. The amide I and carboxylic transitions appeared prior to 50 ps suggesting that the primary electron transfer event is coupled with a specific piece of the protein backbone and to Glu or Asp residues nearby to the special pair. Infrared absorption changes accompanying bacteriochlorophyll dimer cation formation, dominated the signal at all times investigated.

IR spectral changes observed in hydrated and partially dehydrated reaction centers were distinctly different; a band at 1665 cm^{-1} with a spectral width of 6 cm^{-1} in the hydrated protein corresponding to a protein amide I bleach was not present in the dehydrated film. These differences point to different electron-transfer kinetics observed in the presence of water.

Femtosecond IR was used recently to investigate the earliest steps in electron transfer (Cowen et al., 1993). Some data are shown in Fig. 2. The 9-ketocarbonyl region around 1702 cm^{-1}, curve (a) in Fig. 2 shows non-single-exponential growth kinetics which is influenced by sample heterogeneity. Besides the expected 3.5 ps response we have seen in this region even stronger signals exhibiting

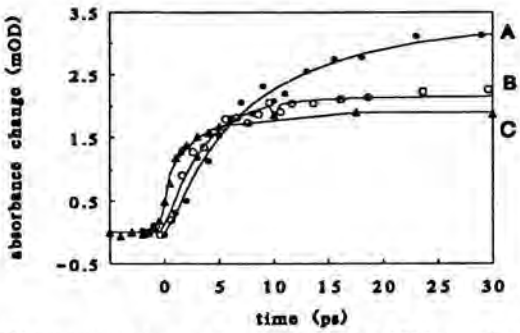

Fig. 2. Some ultrafast IR transients in reaction centers. (a) 1702 cm^{-1}; (b) 1710 cm^{-1}; (c) 1960 cm^{-1}

growth times of ca. 11 ps. At 1708 cm^{-1}, curve (b) only the 3.5 ps rise has been seen. These results are not yet understood but they clearly present another perspective on this electron transfer step.

Trace (c) in Fig. 2 shows a response typical for the 1800-2000 cm^{-1} region where we have seen transitions in the IR due to electronic excitation of $BChl_2^*$ and $BChl_2^+$. In the case of $BChl_2^*$ we observe an interexciton transition which is between states that are symmetric and antisymmetric to interchange of the excitation. For $BChl_2^+$ we confirm the existence of a transition between states that are symmetric and antisymmetric to the transfer of a positive hole. Such a state was already conjectured to be present (Parson et al., 1990; Breton et al., 1992).

These new results, taken together with our measurements on hemoglobin and bacteriorhodopsin suggest a wide variety of new insights can be obtained on protein dynamics using transient IR spectroscopy.

Partial Dephasing

The occurrence of rapid electron transfer in reaction centers suggest that careful consideration be given to dephasing effects involving the various states involved. Some aspects of this were brought out in the paper by Jean and coworkers (Jean et al., 1992). We have noted (Wynne and Hochstrasser, 1993; Galli et al., 1993) the similarity in the expected dephasing processes in porphyrin-like electronic states and dimers: the reaction center contains both such structures. Although this part of the research does not involve IR spectroscopy it does concern Raman transitions and the results are very different for the various vibrational symmetries that occur in porphyrins and chlorins.

The notion of partial dephasing is related to Raman dephasing and arises from consideration of a pair (or multiplet) of states that are nearly degenerate by symmetry or by accident, in contact with a bath. These could be the Q_x and Q_y states of a porphyrin or the accidentally degenerate states Q_{yL} and Q_{yM} of $BChl_2^*$. When driven by a short enough linearly polarized light pulse a molecule having two levels $|a\rangle$ and $|b\rangle$ acquires the density matrix:

$$\sigma = (\varepsilon_x^2 + \varepsilon_y^2)\,\sigma_0 + (\varepsilon_x^2 - \varepsilon_y^2)\,\sigma_z + 2\varepsilon_x\varepsilon_y\sigma_x$$

where σ_0, σ_z and σ_x are the Pauli spin operators and ε_i is the projection of the polarized pump field on the ith molecular dipole allowed state. In a pump probe experiment all three components of σ can be probed but the signals have different anisotropy. We have shown that the pump-probe anisotropy signal acts as if there were a three state kinetic system of the form:

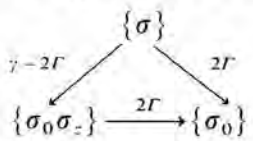

where $\{\sigma_i\}$ means σ_i is determining the ensemble averaged pump-probe signal. The 'rate' coefficients γ and 2Γ satisfy a three state anisotropy equation:

$$r(t) = 0.7\, e^{-\gamma t} + 0.4(e^{-2\Gamma t} - e^{-\gamma t}) + 0.1(1 - e^{-2\Gamma t})$$

The evolution of σ under the influence of bath fluctuations corresponds to the transition to the statistically averaged state $\{\sigma_0\}$ through the partially coherent state characterized by the loss of σ_x only. In the experiment with MgTPP (Galli et al., 1993) the coefficients γ and 2Γ were measured to be 210 fs^{-1} and 1.6 ps^{-1} respectively indicating that the partial dephasing rate $\gamma - 2\Gamma$ is 240 fs^{-1}, quite similar to the rate 2Γ of creating of a statistical mixture. The application of this idea to higher symmetry cases (e.g. $A \rightarrow T$ transitions) and to dimers and trimers is straightforward. Furthermore the influence of such effects on determining pathways of electron transfer from such structures to nearby donors is evident. In recent experiments with porphyrin-quinones (Wynne et al., 1993) we believe that the rate of electron transfer is demonstrably limited by the partial dephasing rate.

Acknowledgments

This work was supported by NIH and NSF. Thanks are due to my colleagues, post-Doctorals and students who contributed to the research projects described in this lecture.

References

Anfinrud, P.A., Han, C., and Hochstrasser, R.M., *Proc. Natl. Acad. Sci.* **86**, 8387, 1989.

Anfinrud, P.A., Han, C., Lian, T., and Hochstrasser, R.M., *J. Phys. Chem.* **94**, 1180, 1990.

Anfinrud, P.A., Johnson, C.K., Sension, R., and Hochstrasser, R.M., 'Ultrafast Spectroscopic Methods,' in Applied Laser Spectroscopy; Techniques, Instrumentation and Applications, ed. Andrews, D.L. (VCH Publishers, NY), 1992.

Breton, J., Martin, J.-L., Migus, A., Antonetti, A., and Orszag, A., *Proc. Natl. Acad. Sci.* **83**, 5121, 1986.

Breton, J., Nabedryk, E., and Parson, W.W., *Biochemistry* **31**, 7503, 1992.

Cowen, B.R., Walker, G.C., Maiti, S., Moser, C.C., Dutton, P.L., and Hochstrasser, R.M., *Biophys. J.* **64**, A213, 1993.

Davis, D.D., Braum, W., and Bass, A.M., *Intern. J. Chem. Kinetics* **2**, 101, 1970.

Diller, R., Iannone, M., Cowen, B.R., Maiti, S., Bogomolni, R.A., and Hochstrasser, R.M., *Biochemistry* **31**, 5567, 1992.

Galiba, F., Tedder, J.M., and Walton, J.C., *J. Chem. Soc. B*, 604, 1966.

Galli, C., Wynne, K., LeCours, S., Therien, M. J., and Hochstrasser, R.M., *Chem. Phys. Lett.* **206**, 493, 1993.

Hansen, P.A., Moore, J.N., and Hochstrasser, R.M., *Chem. Phys.* **131**, 49, 1989.
Heilweil, E.J., Doany, F.E., Moore, R., and Hochstrasser, R.M., *J. Chem. Phys.* **76**, 5632, 1982.
Jean, J.M., Friesner, R.A., and Fleming, G.R., *J. Chem. Phys.* **96**, 5827, 1992.
Kondratiev, V.N., Constants of Gas Phase Reactions Reference Book, ed. Fristrom, R. M. (NBS, Washington), 1972.
Laubereau, A., in Topics in Applied Physics, ed. Kaiser, W. (Springer-Verlag, Berlin) vol. 60, p. 35, 1992.
Li, M., Owrutsky, J., Sarisky, M., Culver, J.P., Yodh, A., and Hochstrasser, R.M., *J. Chem. Phys.* **98**, 7, 1993.
Lian, T., Locke, B., and Hochstrasser, R.M., *Biophys. J.* **61**, A53, 1992.
Locke, B., Diller, R., and Hochstrasser, R.M., 'Ultrafast infrared spectroscopy and protein dynamics,' in Biomolecular Spectroscopy, vol. 20, eds. Clark, R.J.H., Hester, R.E. (by John Wiley & Sons, Ltd.), in press, 1993.
Locke, B., Lian, T., and Hochstrasser, R.M., *Chem. Phys.* **158**, 409, 1991.
Maiti, S., Cowen, B.R., Diller, R., Iannone, M., Moser, C.C., Dutton, P.L., and Hochstrasser, R.M., *Proc. Natl. Acad. Sci.* **90**, 5247, 1993.
Moore, J.N., Hansen, P.A., and Hochstrasser, R.M., *Chem. Phys. Lett.* **138**, 110, 1987.
Owrutsky, J.C., Culver, J.P., Li, M., Kim, Y.R., Sarisky, M.J., Yeganeh, M.S., Yodh, A.G., and Hochstrasser, R.M., *J. Chem. Phys.* **97**, 4421, 1992.
Owrutsky, J.C., Kim, Y.R., Li, M., Sarisky, M.J., and Hochstrasser, R.M., *Chem. Phys. Lett.* **184**, 368, 1991.
Parson, W.W., Chu, Z.-T., and Warshel, A., *Biochim. Biophys. Acta.* **1017**, 251, 1990.
Raftery, D., Iannone, M., Phillips, C.M., and Hochstrasser, R.M., *Chem. Phys. Lett.* **201**, 513, 1993.
Raftery, D., and Hochstrasser, R.M., in process of publication, 1993.
Sension, R.J., Repinec, S.T., Szarka, A.Z., and Hochstrasser, R.M., 'Ultrafast photoreactions of cis-Stilbene,' in Ultrafast Phenomena VIII, eds. Martin, J.L., Migus, A., Mourou, G., Zewail, A.H., Springer Series in Chemical Physics, Vol. 55, 1993.
Steinfeld, J.I., Francisco, J.S., and Hase, W.L., Chemical Kinetics and Dynamics (Prentice Hall, Englewood Cliffs, NJ), 1989.
Wynne, K., Galli, C., LeCours, S., Therien, M.J., and Hochstrasser, R.M., in process of publication, 1993.
Wynne, K., and Hochstrasser, R.M., *Chem. Phys.* **171**, 179, 1993.

Author's Address

Department of Chemistry
231 South 34th Street
University of Pennsylvania
Philadelphia, PA 19104-6323
USA

R.A. Mathies, R.W. Schoenlein, L.A. Peteanu, Q. Wang and C.V. Shank

Femtobiology: Mechanism and Dynamics of the First Step in Vision

Abstract

The kinetics of the primary event in vision have been resolved by using femtosecond optical measurement techniques. The 11-*cis* retinal chromophore in rhodopsin is excited with a 35-fs pump pulse at 500 nm and the transient absorption changes are monitored with 10-fs probe pulses. Within 200 fs, increased absorption is observed between 540 and 620 nm demonstrating that the first step in vision, the 11-*cis* → all-*trans* isomerization of the rhodopsin chromophore, is complete in only 200 fs. The short time scale for this process suggests that the surface crossing from the 11-*cis* excited state to the all-*trans* photoproduct ground state involves nonstationary or coherent vibrational states and that the torsional *velocity* of the excited-state wavepacket in the 90° twisted transition state region is a critical parameter for determining the quantum yield of this important reaction. This new paradigm for visual photochemistry may be relevant for a variety of photochemical and photobiological processes.

Introduction

Visual excitation and photosynthesis are the most important photochemical reactions in biology. This paper will focus on the primary photoisomerization that initiates vision. These studies of femtobiology are important not only because they have elucidated the dynamics of the first step in vision, but also because they have uncovered a new paradigm for the mechanism of photochemical reactions. We begin by describing the protein rhodopsin that initiates visual excitation. This is followed by the presentation of our femtosecond optical studies on the photoexcitation of rhodopsin (Schoenlein et al., 1991b; Peteanu et al., 1993). The importance of nonstationary vibrational states or vibrational coherence in the photochemical isomerization reaction will be emphasized.

The Visual Protein Rhodopsin

Rhodopsin ($\lambda_{max} \cong 500$ nm) is an intrinsic membrane protein found in retinal rod cells. Light absorption by its bound 11-*cis* retinal prosthetic group initiates

a photochemical *cis* → *trans* isomerization that results in the excitation of the retinal rod cell (Wald, 1968). The initial red-absorbing (~ 550 nm) photochemical product is thought to contain a distorted all-*trans* chromophore (Eyring et al., 1980; Yoshizawa & Wald, 1963). Previous transient absorption experiments have shown that the red-absorbing photoproduct is formed in less than 6 ps (Busch et al., 1972). Time-resolved resonance Raman as well as Raman intensity analyses have argued that there is a very fast femtosecond photochemical isomerization (Hayward et al., 1981; Loppnow & Mathies, 1988). However, until the work presented here, the time scale for the first step in vision has remained unresolved.

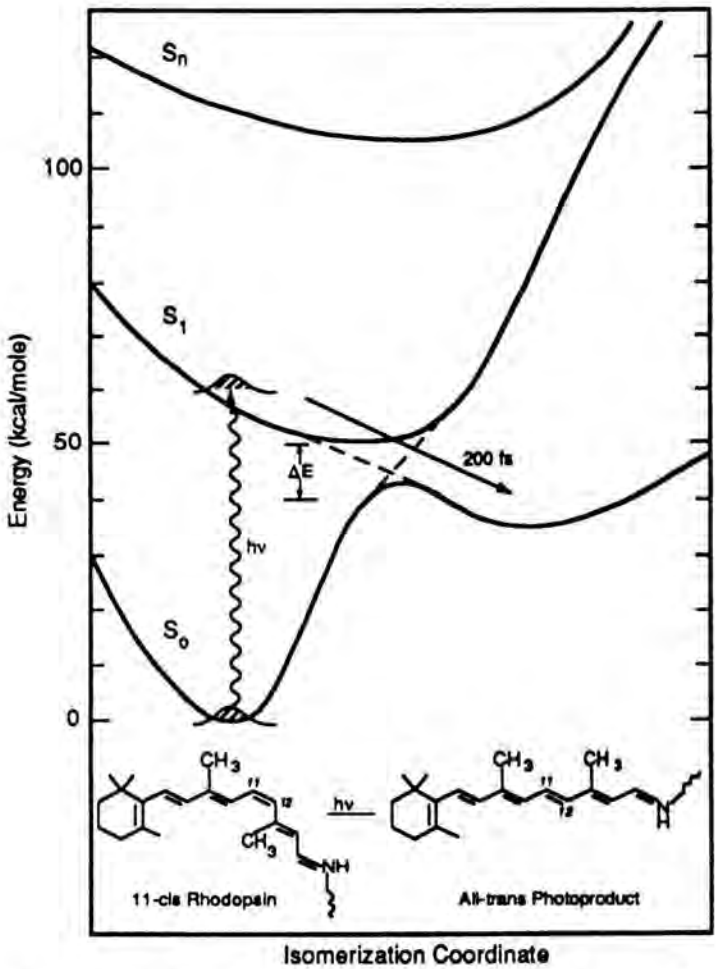

Fig. 1. Schematic ground and excited state potential surfaces for the 11-*cis* → all-*trans* isomerization in rhodopsin. The reaction path of the photoisomerization is indicated by the nonadiabatic potential surfaces (broken lines).

The time course of many photochemical and photobiological reactions can be studied by using compressed femtosecond (fs) optical pulses (Shank, 1986). Such pulses in the red were previously used to observe the isomerization of the retinal chromophore in bacteriorhodopsin, a related pigment that functions as a light-driven proton pump (Mathies et al., 1988). Recent advances in the generation of femtosecond pulses in the blue-green region of the spectrum now make it possible to study the primary photo-processes in vision as well (Schoenlein et al., 1991a). The work presented here reveals that the primary *cis-trans* isomerization in vision occurs in only 200 fs and is one of the fastest photochemical reactions ever studied.

Femtosecond Spectroscopy of Rhodopsin

The femtosecond laser system consists of a colliding-pulse, mode-locked dye laser with a 400 Hz excimer-pumped dye amplifier system (Schoenlein et al., 1991a). This laser system produces 35 fs pump pulses at 500 nm and ~ 10 fs probe pulses (centered either at 620 nm or at 500 nm). The bandwidth of the compressed probe pulses permits the resolution of spectral dynamics of the rhodopsin molecule following the narrow band (~ 15 nm) pump. The probe pulse is then dispersed and detected *after* passing through the sample, providing simultaneously both high spectral and time resolution. Rhodopsin from 400 cattle retinas was purified and solubilized in detergent solution at a concentration of 15 OD/cm at 500 nm. The 3 ml sample was flowed through a 300 μm pathlength wireguided drip jet. In all measurements the maximum signal ($\Delta T/T$) is $<2\%$ and linearity in both the pump and probe powers has been verified.

Fig. 1 presents the structures of the chromophore in 11-*cis* rhodopsin and in its all-*trans* photoproduct along with schematic potential surfaces for the torsional isomerization. In the traditional picture of photochemical processes, vertical excitation would be followed by vibrational dephasing and relaxation, surface crossing to the ground state (and back to the reactant since the quantum yield is not unity) and photoproduct cooling. The rate of photoproduct production can be followed by probing at ~ 570 nm. Fig. 2 presents transient absorption spectra of the primary photochemistry and Fig. 3 presents the corresponding single wavelength kinetic traces. At early times (~ 33 fs) there is a dramatic increase of absorption at 500 nm. This is due to absorption to a higher-lying excited state from the pump-induced nuclear wavepacket produced near the Franck-Condon region on S_1. By 200 fs, this signal has completely disappeared, revealing the full bleach of the rhodopsin ground state absorption at 500 nm. The prompt dissipation of the excited-state absorption demonstrates that rhodopsin exhibits very rapid excited-state torsional nuclear dynamics. The photoproduct absorption in the 550-570 nm region increases rapidly and is fully formed in only 200 fs. After this time the photoproduct absorption band relaxes by shifting slightly to the blue but does not further increase in area. These data show that the all-*trans* photoproduct is formed in only 200 fs and that little to

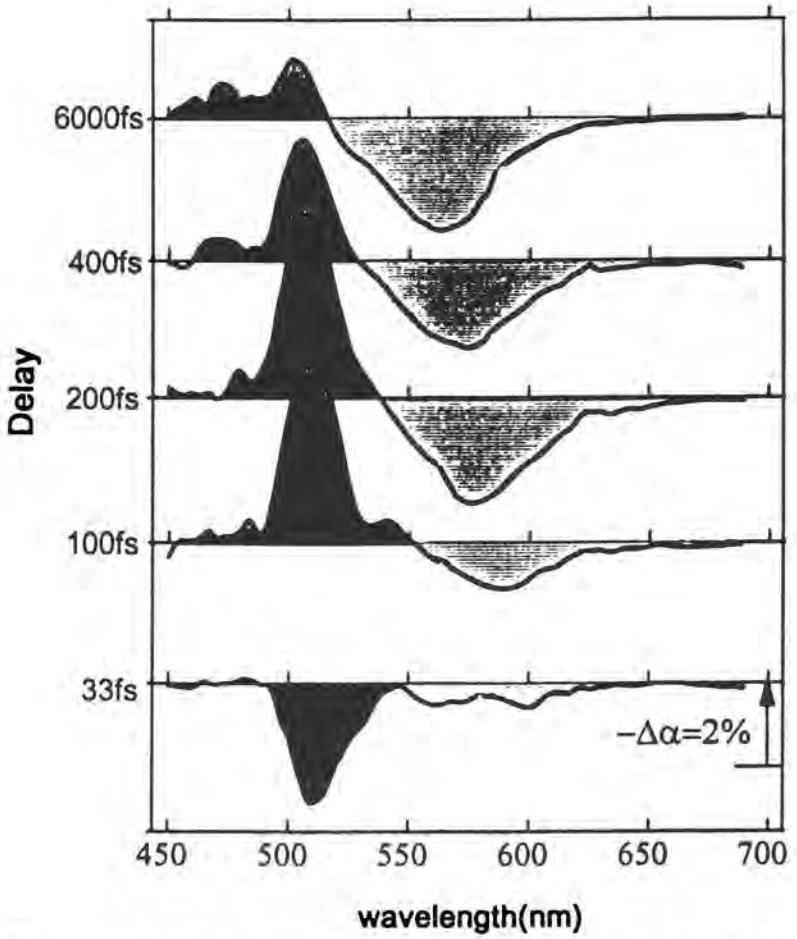

Fig. 2. Difference spectra of 11-*cis* rhodopsin (~ 10 fs probe) at various delays following a 35-fs pump pulse at 500 nm.

no photoproduct is formed after this time. The kinetic traces at 570 nm in Fig. 3 confirm this conclusion.

The time course of the absorption traces at 500 nm, within the rhodopsin bleach, is more complicated. The spectral traces in Fig. 2 suggest that the filling-in of the reactant bleach is slower than the photoproduct production. The kinetic traces in Fig. 3 at 500 nm quantify this observation. There is an initial absorption increase due to excited state absorption. Rapid wavepacket dynamics reveal the full bleach by ~ 150 fs. This bleach is filled in with a biphasic process having a fast (~ 200 fs) and a slow (~ 5 ps) time constant. The slow recovery that occurs after photoproduct formation is most likely due to cooling of hot reactant and photoproduct molecules and/or conformational relaxation on the ground state surface.

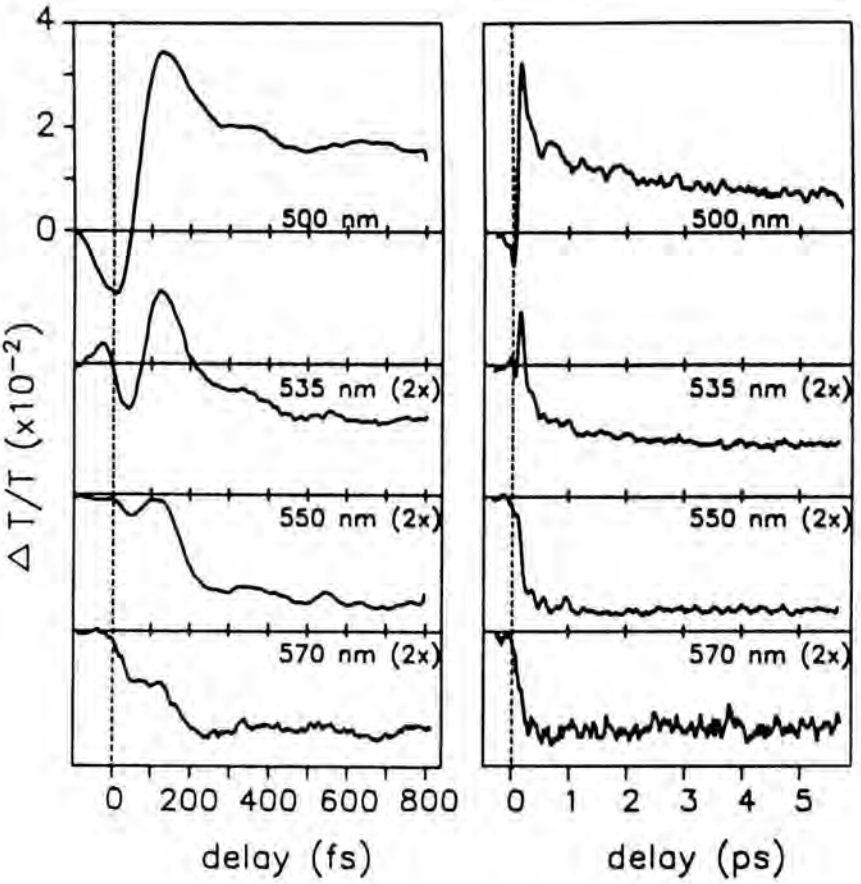

Fig. 3. Transient absorption measurements (~ 10 fs probe) of 11-*cis* rhodopsin at the indicated wavelengths following a 35-fs pump pulse at 500 nm.

A New Paradigm for Visual Photochemistry

Our observation that the *cis-trans* isomerization of rhodopsin is complete in only 200 fs has important implications for the photochemistry of vision and for photochemistry in general. First, 200 fs is faster than typical vibrational dephasing and vibrational relaxation times (Fragnito et al., 1989) suggesting that the photochemistry occurs from a nonstationary vibrational state. The idea that the photochemistry occurs through a vibrationally coherent process is also consistent with the fact that 200 fs is approximately the half-period of a 50 cm^{-1} torsional vibration. This frequency is appropriate for modeling the excited-state torsional isomerization potential energy surface of rhodopsins (Pollard et al., 1990). We conclude that the isomerization occurs in one continuous coherent

torsional motion as indicated in Fig. 1. In contrast, the traditional picture of photochemistry assumes that vibrational relaxation and dephasing bring the system to the bottom of the excited-state potential energy surface. Surface crossing then occurs from these perhaps thermally excited but stationary vibrational states. Our observations indicate that this traditional picture is not correct for rhodopsin; the surface crossing that leads to photoproduct occurs through vibrationally coherent states.

How should one model the rapid photoisomerization in rhodopsin? Our results suggest that after excitation the photoproduct is formed in an essentially barrierless transition following the nonadiabatic potential surface indicated by the broken lines in Fig. 1. The nonadiabatic surface carries the wavepacket rapidly and directly from the *excited state* of the reactant to the *ground state* of the product. This is envisioned as a dynamic coupling where the time-dependent wavepacket tunnels through the avoided crossing between the excited-state and ground-state potential surfaces. Such crossings can be described as a Landau-Zener process where the probability of crossing from the excited state of the reactant to the ground state of the product is given by (Bagchi & Fleming, 1990): $P_{LZ} \propto \exp -\{\Delta E^2/(2h\,|\Delta F|\,v)\}$. Here ΔE is the minimum energy gap between the adiabatic (solid) surfaces (see Fig. 1), h is Planck's constant, v is the wavepacket torsional velocity in the transition state and ΔF is the difference in slope of the two dashed (nonadiabatic) potential surfaces. For reasonable estimates of these parameters ($\Delta E = 5$ kcal/mole, $v\,|\Delta F| = 100\ \mathrm{cm}^{-1}/\mathrm{fs}$) we calculate that P_{LZ} is very close to the experimental value of the isomerization quantum yield (2/3). This shows that the Landau-Zener tunneling mechanism is a competent 1-dimensional model for the isomerization process in vision and supports the idea that vibrational coherence plays an important role in determining the quantum yield of this reaction.

The idea that the isomerization process in rhodopsin involves a vibrationally coherent tunneling process leads to several important predictions. (1) In the first pass through the transition state only 2/3 of the molecules in the ensemble couple through the surface to form product so the other 1/3 must reflect off and presumably vibrationally dephase on the excited-state potential surface. This residual dephased excited-state population may then undergo an incoherent internal conversion. However, the photoproduct is predominantly made through the initial fast vibrationally coherent process. Vibrational coherence and the femtosecond nuclear dynamics are thus critical for the process of vision. If the isomerizing rhodopsin chromophore lost its torsional kinetic energy before reaching the transition state, the quantum yield and hence the exquisite sensitivity of vision would be dramatically reduced. (2) One would expect that if the initial nuclear dynamics are slower then the quantum yield would be reduced. Indeed, femtosecond experiments on isorhodopsin, whose quantum yield is reduced to 0.2 (Suzuki & Callender, 1981), show that the initial dynamics are significantly slower (Schoenlein et al., 1993). Finally, the dynamic crossing of a wavepacket to the ground-state potential surface would predict that oscillations may be seen in the ground state of the product as has been observed in the case of ozone

(Banin & Ruhman, 1993). Indeed, close inspection of the 500 nm and 570 nm traces in Fig. 3 reveals oscillations that are experimentally reproducible. The vibrational frequency of these oscillations ($\sim 100\ cm^{-1}$) is qualitatively consistent with low-frequency torsional modes of rhodopsins (Loppnow & Mathies, 1988) suggesting that rapid dynamic passage through the transition state may be producing impulsive torsional excitation of the photoproduct. Detailed analysis of these oscillations may provide a basis for more accurate modeling of the photochemical potential surfaces in rhodopsin. In conclusion, this work presents experimental evidence for a new paradigm for visual photochemistry that may also be relevant for a wide variety of efficient photobiological processes (Vos et al., 1993).

References

Bagchi, B., and Fleming, G.R., *J. Phys. Chem.* **94**, 9-20, 1990.

Banin, U., and Ruhman, S., *Journal of Chemical Physics* **98**, 4391-4403, 1993.

Busch, G.E., Applebury, M.L., Lamola, A.A., and Rentzepis, P.M., *Proc. Natl. Acad. Sci. USA* **69**, 2802-2806, 1972.

Eyring, G., Curry, B., Mathies, R., Fransen, R., Palings, I., and Lugtenburg, J., *Biochemistry* **19**, 2410-2418, 1980.

Fragnito, H.L., Bigot, J.-Y., Becker, P.C., and Shank, C.V., *Chemical Physics Letters* **160**, 101-104, 1989.

Hayward, G., Carlsen, W., Siegman, A., and Stryer, L., *Science* **211**, 942-944, 1981.

Loppnow, G.R., and Mathies, R.A., *Biophys. J.* **54**, 35-43, 1988.

Mathies, R.A., Brito Cruz, C.H., Pollard, W.T., and Shank, C.V., *Science* **240**, 777-779, 1988.

Peteanu, L.A., Schoenlein, R.W., Wang, Q., Mathies, R.A., and Shank, C.V., *Proc. Natl. Acad. Sci. USA* **90**, 11762-11766, 1993.

Pollard, W.T., Lee, S.-Y., and Mathies, R.A., *J. Chem. Phys.* **92**, 4012-4029, 1990.

Schoenlein, R.W., Bigot, J., Portella, M.T., and Shank, C.V., *Appl. Phys. Lett.* **58**, 801, 1991a.

Schoenlein, R.W., Peteanu, L.A., Mathies, R.A., and Shank, C.V., *Science* **254**, 412-415, 1991b.

Schoenlein, R.W., Peteanu, L.A., Wang, Q.W., Mathies, R.A., and Shank, C.V., *J. Phys. Chem.* **97**, 12087-12092 (1993).

Shank, C.V., *Science* **233**, 1276-1280, 1986.

Suzuki, T., and Callender, R.H., *Biophys. J.* **34**, 261-265, 1981.

Vos, M.H., Rappaport, F., Lambry, J.-C., Breton, J., and Martin, J.L., *Nature (London)* **363**, 320-325, 1993.

Wald, G., *Science* **162**, 230-239, 1968.

Yoshizawa, T., and Wald, G., *Nature (London)* **197**, 1279-1286, 1963.

Authors' Addresses

R.A. Mathies, L.A. Peteanu, Q. Wang and C.V. Shank; Chemistry Department and R.W. Schoenlein, Q. Wang and C.V. Shank; Lawrence Berkeley Laboratory, University of California, Berkeley CA 94720, USA.
L.A. Peteanu; Current Address: Chemistry Department Carnegie-Mellon University, Pittsburg PA 15213.

Jean-Louis Martin, Jacques Breton and Marten H. Vos

Temperature Dependence of Low-Frequency Coherent Vibrational Motions in Bacterial Reaction Centers

Abstract

We report on the temperature dependence of the oscillatory features in the near-infrared emission band induced by direct excitation in the dimer absorption band of a bacterial reaction center.

Introduction

A major achievement allowed by the development of femtosecond spectroscopic techniques has been the real time vizualization of nuclear motion during the course of a chemical reaction (Khundkar and Zewail, 1990). In these studies, a wave packet is created on the potential energy surface of an electronic state by impulsive perturbation of an ensemble of molecules by a short light pulse and the dynamics of such a packet is subsequently inspected by a delayed probe pulse. The pioneering studies in this field were performed with simple alkali molecules in the gas phase, where dephasing mechanisms by intra- and intermolecular energy exchange between vibrational modes is virtually absent on the picosecond time scale. Extension of these studies to simple molecules in liquids has allowed to study the dephasing process by the solvent bath.

Oscillatory features have also been observed in the hexameric chromophore complex bound to the bacterial reaction center, a very complex protein macromolecule (Vos et al., 1991). We have recently demonstrated the vibrational origin of these features (Vos et al., 1993). The fact that specific frequencies ($< 100\ cm^{-1}$) dominate the oscillations in femtosecond transients implies that a) only a few low-frequency vibrational modes are strongly activated upon impulsive population of the excited state and b) these vibrational modes are underdamped. The latter result may seem surprising in view of the manifold of vibrational modes of the protein with which energy might be exchanged. The specific structure of the protein 'solvent' and the reduced degrees of freedom of the surrounding membrane (two-dimensional) solvent may prevent the fast randomization of the activated motion.

The ability to directly vizualize vibrational motion in a protein enables studies of the relation between nuclear motion and functioning. In the case of reaction

centers the coherence time of the observed vibrations strongly suggests that the highly efficient primary charge transfer reaction does not take place in a regime of thermally equilibrated vibrational motion, as usually assumed in conventional theories (Bixon and Jortner, 1986; Marcus and Sutin, 1985). The oscillatory features have mainly been studied at cryogenic temperatures, but they are also observable, albeit much weaker, at physiological temperatures (Vos et al., 1993). In the present paper the temperature dependence of the oscillatory features is analyzed in terms of the construction of the initially created wave packet and of the dephasing mechanisms.

The protein under study is a genetically modified bacterial reaction center from the purple bacterium *Rhodobacter capsulatus*, the D_{LL} mutant, which has been constructed by D.C. Youvan and his collaborators at MIT (Robles et al., 1990a, b). This mutant lacks the bacteriopheophytin acceptor, so upon excitation directly into the lowest electronic transition (P_-) the system evolves on the P^* excited state potential energy surfaces only on the picosecond time scale. Detection in the stimulated emission region, at lower energy than the P_- transition, ensures, in principle, that only excited state dynamics, and no ground state dynamics, are monitored. Oscillatory features which have the fundamental frequencies of the vibrational motions they reflect, are best observed at both sides of the stimulated emission spectrum, i.e. when probing the turning points of the potential energy surface. The detection wavelength in this study is 945 nm, which is at the red side of the stimulated emission spectrum for all temperatures.

Materials and Methods

Chromatophores of *R. capsulatus* D_{LL} devoid of antenna proteins were prepared at MIT by S.J. Robles and D.C. Youvan as described elsewhere (Robles et al., 1990a, b). The samples were diluted in glycerol (60% vol/vol) to an optical density of 0.5 at 870 nm (at room temperature) in a plexiglass cuvette with an optical path length of 1 mm. The samples were cooled in the dark in a convection cryostat with helium (< 100 K) or nitrogen gas. The temperature was measured with a calibrated thermodiode and maintained within ± 3 K. At each temperature, the sample was equilibrated for at least 15 minutes before each measurement. At intermediate temperatures, results obtained after cooling of the sample to a given temperature were identical to results obtained after warming to the same temperature.

The experimental apparatus is described in detail elsewhere (Martin and Vos, 1993). Briefly, pump pulses centered at 870 nm (spectral width 10 nm and temporal width 80 fs) were used to excite $\sim 20\%$ of the reaction centers with a repetition rate of 30 Hz. Continuum probe pulses, compressed to 30 fs at the detection wavelength, were used to monitor the excited state dynamics at $\lambda = 945$ nm, in the stimulated emission region of the excited state P^*. The relative transmission was obtained by shot-to-shot normalizing the intensity of the probe beam

to the intensity of the reference beam which does not pass through the sample. Noise due to fluctuations in the pump beam was minimized by normalizing the transmission change to the pump beam intensity at each shot.

Results

As charge separation does not take place in the D_{LL} mutant due to the absence of the bacteriopheophytin acceptor H_L, the excited state remains populated for a few hundred picoseconds (Breton et al., 1990). The overall stimulated emission therefore does not decay within a few picoseconds, but oscillations are superimposed on the kinetics, which has been interpreted as reflecting vibrational motion in the excited state (Vos et al., 1993). Fig. 1 shows that the oscillations are

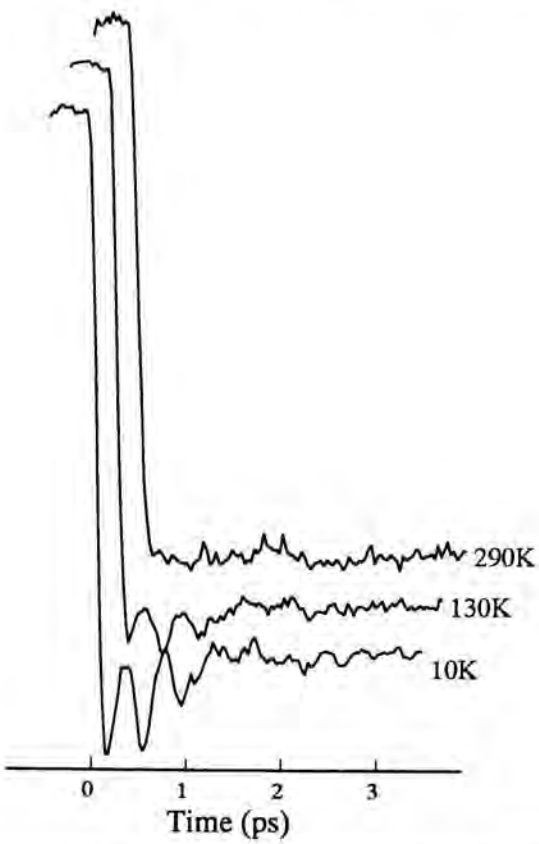

Fig. 1. Kinetics of stimulated emission at selected temperatures of chromatophores of *R. capsulatus* containing D_{LL} mutant reaction centers and devoid of light harvesting proteins. 80 fs Fourier transform limited pump pulses centered at 870 nm and 30 fs continuum probe pulses were used. The detection wavelength was 945 nm. The traces are normalized to the average amplitude of the overall signal.

most prominent at 10 K (amplitude ~20% of total signal) but are still clearly present at room temperature (amplitude ~4% of total signal). The oscillatory parts, isolated by subtracting a heaviside function from the data, (Fig. 2) show that increasing the temperature mainly causes a decrease in the amplitude of the oscillations, and does not strongly affect the damping of the oscillations.

The data were further analysed by Fourier transforming the data after the pump-probe overlap time (Fig. 3). Two bands (low temperature peaks at 15 and 77 cm^{-1}) are present. The 77 cm^{-1} band clearly broadens at higher temperatures and disappears at room temperature. The 15 cm^{-1} band decreases somewhat slower and broadens clearly only at 290 K. The limited spectral resolution (± 8 cm^{-1}) may mask broadening effects at higher temperatures. Fig. 4 shows the normalized amplitude of the two peaks at 15 and 77 cm^{-1} as a function of temperature.

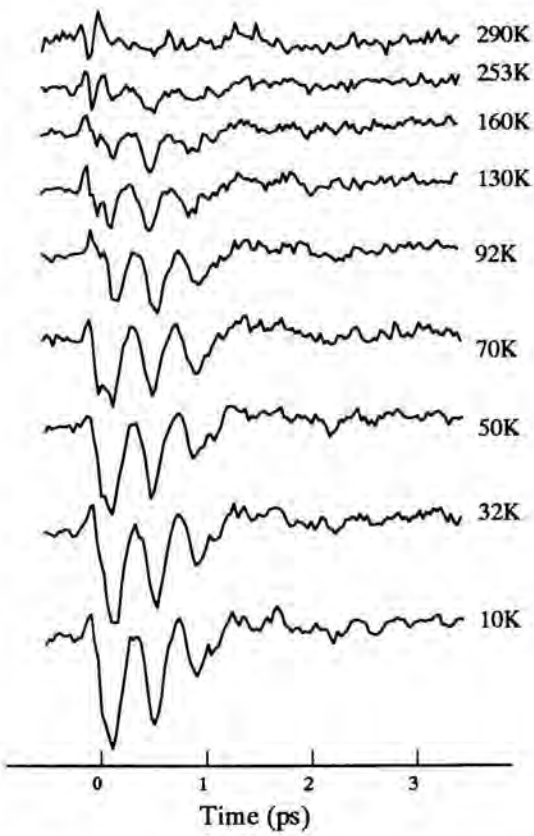

Fig. 2. Oscillatory parts of the data of Fig. 1 and of data obtained at intermediate temperatures. The oscillatory part is obtained by taking the residuals of a fit to a step function convoluted with the instrument response function.

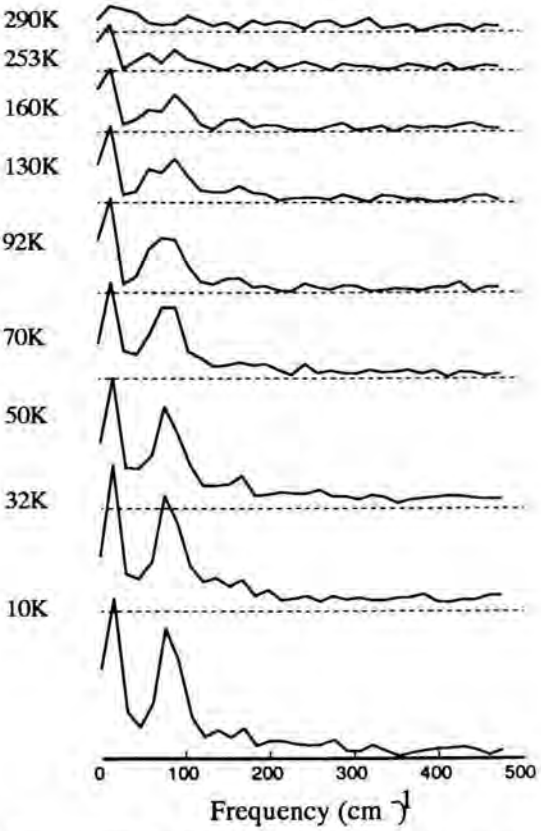

Fig. 3. Fourier transforms (FT) of the oscillatory parts of Fig. 2. Discrete FT describes the input signal $I(t)$ by its amplitudes A and phases ϕ as a function of the frequency ν as $\Sigma_n A_n Re(e^{i(2\pi\nu_n t - \phi_n)})$ (Re: real part) and was taken over a 2.13 ps data interval (64 points), yielding a spectral resolution of 15 cm^{-1}. The FT window was started at $t = 0.10$ ps, i.e. excluding the pump-probe overlap time interval. The spectral region above $\sim 200\ cm^{-1}$ represents the noise level of the data.

Discussion

We will discuss our results in terms of wave packet preparation and its subsequent time evolution on the excited state potential energy surface. The temperature is expected to affect both the efficienty of the dephasing process of the vibrational wave packet through collisional type of events and the quality of the impulsive preparation of the initial wave packet from the ground state, which vibrational levels are thermally populated in the steady state.

The damping observed in the femtosecond kinetics may be due to dephasing of the wave packets through collisions which randomizes the nuclear motion (incoherent dephasing). On the other hand, damping may also be due to frequency dispersion (coherent dephasing). In the latter case, a distribution of vibrational modes or levels is activated with slightly differing frequencies. The

initial phase correlation is then lost in a time related to the width of the frequency distribution, but the phase memory within each vibrational level is not lost and the distribution may in principal rephase (cf. Dantus et al., 1990). At 10 K the observed oscillations damp in about 2 ps for both the 15 and the 77 cm^{-1} mode (Figs. 1 and 2). If incoherent dephasing processes were the main source of the damping of the oscillations at 10 K, one would expect a decrease of the damping time upon warming, as the low frequency modes are expected to couple more strongly to the bath at higher temperatures. The fact that this is not observed (Fig. 2) suggests that incoherent dephasing is at least not the only source of dephasing; hence the incoherent vibrational dephasing time probably exceeds the lower limit of ~ 1 ps.

The temperature dependence of the initial preparation of the wave packet thus may be largely responsible for the decay of the amplitude of the oscillations at higher temperatures. The population distribution of the excited state vibrational levels is mainly determined by the pump bandwidth (130 cm^{-1}) at 10 K ($kT =$ 8 cm^{-1}) and by the ground state Bolzmann distribution at 290 K ($kT = 235$ cm^{-1}). Increasing the temperature from 10 K to 290 K relatively increases the initially populated excited state levels in a very similar manner: from ~ 9 to ~ 16 levels for the 15 cm^{-1} mode and from ~ 2 to ~ 3 for the 77 cm^{-1} mode. This may explain the general similarity of the amplitude decreases for both features (Fig. 4).

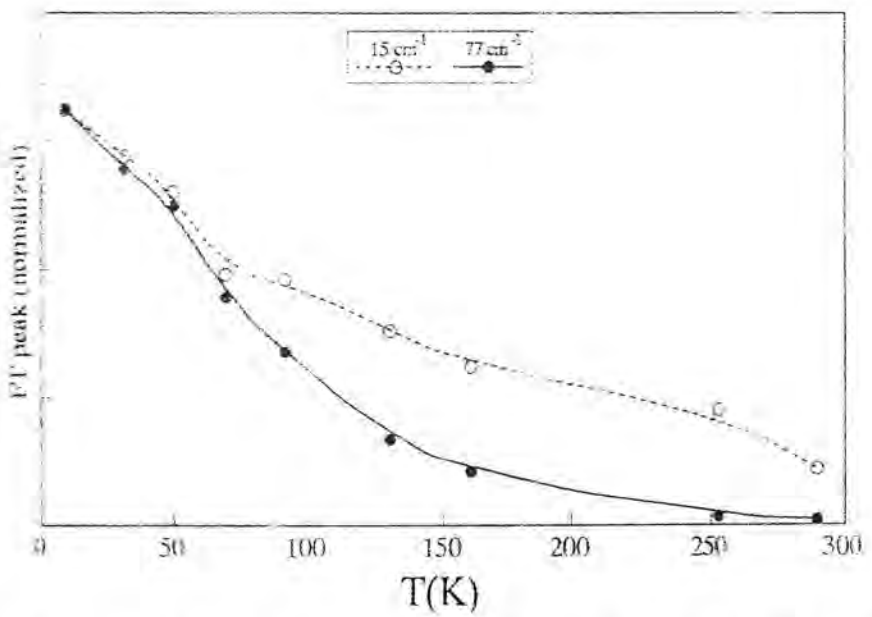

Fig. 4. Dependance of the amplitude of the FT peaks at 15 and at 77 cm^{-1} of Fig. 3 on the temperature. The curves are normalized at 10 K.

Apart from the distribution of vibrational levels, also the distribution of the initial phases within the wave packet may be affected by the temperature. At low temperature the ground state velocities are small and for a displaced mode the initially prepared wave packet will be near the turning point (where the wave packet velocity is zero). At higher temperature the initial velocities are higher and the phase of the wave packet is less well defined, leading to broader wave packets and lower amplitudes of the oscillations. Finally, the site inhomogeneous broadening ($\sim 170\ cm^{-1}$ at 10 K (Johnson et al., 1990)) probably increases at higher temperature, although no data are available on this issue. This would lead to effective broadening on warming of the distribution of levels excited by the pump pulse and of the distribution of nuclear coordinates probed by the probe pulse.

The decay of the amplitudes of both oscillatory features (Fig. 4) is roughly similar, but the decay of the amplitude of the $15\ cm^{-1}$ feature is less pronounced. This effect may in part be due to the fact that the relative broadening of the two features more strongly affects the peak amplitude of the higher frequency component, as the Fourier transform is discrete. Further, it seems that the broadening is biased towards higher frequencies, which selectively reduces the $77\ cm^{-1}$ component, which is at the edge of the vibrational bandwidth for the experiments (due to the 80 fs pump pulse).

A more quantitative analysis of the temperature dependence of the amplitudes of the oscillatory features must await the measurement of the probe wavelength dependence at different temperatures, as the maxima and width of the absorption, and presumably the stimulated emission, spectra are temperature-dependent. Nevertheless, an important result from this work for the functioning of reaction centers is that phase conservation also persists at physiological temperatures, thus stressing the possible importance of vibrational coherence for the primary electron transfer reaction in wild type reaction centers. In this latter case we will have to reconcile our observations with those from other groups using different experimental approaches including hole burning and resonance Raman experiments.

References

Bixon, M., and Jortner, J., *J. Chem. Phys.* **90**, 3795-3800, 1986.

Breton, J., Martin, J.-L., Lambry, J.-C., Robles, S.J., and Youvan, D.C., in: Reaction Centers of Photosynthetic Bacteria (ed. M.E. Michel-Beyerle), pp. 293-302 (Springer, Berlin), 1990.

Dantus, M., Bowman, R.M., and Zewail, A.H., *Nature* **343**, 737-739, 1990.

Khundkar, L.R., and Zewail, A.H., *Annu. Rev. Phys. Chem.* **41**, 15-60, 1990.

Marcus, R.A., and Sutin, N., *Biochim. Biophys. Acta* **811**, 265-322, 1985.

Martin, J.-L., and Vos, M.H., *Meth. Enzym.*, in press, 1993.

Robles, S.J., Breton, J., and Youvan, D.C., *Science* **248**, 1402-1405, 1990.

Robles, S.J., Breton, J., and Youvan, D.C., in: Reaction Centers of Photosynthetic Bacteria (ed. M.E. Michel-Beyerle), pp. 283-291 (Springer, Berlin), 1990.
Vos, M.H., Lambry, J.-C., Robles, S.J., Youvan, D.G., Breton, J., and Martin, J.-L., *Proc. Natl. Acad. Sci. USA* **88**, 8885-8889, 1991.
Vos, M.H., Rappaport, F., Lambry, J.-C., Breton, J., and Martin, J.-L., *Nature* **363**, 320-325, 1993.

Author's Addresses

Laboratoire d'Optique Appliquée
INSERM U275
École Polytechnique ENSTA
91120 Palaiseau
France
(J.-L.M. and M.H.V.)

SBE/DBCM
CEN Saclay
91191 Gif-sur-Yvette Cedex
France
(J.B.)

W. Zinth K. Dressler, P. Hamm, S. Buchanan and H. Michel

Is there a Bacteriochlorophyll Anion in the Primary Electron Transfer of Reaction Centers?

Abstract

Femtosecond transient absorption spectroscopy is used to study the primary reaction dynamics of bacterial reaction centers from *Rhodopseudomonas viridis*. Experiments at a variety of probing wavelengths give strong indication, that the electron transfer proceeds via the monomeric bacteriochlorophyll molecule as a real electron carrier.

1. Introduction

Important questions on the organization of the reaction centers (RC's) have been answered by x-ray structural analysis (for a review see Deisenhofer 1989). From these studies one knows that the different chromophores are arranged in two symmetry related branches A and B. Starting at the special pair P, a strongly coupled pair of bacteriochlorophyll (BChl) molecules, the two branches contain the monomeric bacteriochlorophyll (BChl) molecules B_A and B_B, the bacteriopheophytins (BPhe) (H_A, H_B) and the quinones (Q_A, Q_B). Spectroscopy on reaction centers has revealed that the two pigment branches are spectroscopically non-equivalent and that electron transfer uses predominantly the A branch. In functional reaction centers the photosynthetic action is initiated by optical excitation of the special pair, which acts as the primary electron donor. It is generally accepted that the electron transfer (ET) starts at the special pair P and that the primary reaction is finished by the ET from the bacteriopheophytin H_A to the quinone Q_A which occurs with a time constant of 200 ps. However, there exist different opinions on the processes of the first part of the ET reaction which transfer the electron from the special pair P to the BPhe H_A: Experimental observations have presented different kinetic processes which are related to the first ET steps. At room temperature, the decay of the electronically excited state P^* of the special pair was found to proceed with approximately 3 ps (Breton 1986, Martin 1986, Holzapfel 1989, 1990). An additional subpicosecond component was found with timeconstants of 0.9 ps and 0.65 ps in *Rhodobacter* (*Rb.*) *sphaeroides* and *Rhodopseudomoras* (*Rps.*) *viridis* respectively. Recently, emission experiments with high dynamic range have shown bi(multi)-exponential features

in the decay of P^* (Du 1992, Hamm 1993): There is a dominating 2.3 ps decay and a weak (relative amplitude around 20%) 7 ps contribution (Hamm 1993). Very weak slower emission processes occur in the ten to houndred picosecond regime. At cyrogenic temperatures the 3 ps and the subpicosecond process become faster and some oscillations appear in transient absorption traces. The basic interpretations of the experimental data follow two major lines:

(i) In the superexchange ET model the electron is transferred directly from the special pair P to the bacteriopheophytin H_A on the A branch. The monomeric bacteriochlorophyll is only used as a virtual electron carrier (Breton 1986, 1988, Martin 1986, Fleming 1988). The additional time constants observed must be assigned in the superexchange model to an excited state vibrational relaxation or to a functional heterogeniety of the RC's.

(ii) In the stepwise ET model the monomeric bacteriochlorophyll B_A is a real electron carrier and the electron undergoes two reaction steps, before it reaches the bacteriopheophytin. In this model the initial electron transfer to B_A occurs in approximately 3 ps while a second transfer step to the bacteriopheophytin H_A should be faster taking less than one picosecond (Holzapfel 1989, 1990). It causes the 0,65 ps (0,9 ps) time constant.

In this paper we present a discussion of the primary ET reaction. We will focus on the ET at room-temperature corresponding much better to physiological conditions than cryogenic temperatures. We will begin with a description of first order processes, which are well visible at least at one probing wavelength in transient absorption experiments. By this way, we believe to explain the photosynthetic action of the majority of RC's. In a second step, we extend the discussion to the more detailed measurements and will present working models for the description of the whole RC set.

2. Theoretical Aspects of Ultrafast Spectroscopy of Electron Transfer Reactions

In the standard nonadiabatic description of transient absorption spectroscopy one treats the molecular system as a set of electronic states where the vibrational levels of each state are in thermal equilibrium at some temperature T. As a consequence these states have well defined absorption properties. Transitions between the states are governed by reaction rates and the population of intermediate states may be calculated from a rate-equation system (Holzapfel et al. (1990) and Finkele et al. (1990)). For weak excitation the absorbance change is a sum of exponentials convolved with the instrumental response function. The number of exponentials is equal to the number of intermediate states populated during the reaction.

The situation becomes considerably more complicated when the selective, non-thermal population of specific vibrational levels has to be considered (see for instance Bixon et al. (1991) and references therein). Adiabatic processes have to be taken into account when the reaction i.e. the transition between different electronic states is faster than thermalization of the vibrational states within

each electronic state. An estimate for the relevant time scales is given by the vibrational relaxation times.

In photosynthesis large chromophore molecules with many vibrational modes are of relevance. Here relaxational processes of vibronic modes in the excited electronic state are known to be very fast; e.g. at room temperature and in the condensed phase, vibrational relaxation in the excited electronic state even of medium sized dye molecules was found to have dephasing times below 100 fs and vibrational energy relaxation times of a few 100 fs (Brito Cruz et al., 1988). As a consequence non-adiabatic theory is well suited to describe room temperature ET processes slower than 500 fs (Bixon et al., 1991).

3. Primary Reaction Dynamics in Rps. viridis

The experimental results presented in this paper are obtained on RC from *Rps. viridis*. The preparation of the reaction centers and details of the experimental system are described in Dressler et al. (1991). Characteristic experimental results are depicted in Fig. 1 and 2: The first state in the photosynthetic reaction sequence is the excited electronic level P^* of the special pair P populated directly by the optical excitation process. P^* is readily studied by its stimulated emission on the long wavelength side of the special pair Q_y absorption band. In Fig. 1 at the probing wavelength of 1050 nm, the absorption decrease around delay time zero is due to stimulated emission and depopulation of the ground state. Subsequent relaxation of the signal reflects the decay of P^*. Weak absorption changes seen at later delay times, $t_D > 50$ ps, can be related with the ET to the quinone Q_A. A more carefull inspection of the signal decay in the 0 ps to 50 ps regime leads to the following results: The best monoexponential fit of the data points

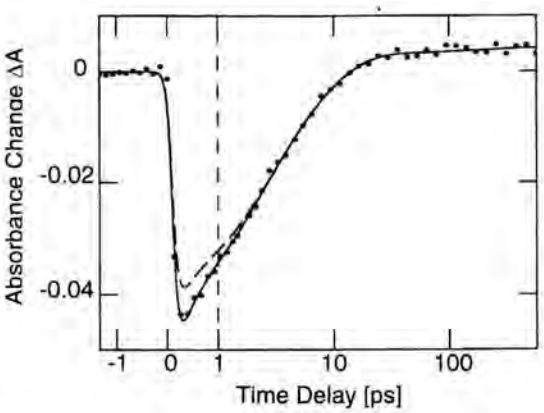

Fig. 1. Time resolved absorption data (circles) for RC from *Rps. viridis*. The curves are calculated model functions. For the solid curve five time constants, 0.65 ps, 2.3 ps, 7 ps, 200 ps, and infinity were used while the broken curve was calculated without the 0.65 ps component. A linear scale of the delay time is used for $t_D < 1$ ps; a logarithmic scale is applied at later delay times.

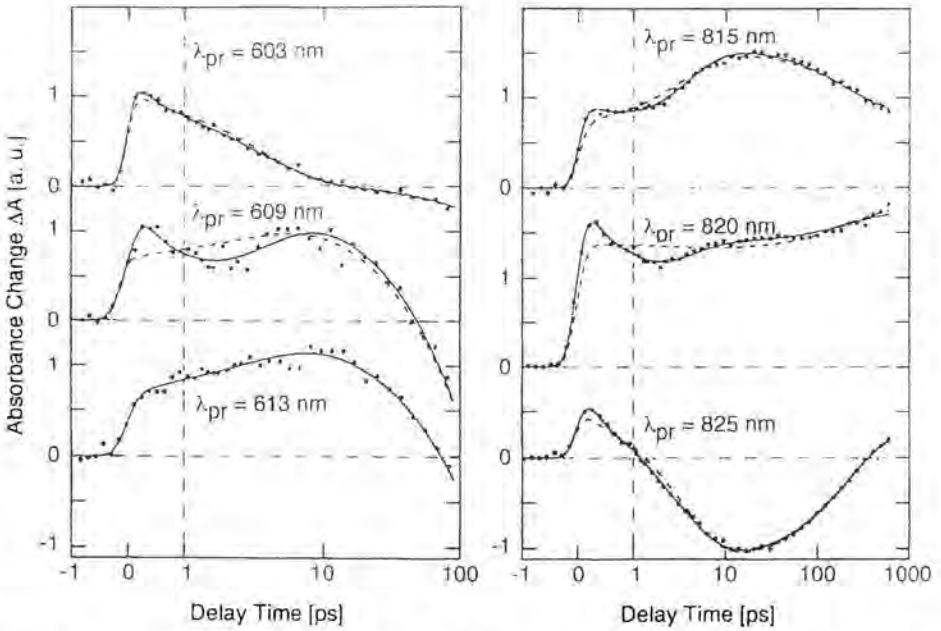

Fig. 2. Transient absorption data (points) for RC from *Rps. viridis* recorded in the Q_x (left) and Q_y (right) absorption band of the accessory bacteriochlorophyll. The solid curves are calculated for a four component (0.65 ps, 3.5 ps, 200 ps, infinity) the broken curve for a three component model (3.5 ps, 200 ps, infinity).

results in a time-constant of $\simeq 3.5$ ps. However there are deviations from the experimental data points at early delay times (which can be explained by a 0.65 ps component with negative amplitude, see below) and weaker ones around 10 ps (for details see last section). Additional information is obtained from probing wavelengths in the Q_x absorption band of the BChl (Fig. 2, left) and in the vicinity of the BChl Q_y absorption bands (Fig. 2, right). Here a fine tuning of the probing wavelength revealed rapidly changing spectral features with a clearly visible subpicosecond component. The distinct visibility of the fast component (time constant $\simeq 0.65$ ps) is restricted to very narrow spectral ranges. Nevertheless it amounts at some wavelengths to more than 30% of the peak absorption change. The fast kinetic component is also visible in the spectral range around 650 nm where the anions of BChl and BPhe absorb. At these wavelengths a final absorption transient occurs which is ($\tau \simeq 200$ ps) related with the ET from H_A to the quinone Q_A.

The observation of three kinetic components with two time constants below 5 ps parallels the previous findings for *Rb. sphaeroides* (Holzapfel 1989, 1990). The experimental data strongly support the idea that the primary ET reactions of *Rb. sphaeroides* and *Rps. viridis* proceed via similar reaction models (Dressler 1990). While the qualitative agreement of the experimental results is striking it should be recalled that the subpicosecond kinetic component is somewhat faster

in RC of *Rps. viridis* than in RC of *Rb. sphaeroides*. In both RC's the fast kinetic component has the following properties: (i) At most wavelengths it appears with a rather small amplitude. (ii) Its amplitude is largest in spectral ranges where BChl (Q_x, Q_y) or BChl anions (660 nm) are known to have a strong absorption. While a qualitative inspection of the spectral dependence seems to relate the subpicosecond component with the monomeric BChl B_A a sound interpretation has to take into account the mathematical description of the transient absorption experiment.

4. A First-Order Description of the Primary Electron Transfer

The structural arrangement of the RC supports the idea that the electron is transferred in several steps from the special pair P via B_A, H_A to Q_A. We now discuss this model in more detail (Model A of Fig. 3): The transient experimental data presented above do not give any contradiction against this reaction model. Far from it, the analysis of the transient data using reaction model A yields the spectra of the intermediates and would expect from in vitro measurements of the chromophores (Fajer 1973, 1976). This finding can be illustrated using the data of Fig. 1. In this experiment the transient absorption at 1050 nm in the gain region was investigated. Surprisingly there was some faster initial decay of the signal at early delay times which is not seen in the short wavelength side of the gain. Within a stepwise ET-model one would not expect to see a rapid initial decay of the gain. Therefore this decay must be due to another mechanism: Data analysis using reaction model A indicates that such a rapid initial decay of the signal occurs if the second intermediate I_2 has an increased absorption in this spectral range. This observation fits well to the interpretation of I_2 being the radical pair state $P^+B_A^-$ as spectra of the BChl *b* anion show a distinct absorption band around 1050 nm (Fajer 1973, 1976). A similar qualitative estimate holds at all wavelengths, where the in vitro spectra of BChl *b* and its anion differ strongly: in a spectral region where a bleaching of a BChl band upon anion formation should occur (605 nm and 825 nm) a positive amplitude of the 0.65 ps kimetic component is expected. On the other hand in spectral regions where the BChl anion has stronger absorption (around 650 nm and 1050 nm) a negative amplitude should occur. In Fig. 4b, the amplitude ΔA of the 0.65 ps kinetic component determined from a number of different transient experiments is plotted as a function of the probing wavelength. The experimentally found values of ΔA agree well with the predictions given by the in vitro spectra.

In model B based on the superexchange ET there is no intermediate which could be related to the subpicosecond kinetic component. In order to consider the subpicosecond kinetic component one has to introduce another intermediate or a modified reaction scheme: a first possibility would use two excited electronic states related by vibrational relaxation. However this assumption does not fit to the temperature dependence of the reaction rates (Lauterwasser 1992).

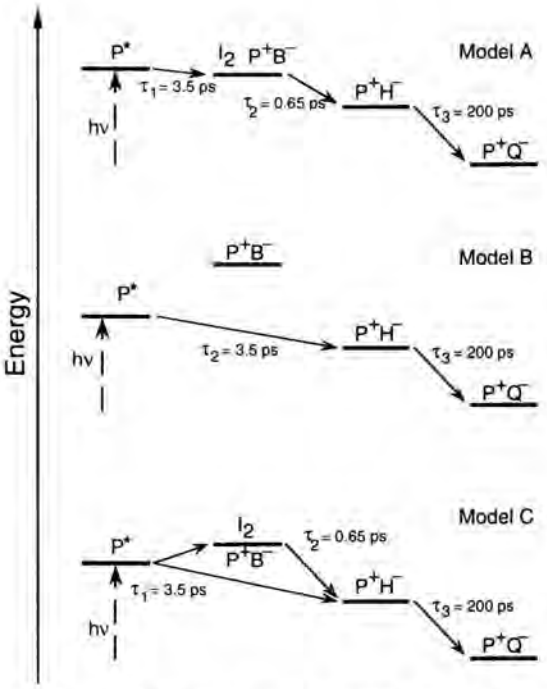

Fig. 3. Schematic representation of possible reaction models for the primary photosynthetic ET. The time constants shown in the figure represent the values for room temperature.

Another interpretation would involve a distribution of reaction rates (Kirmaier 1990, Du 1992). This possibility will be dicussed below in more detail.

Very promising is model C which interpolates between the stepwise and the superexchange ET in a consistent picture (Bixon 1989, 1991): Here the energy of state $P^+B_A^-$ is the relevant parameter. For an energy of state $P^+B_A^-$ far below and above the energy of P^* the stepwise ET-mechanism and the (coherent)

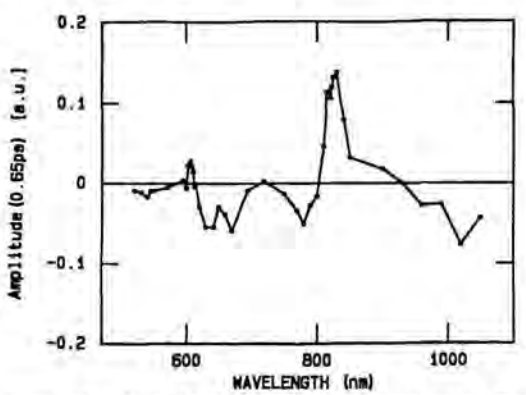

Fig. 4. Amplitude spectrum related to the 0.65 ps kinetic component. The bands fit well the in vitro spectral properties of BChl anions.

superexchange-mechanism applies respectively. For an energy of state $P^+B_A^-$ close to the energy of P^* both reaction mechanisms may occur in parallel. In model C I_2 must have the spectral properties of a radical pair state $P^+B_A^-$. From this one obtains restrictions for the model parameters. We find a consistent spectra for an energy of state $P^+B_A^-$ which is about 200 $cm^{-1} \pm 150$ cm^{-1} below that of P^*. As a consequence, a maximum yield of the direct superexchange transfer at room temperature is below 10%.

5. Higher-Order Effects in Primary Electron Transfer

Very careful inspection of the measurements at $\lambda = 1050$ nm (see Fig. 1a) suggests a weak systematic deviation of the data from a model function with a 3.5 ps decay time in the later part of the decay (for this reason the curve in Fig. 1 was calculated using a 2.3 ps and a 7 ps kinetic component). This observation is an indication for additional kinetic components in the decay of P^*. While it is difficult to observe this deviation from a monoexponential decay in transient absorption experiments, transient stimulated emission techniques having a larger signal to background ratio show this phenomenon convincingly (Hamm 1993, Du 1992). The results of such experiments are: In standard RC preparations of *Rb. sphaeroides* the time constant of 3.5 ps breaks up into a 2.3 ps process with large amplitude and a 7 ps process with a small amplitude of approximately 20% (Hamm et al. 1992, 1993). Similar results were obtained by Du et al. (1992). When we introduce the additional time constant in the fit of the transient absorption data, we obtain a small amplitude of the 7 ps kinetic component, which is, within experimental accuracy, at all wavelengths proportional to the amplitude of the strong 2.3 ps component.

The observation of an additional time constant requires an extension of the reaction models: Assuming a homogeneous sample with only one type of RC one has to assign the longer emission decay time to a new intermediate state (we call it N). The experimental observation of N in emission indicates that it is coupled directly to P^*. There are several possibilities to introduce the new state in a reaction model. Most promising is the assignment of N being the radical pair state $P^+B_B^-$. In this model the electron can transiently reach the monomeric BChl on the inactive *B*-branch. Another explanation is given by the assumption of a functional heterogeneity of the RC in the sample (Kirmaier 1990, Du 1992). In this case one would deal with two or more types of RC having different speeds of the primary ET reaction. This possibility explains well the bi-(multi-) exponential decay of the emission and the fixed amplitude ratio observed in the experiment for the amplitudes of the 2.3 ps and the 7 ps components. The origin of the 'heterogeneity' of the RC may be a distribution of the energy of an intermediate level or a distribution of the distance between two chromophores. Recently it was argued whether a microheterogeniety or a distribution of RC' properties may also account for the subpicosecond kinetic component. Taking this assumption for serious one obtains quite unusual spectral

properties of this subset of RC (In detail: Their special pair absorption remains unchanged but their emission is red-shifted; the BChl absorption decreases upon decay of P^* but the electrochromic shift due to the formation of $P^+H_A^-$, which is observed for the other RC's, is missing; around 650 nm, the P^* absorption must be weaker or the BPhe anion absorption must be higher than in the slower RC's; however in the 605 nm region the opposite behaviour occurs: the P^* absorption must be higher or the BPhe anion absorption must be weaker than in the slower RC's). As this combination of properties is quite unlikely we may use this as an argument to support the notion, that the subpicosecond kinetic component is due to an intermediate state and not to a heterogeniety of the RC.

6. Conclusions

Time resolved spectroscopy on reaction centers of the purple bacterium *Rps. viridis* indicate that electron transfer for the major fraction of native RC occurs stepwise using the different chromophores of the *A*-branch as real intermediate electron carriers. The observation of the bi-(multi-)exponentiality seen in emission and in transient absorption spectroscopy may be taken as an indication for a transient population of the radical pair state $P^+B_B^-$ on the 'inactive' *B* chromophore branch or for a microheterogeniety of the reaction centers. The relative amplitudes observed in the experiments suggest, that only a minor fraction of the reaction centers follows the slower reaction mechanism.

7. References

Bixon, M., Jortner J., Michel-Beyerle, M.E., and Ogrodnik, A., *Biochim. Biophys. Acta* **977**, 273, 1989.

Bixon, M., Jortner, J., and Michel-Beyerle, M.E., *Biochim. Biophys. Acta* **1056**, 301, 1991.

Breton, J., Martin, J.-L., Migus, A., Antonetti, A., and Orszag A., *Proc. Natl. Acad. Sci. USA* **83**, 5121, 1986.

Breton, J., Martin, J.-L., Fleming G.R., and Lambry J.-C., *Biochemistry* **27**, 8276, 1988.

Brito Cruz, C.H., Gordon, J.P., Becker, P.C., Fork, R.L. and Shank, C.V., *IEEE J. Quantum Electron.* **24**, 261, 1988.

Deisenhofer, J., and Michel H., *EMBO J.* **8**, 2149, 1989.

Dressler, K., Finkele, U., Lauterwasser, C., Hamm, P., Holzapfel, W., Buchanan, S., Kaiser, W., Michel, H., Oesterhelt, D., Scheer, H., Stilz, H.U., and Zinth, W., In: *Springer series in biophysics*, Vol. 6. Reaction centers of photosynthetic bacteria (ed. M.E. Michel-Beyerle), pp. 135, 1990.

Dressler, K., Umlauf, E., Schmidt, S., Hamm, P., Zinth, W., Buchanan, S., and Michel, H., *Chem. Phys. Lett.* **183**, 270, 1991.

Du, M., Rosenthal, S.J., Xie, X., Di Magno, T.J., Schmidt, M., Hanson, D.K., Schiffer, M., Norris, J.R., and Fleming, G.R., *Proc. Natl. Acad. Sci. USA* **89**, 8517, 1992.
Fajer, J., Borg, D.C. , Forman, A., Dolphin, D., and Felton, R.H., *J. Am. Chem. Soc.* **95**, 2739, 1976.
Fajer, J., Davis, M.S., Brune, D.C., Spaulding, L.D., Borg, D.C., and Forman, A., *Brookhaven Symp. Biol.* **28**, 74, 1976.
Finkele, U., Dressler, K., Lauterwasser, C., and Zinth, W., In: *Springer series in biophysics*, Vol. 6. Reaction centers of photosynthetic bacteria (ed. M.E. Michel-Beyerle), pp. 127, 1990.
Fleming, G.R., Martin, J.L., and Breton, J., *Nature* **333**, 190, 1988.
Hamm, P., Gray, K.A., Oesterhelt, D., Feick, R., Scheer, H., and Zinth, W., *Biochim. Biophys. Acta* **1142**, 99, 1993.
Hamm, P., and Zinth, W., Ultrafast Phenomena VIII, *Springer Series in Chemical Physics* Vol. 55, 541, 1993.
Holzapfel, W., Finkele, U., Kaiser, W., Oesterhelt, D., Scheer, H., Stilz, H.U., and Zinth, W., *Chem. Phys. Lett.* **160**, 1, 1989.
Holzapfel, W., Finkele, U., Kaiser, W., Oesterhelt, D., Scheer, H., Stilz, H.U., and Zinth, W., *Proc. Natl. Acad. Sci. USA* **87**, 5168, 1990.
Kirmaier, C., and Holten, D., *Proc. Natl. Acad. Sci. USA* 87, 3552, 1990.
Lauterwasser, C., Finkele, U., Scheer, H., and Zinth, W., *Chem. Phys. Lett.* **183**, 471, 1991.
Martin, J.-L., Breton, J., Hoff, A. J., Migus, A., and Antonetti, A., *Proc. Natl. Acad. Sci. USA* **83**, 957, 1986.
Michel-Beyerle, M.E., Plato, M., Deisenhofer, J., Michel, H., Bixon, M., and Jortner, J., *Biochim. et Biophys. Acta* **932**, 52, 1988.
Michel-Beyerle, M.E., Bixon, M., and Jortner, J., *Chem. Phys. Lett.* **151**, 188, 1988.

Addresses:

W. Zinth, P. Hamm
Institut für medizinische Optik der Universität München
Barbarastraße 16/IV, 80797 München , Germany
K. Dressler
Physik Department E 11 der Technischen Universität München, 80333 München, Germany
S. Buchanan, H. Michel
Max-Planck-Institut für Biophysik, Heinrich-Hoffmannstraße 7, 60528 Frankfurt, Germany

E.W. Castner, Jr. and Y.J. Chang

Femtosecond Dynamics in Hydrogen-Bonded Solvents

Abstract

We present results on the ultrafast dynamics of pure hydrogen-bonding solvents, obtained using femtosecond Fourier-transform optical-heterodyne-detected, Raman-induced Kerr effect spectroscopy. Solvent systems we have studied include the formamides, water, ethylene glycol, and acetic acid. Inertial and diffusive motions are clearly resolved. We comment on the effect that such ultrafast solvent motions have on chemical reactions in solution.

Introduction

Many solution-phase chemical transformations have a strong dependence on both the static and dynamic properties of the solvent. When considered in greater detail, macroscopic properties of solvents such as viscosity or dielectric constant are actually a measure of the microscopic structure and dynamics of molecular liquids. One class of solution-phase reactions for which the solvation-coordinate is strongly coupled to the reaction coordinate is that of adiabatic charge-transfer reactions. In particular, certain electron-transfer reactions in the barrierless regime have effective rates that are predicted to be limited by the solvent relaxation dynamics. In turn, specific features of the solvent relaxation dynamics in molecular liquids have long been studied by techniques such as magnetic resonance T_1-relaxation, dielectric relaxation, Rayleigh and Raman light-scattering, and far-infrared absorption spectroscopy, in addition to the more recent ultrafast laser techniques, such as the time-dependent fluorescence Stokes-shift (TDFSS).

We present results using a femtosecond laser polarization spectroscopy technique that encompass all of the ultrafast dynamical results of the above mentioned experiments. Our ultrafast laser spectroscopy data provide a holistic solvent relaxation profile that includes the longer-time diffusive solvent relaxation dynamics, in addition to the more rapid inertial motions. The inertial motions include librations, translations, and collisions. By obtaining a complete profile of the neat solvent dynamics on all relevant time-scales, we can then test theoretical predictions and molecular dynamics simulations that model the effect of solvent relaxation on the solvation dynamics. These solvent dynamics can directly

affect the outcome of chemical reactions. In this contribution, we present the results of our recent experiments on the femtosecond relaxation of the dipolar, strongly associated, and hydrogen-bonding liquids formamide, *N*-methylformamide (NMF), *N*,*N*-dimethylformamide (DMF), acetic acid, water, and ethylene glycol.

The time-resolved optical Kerr effect has been used to study molecular liquids since Duguay and Hansen generated an optical gate in CS_2 (Duguay and Hansen, 1969). In the past decade, several workers have used a heterodyne scheme (Levenson and Eesley, 1979) to make the detected signal linear in the molecular nonlinear optical response (Greene and Farrow, 1982; McMorrow, et al., 1988; McMorrow, 1991; McMorrow and Lotshaw, 1991; Cho, et al., 1992; McMorrow, et al., 1992; Wynne, et al., 1992; Chang and Castner, 1993; McMorrow and Lotshaw, 1993). Optical-heterodyne detected, Raman-induced Kerr-effect spectroscopy (OHD-RIKES) is a very sensitive nonlinear optical technique that measures the time-dependent relaxation of a coherent macroscopic polarization induced in the transparent liquid sample by an intense femtosecond pulse with a peak power-density of $\leqslant 2\,GW/cm^2$, and probed by a probe pulse about 20 times weaker. As the molecules of the neat liquid sample relax both individually and collectively, they rotate, librate, vibrate, translate, and collide. The coherent macroscopic polarization oscillates and decays as a result of the molecular motions. While the technique is electronically non-resonant, i.e., the samples do not absorb the near-infrared or visible pulses used, the low-frequency intermolecular vibrations are impulsively excited. Using laser pulses of $\leqslant 50$ femtoseconds, all of the single-molecule and collective motions can be impulsively excited by the broad, Fourier-transform limited spectrum of the actinic pulse. As in the solid state, the low-frequency collective vibrations are expected to couple most strongly with excited states or transition states of reacting species. Hattori, et al. (Hattori, et al., 1991) have developed an analogous technique that also yields the same molecular information.

The impulsive-stimulated-Raman-scattering (ISRS) technique (Ruhman, et al., 1988; Yan, et al., 1988) measures the same ultrafast solvent dynamical properties as our OHD-RIKES experiment, because in both cases, the signal arises from the same molecular nonlinear optical (polarizability) response. When performed in a polarization-sensitive transient-grating/four-wave-mixing folder BOXCARS geometry, the ISRS experiment has the distinct advantage of being able to measure either pure nuclear-coordinate or pure electronic dynamics directly (Etchepare et al., 1987). In this case, suppression of the electronic hyperpolarizability is clearly advantageous for the study of liquids such as water and ethylene glycol, where the electronic contribution to the molecular nonlinear optical response dominates the signal. There are two drawbacks of ISRS relative to OHD-RIKES. They are: i) ISRS requires pulse-energies in the range of 100 nJ-1 μJ, while OHD-RIKES pulse energies need only be in the 100 pJ-5 nJ range, and ii) the ISRS signal is proportional to the square of the molecular nonlinear optical response, while OHD-RIKES signals are linear in the same response. Point i) is not a limitation in many laboratories, where femtosecond

pulse energies after amplification of a pico-/nano-Joule oscillator to up to > 1 mJ is now a standard technology. However, it is quite convenient to be able to do the OHD-RIKES experiment with an un-amplified Ti:Sapphire femtosecond oscillator. With regard to point ii): the square of the molecular response will contain cross-terms that complicate the analysis of ISRS data relative to OHD-RIKES data, without adding any additional molecular dynamical information. On the other hand, strain-birefringence is a difficult problem in extending the OHD-RIKES experiment to extremes of low-temperatures (in cryostats) and high-pressures (in diamond-anvil cells). These limitations have been overcome for the study of the femtosecond dynamics of CS_2 using the ISRS technique (Ruhman, et al., 1987; Kohler and Nelson, 1992). Thus, because each technique has clear merits and disadvantages, the ideal will be to select one or the other based on the limitations imposed by the liquid under study, such as the magnitude of the total molecular nonlinear optical response, and the relative amplitudes of the electronic versus the nuclear contributions to this response.

A general feature of our femtosecond solvent dynamical results is that in all liquids there appears a clear separation of time-scales between diffusive and inertial dynamics. The diffusive dynamics are temperature-dependent, while the inertial (or non-diffusive) dynamics are only weakly temperature dependent. Previous studies of solvent dynamics by dielectric relaxation, NMR T_1 relaxation, and Rayleigh light scattering have tended to concentrate on the diffusive component of the dynamics, which leads to predictions for solvent-dependent chemical reaction rates that are too slow. Rayleigh and Raman spectroscopy signals arise from the same molecular polarizability tensor that is the laser-molecular coupling responsible for the OHD-RIKES signal, but because of our time-domain measurement, we can easily separate the diffusive (Lorentzian) and inertial parts of the low-frequency dynamics. By combining data analysis in the time and frequency domains, which is possible because we use Fourier-transform limited laser pulses, we can develop appropriate models that take into account lineshapes, dephasing rates, lifetimes, and relative amplitudes of the different motions contributing to the ultrafast solvent relaxation.

Experimental

The experimental setup we use to measure femtosecond solvent dynamics by the OHD-RIKES experiment has been described in detail recently by several authors (McMorrow, Lotshaw et al., 1988; McMorrow and Lotshaw, 1991; Chang and Castner, 1993; Chang and Castner, 1993). Thus only a few brief comments will be given here. One important feature of our experiment is that we are using an ultra-stable modelocked Ti:Sapphire laser for our source of femtosecond pulses. We routinely use pulses of ~ 50 fs, with a sech^2 pulse shape. The Spectra-Physics Tsunami laser gives an output at 780 nm of ~ 650 mW at 82 MHz repetition rate, or ~ 8 nJ/pulse, when pumped by 6.0 W from an all-lines BeamLok 2060-7S Ar^+ laser in a TEM_{00} spatial mode.

A schematic diagram of the experimental setup is shown in Figure 1. The geometry is that of a standard pump-probe polarization experiment, where an uncoated wedge splits off $\sim 5\%$ of the beam for the probe, with the remainder used for the pump. A Glan-Laser calcite polarizer sets the vertical polarization of the pump beam, while the probe beam is rotated to $+45^\circ$ for a maximal projection of the probe onto both axes of the induced birefringence. Glan-Thompson calcite polarizers are used in the probe beam, with a mica quarter-wave retarder located before the sample. When all optics in the probe beam are set for maximum extinction, the ratio of probe transmitted through blocked and fully open polarizers has been measured to be 1.6×10^{-8}, including the sample cell, sample, and focusing lenses. The calcite polarizers are obtained from Karl Lambrecht Corp., and the mica waveplates from Optics for Research. The zero-order half-wave retarders were from Newport Corp., and the 1 mm path fused silica sample cells were from NSG Precision Cells.

An out-of-phase local-oscillator is generated for the optical-heterodyne detection by rotating the input polarizer by 1°. The out-of-phase local-oscillator

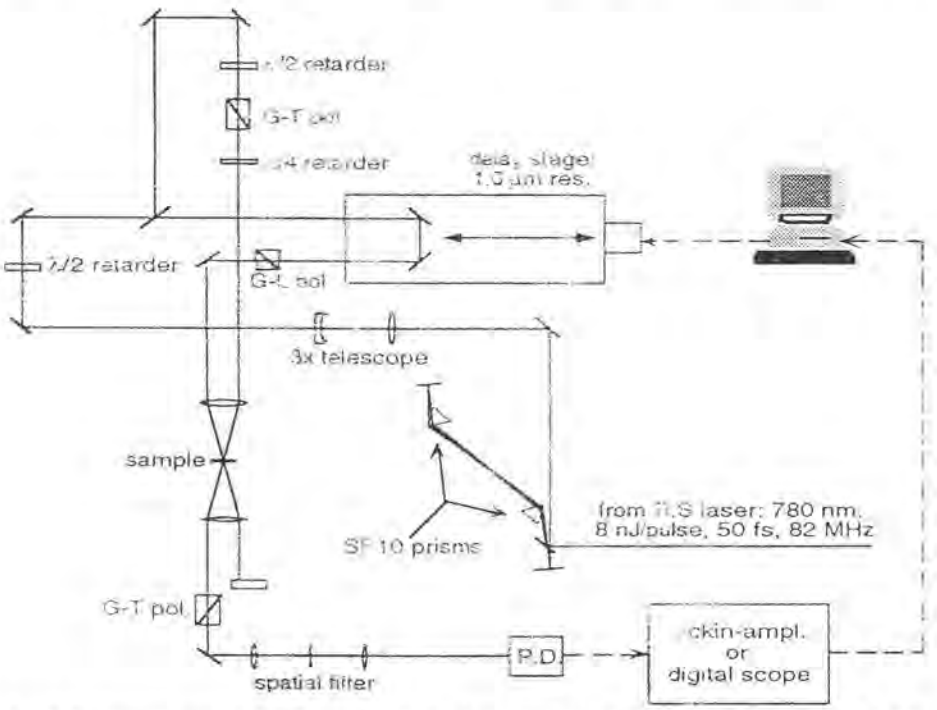

Fig. 1. Schematic diagram for the OHD-RIKES experimental setup. G-T pol. and G-T pol. represent Glan-Thompson and Glan-Laser calcite polarizers, respectively. The pinhole in the spatial filter is 100 μm diameter. P.D. represents the photodetector, either a Hamamatsu R928 photomultiplier or a Thorlabs PDA50 photodiode. The near-retroreflecting SF10 prism pair is a phase compensator for correcting for the group-velocity-dispersion mismatch arising from the normal dispersion of the polarizers and other optics.

heterodyne signal is measured to be a factor of 30-50 times greater than the homodyne signal obtained when the polarizers are crossed. The pump beam is scanned with 1.0 μm precision using an Aerotech DC-servo motor stage under real-time computer control via a nuLogic, Inc. interface. Either a Hamamatsu R928 photomultiplier tube or a Thorlabs PDA50 photodiode is used to detect the heterodyned probe beam. Data is acquired either by using the stage as a stepper system, or by rapidly scanning it (3 cm/sec) and acquiring the data on a digital oscilloscope (5 μs = 1 femtosecond delay). In either case, a number of scans ranging from 10 to 1000 are averaged either on a computer reading a lockin-amplifier (stepper case) or on the digital scope (fast scan case). Water has the smallest nonlinear optical response of the liquids we have studied thus far, yet a signal-to-noise ratio of 1000 relative to the peak of the signal was obtained by averaging 10 scans for a room-temperature water sample. A far superior signal-to-noise is of course obtained for liquids with a large nonlinear optical response, such as CS_2. Such a high signal-to-noise ratio is required to be able to make best use of the data in later analysis, such as when the electronic response is deconvoluted and the pure nuclear-coordinate motions are considered in the frequency domain.

All solvents were reagent, spectrophotometric, or HPLC grade, and were purified by fractional vacuum distillation immediately prior to use, with the exception of the freshly-opened acetic acid, which was Baker Ultrex grade. Water was obtained from a MilliPore Milli-Q purification system.

Theoretical Background

In the OHD-RIKES experiment, an intense femtosecond pump pulse interacts with the liquid sample non-resonantly with respect to electronic states, inducing a macroscopic polarization arising from a coupling between the electric field and the nonlinear optical response, $R(t)$. The signal is detected as a birefringence transient. Because the Born-Oppenheimer approximation applies, the nonlinear optical response $R(t)$ is separable into electronic and nuclear components. These components include an effectively instantaneous electronic hyper-polarizability response, $\sigma(t)$, and a slower response limited by the nuclear motions of the sample, $r_i(t)$. $R(t)$ is written as:

$$R(t) = \sigma(t) + \sum_i r_i(t). \tag{1}$$

While our 50 fs pulses are short, they are certainly not instantaneous. Thus, the birefringence transient that we observe, $T(\tau)$, is the convolution of the molecular nonlinear optical response $R(t)$ with the laser pulse autocorrelation, $G_0^{(2)}(t)$. $T(\tau)$ is given by:

$$T(\tau) \propto \int dt\, R(t-\tau)\, G_0^{(2)}(t). \tag{2}$$

To obtain the desired solvent relaxation information contained in the nuclear-coordinate part of the response $R(t)$, we must deconvolute the effects of the non-zero impulse width. McMorrow has shown (McMorrow, 1991) that a frequency-domain representation of our data is a means to a straightforward and exact deconvolution method. The frequency-domain susceptibility is defined by

$$D(\omega) = \int_{-\infty}^{\infty} dt \cdot \exp(i\omega t) \cdot R(t) = \mathcal{F}\{R(t)\}, \tag{3}$$

where $\mathcal{F}$ denotes a forward complex Fourier-transform. We may now write the deconvolution relation as

$$D(\omega) = \frac{\mathcal{F}\{T(\tau)\}}{\mathcal{F}\{G_0^{(2)}(\tau)\}}. \tag{4}$$

$D(\omega)$ now contains the low-frequency spectral-density free from effects of the non-zero pulse width. For all of the solvents we have studied, our 780 nm laser pulse is electronically non-resonant. The electronic hyperpolarizability component of the nonlinear optical response, $\sigma(t)$, is then symmetric and real (following the temporal profile of the autocorrelation of the femtosecond optical pulse). Thus, we can eliminate the electronic hyperpolarizability component from our spectral density by considering only the imaginary part of $D(\omega)$. We define

$$D_{\text{nucl}}(\omega) = \text{Im}[D(\omega)] \tag{5}$$

as the pure nuclear-coordinate frequency-domain representation of our solvent dynamics. We proceed to analyze the low-frequency spectral density in the frequency domain, as well as in the time domain. Time domain analysis of the dynamics can of course be obtained by convolute-and-compare nonlinear least-squares fitting. However, it is convenient to construct the pure nuclear-coordinate component of the nonlinear optical response $r(t) = \sum_i r_i(t)$ from the inverse Fourier-transform by

$$r(t) = 2\mathcal{F}^{-1}\{\text{Im}[D(\omega)]\}\, H(t - t_0) \tag{6}$$

where $H(t)$ is the Heaviside step-function. The latter technique has the advantage of being model-independent.

A major advantage of femtosecond nonlinear optical spectroscopy, such as OHD-RIKES, over conventional Rayleigh light scattering is that there is a clear and obvious separation of time-scales between diffusive rotational reorientation and faster inertial, non-diffusive dynamics. The longest time-scales in the OHD-RIKES experiment correspond to diffusive relaxation, and can in fact be subtracted away to allow for simpler and more accurate modeling of the inertial parts of the spectral density. The model used for fitting the diffusive relaxation is given in the following equation:

$$r_1(t) = A_{rot} \sum_i c_i \exp(-t/\tau_{ir})[1 - \exp(-2\omega_0 t)], \tag{7}$$

where the τ_{ir} are the lifetimes for rotational diffusion, the c_i are the relative weights between the lifetimes, A_{rot} is the overall amplitude of rotational diffusion in the nuclear-coordinate response, and ω_0 is the first moment of the inertial intermolecular vibrational band. For the hydrogen-bonding solvents we have studied, at least two exponential components, sometimes three or more, were required to properly fit the long-time tail of the OHD-RIKES birefringence transient data. This multi-exponential character of the solvent rotational diffusion is a manifestation of the fact that these solvent molecules are in general asymmetric rotors with substantially different inertial moments about the different axes.

To make the connection between the pure solvent relaxation data measured in our OHD-RIKES experiments and the solvation coordinate for a charge-transfer reaction, we have implemented an ansatz based upon the recent theory of Maroncelli, et al. (Maroncelli, et al., 1993). The Maroncelli model yields a correlation function $C_V(t)$ for the response of a solvent to an instantaneously created charge. $C_V(t)$ is based on the single-molecule rotational correlation function taken to the power of the normalized dipole density α_{MKP}. Our approximation to $C_V(t)$, based on our pure nuclear-coordinate solvent dynamical response, $r(t)$, is (Chang and Castner, 1993):

$$C_V(t) \approx \left\{1 - \frac{\int_0^t r(t')\,dt'}{\int_0^\infty r(t')\,dt'}\right\}^{\alpha_{MKP}/3} \tag{8}$$

Though a microscopic model including all interactions between the many solvent molecules and the reactant should smooth out much of the oscillatory character of the coherent, inertial solvent response, we find that a rapid femtosecond response occurs in our constructed $C_V(t)$ functions with a Gaussian shape in the first hundreds of femtoseconds, with a non-exponential component to the solvation relaxation occurring on time scales correlated with the diffusive solvent relaxation.

Results and Discussion

On the longest time scales of our OHD-RIKES experiment, ranging from 1-150 picoseconds, only diffusive molecular rotation is occurring in the hydrogen-bonding liquids. In all cases, this rotational diffusion correlation cannot be modeled by an exponential decay. Two, three, or more time constants are required. Fig. 2 shows the longer time-scale rotational diffusion relaxation for acetic acid at 296 K. An excellent fit is obtained for acetic acid when three exponential time constants are used, of lifetimes 0.67, 3.34, and 22.1 ps, respectively. The quality of the fit may be judged by the residuals from the nonlinear least-squares fit; systematic deviations occur when only one or two exponential time constants are used. A quite similar effect is shown to occur for formamides over a range of concentrations in other polar solvents (Chang and Castner, 1993) and over

a range of temperatures between 290-360 K. Water and ethylene glycol require two exponential components, with the longer lifetimes being 1.2 and 9.4 ps, respectively.

The shorter time-scale dynamics of the hydrogen-bonding liquids studied are shown in Figs. 3 and 4. The raw data are presented in semi-log form, and the frequency-domain representation of the dynamics are shown after deconvolution of the electronic hyperpolarizability response, done using Equations 4 and 5.

All of the OHD-RIKES data sets have a sharply rising leading edge that initially follows the laser-pulse autocorrelation signal. This pulse-response shaped signal component arises from the electronic hyperpolarizability part of the molecular nonlinear optical response, labelled $\sigma(t)$ in Equation 1. The signal continues to grow after the peak of the laser-pulse autocorrelation for another 150-300 femtoseconds. This further growth of the nonlinear optical polarization

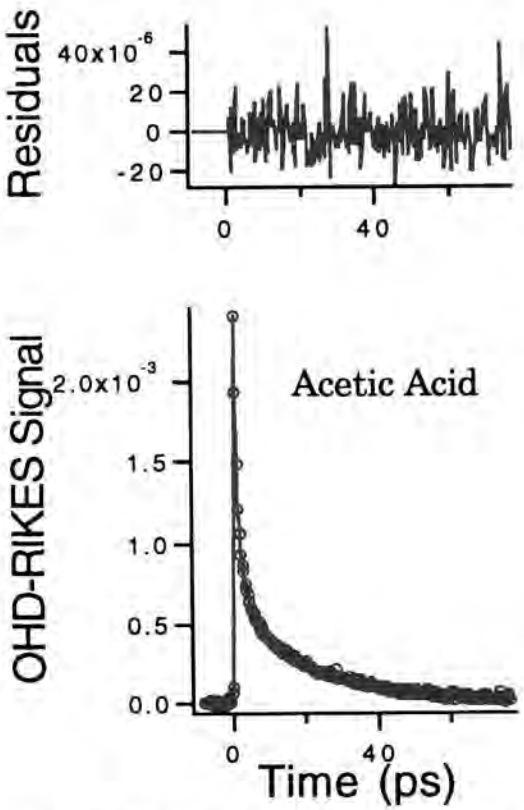

Fig. 2. The longer time-scale diffusive rotational reorientation decay is shown for acetic acid at 296 K. The data near zero-time-delay are off-scale. The open circles are the data, and the solid line is the nonlinear least squares fit. The residuals from the fit are shown at the top of the figure. Three exponential time constants are required to fit the data in the range from 1-80 ps. The relative amplitudes and lifetimes are: $c_1 = 2.958 \times 10^{-3} \pm 3.4 \times 10^{-4}$, $c_2 = 5.593 \times 10^{-4} \pm 6.9 \times 10^{-5}$, $c_3 = 5.775 \times 10^{-4} \pm 1.3 \times 10^{-5}$, and $\tau_1 = 0.668 \pm 0.065$ ps, $\tau_2 = 3.34 \pm 0.67$ ps, and $\tau_3 = 22.1 \pm 0.4$ ps.

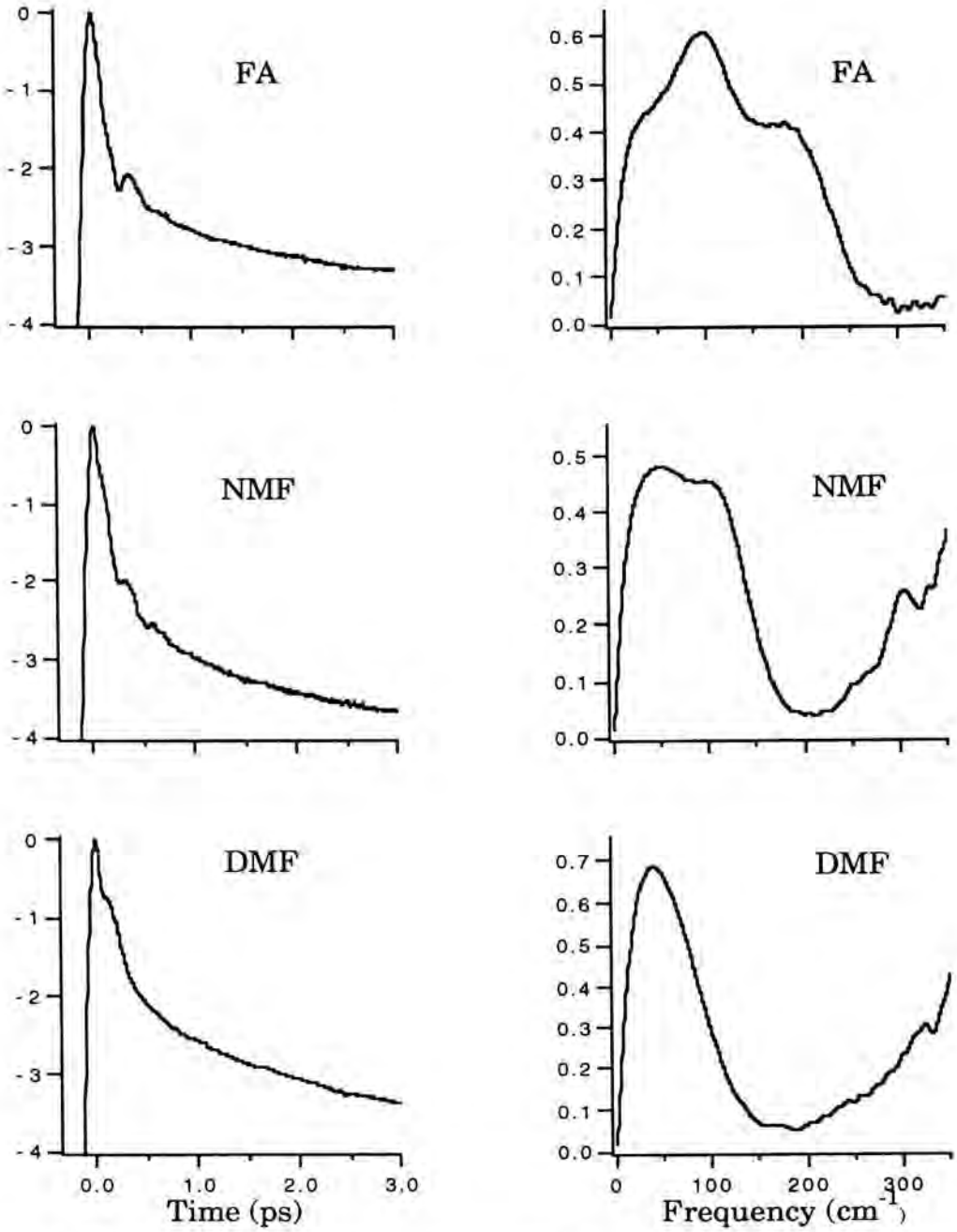

Fig. 3. The OHD-RIKES data for formamide, *N*-methylformamide, and *N*,*N*-dimethylformamide are shown. The raw data in the time domain are presented in semi-log form in the left column, with the deconvoluted frequency-domain data obtained from Equations 4 and 5 are shown in the right column with linear ordinate scales.

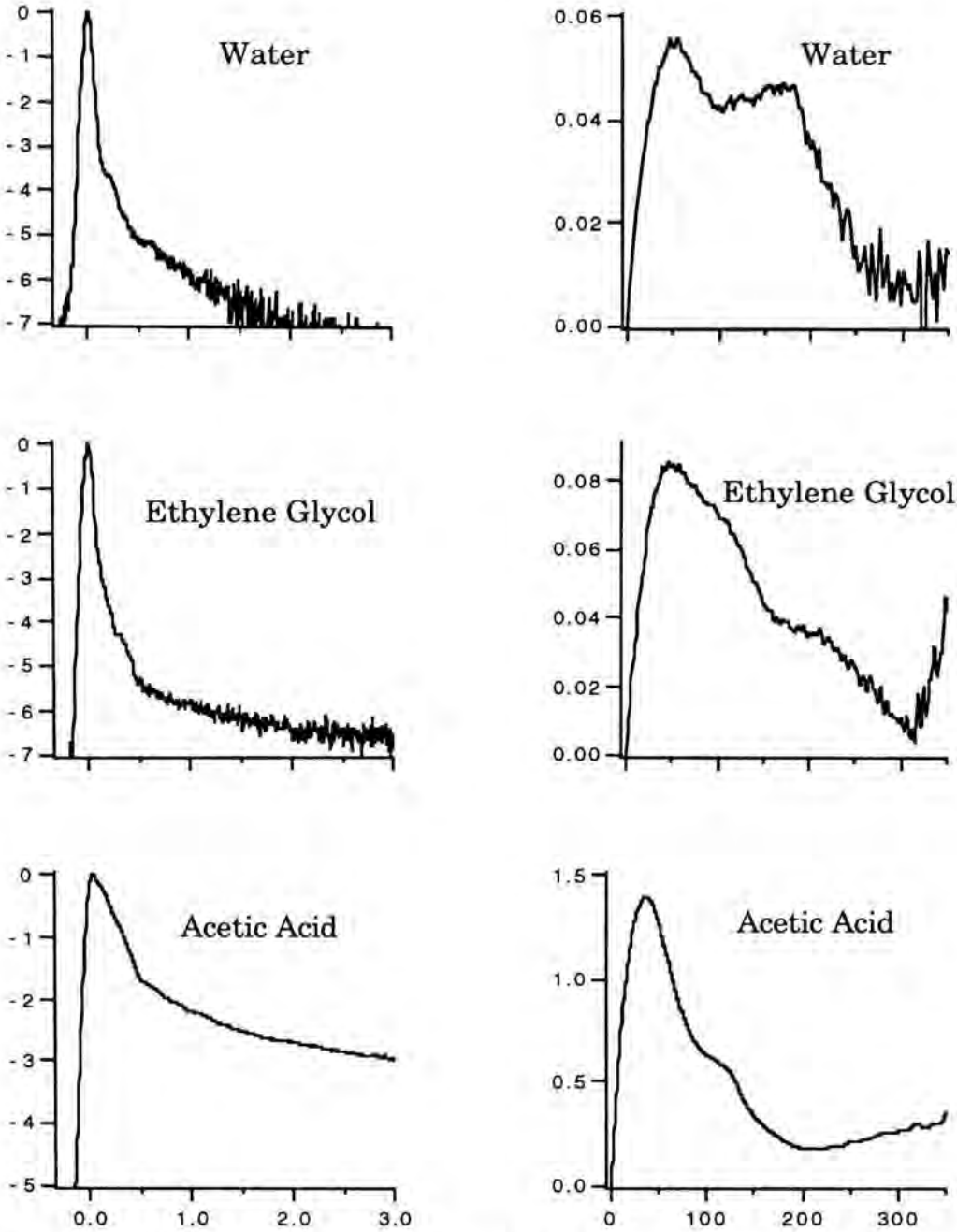

Fig. 4. The OHD-RIKES data for water, ethylene glycol, and acetic acid are shown. The raw data in the time domain are presented in semi-log form in the left column, with the deconvoluted frequency-domain data obtained from Equations 4 and 5 are shown in the right column with linear ordinate scales.

arises from the nuclear-coordinate inertial motions of the solvent molecules. At the longer time-scales beyond 1.0-1.5 picoseconds, all inertial components of the molecular nonlinear optical response are damped out, and only the diffusive rotational reorientation processes contribute to the polarization decay.

For all of the hydrogen-bonding solvents presented here, with the exception of acetic acid, a rather rapid decay of the birefringence transient occurs after the peak of the signal. Partly this is caused by the very rapid decay of the intermolecular vibrations convoluted with the laser impulse, and partly this is simply a result of the fact that the electronic hyperpolarizability component of the response dominates the overall molecular response, $R(t)$. For acetic acid, the nuclear components dominate, leading to a much slower decay of the OHD-RIKES transient in the first 0.5 ps.

For the formamides, water, and ethylene glycol, a substantial change in curvature occurs in the OHD-RIKES birefringence transients at a time delay between 200-300 femtoseconds. In each of these cases, this 'knee' of the curve results from the underdamped intermolecular vibrations: out-of-plane librations for the formamides, (Chang and Castner, 1993) and translational density fluctuations for water (Chang and Castner, 1993).

When the OHD-RIKES femtosecond dynamics are considered in the frequency domain, it is possible to remove the rotational diffusion response exactly in the time domain, prior to deconvolution of the electronic response. This is done by fitting the longer time multi-exponential tails, tail matching, and subtracting this part away using Equation 7. We have done this analysis for all of our data sets, and the results are shown in the right hand columns of Figures 3 and 4. The resulting nuclear-coordinate spectral-density then contains only the inertial parts of the solvent relaxation. For all the liquids studied, there is a peak in the low-frequency spectral-density occurring near 50 cm^{-1}. This low-frequency band results from a complex sum of intermolecular interactions including overdamped librations, and interaction-induced Raman modes resulting from intermolecular collisions. The higher frequency modes with band centers in the 100-250 cm^{-1} range have been assigned to librations and translations for acetic acid (Faurskov Nielsen and Lund, 1983), formamide (Faurskov-Nielsen, et al., 1982), ethylene glycol (Manisse-Morgant et al., 1971; Schwartz, 1977), and water (Walrafen, 1990) based on low-frequency Raman studies in the frequency domain.

We analyze our low-frequency spectral density obtained from applying Equations 7, 4, and 5 to our data, in terms of a sum of different classical oscillators. The librational and translational bands are fit to Gaussian or anti-symmetrized Gaussians models. The broadest asymmetric lowest-frequency band has been assigned to collisional interaction-induced effects in simpler liquids, and is often fit to a function form of the type $I(\omega) = \omega^{\alpha} \exp(-\omega/\omega_0)$, where the exponent α is usually near to unity.

Figures 5A and 5B show the solvation time-correlation functions, for an instantaneously-created charge, $C_V(t)$, for the three formamides, and acetic acid, ethylene glycol, and water, respectively. These curves were calculated using

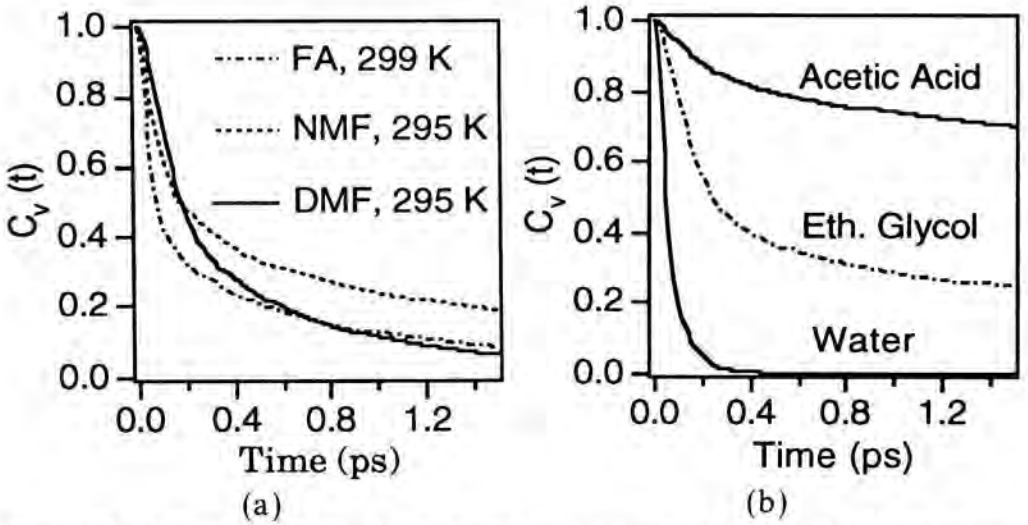

Fig. 5. The solvation correlation-function for an instantaneously created charge, $C_V(t)$, are shown. $C_V(t)$ is calculated using Equation 8. A. $C_V(t)$ for formamide, *N*-methylformamide, and *N*,*N*-dimethylformamide are shown. B. $C_V(t)$ for acetic acid, ethylene glycol, and water are shown.

Equation 8. The intial parts of the decays of $C_V(t)$ all show a Gaussian shape, indicating the inertial character of this part of the solvation response. For longer times beyond ~ 250 fs, the Gaussian initial decay trails into a non-exponential response arising from the diffusive rotational reorientation. For comparison with TDFSS experiments and molecular dynamics simulations, we define an effective integrated solvation time constant τ_S as $\tau_S = \int_0^\infty C_V(t)\, dt$. The effective solvation times, τ_S, are given in Table 1. Though the effective solvation times for NMF, acetic acid, and ethylene glycol all exceed 1.0 picosecond, Figure 5 clearly shows that extremely rapid inertial processes are present in all of the six hydrogen-bonding solvents that we have measured.

Recent theoretical work has concentrated on understanding the ultrarapid inertial motions in terms of multi-mode Brownian oscillators (Fried and Mukamel, 1993) and using an intermolecular normal vibrational mode analysis (Buchner et al., 1992). We are presently extending our data analysis to include these newer and more sophisticated models for the inertial dynamics and low-frequency spectra.

Table 1

Solvent	τ_S (ps)
formamide	0.75
NMF	1.1
DMF	0.48
acetic acid	15.2
ethylene glycol	1.76
water	0.074

Acknowledgments

This research was carried out at Brookhaven National Laboratory under contract DE-AC02-76CH00016 with the U.S. Department of Energy and supported by its Division of Chemical Sciences, Office of Basic Energy Sciences.

References

Buchner, M., Ladanyi, B.M., and Stratt, R.M., The short-time dynamics of molecular liquids. Instantaneous-normal-mode theory. In: *J. Chem. Phys.* **97**, 8522-8535, 1992.

Chang, Y.J., and Castner, E.W., Jr., Fast Responses From 'Slowly-Relaxing' Liquids: A Comparison Between The Femtosecond Dynamics Of Triacetin, Ethylene Glycol, And Water. In: *J. Chem. Phys.* **99**, 7289-7299, 1993.

Chang, Y.J., and Castner, E.W., Jr., Femtosecond dynamics in hydrogen-bonding solvents: Formamide and N-methylformamide in acetonitrile, DMF, and water. In: *J. Chem. Phys.* **99**, 113, 1993.

Cho, M., Rosenthal, S.J., Scherer, N.F., Ziegler, L.D., and Fleming, G.R., Ultrafast solvent dynamics: Connection between time resolved fluorescence and optical Kerr measurements. In: *J. Chem. Phys.* **96**, 5033-5038, 1992.

Duguay, M.A., and Hansen, J.W., An ultrafast light gate. In: *Appl. Phys. Lett.* **15**, 192-194, 1969.

Etchepare, J., Grillon, G., Hamoniaux, G., and Orszag, A., In: *Opt. Commun.* **63**, 329, 1987.

Faurskov Nielsen, O., and Lund, P.-A., Intermolecular Raman active vibrations of hydrogen bonded acetic acid dimers in the liquid state. In: *J. Chem. Phys.* **78**, 652-655, 1983.

Faurskov-Nielsen, O., Lund, P.-A., and Praestgaard, E., Hydrogen bonding in liquid formamide. A low frequency Raman study. In: *J. Chem. Phys.* **77**, 3878-3883, 1982.

Fried, L.E., and Mukamel, S., Simulation of Nonlinear Electronic Spectroscopy in the Condensed Phase. In: *Advances in Chemical Physics* **84**, 435-517, 1993.

Greene, B.I., and Farrow, R.C., Direct measurement of a subpicosecond birefringent response in CS_2. In: *J. Chem. Phys.* **77**, 4779-4780, 1982.

Hattori, T., Terasaki, A., Kobayashi, T., Wada, T., Yamada, A., et al., Optical-heterodyne-detected induced phase modulation for the study of femtosecond molecular dynamics. In: *J. Chem. Phys.* **95**, 937-945, 1991.

Kohler, B., and Nelson, K.A., Femtosecond impulsive stimulated light scattering from liquid carbon disulfide at high pressure: Experiment and computer simulation. In: *J. Phys. Chem.* **96**, 6532-6538, 1992.

Levenson, M.D., and Eesley, G.L., Polarization selective optical heterodyne detection for dramatically improved sensitivity in laser spectroscopy. In: *Appl. Phys.* **19**, 1-17, 1979.

Manisse-Morgant, A., Beaudoin, J.L., Benchenane, A., and Harrand, M., Con-

tribution à l'étude de la structure de l'éthylèneglycol liquide et cristallisé. In: *C. R. Acad. Sci.* **273B**, 293-296, 1971.
Maroncelli, M., Kumar, V.P., and Papazyan, A., A Simple Interpretation of Polar Solvation Dynamics. In: *J. Phys. Chem.* **97**, 13-18, 1993.
McMorrow, D., Separation of nuclear and electronic contributions to femtosecond four-wave mixing data. In: *Opt. Commun.* **86**, 236-244, 1991.
McMorrow, D., Kim, S.K., Melinger, J.S., and Lotshaw, W.T., Probing the microscopic molecular environment in liquids with femtosecond Fourier-transform Raman spectroscopy. In: *Ultrafast Phenomena VIII*, in press, 1992.
McMorrow, D., and Lotshaw, W.T., Evidence for low-frequency ($\sim 15\ cm^{-1}$) collective modes in benzene and pyridine liquids. In: *Chem. Phys. Lett.* **201**, 369, 1993.
McMorrow, D., and Lotshaw, W.T., Intermolecular Dynamics in Acetonitrile Probed with Femtosecond Fourier Transform Raman Spectroscopy. In: *J. Phys. Chem.* **95**, 10395-10406, 1991.
McMorrow, D., Lotshaw, W.T., and Kenney-Wallace, G.A., Femtosecond Optical Kerr Studies on the Origin of the Nonlinear Responses in Simple Liquids. In: *IEEE J. Quantum Electron.* **24**, 443-454, 1988.
Ruhman, S., Joly, A.G., and Nelson, K.A., Coherent Molecular Vibrational Motion Observed in the Time Domain Through Impulsive Stimulated Raman Scattering. In: *IEEE J. Quantum Electron.* **24**, 470-481, 1988.
Ruhman, S., Kohler, B., Joly, A.G., and Nelson, K.A., Intermolecular vibrational motion in CS2 liquid at $165\ K \leqslant T \leqslant 300\ K$ observed by femtosecond time-resolved impulsive stimulated scattering. In: *Chem. Phys. Lett.* **141**, 16-24, 1987.
Schwartz, M., Raman study of the conformational equilibrium of ethylene glycol in dimethyl sulfoxide. In: *Spectrochim. Acta* **33A**, 1025-1032, 1977.
Walrafen, G.E., Raman Spectrum of Water: Transverse and Longitudinal Acoustic Modes Below $\approx 300\ cm^{-1}$ and Optic Modes Above $\approx 300\ cm^{-1}$. In: *J. Phys. Chem.* **94**, 2237-2239, 1990.
Wynne, K., Galli, C., and Hochstrasser, R.M., Femtosecond intermolecular vibrational motion in pyrrole. In: *Chem. Phys. Lett.***193**, 17-22, 1992.
Yan, Y.-X., Cheng, L.-T., and Nelson, K.A., Impulsive Stimulated Light Scattering. In: *Advances in Nonlinear Spectroscopy* **16**, 299-355, 1988.

Authors' Adresses

Brookhaven National Laboratory
Chemistry Department
Building 555A
Upton, NY 11973
USA

S. Takeuchi, M. Yoshizawa and T. Kobayashi

Femtosecond Spectroscopy of Polymers

Abstract

The configuration of main chain with the self-trapped exciton after geometrical relaxation in polydiacetylene was determined directly to be a butatriene-like structure from the femtosecond time-resolved stimulated Raman gain spectroscopy. Formation time of a confined soliton-antisoliton pair was resolved and determined as 98 ± 8 fs for the first time in a substituted polyacetylene.

1. Femtosecond time-resolved stimulated Raman gain spectroscopy in a polydiacetylene

Due to a strong electron-lattice coupling, conjugated polymers have localized excited states with geometrical relaxation such as soliton, polaron, and self-trapped exciton (STE). The geometrical relaxation due to STE formation from free exciton (FE) in a polydiacetylene (PDA) has been directly observed by femtosecond time-resolved stimulated Raman gain spectroscopy for the first time.

1.1. *Experimental*

The femtosecond Raman gain spectroscopy was performed using three femtosecond pulses generated by a colliding-pulse mode-locked (CPM) dye laser and a four-stage dye amplifier (Yoshizawa, 1989, 1991; Kobayashi, 1990). The 1.97 eV pulse (pump 1) with 100 fs duration was used for the generation of excited states in PDA. The probe pulse was the white continuum extending from 400 to 1000 nm generated by self-phase modulation (SPM) in CCl_4. The 1.77 eV pulse (pump 2) with 200 fs duration used as the pump pulse of the Raman gain spectroscopy was generated by further amplifying a spectral portion of the white continuum in another two-stage dye cells. Polarizations of the three beams were parallel to the oriented polymer chain of PDA-C_4UC_4 thin film (side group: $R = (CH_2)_4OCONHC_4H_9$). The transmitted probe pulse was spectrally dispersed using $f = 275$ mm polychromater and detected by CCD. The experiment was performed at room temperature.

1.2. *Results*

Figure 1 shows transient absorption spectra after photoexcitation with the 1.97 eV pulse. At a pump-probe delay time of 0.5 ps, bleaching due to saturation of the excitonic absorption and broad photoinduced absorption below 1.85 eV were observed. The ultrafast relaxation process in PDA has been so far explained in terms of STE (Yoshizawa, 1989, 1991, 1993; Kobayashi, 1990, 1992).

The model potential surface for an excitation in the configuration space is shown in Fig. 2. The photoexcited FEs are coupled with the C – C stretching modes within the phonon periods of 10-20 fs. However, the STEs have not relaxed to the bottom of the potential curve and the binding energy of the STEs remains as the kinetic energy of the lattice oscillation (nonthermal STEs). The nonthermal STEs emit phonons and relax to the bottom of the potential. The time required for the phonon emission is determined by the energy redistribution rate from the strongly coupled phonon to the other low-frequency phonon modes. The emission process is equivalent to the formation process of the quasi-thermalized (relaxed) STEs which was observed as the spectral change with the time constant of 150 fs. The relaxed STEs after phonon emission process are subsequently coupled with low-frequency phonon modes and thermalize. The thermalization process is observed as the spectral change with time from 0.5 to 5.0 ps, and the obtained time constant of the process is about 1 ps. Eventually the STEs go back to the ground state mainly by tunneling through the barrier between the STEs and ground-state potentials.

The observed photoinduced absorption peak at 1.78 eV has been assigned to the transition from the STEs to biexciton states. The pump 2 pulse used in the

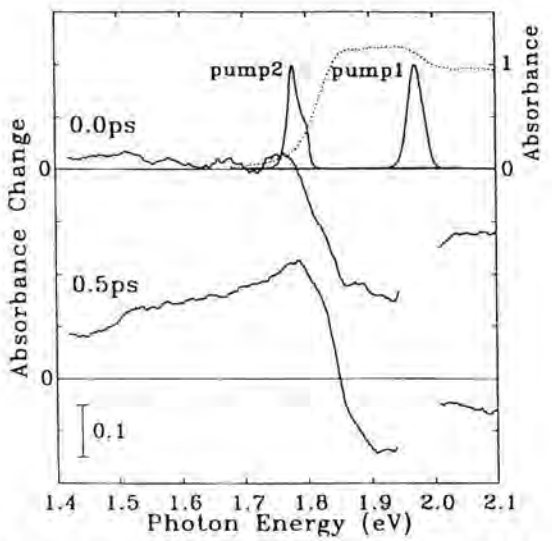

Fig. 1. Photoinduced absorption spectra of PDA-C_4UC_4 at 0.0 and 0.5 ps after the 1.97 eV pump. Stationary absorption spectrum is also shown with dotted curve.

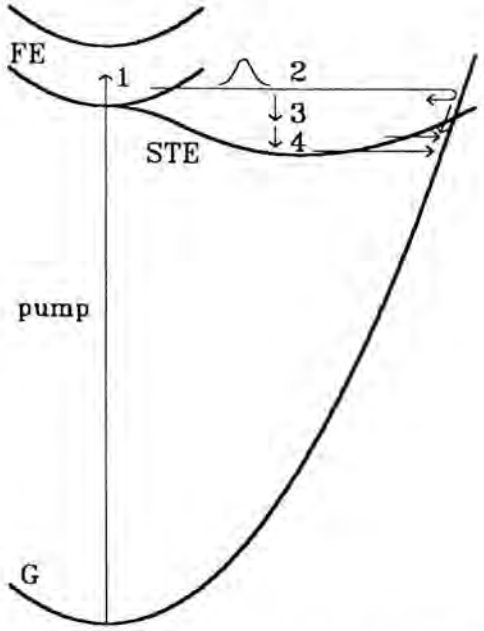

Fig. 2. A model potential curve in a configuration space for excitations in PDA. FE(1): free exciton, STE: self-trapped exciton, 2: nonthermal STE, 3: quasi-thermalized STE, 4: thermalized STE, and G: ground state.

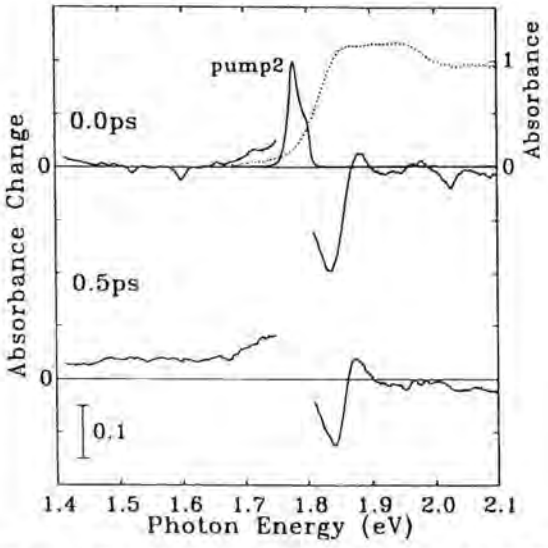

Fig. 3. The same as Fig. 1, but with the 1.77 eV pump.

Raman gain experiment was set just resonant with the peak, so that the Raman process is enhanced.

The transient absorption spectra excited by the 1.77 eV pulse (pump 2) is shown in Fig. 3. Two minima due to the Raman gain were observed at 1.52 and 1.60 eV at a delay time of 0.0 ps. The oscillational structures around 2 eV are mainly due to inverse Raman scattering (Yoshizawa, 1993).

The time-resolved stimulated Raman gain spectra shown in Fig. 4 were obtained from the transient absorption spectra induced by the pump 2 pulse. At a pump 1 - pump 2 delay time of -0.5 ps, two Raman gain peaks were observed at 1450 and 2060 cm^{-1}. They are assigned respectively to the stretching vibrations of the C=C and C≡C bonds in acetylene-type structure $=CR-C\equiv C-CR=$ of the ground state. The 1450 cm^{-1} Raman gain peak at 0.0 ps has a shoulder at lower frequency, and a clear peak is observed at 1200 cm^{-1} at delay times longer than 0.2 ps.

1.3. *Geometrical relaxation in self-trapped excitons*

The Raman peak frequencies were compared with those of several unsaturated hydrocarbons. The Raman frequencies, 2060 and 1450 cm^{-1}, observed for PDA in the ground state correspond respectively to 2235 cm^{-1} of the middle C≡C bond in dimethylacetylene (C−C≡C−C) and 1675 cm^{-1} of the middle C=C bond in transbutene-2 (C−C=C−C). Since the Raman frequency of the new peak (1200 cm^{-1}) compares favorably with 1202 cm^{-1} of the middle C−C bond

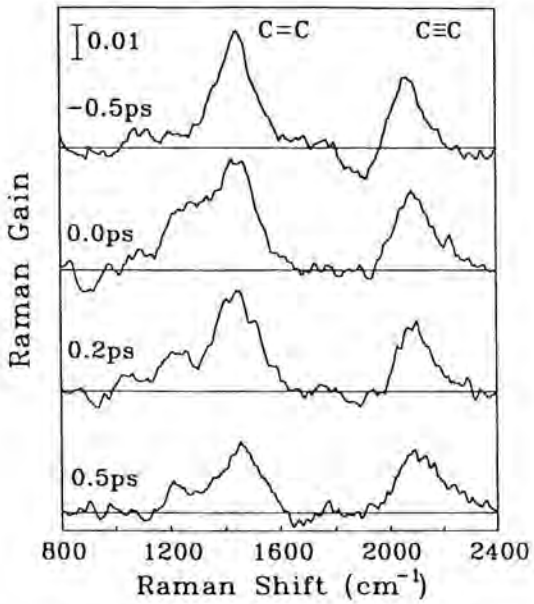

Fig. 4. Time-resolved stimulated Raman gain spectra of PDA-C_4UC_4 at several delay times after the excitation of 1.97 eV pump pulse.

in trans-1,3-butadiene (C=C−C=C), it can be concluded that the formation of STE is associated with the geometrical change of main chain from acetylene-type =CR−C≡C−CR= to butatriene-type −CR=C=C=CR−. The 2600 cm^{-1} Raman peak has no observable change, because the frequency of the middle C=C bond (2079 cm^{-1}) of the butatriene is similar to that of the C≡C bond (2060 cm^{-1}).

2. Ultrafast charge separation in a substituted polyacetylene

In conjugated polymers with degenerate ground states, a photogenerated electron-hole pair is unstable toward separating to each other, forming a soliton-antisoliton pair. The formation time of the soliton-antisoliton pair and the spectrum associated with it were determined experimentally for the first time using femtosecond transient absorption.

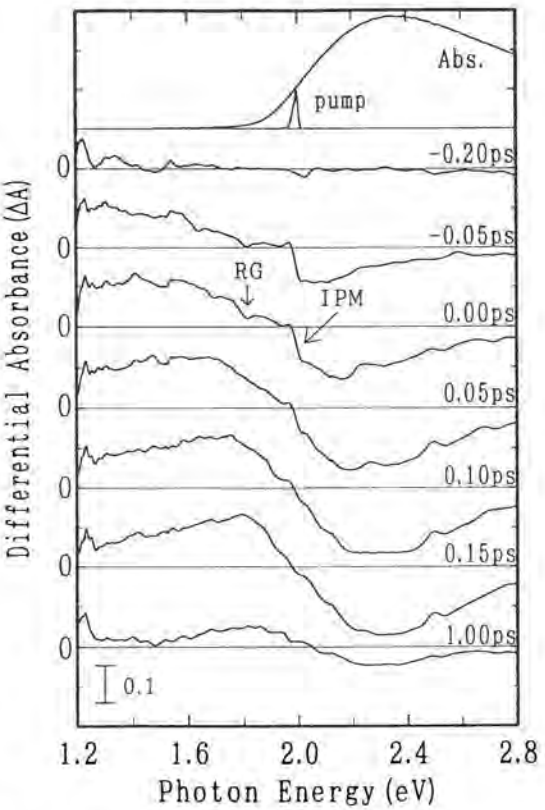

Fig. 5. Photoinduced and stationary (Abs.) absorption spectra of PMSPA at several delay times after the 1.98 eV pump.

2.1. *Experimental Results*

The sample used in this study, poly[(o-trimethylsilyl)phenylacetylene] (PMSPA), has the same back-bone structure as that of trans-polyacetylene, but a bulky side-group ($-C_6H_4Si(CH_3)_3$) is attached to every two carbon sites. The transient absorption measurement was performed by a pump-probe method using femtosecond pulses generated by the CPM dye laser and a four-stage dye amplifier. The photoexcitation was made by 1.98 eV pulse with 100 fs duration and the probe pulse was the white continuum generated by SPM in CCl_4.

The transient absorption spectra measured at 10 K are shown in Fig. 5. The stationary absorption spectrum of the sample and the spectrum of the pump pulse are also shown for a comparison. Besides bleaching of the $\pi - \pi^*$ transition above 2 eV, a broad photoinduced absorption (PA) peaking around 1.2-1.4 eV appeared immediately after the leading edge of the pump pulse reached the sample (-0.05 ps). The PA in this lower energy region decayed exponentially with a time constant of 0.135 ps and almost vanished by 1 ps (Fig. 6a). The PA spectra subsequently showed a gradual blue shift to a peak at 1.8 eV by a delay time of 0.15 ps. The decay profile around the peak, in contrast to that at the lower energy region, obeyed a power-law decay, $erf[(\sigma t)^{-n}]$ with $n = 0.65 \pm 0.05$ and $\sigma = 4.3\ (\mathrm{ps})^{-1}$, where $erf(\ )$ denotes an error function (Fig. 6b).

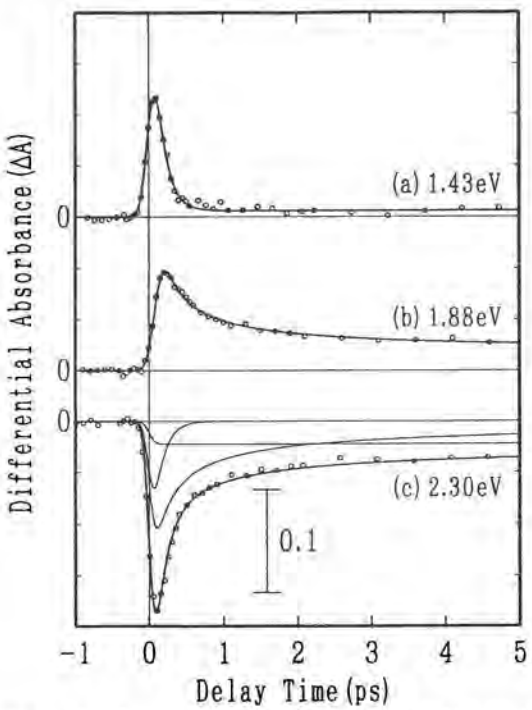

Fig. 6. Time dependence of absorbance change in PMSPA thin film at (a) 1.43, (b) 1.88, and (c) 2.30 eV, respectively.

Since it is characteristic of a geminate recombination process of two excitations on a quasi one-dimensional chain and the peak position agrees well with a transition energy associated with a closely confined pair of charged solitons as well, the peak at 1.8 eV has been interpreted to be due to an oppositely charged, overall neutral, soliton-antisoliton pair confined in a segmented conjugation chain of the polymer (Takeuchi, 1992). The size of the segment is about six repeat unit lengths from our former estimation. It is fairly small, probably due to a reduction of the conjugation length caused by the bulky side-groups.

2.2. *Decomposition of the transient behavior*

The spectral blue shift implies that the PA consists of two different components which are temporally delayed. We could successfully separate the two components by fitting the decay over the entire PA region to the following curve (Takeuchi, 1993):

$$\Delta A(\varepsilon, t) = A(\varepsilon)\, erf[\{\sigma(t - t_d)\}^{-n}] + B(\varepsilon)\exp(-t/\tau) + C(\varepsilon)$$

Here the first term represents a power-law decay, the second term an exponential decay, and the last term a long-lived component which can be regarded as a constant within the observed time range. The time delay between the first two components is also introduced. The fitting was made for A, B, C and t_d with a fixed parameter set: $n = 0.65$, $\sigma = 4.3\ (\text{ps})^{-1}$, and $\tau = 0.135$ ps using the least square method. The magnitude of each component, A, B, and C, is a function of probe photon energy ε. The resultant values of A, B, and C are plotted against probe photon energy in Fig. 7. The exponential component $B(\varepsilon)$ has a broad peak around 1.4 eV and seems to extend below the measured region, while the power-law component $A(\varepsilon)$ has a clear peak at 1.8 eV. The latter corresponds to the spectrum of the confined soliton-antisoliton pair revealed for the first time in the present study.

The exponential component which is responsible for the quick rise of the PA in the lower energy region can be also observed in other various conjugated polymers such as polydiacetylene (Yoshizawa, 1991), polythiophene (Stamm, 1990) and poly(2,5-thienylenevinylene) (Halle, 1992). It is believed that the component in these materials is due to a nonthermal singlet exciton-polaron (self-trapped exciton) which is directly created by intrachain photoexcitation, because the formation of exciton-polarons is less affected by the degeneracy of the main chain structure than that of soliton-antisoliton pairs. In the nondegenerate systems, a photogenerated electron-hole pair undergoes inherent, strong confinement, forming the exciton-polaron. It subsequently thermalizes by emitting phonons with a change of the spectral shape within 1-2 ps. In the degenerate system, on the other hand, it is unstable toward separating each other by using the excess energy of photoexcitation, forming a soliton-antisoliton pair. In the material under current investigation, in particular, an imperfect degeneracy of

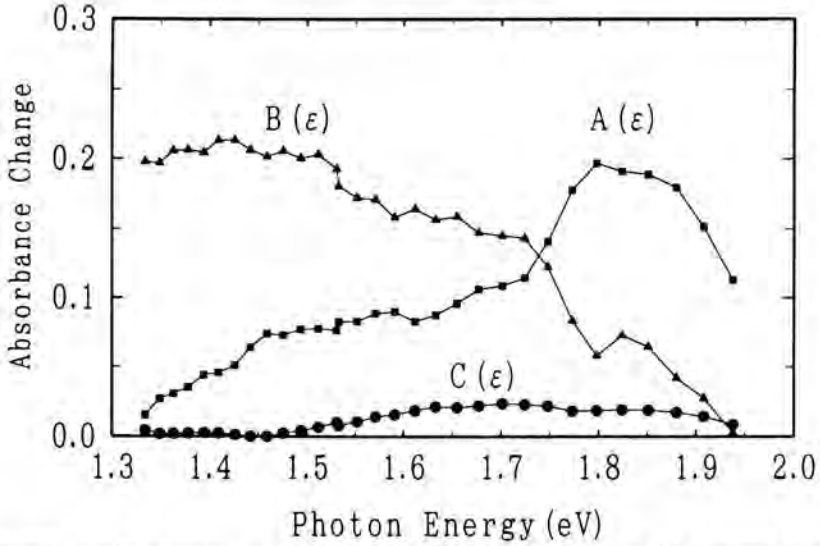

Fig. 7. Fractions of the exponential (triangle), power-law (square), and long-lived (circle) components plotted against the probe photon energy.

the ground state due to bulky side-groups leads to a confinement of the soliton-antisoliton pair.

The transition energy associated with the exciton-polaron can be regarded as a simple sum of an exciton effect (bare electronic binding energy) and a polaron effect (stabilization energy due to lattice relaxation) (Abe, 1992). Using the calculated values of 0.6 (Abe, 1992) and 0.5 eV (Su, 1987) respectively for the two effects, the transition energy from the exciton-polaron state possibly to the conduction band turns out to be 1.1 eV. It compares favorably with the observed broad peak around 1.4 eV of the exponential component $B(\varepsilon)$.

2.3. *Formation time of a soliton-antisoliton pair*

The value of t_d obtained by the above fitting is plotted against probe photon energy in Fig. 8. Since it is the time delay between the exponential component associated with the exciton-polaron and the power-law component associated with the soliton-antisoliton pair, it can be physically regarded as a time required for an exciton-polaron to decay to form a soliton-antisoliton pair. The t_d holds almost the same value over the entire PA region, indicating the finite formation time of the soliton-antisoliton pair to be 98 ± 8 fs. Since a soliton is an electronic excitation with a lattice relaxation, its formation time is essentially determined by the lattice distortion rate. It was shown by numerical simulations made by Su and Schrieffer (Su, 1980) that a photogenerated electron-hole pair decays

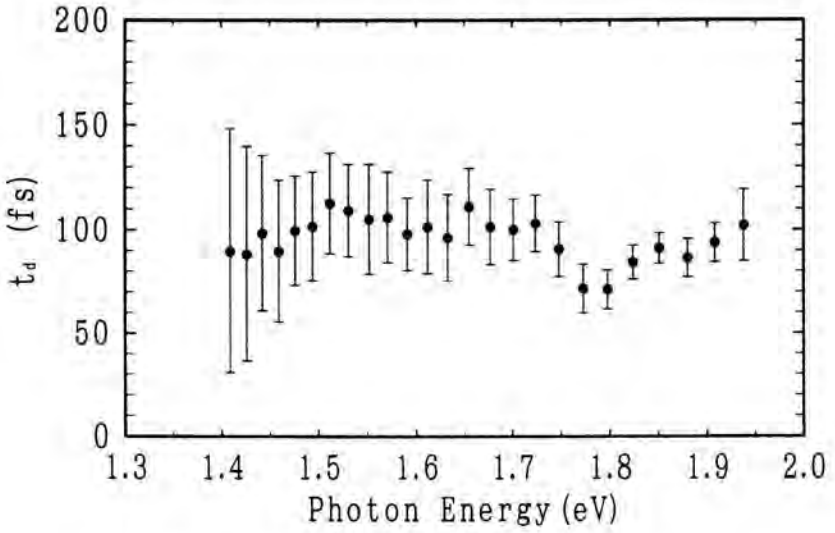

Fig. 8. Delay time t_d plotted against the probe photon energy.

into a soliton-antisoliton pair in a time of order 100 fs. The time corresponds to an oscillation period of optical phonons modulating a chain dimerization. The experimentally determined value for the formation time agrees quite well with the result of the numerical simulation.

References

Abe, S., Yu, J., and Su, W.P., *Phys. Rev. B* **45**, 8264, 1992.

Halle, S.D., Yoshizawa, M., Murata, H., Tsutsui, T., Saito, S., and Kobayashi, T., *Synth. Met.* **49-50**, 429, 1992.

Kobayashi, T., Yoshizawa, M., Stamm, U., Taiji, M., and Hasegawa, M., *J. Opt. Soc. Am. B* 7 (8), 1558, 1990.

Kobayashi, T., *IEICE Trans. Fundament. E* **75**-*A*(1), 38, 1992.

Stamm, U., Taiji, M., Yoshizawa, M., Yoshino, K., and Kobayashi, T., *Mol. Cryst. Liq. Cryst.* **182**A, 147, 1990.

Su, W.P., and Schrieffer, J.R., *Proc. Natl. Acad. Sci. USA* **77** (10), 5626, 1980.

Su, W.P., *Phys. Rev. B* **36**, 6040, 1987.

Takeuchi, S., Yoshizawa, M., Masuda, T., Higashimura, T., and Kobayashi, T., *IEEE J. Quantum Electron.* **28**, 2508, 1992.

Takeuchi, S., Masuda, T., Higashimura, T., and Kobayashi, T., *Solid State Comm.* **87**, 655, 1993.

Yoshizawa, M., Taiji, M., and Kobayashi, T., *IEEE J. Quantum Electron.* **25**, 2532, 1989.

Yoshizawa, M., Yasuda, A., and Kobayashi, T., *Appl. Phys. B* **53**, 296, 1991.
Yoshizawa, M., Hattori, Y., and Kobayashi, T., *Phys. Rev. B* **47**, 3882, 1993.

Author's Address

Department of Physics, Faculty of Science, University of Tokyo
7-3-1 Hongo, Bunkyo-ku, Tokyo 113, Japan
Tel +81-3-3812-2111 ext. 4227
Fax +81-3-3818-7812

B. Broers, L.D. Noordam and H.B. van Linden van den Heuvell

Two-Photon Processes with Chirped Pulses

Abstract

Two-photon excitation processes are studied with visible, chirped, picosecond, laser pulses. Two classes of processes are distinghuised: 1) the situation where intermediate resonances at the one-photon level form a wavelength selection and therefore, due to the chirp of the optical pulse, also a time selection and 2) the non-resonant processes which are described by interference of many excitation paths. This interference has a close analogy with Fresnel diffraction. For all cases experiments have been performed with two-photon excitation in rubidium atoms. In the non-resonant situation also second-harmonic generation in thin KDP crystals is used.

Relevance of these processes for the vibrational excitation and dissociation of molecules is discussed.

Introduction

General

Time-resolved molecular spectroscopy was always one of the first areas of application when the technique of making ultrashort optical pulses progressed in the course of years. Undoubtedly, one of the reasons for this favorable situation is that molecular spectroscopy is not only benefiting from ultra-fast laser spectroscopy but also was and still is contributing to this field.

Despite the fact that picosecond lasers have been available for decades and also femtosecond laser pulses are routinely produced in many laboratories in the world, the use of pulses with a well-defined and quantified chirp is still not widespread. But the prospects for the use of chirped light pulses in laser chemistry are good. An argument in favor of this is that it might turn out that chirped pulses form a feasible realisation of what is commonly called 'phase-controlled chemistry' (e.g. Brumer and Shapiro, 1986). In general, a problem of this approach is (as with many other forms of interferometric use of visible light) that is is a very unstable process. It is anticipated that the use of chirped pulses in combination with adiabatic passage can prevent this instability.

In this context we limit the meaning of the word chirp to linear chirp. This

describes the smallest deviation of a 'bandwidth limited' or 'Fourier limited' pulse. Assume a pulse, $E(t)$, that has a spectrum $E(\omega)$, giving the amplitudes of the frequency components $\exp(i\omega t)$. Due to technical limitations, in practice the spectrum is a fairly narrow band $\Delta\omega$ around ω_0 (typically $\Delta\omega$ is no more than a few percent of ω_0). When at $t=0$ all frequency components are in phase (e.g. $E(\omega)$ is real for all ω's), then the smallest possible pulse, given the spectrum $E(\omega)$, is realized around $t=0$. An additional phase factor that is linearly depending on the frequency, $\exp(i(\omega-\omega_0)\,t_0)$ is not changing this pulse; only the origin is moved in time. If the original pulse, with the spectrum $E(\omega)$, was peaked at $t=0$ then a pulse described by $\exp(i(\omega-\omega_0)\,t_0)\,E(\omega)$ is peaked around $t=t_0$. The first non-trivial modification of the pulse is given by a phase factor that depends quadratic on the frequency: $\exp(i\alpha(\omega-\omega_0)^2)\,E(\omega)$. The absolute value of the additional factor is always unity so the power spectrum of the pulse, $|E(\omega)|^2$ is not changed. The numerical value of α can be put in perspective if it es expressed as a stretching factor of the original pulse (in the present experiments this factor is between 1 and 50). Alternatively, the chirp can be seen as the rate of change of the central frequency. A typical number of 1 ps^2 corresponds to 0.4 ns/octave or, more in line with electrical units 4 eV/ns. Note that smaller chirps corresponds to faster sweeps.

Perhaps the first impression is that the effect of chirp on a pulse will be rather subtle, because the intensity distribution over various frequency components is not changed by the introduction of chirp. For instance, the rate equations contain only the light intensity and no phase information of the light, so all processes that are adequately described by rate equations are not effected by chirp. However, as will become clear in the rest of this contribution, the effect on **non-linear** processes (including saturated processes) can be large.

Non-resonant excitation

When a two-photon processes is driven by a pulsed field $E(t)$, the effective field that drives the process by means of the induced non-linear polarisation is proportional to $E^2(t)$, assuming that there are no intermediate resonances. The Fourier transform of $E^2(t)$, indicated with $E^{(2)}(\omega)$ gives the frequency response at the two-photon level. The multiplication of $E(t)$ with itself corresponds to a convolution in the frequency domain. Therefore $E^{(2)}(\omega)$ can be expressed as the self-convolution of the spectrum of the original pulse:

$$E^{(2)}(\omega)=\int E(\omega')\,E(\omega-\omega')\,d\omega' \qquad (1)$$

Here we see the phenomenon that is typical for non-resonant two-photon absorption (or emission): the total production is the sum of contribution due to all combinations of frequencies that add up to the final frequency. $E^{(2)}(\omega)$ peaks at $2\omega_0$ if $E(\omega)$ peaks at ω_0. There are no restrictions for the energy of the single photons, only the sum of two photons has to match the energy difference between initial and final state. E.g. a photon that is 'too blue' combines with one

that is 'too red'. In the case that the pulse is bandwidth-limited all the contributions of the different pairs of photons, (all the available paths from initial to final state) are in phase. When the pulse is chirped this is no longer the case.

As an example, that is also realized in the performed experiment, assume a pulse with a linear chirp and with a square power spectrum within a band $\Delta\omega$:

$$\begin{aligned} |E(\omega)| &= E \qquad \text{if } -\tfrac{1}{2}\Delta\omega \leqslant (\omega-\omega_0) \leqslant \tfrac{1}{2}\Delta\omega \\ \arg(E(\omega)) &= \alpha(\omega-\omega_0)^2 + \omega t \end{aligned} \tag{2}$$

In this particular case the sum over all photon-pair contribution, as given in Eq. 1 results in

$$\begin{aligned} E^{(2)}[2(\omega_0+\delta\omega)] &= \int_{-\Delta\omega/2+|\delta\omega|}^{+\omega/2-|\delta\omega|} E^2 \exp(2i\alpha\omega'^2)\, d\omega' \\ &= E^2 \frac{1+i}{2}\frac{\sqrt{\pi}}{\alpha}\operatorname{erf}[(i-1)\sqrt{\alpha}\,(\Delta\omega/2-|\delta\omega|)] \end{aligned} \tag{3}$$

In the above equation we see the well-known Fresnel integral. 'On axis', so for a frequency $\omega = 2\omega_0$ or $\delta\omega = 0$, the result is identical with Fresnel diffraction. 'Off axis', so in the case that the energy of the final state is more or less than two times the central photon energy, the integration limits are different than as they occur in the usual Fresnel diffraction. The strict analogy between the two-photon absorption with a pulse described in Eq. 2 and Fresnel diffraction would be when the width of the slit that occurs in the diffraction problem would be a function of the off-axis distance of the final observation.

Due to the connection with Fresnel diffraction, it is straightforward to extend the two-photon absorption processes with chirped pulses to the use of zone plates and spectral focusing. With spectral focusing we mean the situation that the bandwidth of the effective driving field at two-photon level $E^{(2)}(\omega)$ is considerably smaller than the original pulse $E(\omega)$.

Another situation, not related with chirped pulses, where this process occurs is when the output spectrum after frequency doubling in a non-linear crystal is limited due to phase match restrictions. The frequency-doubled light has in general a spectrum that is $\sqrt{2}$ narrower than the primary pulse, due to the non-linearity of the frequency-doubling process. But there is more: it is observed that 'too red' and 'too blue' photons from the primary pulse are combined to the central wavelength, due to the phase-matching restrictions. The bandwidth of the absorbed light is much wider than the bandwidth of the emitted light of the double frequency.

Here we will create the effect of spectral focusing by use of a zone plate. Frequency components that are not constructively interfering at the final frequency $2\omega_0$ are simply blocked.

So far we assumed that we were dealing with a genuine two-photon process. More specifically, the assumption was that there are no intermediate resonances at the one photon level. The presence of an intermediate state brings both a simplification and a new complication. The simplification is that the sum of contribution of photon pairs is replaced by one single contributing pair, namely the colour combination that is resonant with the intermediate state. The new complication is that the finite lifetime of the intermediate state makes that the response of the medium is not instantaneous anymore as with a simple χ_2 material but also determined by the history of the process.

The most intuitive order of absorption processes is that in the beginning of the pulse the transition from the ground state to the intermediate state is made, while later when due to the chirp of the light the second step has become resonant, the final transition is occurring. However, there are also less intuitive processes possible in such a ladder of states.

In this context we call a counterintuitive chirp, a frequency sweep where the excitation to the final state is resonant first with the light, and the transition from the initial state is resonant at the end of the pulse, or in any case as the last of all involved transitions.

Whether processes should be called intuitive or not is of course subjective. But in this context we connect the word intuitive with the notion that the ladder itself (in more explicit terms, the spectroscopy of the target) is independent of the light intensity. So it is assumed that the AC-Stark shifts or light shifts of the involved levels are negligible for the used intensities. However, when we require a one-photon process rate (e.g. indicated by the Rabi frequency) that is larger than the inverse of the pulse duration of the light, then it is unavoidable that the Autler-Townes splitting is more than the bandwidth of the laser. So intuitive or not, the spectroscopy of the ladder will be affected by the light in cases that the light intensity is high enough to expect an excitation probability per pulse of unity.

Experiments

Experiments, demonstrating the for-mentioned 'spectral diffraction' were performed with use of the following laser system (Noordam et al. 1991). Pulses from a colliding-pulse mode-locked (CPM) ring dye laser (pulse duration around 100 fs, central wavelength around 620 nm) were amplified in so-called Bethune cells which were pumped at 10 Hz by the second harmonic of a seeded Nd:YAG laser. Tunable pulses were obtained by focusing these pulses in water to generate a wavelength continuum. The desired wavelength was selected with a pulse shaper (see Fig. 1), a device that was introduced by Weiner et al. (1988). After the shaper the pulses were amplified again into the μJ range. The shaper was not only used to select the central wavelength and the bandwidth but also to tune

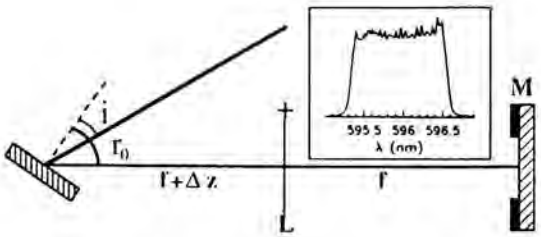

Fig. 1. The pulse shaper. This simple and elegant device consists of a grating, a lens (indicated by L, with a focal length f) and a mirror with an adjustable slit (indicated with M). In the inset the power spectrum is shown, as it is shaped by the slit. Of course, other obstructions can be placed in front of the mirror; see e.g. Fig. 7.

the chirp. The frequency spectrum of the pulse before the shaper, $E(\omega)$, is changed to $E(\omega)\exp(i\phi(\omega))$ after the shaper. The additional phase can be described by a Taylor series in which the lowest useful order is $\phi(\omega) \approx \alpha(\omega - \omega_0)^2$, where α is proportional to Δz (see Fig. 1). The relation between the chirp α and experimental parameters as grating angle, grating spacing and wavelength of the length is given in Broers et al. (1992a).

Non-resonant two-photon processes

The spectral diffraction measurements, given in Fig. 2, are performed with a standard frequency doubling crystal for doubling 100-fs, 620-nm pulses. The bandwidth of the chirp pulses is much less than the shorter above-mentioned pulse, so phase-matching issues are not of any relevance in these experiments. Apart from all the oscillations in the signal due to interference of the various color combinations, it is interesting to compare the absolute signal sizes for the various chirps. The signals are very much reduced when the chirp is increased. It turnes out that this effect of reduction is already apparent for very small chirps, in particular the spectral contribution at the center of the bandwidth (see also Broers et al., 1992a).

In the absence of any chirp a triangular spectrum is expected (the convolution of a block) which is measured indeed (see e.g. Broers et al., 1992a. Note that the power spectrum is the square of the absolute value of the amplitude spectrum). When the chirp is much larger than the ratio of the pulse duration and the spectral bandwidth, a block is expected. Due to the large chirp all frequency components are separated in time. Therefore the photon pairs have to be symmetric. And the spectral block is realised 'sequentially.' The result is almost frequency independent. But in the intermediate case of chirped two-photon excitation the production shows fringes as a function of the final frequency and is not necessarily maximal at the central frequency.

In the shaper (Fig. 1), at the position of the mirror, the spectrum of the pulse is separated geometrically. Therefore it is possible to reduce the original spectrum to a much narrower block spectrum. However, it also gives the oppor-

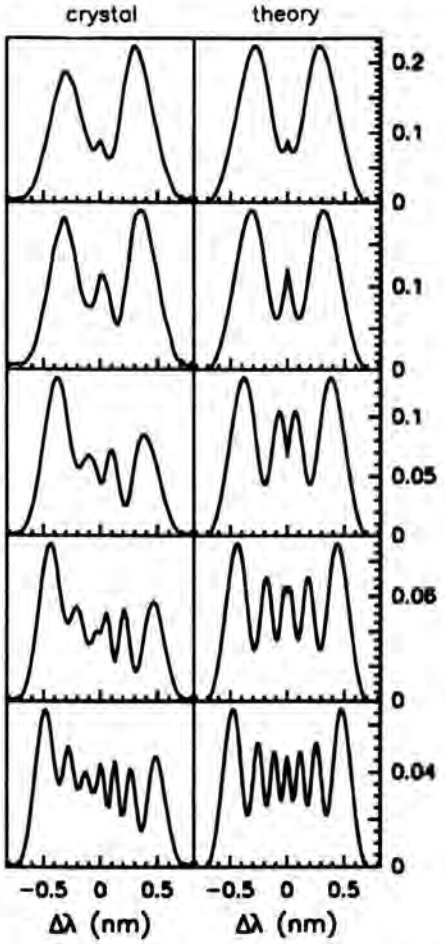

Fig. 2. Measured (left column) and calculated (right column) power spectra of frequency doubled light for increasing chirp of the fundamental pulse. Starting from the top, the bandwidth-time product, relative to that of the chirp-free pulse, has the values: 2.9, 3.5, 5.2, 8.0 and 12.0, respectively.

tunity to include a structure that is clipping the spectrum in a less straightforward way.

What will be discussed in the following is what we would like to call spectral focusing, in analogy with geometrical focusing and inspired by the just mentioned analogy between spectral and geometrical diffraction. The idea is sketched in Fig. 3.

As is said before, the phase profile of a linearly chirped pulse as a function of the frequency is a parabola with its minimum at the central frequency. Both the components at the red and the blue side are retarded with respect to the central frequency. The phase of the total path leading to a final frequency $2\omega_0$ is

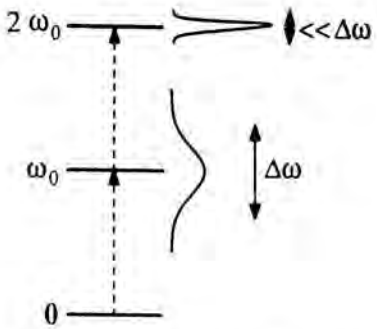

Fig. 3. The basic situation that could be termed spectral focusing, shown for a two-photon process. The effective bandwidth at the two-photon level is much smaller than the bandwidth of the excitation pulse.

$\phi_{tot}(\delta\omega) = 2\alpha(\delta\omega)^2$ if the path consists of the combination $\omega_0 - \delta\omega$ and $\omega_0 + \delta\omega$. The paths can be divided in zones, such that the maximum phase difference in one zone is π. The zone boundaries are given by $\delta\omega_n$, $n = 1, 2, ..., n_{max}$, where $(n-1)\,\pi < \phi_{tot} < n\pi$. The width of the zones is not equal since ϕ_{tot} is not a linear function of $\delta\omega$. The enhancement of energy at ω_0 (focusing) is obtained by blocking all odd zones (n odd) or all even zones (n even). The zone plate that was used blocked the odd zones. The transmission is given in Fig. 4. Since the zones are becoming smaller for off-centred frequencies the number of useful zones is limited. In our case the limit was set by the diffraction limit of lens L (Fig. 1) to the first three even zones. In this arrangement there is a fixed relation between the scale of the zone plate and the magnitude of the chirp.

There is a distinction between spectral focusing and spectral clipping. Clipping is used in the shaper to create a block spectrum by means of a slit. Both with focusing and clipping the width of the spectrum is reduced. With spectral focus-

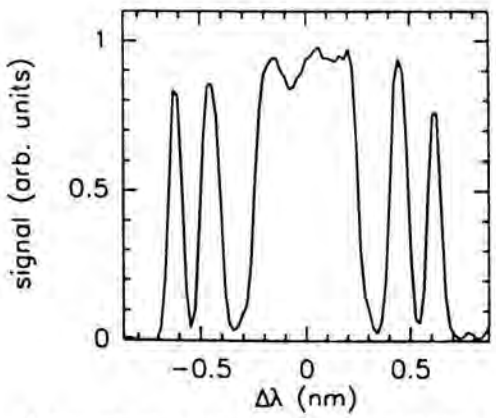

Fig. 4. Power spectrum of the excitation pulse with the Fresnel zone plate put into the shaper. The zone plate blocks the first three even Fresnel zones. Since it is the spectrum at the one-photon level it is independent of the applied chirp.

ing the intensity in the remaining bandwidth is increased, while in the case of clipping spectral components are blocked or left unaffected. Fig. 5 shows that the zone plate gives rise to both a reduction of the bandwidth and an increase of the production for the remaining bandwidth.

Resonant two-photon processes

Because of spectral congestion that is so typical for the spectroscopy of molecules, the prospects for resonant excitation are off hand always better than for non-resonant excitation. It was recently proposed to use chirped pulses to sweep through a chain of resonances (Chelkowski et al. 1990) to obtain an efficient and controlled molecular dissociation. The idea is that the population of the initial molecular ground state is sequentially transferred from one state of the vibrational ladder to the next one higher; all within one laser pulse. The advantage over a multi-pulse approach is that the whole process lasts less than a few ps so that the process is not drained by unwanted decay mechanisms out of the intermediate states (Maddox 1992).

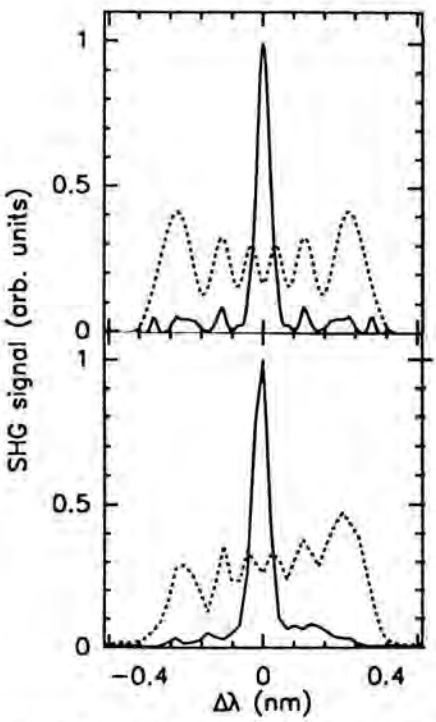

Fig. 5. Experimental (bottom) and theoretical (top) power spectra of frequency doubled light, which show the effect of spectral focusing. The dotted lines result from a pulse with a chirp that amounts to six Fresnel zones. When the even Fresnel Zones are blocked, the yield at $2\omega_0$ is enhanced at the cost of the yield at detuned frequencies (full line).

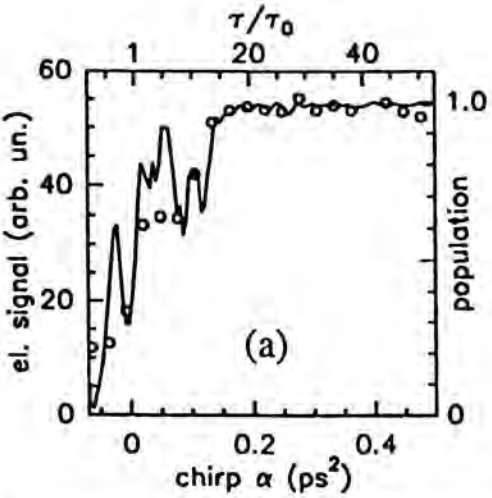

Fig. 6. Measured photoelectron signal (points) and calculated population of the 5d state (line) as a function of the chirp under the following conditions: $\lambda_c = 777.5$ nm, $\Delta\lambda = 5.8$ nm, Fluence = 500 μJ/cm^2.

The referred experiment (Broers et al., 1992c) is not performed with a vibrational ladder in a molecule but with a three-state ladder in atomic rubidium in order to postpone the technological problems of chirped infrared pulses. The experiment is performed with the 5s, 5p and 5d state, connected with a 780-nm and 776-nm transition. The population of the final 5d state is detected my means of photoionization with a long (5 ns), weak (8 MW/cm^2) pulse, but with a high fluence (about 45 mJ/cm^2, a hundred times higher than the chirped pulse). The parameters of the chirped pulse are given in the caption of Fig. 6 and 7.

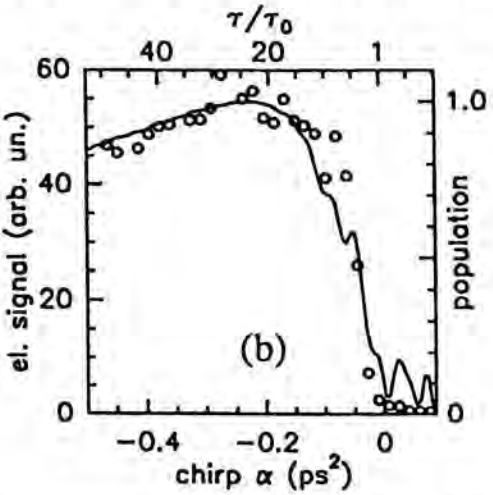

Fig. 7. As in Fig. 6, for the following parameters: $\lambda_c = 780.8$ nm, $\Delta\lambda = 5.8$ nm, $F = 500$ μJ/cm^2.

Fig. 6 shows a typical result. It should be realized that the spectral profile of the pulse is constant over the scan. Still, we see that the population of the 5d state is substantially enhanced with the application of a positive chirp, despite the fact that a chirp is reducing the light intensity of the pulse that is driving the two-photon process. An important observation is that a full population transfer is possible for sufficiently large chirp. Due to problems with Rabi oscillations full transfer is hard to obtain with a bandwidth-limited pulse.

It is rather straightforward to model the chirped excitation process, because apart from the light pulse only three states are involved. The result of the numerical solution of the time-dependent Schrödinger equation is given by the full line in Fig. 6. The calculations have the right-hand scale, the measurements the scale at the left side. The vertical scale of the measurements is fitted to the calculations. But once the connections is established it is consistent with all other measurements, not only the ones of Fig. 6.

When the chirp is reversed also an increase of the population transfer is found, as can be seen in Fig. 7. Also this measurement is confirmed by the solution of the Schrödinger equation describing three states (without loss) in a chirped radiation field.

The mechanism that underlies the population transfer, given in e.g. the Figs. 6 and 7, is adiabatic passage. This is a very general mechanism, relevant in many areas of both quantummechanics and classical mechanics, and subsequently discussed at many places. Because this mechanism is so well established (see e.g. Melinger et al. 1991) an explanation in the form of Fig. 8 will suffice. The three dotted lines 1, 2, and 3 indicate the dressed but uncoupled states 5s, 5p, and 5d, plus, without and minus one photon, respectively, as a function of the wavelength of the light field. The full lines show the effect of the coupling (resonant AC Stark shift or Autler Townes splitting; in the time domain known as the Rabi oscillation time). The effect of the chirp can be seen as a change of the

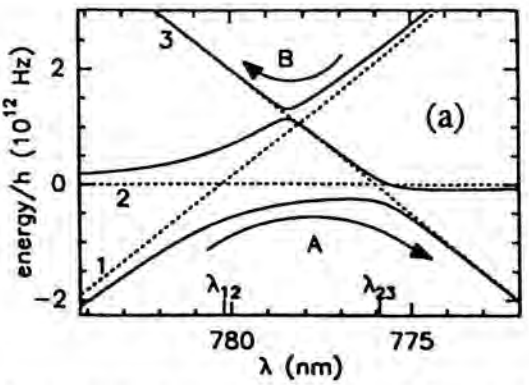

Fig. 8. (a) Calculated dressed-level scheme of the three-state ladder at an fixed intensity of $1.1\ 10^7$ W/cm^2. The dotted lines indicate the dressed, uncoupled states, with 1 for 5s plus one photon, 2 for 5p, and 3 for 5d minus one photon. The full lines give the level positions in the presence of the light field.

instantaneous frequency. Therefore the wavelength scale can also be interpreted as a time scale. If the change of frequency is slow enough an eigenstate in the field stays an eigenstate (a 'sweep' along a line). However, there is no one-to-one relation between the coupled and the uncoupled eigenstates. E.g. the lowest curve in Fig. 8 corresponds to the 5s state far left of the avoided crossings (goes over in the 5s state when the light is turned off), while it corresponds with the 5d state when the coupling is due to light of a higher frequency at the right side of all avoided crossings.

This figure explains why chirped pulses can make full population transfer irrespective of the sign of the chirp. In the intuitive case two avoided crossings are made, indicated with arrow A, in the counterintuitive case, the transition indicated with arrow B is made, consisting of only one avoided crossing. We see the interesting consequence that in the last case state 2 is only slightly populated. In both cases the 'gap' of the avoided crossing has to be large enough to ensure that the passage is adiabatically. This means that the light intensity of the pulse has to be high enough when the instantaneous light frequency matches the resonance condition. Such a constraint is very mild and fulfilled over a large range of intensities, making the process very stable.

Discussion

Undoubtedly, the value of the presented work is, among other considerations, determined by the possibility to extend the observed mechanisms from two-photon to *n*-photon processes. For the resonant processes, this extension is already made in calculations (Chelkowski, 1990), and seems very feasible in real experiments, especially because multi-step adiabatic passage has been demonstrated in other systems (e.g. Hulet and Kleppner, 1983, with a combination of dc and microwave fields instead of visible light).

Given the fact that short pulses are a requirement anyhow, e.g. in order to avoid unwanted processes out of intermediate states, the use of chirped pulses is not a significant complication.

Finally, a two-photon process has advantages over one-photon processes, in the particular case of electronic excitations, because the relevant transitions are (deep) in the UV regime for many molecules and atoms.

Conclusion

We have sketched two types of processes that are both intrinsically fast and that are in principle both applicable to molecules. However, due to the selectivity of the resonant process, the prospects for this one is better.

The experiments with non-resonant two-photon transitions have shown that pulses have to be closer to the Fourier transform limit than is assured by the commercially used classification of 'nearly bandwidth-limited' in order to prevent destructive interference effects in the excitation.

Acknowledgement

This work is part of the research program of the 'Stichting voor Fundamenteel Onderzoek der Materie' (Foundation for Fundamental Research on Matter) and was made possible by financial support from the 'Nederlandse Organisatie voor Wetenschappelijk Onderzoek' (Nederlands Organisation for the Advancement of Research).

References

Broers, B., van Linden van den Heuvell, H.B., and Noordam, L.D., *Optics Comm. 91* **57**, 1992a.

Broers, B., Noordam, L.D., and van Linden van den Heuvell, H.B., *Phys. Rev. A* **46**, 2749, 1992b.

Broers, B., van Linden van den Heuvell, H.B., and Noordam, L.D., *Phys. Rev. Lett.* **69**, 2062, 1992c.

Brumer, P., and Shapiro, M., *J. Chem. Phys.* **84**, 4013, 1986.

Chelkowski, S., Bandrauk, A.D., and Corkum, P.B., *Phys. Rev. Lett.* **65**, 2355, 1990.

Hulet, R.G., and Kleppner, D., *Phys. Rev. Lett.* **51**, 1430, 1983.

Melinger, J.S., Hariharan, A., Gandhi, S.R., and Warren, W.S., *J. Chem. Phys.* **95**, 2210, 1991.

Noordam, L.D., Joosen, W., Broers, B., ten Wolde, A., van Linden van den Heuvell, H.B., and Muller, H.G., *Optics Comm.* **85**, 331, 1991.

Maddox, J., *Nature* **360**, 103, 1992.

Weiner, A.W., Heritage, J.P., and Kirscher, E.M., *J. Opt. Soc. Am. B* **5**, 1563, 1988.

Authors' addresses

B. Broers, L.D. Noordam and H.B. van Linden van den Heuvell; FOM-Institute for atomic and molecular physics,
Kruislaan 407
1098 SJ Amsterdam
The Netherlands
H.B. van Linden van den Heuvell; Van der Waals-Zeeman Laboratory of the University of Amsterdam
Valckenierstraat 65
1018 XE Amsterdam
The Netherlands

D. Goswami, C.W. Hillegas, J.X. Tull and W.S. Warren

Generation of Shaped Femtosecond Laser Pulses: New Approaches to Laser Selective Chemistry

Abstract

We discuss two new approaches to pulse shaping which have major potential advantages over existing techniques for making complex waveforms. These approaches are needed to create nonlinear frequency sweeps and other modulations which are useful for coherent control of chemical dynamics.

Introduction

The idea of using controlled radiation fields to alter molecular states or drive chemical reactions – laser selective chemistry – has a very long and checkered history (for recent reviews see Rice 1992 and Warren 1993). The development of high-power lasers in the 1960s led almost immediately to efforts to dump energy into specific chemical bonds (for example, through overtone absorption) in the hope that this would change reaction dynamics. By the late 1970s (many person-years and guilders later) these studies had produced valuable insights on intramolecular energy redistribution, but the original goal seemed farther away then ever, and the concept of 'photons as chemical reagents' had fallen into disrepute.

Today the coherent control community includes dozens of theoretical and experimental groups, and the prospects for optical control of chemical dynamics seem quite bright. Two major and complementary sets of developments over the last decade have changed the outlook dramatically. First and foremost, the technology for controlling optical fields improved dramatically. Coherent laser spectroscopy has fluorished since the late 1970s and early 1980s (in large part due to contributions from the chairman of this meeting, for example Morsink 1980), but mainly by the clever use of pulse sequences which were extremely insensitive to pulse shape and phase shift effects. Indeed, the first experiments which used even nonoverlapping nanosecond pulses with a completely controlled phase shift came in 1981. Phase shifting technology rapidly evolved in the 1980s into the femtosecond time domain (Mukherjee 1986, Spano 1987, Warren 1988, Scherer 1990). In addition, optical pulse shaping capabilities evolved from nanosecond resolution with pieces chopped out of a continuous laser to < 100 fs time resolution with amplified laser pulses and programmability (Weiner 1986,

1989, Haner 1988). Suddenly the kinds of multiple-pulse experiments which led to such dramatic breakthroughs in magnetic resonance twenty years earlier became technically conceivable in the optical regime, on a timescale which was short enough to compete with molecular relaxation, with high enough powers to significantly perturb populations. Experimental work has demonstrated modulation or enhancement of overall signals (in stimulated Raman scattering, multiphoton ionization, or fluroescence) in a variety of applications. Just as importantly, by the mid-1980s these technological developments had begun to fire the imagination of the theoretical community. Starting with simple model molecules, and gradually evolving into more complex systems, calculations have shown that appropriately shaped and phased optical pulses can prepare selected rotational states, pump up anharmonic vibrational ladders or modify internal relaxation dynamics (for recent reviews see Rice 1992 and Warren 1993).

Despite the tremendous progress over the last decade, there is still a gap between what the experimentalists have achieved and what the theoreticians expect will be possible. This gap is narrowing visibly as calculations get more sophisticated, but it is still clear that technological capabilities provide an ultimate limitation to what will be achieved in the foreseeable future. While 100 femtosecond, programmable pulse shaping has been achieved by several approaches, this does not imply that *any* waveform with such a risetime is possible. For example, nonlinear frequency modulation remains extremely difficult (and, unfortunately, central to many proposed schemes). In addition, schemes to make molecules act as 'quantum mechanical computers' to design their own optimal waveforms (Rabitz, 1992) require the ability to change waveforms quickly, and the most common approach to programmable pulse shaping (multielement LCD modulation of a spatially dispersed waveform) can only be updated at approximately 100 Hz – far lower than the repetition rate of even many amplified laser systems.

We discuss here two new pulse shaping methods developed in our laboratory over the last few months. First we discuss a method for letting molecules design their own optimal pulse shape by absorption within a Michaelson interferometer. This makes it possible to fabricate pulses with dozens or hundreds of different Fourier components, individually matched to specific molecular absorptions. In addition, we show that acousto-optic modulators can be used in place of LCDs to produce programmable pulse shaping. The ultimate potential advantages of this technique include very high resolution, pulse shape updating at MHz repetition rates, and absence of distortions due to gaps between LCD pixels.

Interferometric Pulse Shaping

One of the most important issues in coherent laser spectroscopy is *robustness*. It is one thing to calculate waveforms which in principle would force molecules into a specific state, given the exact Hamiltonian and no inhomogeneities; real-

istic implementation is quite another matter. For this reason, one of our major thrusts over the last few years has been applications of frequency swept laser pulses (Melinger 1991, 1992, Goswami 1993), which in the adiabatic limit produce population inversion or state-to-state transfer even if the sweep is not perfectly linear or if the intensity is not uniform. For example, we have shown that frequency swept pulses can simultaneously invert a large number of transitions in molecular iodine (Melinger 1991). However, the simplest version of this technique (a linear frequency sweep) only works far from the rotational bandheads. Explicitly, the population in state $J'' = N$ will only be transferred into the excited state if the frequency separation between the two transitions including this state ($R(N)$-$P(N)$) is larger than the pulse bandwidth.

It is possible to do much better with more sophististicated laser pulses. In the weak-response limit, the optimum laser pulse for exciting any molecule with discrete spectral lines would be a pulse which contains only those frequency components. Such a pulse would also do the best possible job of selectively exciting a specific molecule in a background of competing absorbers. In the strong-response (adiabatic) limit, pulses with such a frequency structure are a natural and logical starting point for generating efficient inversion, particularly if phase modulation or frequency sweeps can be imposed on this overall structure as well.

Such waveforms could look quite complex. In iodine, for example, the spectrum of a room-temperature bulb has 5-10 intense transitions per wavenumber. Thus even a 1 ps pulse (bandwidth $\approx 13\ \mathrm{cm}^{-1}$) excites approximately 100 different transitions, which are separated only slightly in frequency. No existing pulse shaping techniques have such frequency resolution or could generate waveforms with such complexity. However, the *molecule itself* knows how to generate such a waveform easily; the optical free induction decay after a single short pulse has exactly the right frequency characteristics.

We save the free induction decay while deleting the intense original pulse with a Michaelson interferometer (Fig. 1). When the two arms of the interferometer are exactly equal, it produces constructive interference in one direction and

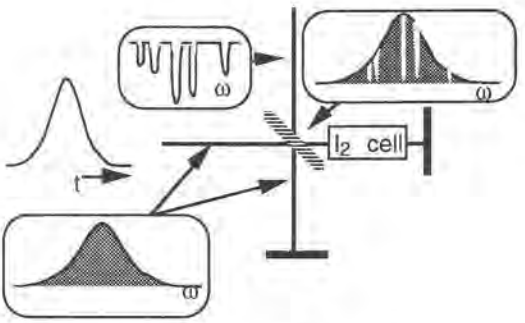

Fig. 1. A Michaelson interferometer plus an iodine cell shapes a picosecond pulse to create a waveform which, when amplified, is extremely efficient for iodine inversion.

destructive interference in the other, independent of wavelength. Inserting a sample cell into one of the arms attenuates the resonant frequency components, and also introduces some phase shifts (depending on the optical density of the cell). This destroys the perfect cancellation in the destructive interference direction (counterpropagating with the entering laser pulse), leaving only the molecular free induction decay. The beams can be separated by polarization rotation (using a polarizing beamsplitter and a quarter-wave plate); we find it more convenient to misadjust the Michaelson by $\lambda/2$, thus separating the destructive interference direction from the input beam. Since the iodine cell is relatively large (10 cm) the delay line is stabilized with a collinear HeNe laser and a PZT on one arm.

Analysis with a 10 ps resolution streak camera (Hamamatsu) verifies that an elongated pulse is produced. We are currently producing amplified shaped pulses with a conventional excimer-pumped dye amplifier.

Generation of Tailored Ultrafast Laser Pulses with Tailored Microsecond Radiofrequency Pulses

Subpicosecond resolution pulse shaping is always achieved by indirect modulation schemes, since no electronic devices are capable of responding that quickly. In one approach, pioneered in our laboratory a few years ago (Haner 1988), fast electro-optic modulators are inserted into a pulse stretcher-compressor combination. After the stretcher, an initial ultrafast pulse can be lengthened to ≈ 100 ps; a programmable microwave pulse generator can act with a risetime of approximately 10 ps, so the stretched pulse can be significantly altered. One major advantage of this idea is that the waveform can be updated quite rapidly (in one application, new pulse shapes were generated within approximately 10 ns). Also, the pulse shape is controlled by a single temporal voltage waveform, which is relatively easy to characterize with modern electronics. However, the effective number of 'bits' of modulation which can be imposed on a pulse is relatively small (6-10). In addition, the technology is cutting-edge and difficult to use.

Heritage and Weiner developed a pulse shaping approach in the mid-1980's using spatial dispersion of an ultrafast pulse within a grating pair (Weiner 1986). Programmability was ultimately achieved with multielement LCD spatial modulators for phase or amplitude modulation (Weiner 1989). The advantage of this approach is that these modulators are commercially available, and thus shaped waveform generation is dramatically simpler than with fast electro-optic modulators. However, the gap between pixels leads to an additional modulation on the desired waveform. In addition, alignment and calibration of each individual pixel can be complex, and the fundamental response time of the devices is relatively slow (a few hundred Hertz). The LCD devices are fundamentally phase modulators, and while they can be used with polarizers to produce amplitude modulation, the isolation is also not particularly good.

We present here a new pulse shaping approach which promises to combine

many of the advantages of the two earlier techniques. It uses a shaped radiofrequency pulse of long duration (up to a few microseconds) to control the ultrafast laser pulse shape. The apparatus is essentially the same as the Heritage-Weiner pulse shaping setup, with the LCD spatial modulators replaced with acousto-optic modulators. In the simplest approach (Fig. 2) the AOM is operated at the Bragg angle. We have previously shown that amplitude and phase modulation applied to the radiofrequency AOM driver is imposed on the laser output; however, this is limited to generating shaped pulses with nanosecond risetimes. In our new approach, the laser pulse entering the AOM is spatially dispersed to a width of approximately 5 mm. The speed of sound in our TeO_2 modulator is 4.2 mm/μs. Thus, the sound wave takes approximately 1.2 μs to traverse the entire laser beam, and a 1.2 μs modulated r.f. pulse produces different diffracted intensities at different positions in the crystal.

Preliminary experimental data is shown in Fig. 3. The output of a LeCroy model 9109 arbitrary waveform generator (resolution 5 ns) was mixed with a 200 MHz frequency source to generate the r.f. driver pulses for a Crystal Tech-

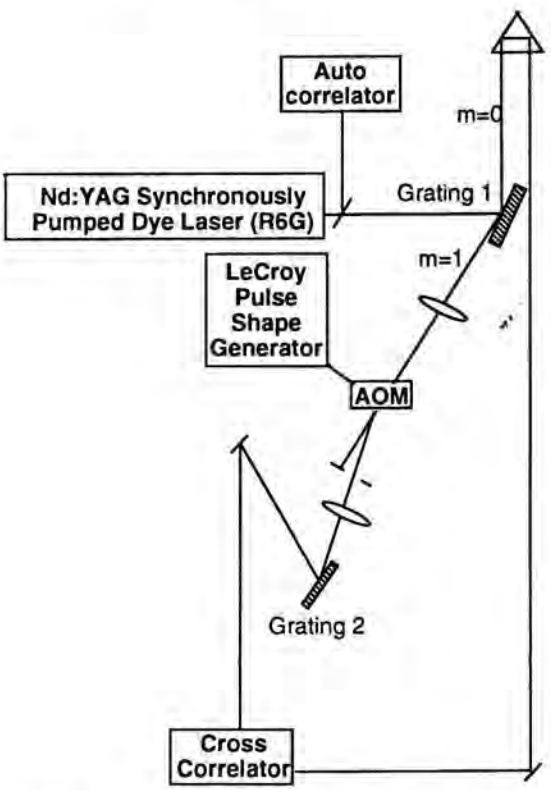

Fig. 2. Pulse shaping apparatus. The gratings were used at near-grazing incidence, and the spatially dispersed pulse was modulated with an acousto-optic modulator and an arbitrary waveform generator.

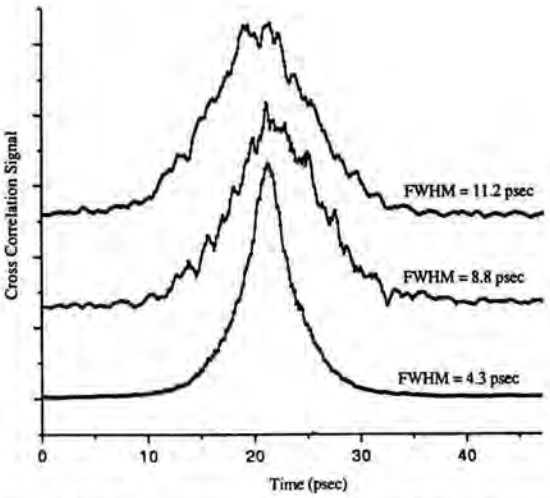

Fig. 3. Cross-correlations of the recompressed AOM output with the initial pulse. Bottom: continuous rf irradiation. Middle and top: irradiation with sinc-envelope rf pulses (30 and 60 ns FWHM). The observed cross-correlations are in good agreement with our predictions.

nology model 3200 AOM (risetime 10 ns). In this experiment, we started with a relatively long laser pulse (autocorrelation width 3.8 ps) from our YAG-pumped dye laser, and applied sinc-function r.f. pulses to lengthen the laser pulse. If the sinc function pulse is sufficiently short (in the crystal) to make the dispersed pulse nearly uniform in intensity, this will create a rectangular laser pulse. In fact, starting from our picosecond pulse, we only dispersed the frequency components over approximately 2.5 mm, and thus the edges are expected to be strongly broadened. Fig. 3 compares cross-correlations generated with continuous r.f. irradiation (4.3 ps, compared to the 3.8 ps autocorrelation); a sinc function with FWHM 60 ns, which is 250 μm in the crystal (8.8 ps); and a sinc function with FWHM 30 ns, which is 125 μm in the crystal (11.2 ps). In the latter case, the crosscorrelation shows the structure expected from the imposed r.f. pulse (with these parameters, a fully rectangular crosscorrelation was not expected). Note that the cross-correlation risetime and falltimes are very similar for the two sinc-modulated laser pulses, and far longer than the risetime of the unmodulated pulse, as expected.

The major advantage of using Bragg diffraction is the very low background; the typical isolation of such a modulator is 40 dB. However, spatial dispersion because of the Bragg condition $\mathbf{k}_{in} = \mathbf{k}_{out} + \mathbf{k}_{rf}$ must be taken into account. The variation of Bragg angle with optical wavelength is not a serious issue, even for femtosecond pulses; the extra spatial dispersion could be corrected by prisms. However, the Bragg angle also varies as the r.f. frequency is changed, which could send different frequency components in different directions. In TeO_2, the Bragg angle varies by 0.1 mrad/MHz of r.f. frequency at $\lambda = 600$ nm, so a waveform with 10 MHz modulation bandwidth would spread the output beam by

only 1 mrad. Larger r.f. bandwidths might create an intolerable spreading (unless the modulator is double-passed). However, even restriction to a 10 MHz bandwidth (risetime 40 ns) would imply an effective 'pixel size' in the AOM of 0.17 mm. Our modulator has a clear aperture of 0.5 cm, but this is not a fundamental limitation (far longer modulators are available; the acoustic attenuation across the crystal was less than 10%). An inexpensive AOM and a much lower resolution waveform generator could still be equivalent to a 100-pixel LCD array, with additional advantages of no pixel gap, rapid waveform updating, high isolation, and simple calibration.

It is also possible to consider using the acousto-optic modulator in other modes, and in this case far higher resolution can be achieved. For example, the undiffracted beam can be used if pure amplitude modulation is desired, and then the full bandwidth of the modulator can be employed. Here the major disadvantage would be decreased isolation (20 dB, comparable to an LCD modulator, implies 90% diffraction efficiency), but again a double-pass configuration would work. Raman-Nath mode (perpendicular to the transducer) would convert the device into a phase modulator.

Summary

We have briefly discussed here two new approaches to pulse shaping which have major potential advantages over existing techniques for making complex waveforms. The interferometric approach can make laser pulses with high complexity, but tailored in a robust manner to the real absorption spectrum of individual molecules. The acousto-optic approach promises to substantially simplify the process of complex pulse shape generation. Both of these approaches can be expected to contribute significantly to the next generation of experiments for coherent control of chemical reactions.

This work is supported by the National Science Foundation under grant CHE-9101544. We also wish the thank LeCroy Instruments for loan of the waveform generator.

References

Goswami, D., and Warren, W.S., In: *J. Chem. Phys.* **99**, 4509, 1993.

Haner, M., and Warren, W.S., In: *Appl. Phys. Lett.* **52**, 1458, 1988.

Judson, R., and Rabitz, H., In: *Phys. Rev. Lett.* **68**, 1500, 1992.

Melinger, J.S., Hariharan, A., Gandhi, S.R., and Warren, W.S., In: *J. Chem. Phys.* **95**, 2210, 1991.

Melinger, J.S., Gandhi, S.R., Hariharan, A., Tull, J., and Warren, W.S., In: *Phys. Rev. Lett.* **68**, 2000, 1992.

Morsink, J.B.W., Kruizinga, B., and Wiersma, D.A., In: *Chem. Phys. Lett.* **76**, 218, 1980

Mukherjee, A., Mukherjee, N., Diels, J.-C., and Arzumanyan, G., In: *Ultrafast Phenomena V* (G. Fleming and A. Siegman, editors; Springer, Berlin) p. 266, 1986.
Rice, S., In: *Science* **248**, 412, 1992.
Scherer, N., Ruggiero, A.J., Du, M., and Fleming, G.R., In: *J. Chem. Phys.* **93**, 856, 1990.
Spano, F., Haner, M., and Warren, W.S., In: *Chem. Phys. Lett.* **135**, 97, 1987.
Warren, W.S., and Haner, M., In: *Atomic and Molecular Processes with Short Intense Laser Pulses*, (A. Bandrauk, ed., Plenum, New York), p. 1, 1988.
Warren, W., Rabitz, H., and Dahleh, M., In: *Science* **259**, 1581, 1993.
Weiner, A.M., Heritage, J.P., and Thurston, R.N., In: *Opt. Lett.* **11**, 153, 1986.
Weiner, A.M., Thurston, R.N., Tomlinson, W.J., Heritage, J.P., Leaird, D.E., and Kirschener, E.M., In: *Opt. Lett.* **14**, 868, 1986.

Department of Chemistry, Princeton University, Princeton, NJ 08544 USA and the Princeton Center for Photonics and Opto-Electronic Materials

K. Yoshihara, R. Inaba, H. Okamoto, M. Tasumi, K. Tominaga and K.A. Nelson

Vibrational and Rotational Dynamics of Molecules in Solution Studied by Femtosecond CARS and Raman Echo

Abstract

Vibrational dephasing in liquids has been studied systematically by polarized femtosecond time-resolvent coherent anti-Stokes Raman scattering (CARS), using C≡N and C≡C stretchings as probe vibrations. Dependence of the inter- and intramolecular dephasing process on molecular size is examined. Reorientational motion of molecules in liquid have also been observed from anisotropic component of Raman tensor by a proper choice of polarization conditions. In addition to picosecond decay component, a faster decay component presumably due to the non-dissipative free rotation has been found in the case of neat benzonitrile. An observation of ultrafast Raman echo with a new method is reported for the C≡N stretching of benzonitrile in the liquid phase. It is found that the vibrational line broadening is mainly due to homogeneous effect.

Introduction

Vibrational dephasing of molecules in condensed phase is a fundamental physical process and carries many important information on molecular interactions, and structure and dynamics of liquids. It gives the first step in the energy transfer pathway of chemical reaction. Since molecular vibration takes place in the femto- to picosecond timescale it is necessary to have time resolution in such a time region. Several groups have applied subpicosecond and femtosecond light pulses to time-resolved coherent anti-Stokes Raman scattering (CARS) measurements (Leonhardt et al, 1987; Bron et al, 1989; Fickenscher and Laubereau, 1990; Okamoto and Yoshihara, 1990; Joo et al., 1991). The main interests of these works have been the observation of vibrational dephasing and/or beating phenomena among several vibrational modes. We have developed an experimental apparatus for measuring femtosecond time-resolved CARS with the capability of selecting any arbitrary polarization conditions (Okamoto and Yoshihara, 1990) and have been studying systematically vibrational dephasing of C≡N stretching in series of alkanenitriles and alkanedinitriles (Inaba et al. 1991; Inba et al. 1992; Okamoto et al. 1993(a)) and of C≡C stretching in monoalkylace-

tylenes and dialkylacetylenes (Inaba et al. 1993(a)) in neat liquids as well as in mixtures with either hydrogen donating or accepting solvents. In this article we firstly describe intra- and intermolecular effects of vibrational dephasing.

One of the advantages of applying CARS is the feasibility of obtaining purely isotropic and anisotropic Raman components separately from independent experiments upon choosing proper polarization conditions (Dick, 1987). We secondly describe the anisotropic decay of C≡N stretching mode of benzonitrile in various conditions (Okamoto et al. 1993(b)).

One extension towards exciting higher order non-linear susceptibility of the time-resolved CARS measurement is the ultrafast Raman echo experiment, and it was suggested theoretically to be a method which gives a distinct separation between homogeneous and inhomogeneous contribution to the Raman band (Loring and Mukamel, 1985). The observation of Raman echo signal has recently been reported by Vanden Bout et al. (1991) for the first time. In this article we finally describe a Raman echo experiment with high repetition rate pulses and actual observation of echo signal of C≡N stretching of benzonitrile (Inaba et al, 1993(b)).

Intramolecular Effects on Vibrational Dephasing

We reported that the time-resolved CARS for C≡N stretching of relatively small alkanenitriles ($C_nH_{2n+1}CN$, $n=1\sim5$) and found molecular size has significant effects on the vibrational dephasing (Inaba et al., 1991). We expected that further extensive studies on the chain length dependence might provide information on the mechanism of intramolecular relaxation.

Typical experimental results of the time-resolved CARS for the C≡N stretching vibration ($\sim 2250\ cm^{-1}$) of neat alkanenitriles ($C_nH_{2n+1}CN$, $n=2\sim17$) are given in Fig. 1. The strong peak at zero delay is due to the nonresonant background. All the observed profiles nearly fit to a single-exponential decay function.

Within the framework of Fermi's Golden Rule, the intramolecular vibrational relaxation rate of an isolated molecule should be linearly correlated with the density of states, if the other factors can be regarded as practically constant. We find that the dephasing rates for the neat alkanenitriles are approximately proportional to the logarithm of the density of vibrational states as shown in Fig. 2. If the inter-state vibrational couplings between the optically allowed state and the background dark states are equivalent, the relaxation rate is expected to be governed by an integrated strength of the inter-state couplings. The present observation suggests that an average of the inter-state matrix elements for the coupling between the C≡N stretching and the dark states decreases as the alkyl chain becomes longer. It is interesting to note that there is no asymptotic limit for the value of T_2 up to $n=17$ (Fig. 2).

In contrast to the case of nitriles, the dephasing rates of C≡C stretching ($\sim 2120\ cm^{-1}$) of alkylacetylenes ($C_nH_{2n+1}C\equiv CH$, $n=4\sim10$) are almost in-

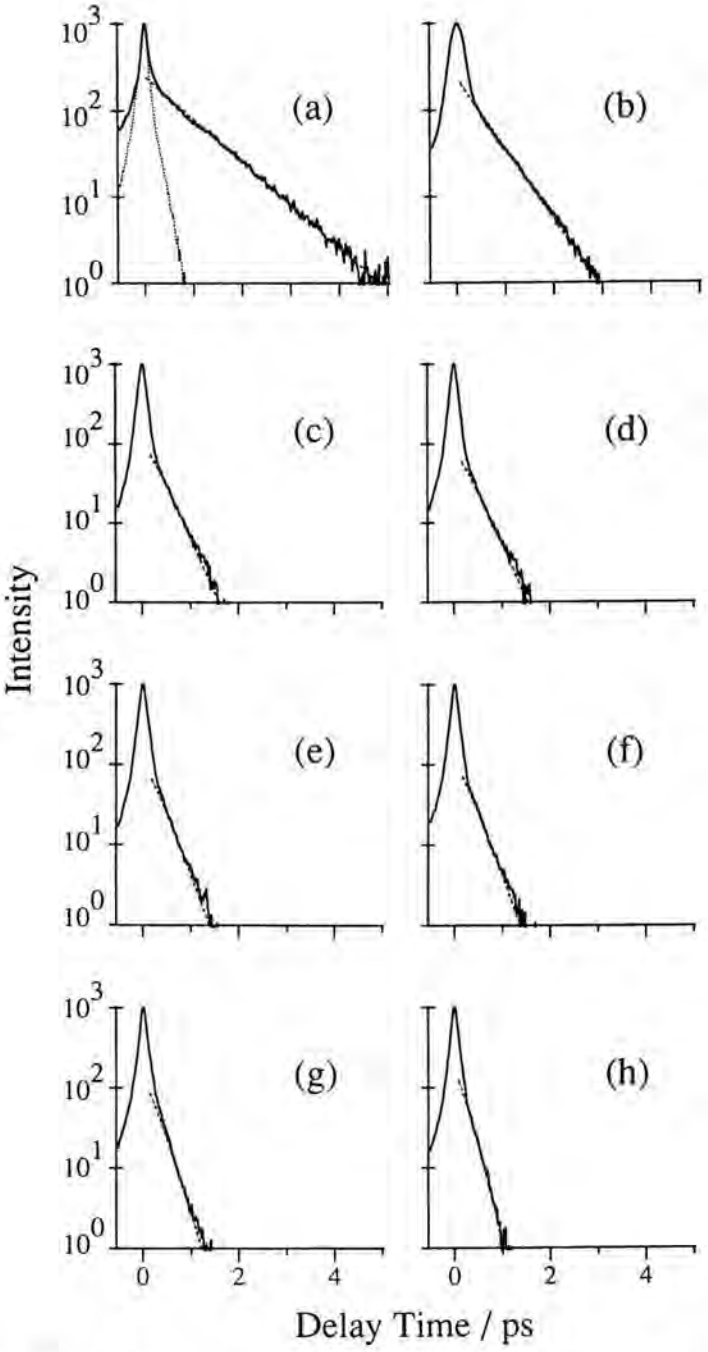

Fig. 1. Time-resolved CARS signals for the C≡N stretching of alkanenitriles. (a) C_2H_5CN, (b) $C_5H_{11}CN$, (c) $C_7H_{15}CN$, (d) $C_8H_{17}CN$, (e) $C_{10}H_{21}CN$, (f) $C_{11}H_{23}CN$, (g) $C_{14}H_{29}CN$, (h) $C_{17}H_{35}CN$. The dotted curve in (a) shows the nonresonant background signal from CCl_4.

dependent of the chain length in the region under study. Such a difference may be attributed to the presence and absence of the dipole associated with the C≡N and C≡C bonds, respectively. It is conceivable that the dephasing of C≡N stretching is affected by interactions between its own dipole and dipoles associated with the methylene groups in the same molecule but located far from the C≡N group.

Intermolecular Effects on Vibrational Dephasing

Fig. 2 shows the dephasing time of C≡N stretching of alkanenitriles mixed with methanol (proton donating solvent) in 1:1 mole ratio. The dephasing rates in-

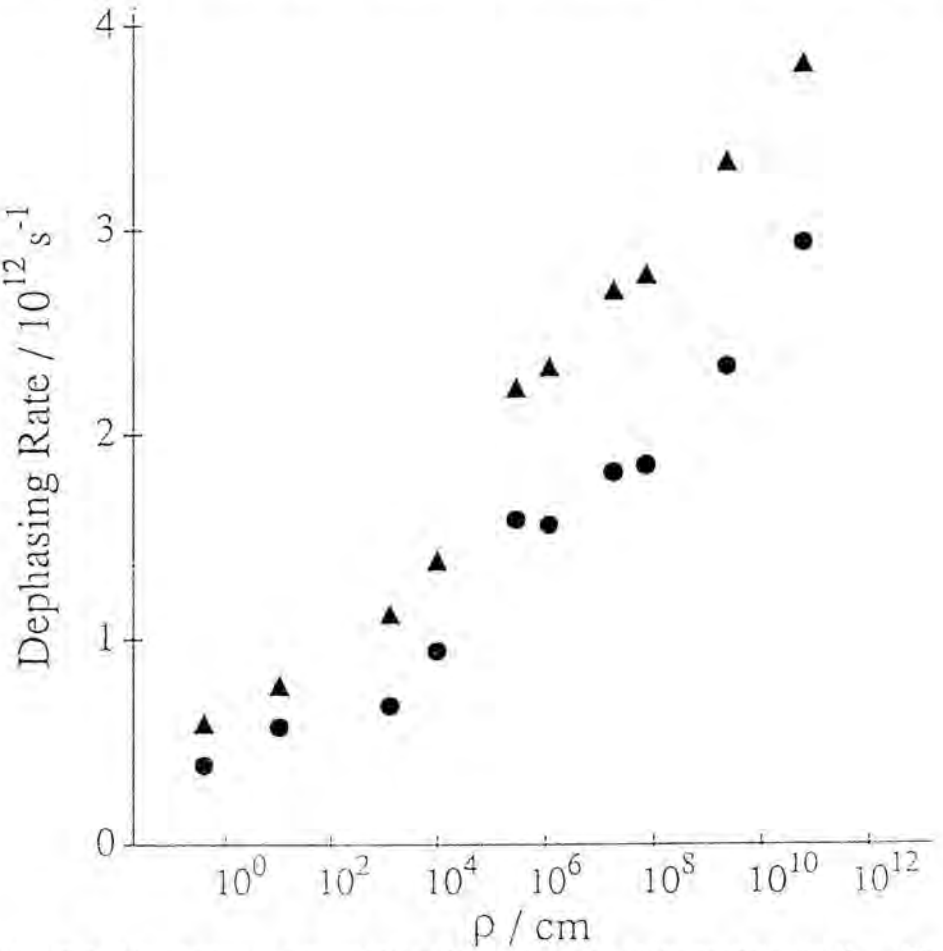

Fig. 2. Plot of the dephasing rates ($1/T_2$) of C≡N stretching of alkanenitriles ($C_nH_{2n+1}CN$, $n = 2 \sim 17$) against the density of vibrational states (ρ, in cm = states/cm^{-1}) at the C≡N stretching energy. ●: neat liquids; ▲: 50 mol% mixtures with methanol.

crease by about 30%, *regardless* of the chain length (filled triangles). This observation does not support a general expectation that the contribution of intermolecular process to the dephasing would decrease with increasing chain length. If we would divide the dephasing process into intra- and intermolecular parts, the present observation indicates that the weight of the inter-molecular dephasing due to the hydrogen bonding is independent of the molecular size. Therefore, the rate of intermolecular dissipation of vibrational coherence increases with chain length, since the total (intramolecular and intermolecular) dephasing rate also increases with the chain length. This suggests that hydrogen bond is increasingly tightened as the alkyl chain becomes longer. Such a situation may be explained by assuming the formation of a structure similar to lipid bilayer. It would be conceivable that the stability of such an aggregate is increased for longer alkyl chain.

Another explanation may be possible, if we assume that a significant part of the whole dephasing process originates from a correlation (or cross term) between intra- and intermolecular processes. If such a mechanism works, an increase in the dephasing rate of intramolecular origin (due to increasing chain length) could automatically result in greater contribution from the cross term. In the present experiment which measures the acceleration of dephasing in the mixtures with hydrogen bonding solvents, the contribution from the cross term cannot be differentiated from the purely intermolecular contribution, and both of them would appear like the contribution arising from a single origin (formation of intermolecular hydrogen bonding between the OH and CN groups, for example). These two kinds of contributions could amount to the constant degree of increases in the dephasing rate. It has been pointed out theoretically that they are generally neither independent nor simply additive when different dephasing mechanisms are simultaneously operative (Oxtoby et al., 1978). Further studies are needed in order to clarify the dephasing mechanism induced by hydrogen bonding.

Reorientational Relaxation

One can obtain purely isotropic and anisotropic component of Raman tensor separately from independent measurements in CARS, if we adopt proper polarization conditions (Dick, 1987). We have obtained the rotational correlation function, directly in the time domain, of C≡N stretching vibration ($\sim 2230\ cm^{-1}$) of benzonitrile (BN) mixed with various solvents as shown in Fig. 3. In order to extract the rotational correlation function, we have divided the anisotropic signal by the isotropic signal. (Okamoto et al., 1993(a)). All the mixtures under study give exponential correlation functions. The decay time constants ($=\tau_{OR}/2$) obtained are 2.79 ps for neat BN, 2.00 ps for BN + 1-pentanol (1:1 mole ratio), and 1.87 ps for BN + benzene (1:1). A roughly linear relationship between the reorientational relaxation time and viscosity was found in the mixtures with low

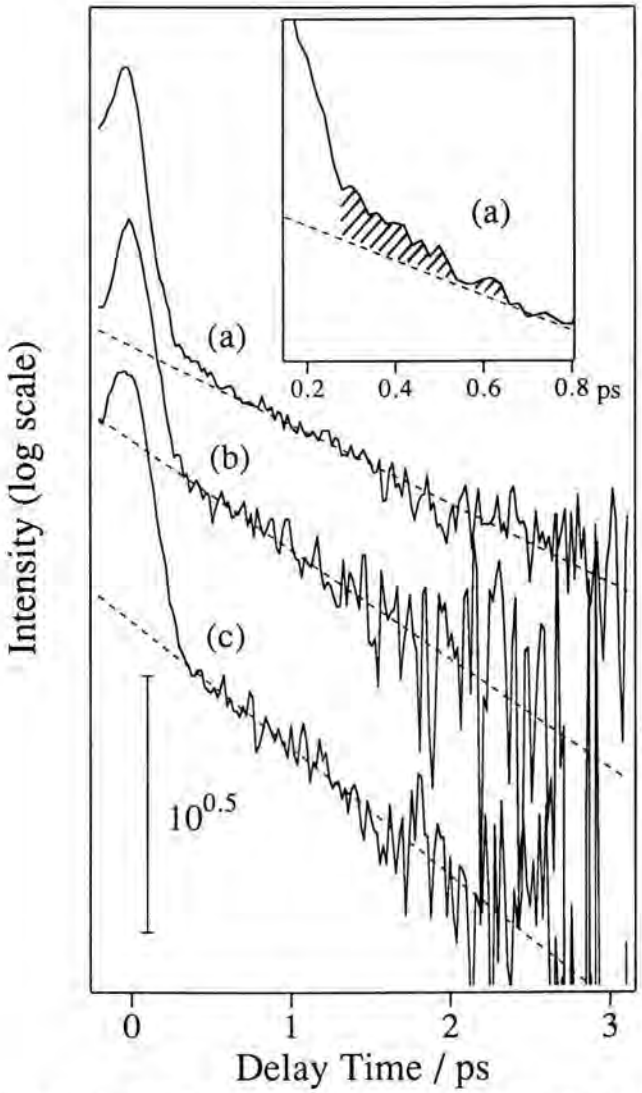

Fig. 3. Correlation functions of anisotropic component obtained by polarized CARS measurements. (a) neat benzonitrile (BN), (b) BN + 1-pentanol (1:1 mole ratio), (c) BN + benzene (1:1 mole ratio). The time constants ($=1/2\tau_{OR}$) obtained are (a) 2.79, (b) 2.00, (c) 1.87 ps.

viscosity. This observation indicates that the macroscopic Stokes-Einstein model is applicable to these mixtures.

Neat BN showed slightly non-exponential behavior in short-time region (hatches part in the inset, <0.7 ps). An exponential decay of the correlation function is expected when molecules undergo a number of stochastic collisions (dissipative process) in the course of the reorientational motion. On the other hand, before the molecule collides with neighboring molecules, it rotates freely

like an isolated molecule in the gas phase (non-dissipative process). Then, the rotational correlation function decays rapidly in the short-time regime before the collision occurs. Existence of the non-dissipative process has been pointed out from the band shape analysis of spontaneous Raman spectra (Gordon, 1965). The presence of the fast decay component in the rotational correlation function observed in the present time-resolved experiment may be attributed to the non-dissipative process.

Another interpretation may be possible on the basis of a recent theoretical work by Hayashi et al. (1992) who discussed intermolecular rotational coherence in liquid. They have pointed out a possibility that the interference among rovibrational Raman transitions of molecules at various sites causes the subpicosecond decay of anisotropic part of the coherent Raman signal. The idea seems to be consistent with the present observation.

Ultrafast Raman Echo Measurements

In time-resolved CARS or other time-resolved coherent Raman spectroscopic methods based upon the third-order nonlinear process, it is practically impossible to differentiate dephasing due to homogeneous and inhomogeneous contributions. In the previous sections, we have implicitly assumed that the dephasing is not seriously affected by the inhomogeneous contributions. In general, however, vibrational dephasing is influenced by both homogeneous and inhomogeneous contributions.

Homogeneous dephasing arises from an interaction with a bath on a very fast time scale, such as rapid fluctuation of the local environment. The resulting dephasing process usually shows an exponential decay, corresponding to a Lorentzian line shape in the frequency domain. On the other hand, inhomogeneous dephasing takes place when the frequencies of radiation field which interacts with molecules depend on local environments. In this case, the dephasing is static in nature, reflecting the spread in molecular transition energies. A Gaussian inhomogeneous distribution function is sometimes assumed in order to separate the homogeneous and inhomogeneous contributions. However, a non-Gaussian inhomogeneous contribution has been sometimes observed. Therefore, it is difficult to unambiguously determine the extent of inhomogeneous contribution to the dephasing process by means of the time-resolved coherent Raman spectroscopies or the frequency domain band shape analyses.

The homogeneous dephasing can be clearly separated from the inhomogeneous contribution by using Raman echoes, if the vibrational dephasing in liquids is described as a convolution of inhomogeneous and homogeneous contributions (Loring and Mukamel, 1985). An ultrafast Raman echo experiment in liquids has recently been reported for the dephasing of the symmetric stretching mode of methyl group of acetonitrile (Vanden Bout et al., 1991).

The Raman echo is a seventh-order nonlinear process, for which the energy diagram is shown in Fig. 4. Levels a and b represent ground and excited vibra-

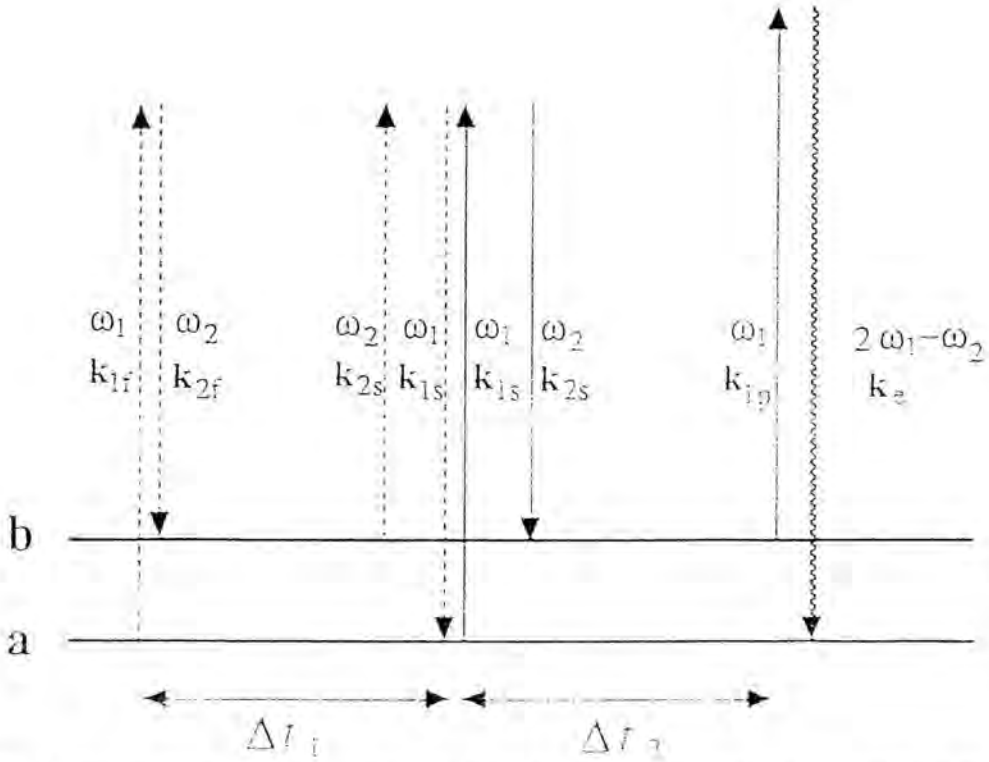

Fig. 4. Energy and time evolution diagram of the Raman echo. Time elapses from left to right. The longitudinal solid and broken arrows represent the ket- and bra-side dipole transitions, respectively. The wavy arrow indicates the light emitting transition by the induced polarization.

tional states, respectively. Initially, all the molecules in the system are assumed to be in state *a*. Coherence between *a* and *b* is prepared by applying simultaneously two light pulses with frequencies ω_1 and ω_2, where $\omega_1 - \omega_2$ is tuned to the transition from *a* to *b*. After a delay time Δt_1, the system interacts with another pair of excitation pulses at ω_1 and ω_2, which induce two sequential Raman transitions. These transitions cause a rephasing of vibrational coherence partially lost due to inhomogeneity during the delay time Δt_1. After another delay time Δt_2, the system is probed with a pulse at ω_1. Then, the echo signal with a frequency of $2\omega_1 - \omega_2$ is generated, reflecting the amount of the vibrational coherence, if the incident radiation fields satisfy the phase-matching condition (Loring and Mukamel, 1985),

$$\mathbf{k}_e = \mathbf{k}_{1p} + 2(\mathbf{k}_{1s} - \mathbf{k}_{2s}) - (\mathbf{k}_{1f} - \mathbf{k}_{2f}) \tag{1}$$

where $\mathbf{k}_e$ is the wave vector of the echo signal, $\mathbf{k}_{1f}$, $\mathbf{k}_{1s}$, and $\mathbf{k}_{1p}$ are those of the incident ω_1 radiation, and $\mathbf{k}_{2f}$ and $\mathbf{k}_{2s}$ are those of the ω_2 radiation. Subscripts '*f*', '*s*', and '*p*' denote the first and second pulse pairs, and the probe pulse,

respectively. When the signal intensity is plotted as a function of Δt_2 with a fixed value of Δt_1, the signal shows a maximum intensity when $\Delta t_2 = \Delta t_1$ for an extremely inhomogeneously broadened system. For a homogeneously broadened system, on the other hand, the echo signal decays exponentially with increasing Δt_2 regardless of Δt_1.

The ultrafast Raman echo experiment was performed using a system consisting a home-made CW mode-locked Nd:YAG laser, picosecond and femtosecond dye lasers. The pulses from synchronously pumped dye lasers were amplified by dye jet amplifiers excited by a copper-vapor laser operated at 6 kHz. The picosecond pulse was lasing at ~ 685 nm with ~ 7 ps in duration and amplified as high energy as $\sim 5\mu$J. The femtosecond pulse at ~ 592 nm with a duration of ~ 200 fs was amplified to 0.7 μJ.

The amplified femtosecond radiation is divided into three portions and used as $\mathbf{k}_{1f}$, $\mathbf{k}_{1s}$, and $\mathbf{k}_{1p}$. The amplified picosecond beam is used as $\mathbf{k}_{2f}$ and $\mathbf{k}_{2s}$ without dividing into two, i.e., $\mathbf{k}_{2f} = \mathbf{k}_{2s}$. These four beams are focused onto the sample to satisfy the phase matching condition for the Raman echo shown by Eq. (1). The echo signal can be separated from the CARS signals, of which the frequency is same as that of the Raman echo, with the aperture by making use of the difference in the phase-matching conditions. However, the aperture is not effective to completely remove the CARS signals, because the difference in the wave-vector mismatch between the CARS and Raman echo is sometimes very small. In order to separate the Raman echo from the CARS signals, the $\mathbf{k}_{1f}$ and $\mathbf{k}_{1s}$ beams are mechanically chopped with frequencies of $f_f \approx 840$ Hz and $f_s \approx 700$ Hz, respectively, by a dual chopper wheel. The Raman echo signal is modulated at the frequency of $f_d = f_f - f_s \approx 140$ Hz, while the CARS signal is modulated at f_f or f_s, except for the CARS signal which is scattered in the direction of $\mathbf{k}_{1f} + \mathbf{k}_{1s} - \mathbf{k}_{2f}$. The CARS signal in this direction is modulated at the same frequency as that of the Raman echo, but the intensity of this CARS signal is independent of Δt_2. Therefore, a plot of the f_d-modulated signal intensity as a function of Δt_2 reflects the decay of the Raman echo signal. The f_d-modulated component of the signal from the photomultiplier tube is detected by a lock-in amplifier.

In Fig. 5, the Raman echo intensities are shown for the C≡N stretching of benzonitrile as a function of Δt_2. The other delay time Δt_1 is fixed at 0 ps and 2 ps in Fig. 5 (a) and (b), respectively. A strong signal at around $\Delta t_2 = 0$ ps is due to a coherence artifact resulting from a seventh-order nonresonant response. It is found that the echo signals show exponential decay profiles with time constants of ≈ 0.6 ps for both $\Delta t_1 = 0$ ps and $\Delta t_1 = 2$ ps, within experimental uncertainty.

If the inhomogeneous distribution in Raman transition frequency is assumed to be a Gaussian with a characteristic width (i.e., standard deviation of the transition frequencies) δ, the intensity of Raman echo signal $I(\Delta t_1, \Delta t_2)$ is given by the following equation (Loring and Mukamel, 1985),

$$I(\Delta t_1, \Delta t_2) = \exp(-2(\Delta t_1 + \Delta t_2)/T_2) \exp(\delta^2(\Delta t_2 - \Delta t_1)^2) \qquad (2)$$

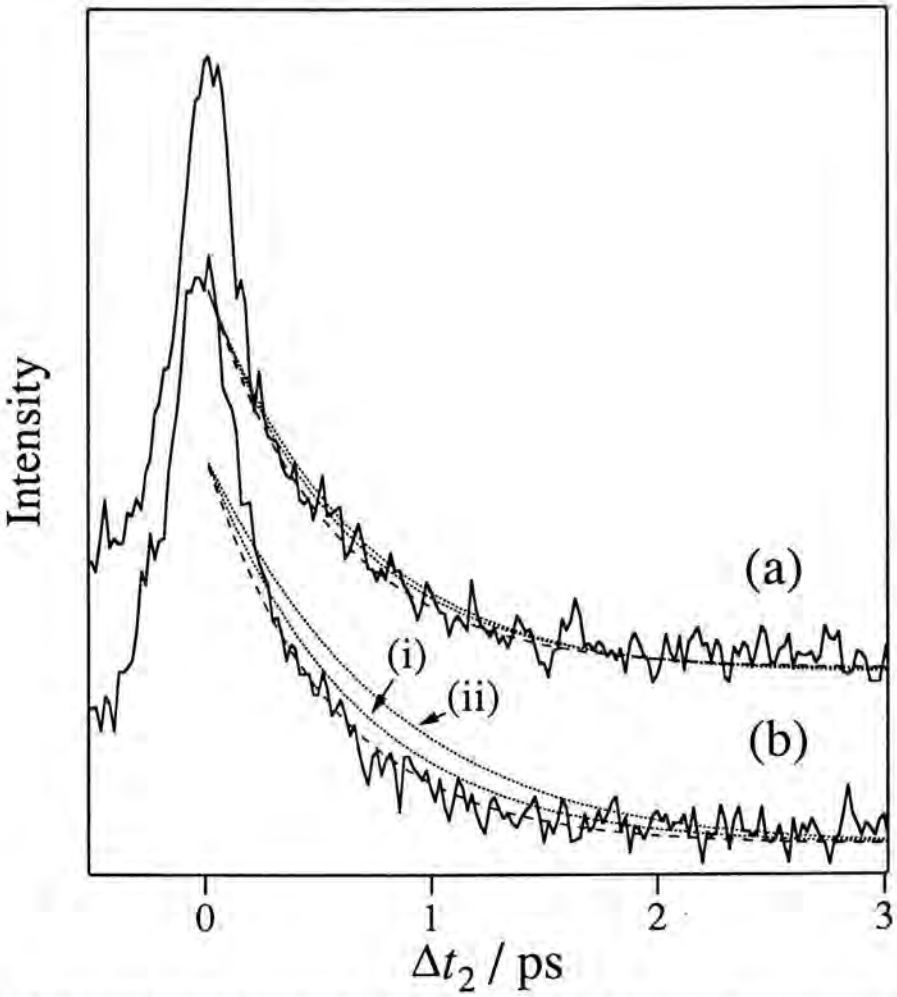

Fig. 5. Raman-echo signal intensities for the C≡N stretching of benzonitrile as functions of Δt_2. (a) $\Delta t_1 = 0$ ps. (b) $\Delta t_1 = 2$ ps. The broken curve indicates the exponential decay with a time constant 0.6 ps ($= T_2/2$). The dotted curves represent the calculated decay profiles. The parameters for the calculation are: (i) $T_2 = 1.22$ ps and $\delta = 0.92$ cm^{-1}; (ii) $T_2 = 1.33$ ps and $\delta = 1.41$ cm^{-1}.

where T_2 is the homogeneous dephasing time constant. Therefore, if the inhomogeneous broadening has a significant contribution to the dephasing, the decay of the signal should be retarded further as Δt_1 increases, or in an extremely inhomogeneous broadening case, the signal should show a rise-and-decay profile. The decay profile of Raman echo for $\Delta t_1 = 0$ ps corresponds to that of the time-resolved CARS signal, i.e., the Fourier transform of the isotropic Raman band shape in the frequency domain. The decay time constant of 0.6 ps obtained in this experiment for $\Delta t_1 = 0$ ps is in good agreement with that obtained in the CARS experiment of 0.74 ps (Okamoto et al., 1993).

In Fig. 5, the calculated decay profiles are also indicated for (i) $T_2 = 1.22$ ps and $\delta = 0.92\ \mathrm{cm}^{-1}$, and (ii) $T_2 = 1.33$ ps and $\delta = 1.41\ \mathrm{cm}^{-1}$. In each condition, the predicted isotropic Raman linewidth (half-width at half maximum) is $\approx 4.6\ \mathrm{cm}^{-1}$, which corresponds to 0.6 ps decay of the echo signal for $\Delta t_1 = 0$ ps. From the comparison of the observed decay profile with the calculated one, the characteristic width of inhomogeneous broadening, δ, is estimated to be less than $1\ \mathrm{cm}^{-1}$. In other words, the C≡N stretching Raman band of benzonitrile is almost completely homogeneously broadened. This observation indicates either that the C≡N stretching is only weakly coupled to inhomogeneity in the local environment, or that the lifetime of the fluctuation of liquid structure which is coupled to the C≡N stretching is shorter than the homogeneous dephasing time constant ($T_2 \approx 1.2$ ps) in liquid benzonitrile.

References

Dick, B., *Chem. Phys.* **113**, 131, 1987.

Gordon, R.G., *J. Chem. Phys.* **43**, 1370, 1965.

Fickenscher, M. Laubereau, *J. Raman Spectry.* **21**, 857, 1990.

Hayashi, M., Fujimura, Y., Okamoto, H., and Yoshihara, K., *Chem. Phys. Lett.* **196**, 44, 1992.

Inaba, R., Okamoto, H., Yoshihara, K., and Tasumi, M., *Chem. Phys. Lett.* **185**, 56, 1991.

Inaba, R., Okamoto, H., Yoshihara, K., and Tasumi, M., *J. Phys. Chem.* **96**, 8385, 1992.

Inaba, R., Okamoto, H., Yoshihara, K., and Tasumi, M., *J. Phys. Chem.* **97**, 7815, 1993.

Inaba, R., Tominaga, K., Tasumi, M., Nelson, K.A., and Yoshihara, K., *Chem. Phys. Lett.*, **211**, 183, 1993.

Joo, T., Dugan, M.A., and Albrecht, A.C., *Chem. Phys. Lett.* **177**, 4, 1991.

Leonhardt, R., Holzaphel, W., Zinth, W., and Kaiser, W., *Chem. Phys. Lett.* **133**, 373, 1987.

Loring, R.F., and Mukamel, S., *J. Chem. Phys.* **83**, 2116, 1985.

Okamoto, H., and Yoshihara, K., *J. Opt. Soc. Am.* **B7**, 1702, 1990.

Okamoto, H., Hayashi, H., Yoshihara, K., and Tasumi, M., *Chem. Phys. Lett.* **182**, 96, 1991.

Okamoto, H., Inaba, R., Tasumi, M., and Yoshihara, K., *Chem. Phys. Lett.* **206**, 388, 1993.

Okamoto, H., Inaba, H., Yoshihara, K., and Tasumi, M., *Chem. Phys. Lett.* **202**, 161, 1993.

Oxtoby, D.W., Levesque, D., and Weis, J.-J., *J. Chem. Phys.* **68**, 5528, 1978.

Vanden Bout, D., Muller, L.J., and Berg, M., *Phys. Rev. Lett.* **43**, 3700, 1991.

Authors' Address

K. Yoshihara, R. Inaba, K. Tominaga and K.A. Nelson; Institute for Molecular Science, Myodaiji, Okazaki 444, Japan
R. Inaba, H. Okamoto and M. Tasumi; Department of Chemistry, University of Tokyo, Hongo, Bunkyo, Tokyo 113, Japan
R. Inaba; Present address; Hitachi Research Laboratory, Hitachi Ltd., Ohmika, Hitachi, Ibaraki 319-12, Japan
K.A. Nelson; Permanent address, Department of Chemistry, Massachusetts Institute of Technology, Cambridge, MA 02139, USA